BORON-FUNCTIONALIZED HOMO AND BLOCK COPOLYMERS

FOR OPTOELECTRONIC AND SENSORY APPLICATIONS

by

FANG GUO

A Dissertation submitted to the

Graduate School – Newark

Rutgers, The State University of New Jersey

in partial fulfillment of requirements

for the degree of

Doctor of Philosophy

Graduate Program in Chemistry

written under the direction of

Professor Frieder Jäkle

and approved by

_____

_____

_____

_____

Newark, New Jersey

October, 2015

© 2015

Fang Guo

ABSTRACT OF THE THESIS

BORON-FUNCTIONALIZED HOMO AND BLOCK COPOLYMERS

FOR OPTOELECTRONIC AND SENSORY APPLICATIONS

By Fang Guo

Thesis Director: Professor Frieder Jäkle

Conjugated polymers have been explored as an important class of organic electronics, such as organic light emitting diodes (OLEDs), organic field-effect transistors (OFETs) and organic solar cells. With the development of various synthetic methods and characterization techniques, the family of conjugated polymers have grown to a scope which goes beyond any single discipline. Functionalization of conjugated organic systems with main group elements represents an active research area of significant interest in the scientific community. One of the most employed elements is the electron-deficient boron that features an empty p orbital that enables the overlap with π orbitals of attached aryl groups. This leads to novel optical and electronic properties for organoborane containing conjugated polymers. The focus of this thesis is on the investigation of incorporation of organoborane into different conjugated systems.

Chapter 1. **Regioregular Organoborane-Functionalized Poly(3-alkynylthiophene)s**

A series of new alkynylphenylborane-functionalized monomers were synthesized and

utilized to prepare regioregular borane acceptor-functionalized polythiophenes *rr*-**P1**, *rr*-**P2** using Stille-type polymerization and **P1** using Kumada technique. Theoretical calculations on model systems and fluoride anion binding studies confirm the assignment of the lowest energy absorption at ca. 500 nm to the polymer backbone and the higher energy bands at ca. 330-340 nm to a charge transfer state which is localized on the borane moieties. A comparison between polymer **P1** and **rr-P1** suggests a higher regioregularity which results in significant bathochromic shifts in both absorption and emission spectra. The borane acceptor effect is also reflected in the bathochromic shift of the lower energy absorption maximum of polymers *rr*-**P1**, *rr*-**P2** and rr-P3HT which is envisioned as possible candidates for optical and sensory materials.

Chapter 2.   Amphiphilic Polythiophene Block Copolymers Containing

Phenylboronic Acid Functionality

The amphiphilic block copolymers poly (3-hexylthiophene)-block-polystyrene boronic acid   (P3HT-*b*-PSBA)   and   poly   (3-hexylthiophene)-block-poly (4-vinylpyridine-stat-styrene boronic acid) (P3HT-*b*-P(4VP-*stat*-SBA) are prepared using a combination of Grignard metathesis (GRIM), controlled radical polymerization (CRP) and click chemistry. This polymers represent a new type amphiphilic polythiophene block copolymers containing boronic acid-functionality for potential applications in material chemistry.

Chapter 3.   The First 1, 2-azaborine Polymer

With a collaborative effort with Prof. Liu's group (Boston College) who provided Bpin/Br-functionalized AB-type monomers and regioregular model compounds, we incorporated monocyclic 1,2-azaborine into extended π-conjugated systems using the Suzuki-Miyaura polymerization technique. Though the polymer main chain is isoelectronic to poly (paraphenylene), photophysical and computational studies indicate a closer similarity to polyacetylene which indicates promising applications as a new class of conjugated materials.

Acknowledgments

First, I would like to thank my advisor Prof. Frieder Jäkle for taking me at the most difficult time in my graduate years and opening wide learning opportunity for me. Thanking him for his tireless enthusiasm in encouraging me to learn, to practice. Without his training and mentoring, I would not have had the opportunity to have a taste of the State of the Art. Most of all, I am very impressed by his passion and dedication as a scientist in always striving for the excellence which made him a role model in my academic career.

I would like to acknowledge my committee members, Prof. Agostino Pietrangelo, Prof. John Sheridan, and Prof. Qiao-Sheng Hu (City University of New York), for spending their time reading and correcting my thesis, and for their helpful advice and encouragement.

I would like to thank all the Rutgers University-Newark chemistry faculty and staff for their kind help over the past years: especially thank Prof. Piotr Piotrowiak for his understanding and support when I made the bold decision to move, Prof. Roger Lalancette for helping to solve crystals' structure, Prof. Michele Pavenello and Prof. Phillip Huskey for helping with DFT calculation questions, Dr. Lazaros Kakalis for 2D NMR measurement, Dr. Roman Brukh for MALDI-MS training, Dr. Karen Chaffee for helping me to prepare the interviews. My thanks also goes to the former and current

Table of Contents

List of Schemes

List of Figures

List of Tables

General Introduction

π-conjugated polymers have garnered much attention as promising materials for the development of the next generation of organic electronics since the award of the Nobel Prize for Chemistry in 2000 to Professors Alan Heeger, Alan MacDiarmid, and Hideki Shirakawa for their discovery of highly conductive polyacetylene by doping.[1] In a conjugated organic polymer (Figure 1), the bonds between carbon atoms are alternatively single (σ bond) and double (π bond). The overlap of π bonding between neighboring atoms leads to electron delocalization along the polymer backbone and provide a pathway for charge mobility along the backbone of the polymer chain.[2] Figure 2 gives an example of the development of a band structure of polythiophenes (PT) and the lowering of the HOMO-LUMO energy gap while the polymer chain extends.[3]

Polyacetylene (PA), **1**

Poly(para-phenylene vinylene) (PPV), **4**

Poly(para-phenylene) (PPP), **2**

Polythiophene (PT), **5**

Polyaniline (PANI), **3**

Polypyrole (PPy), **6**
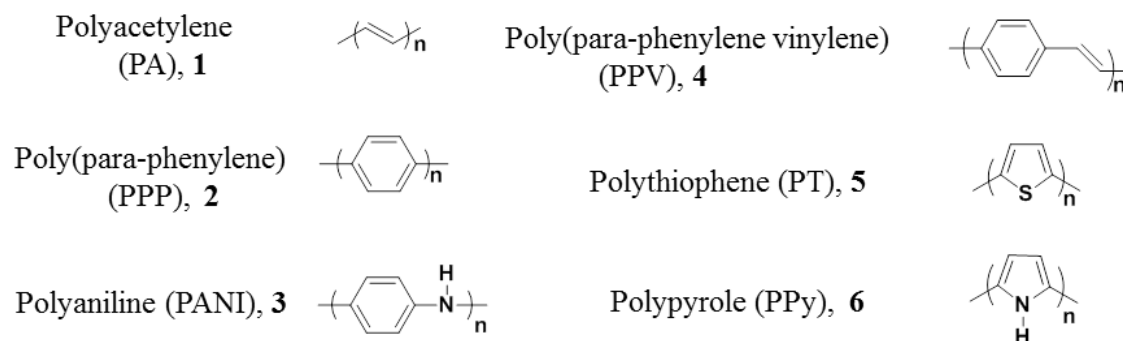
Figure 1. Examples of some conjugated polymers.
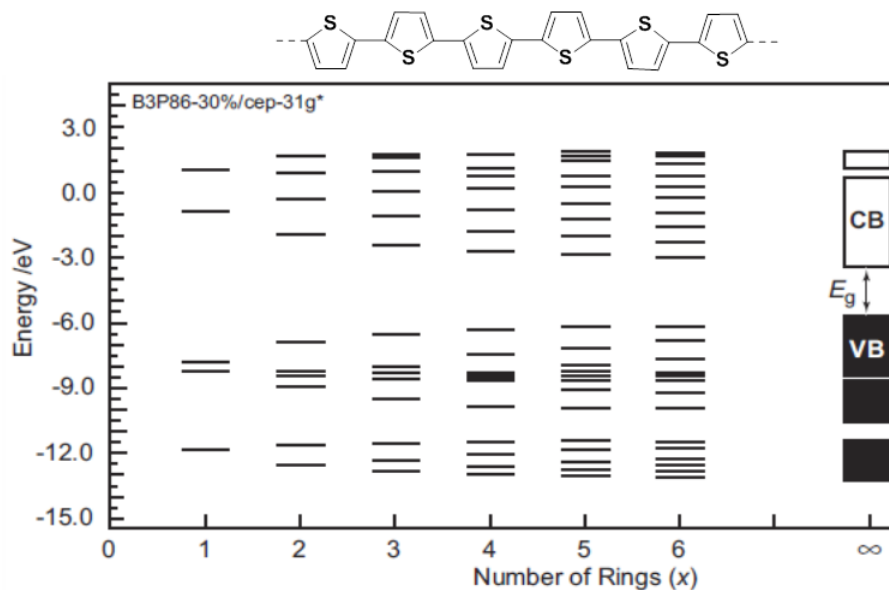
Figure 2. (a) Development of band structure of PT (adapted with permission from reference 3).

Practically, in semiconducting polymers, the energy gap between the highest occupied molecular orbital (HOMO) and the lowest unoccupied molecular orbital (LUMO) determines the conductivity and the color of the neutral polymers. In general, a lower HOMO/LUMO energy gap can be realized by extension of π-conjugation, transition from aromatic to quinoidal structures, incorporation of alternating donor-acceptor (D-A) moieties in the polymer backbone, or introduction of main group elements such as N, P, S, Si.[4] The combination of the optical and electronic properties of semiconductors with the advantages of low-cost, lightweight, easy processing, and structural versatility led to wide applications of conjugated polymers in organic electronic devices such as organic light-emitting diodes (OLEDs), solar cells, and organic field-effect transistors (OFETs).[5]

Tricoordinate boron provides a vacant p-orbital which can overlap with an adjacent π-system to facilitate π-delocalization and lower the HOMO-LUMO energy gap

that is often accompanied by interesting photophysical properties.[6] Especially, the enhanced electron-acceptor character due to organoboron incorporation is advantageous for the detection of anions and toxic chemicals such as fluoride and cyanide species. Hydroboration[7] and metathesis[8] reactions developed by Chujo have been widely used to incorporate boron into π-conjugated systems (Figure 3). Very often, the attachment of bulky mesityl (2,4,6-trimethylphenyl) (Mes), tripyl (2,4,6-triisopropylphenyl) (Tip), or less often (2,4,6-tri-tert-butylphenyl (Mes*) groups to boron is necessary to protect the boron center from nucleophilic attack and subsequent oxidative degradation.
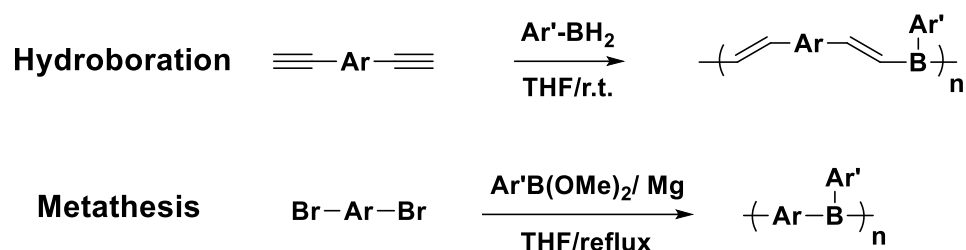
Figure 3. Methods developed by Chujo to incorporate boron into π-conjugated systems.

1. Polythiophenes (PTs)

Polythiophenes are one of the most investigated semiconducting materials for applications in organic electronics due to their relatively high stability and processibility, as well as excellent properties upon substitution.[9] Substituted polythiophenes (Figure 4) show electroluminescence varying from the blue (PCHMT), green (PCHT), orange (PTOPT) to red (and NIR) (POPT) due to different degrees of torsion in the conjugated main chain.[9e,10] Voltage-controlled electroluminescence and white light emitters were thus obtained by blending the polymers of different emission.
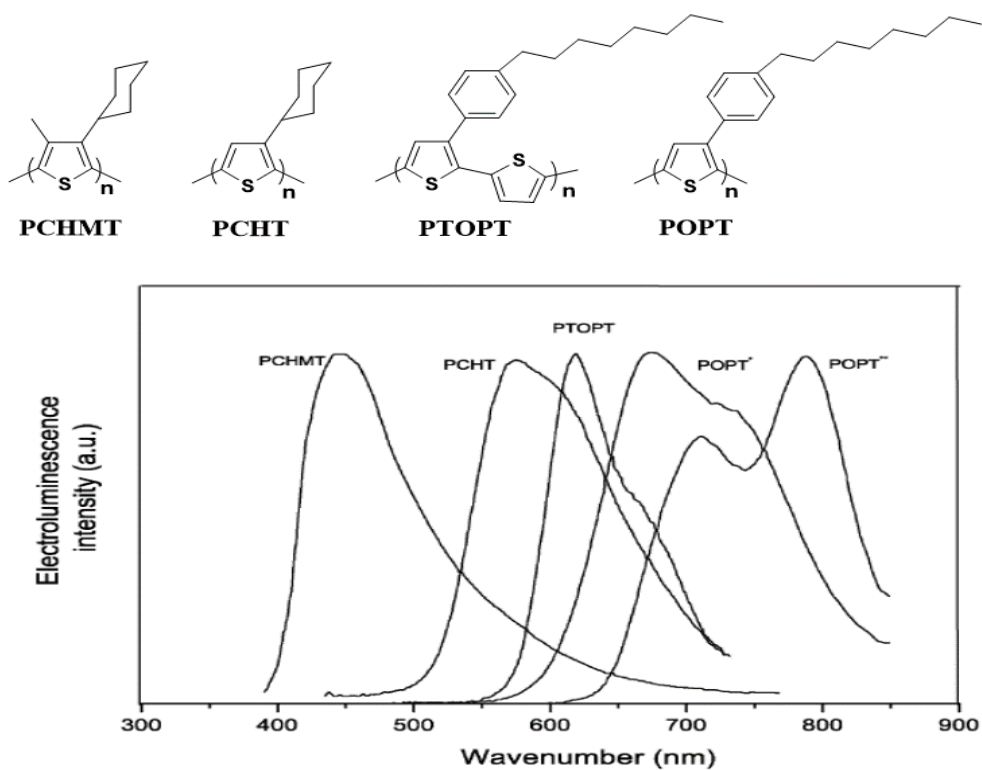
Figure 4. Effect of substitution on the emitting properties of polythiophenes. POPT* is more ordered film of POPT and shows more red-shift electroluminescence. (reproduced with permission from reference 9e)

Another important aspect that influences the optical and charge transport properties of polythiophenes is regioregularity.[11] The absorption peak of the regiorandom poly (3-hexylthiophene) (*rra*-P3HT) occurs at 420 nm which is blue-shifted about 34 nm compared to regioregular poly (3-hexylthiophene) (*rr*-P3HT). The emission maxima of *rra*-P3HT and *rr*-P3HT appear 572 and 577 nm, respectively (Figure 5).[11b] The blue-shift of *rra*-P3HT was attributed to the decrease of the effective conjugation length due to twisting of polymer chains by repulsive interactions between two alkyl chains and a sulfur lone pair.[12]
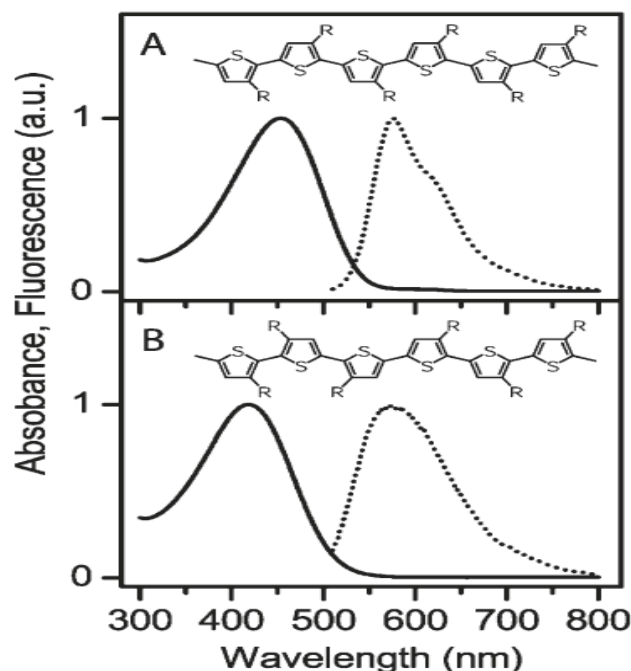
Figure 5. Effect of regioregularity on the absorption (solid) and emission (dotted) spectra of (A) *rr*-P3HT (97% HT-HT) and (B) *rra*-P3HT (64% HT-HT) in chloroform. (reproduced with permission from reference 11b)

1.1 Main-Chain Organoboron-Functionalized Polythiophenes

The functionalization of polythiophenes with tricoordinate boron has a strong π-acceptor effect on the conjugated polymer backbone resulting in novel optical and electronic properties. In 1998, Siebert and coworkers reported the formation of conjugated main chain-functionalized polythiophenes **7** through hydroboration of 2,5-diethynylthiophene derivatives with BCl_3/Et_3SiH mixture (Figure 6).[13] The resulting polymers showed tunable color depending on the substituents on the alkynyl groups and the boron center itself. However, the high sensitivity to moisture and oxygen prevented further characterization of the molecular weight and photophysical properties. One year later, the Chujo group developed the relatively more stable organoboron-functionalized polythiophene **8** through hydroboration.[7b] The resulting polymer showed only 10% weight loss at 190 °C in thermogravimetric analysis (TGA) measurement. An absorption

maxim at 350 nm and an emission maxim at 488 nm (visible green) were observed. The unusually large Stokes shift was thought to be due to possible energy transfer in the excited states.

R = Ph, turquoise powder
R = SiMe$_3$, red powder
R = ^{t}Bu, Orange-brown paste
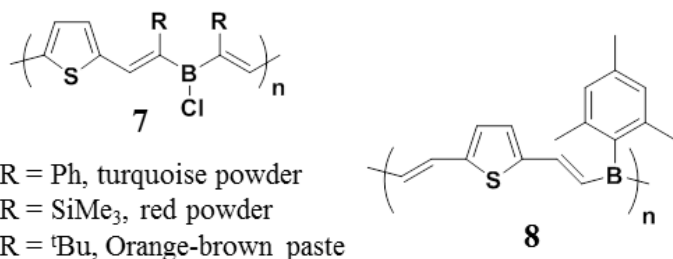
Figure 6. Main-chain organoboron-functionalized PTs.

Our group has explored a mild and highly selective Sn/B exchange method to obtain boron-containing polythiophenes (Figure 7).[14] One important aspect of this approach is the use of non-coordinating solvents such as CH$_2$Cl$_2$ or toluene avoiding the need for ether solvents which tend to form Lewis acid-base complex with highly Lewis acidic borane centers or elicit ether cleavage. The obtained polymers are readily soluble in common organic solvents and thermally stable to ca. 200 ºC but need to be handled under nitrogen atmosphere due to some oxygen sensitivity.
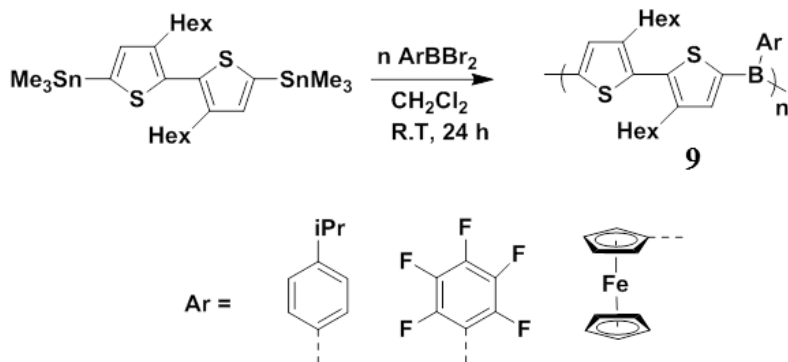
Figure 7. Preparation of main-chain organoboron-functionalized PTs by B/Sn exchange.

Recently, our group has utilized the Sn/B exchange method to prepare a series of very stable conjugated thienylboranes (Figure 8:**10-11**) and explored the derivatization of

these molecules with halogens.[15] The halogenated compound can react with diboronated fluorene by Suzuki-Miyaura cross-coupling to generate polymers (Figure 8) with $M_n = 8.4$ kDa in a yield of 61%. The results of this preliminary study are very encouraging for the future use of these molecules as electron-deficient building blocks in organic electronics and sensory materials.
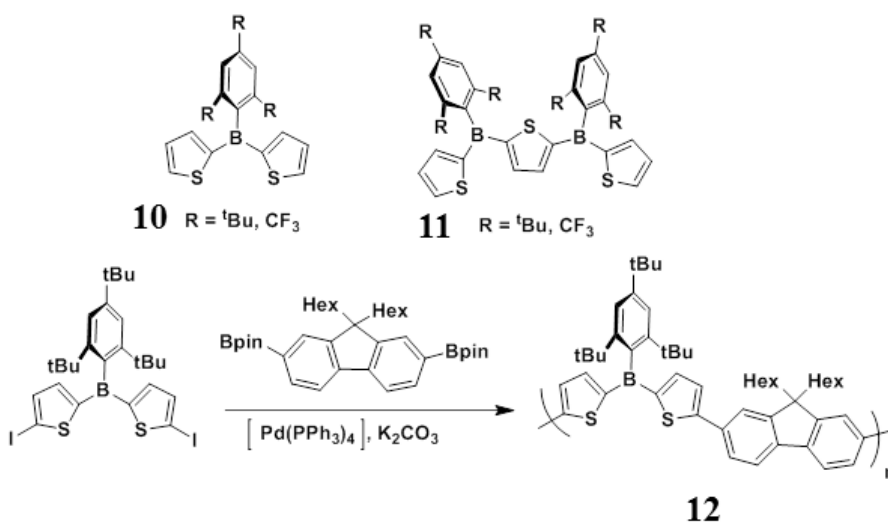
Figure 8. Main-chain organoboron-functionalized thiophene derivatives **10-11** and preparation of PT **12** by Suzuki-Miyaura cross-coupling method.

1.2 Side-Chain Organoboron-Functionalized Polythiophenes

Compared to main-chain organoboron-functionalized conjugated polymers,[6b,14-16] the side-chain functionalization of conjugated materials with organoborane groups has been underdeveloped. Similar methods as mentioned above have been used to prepare conjugated polymers with tricoordinate boron incorporated in the side chains (Figure 9).[17]
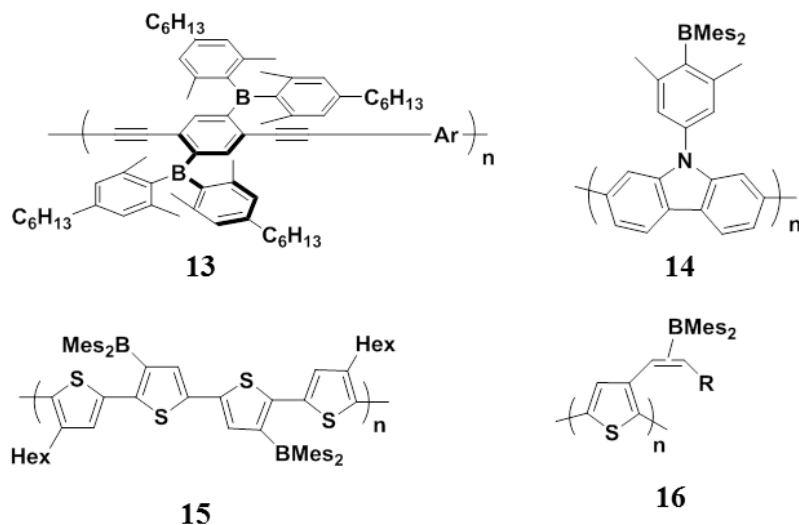
Figure 9. Examples of side-chain organoboron-functionalized conjugated polymers.

The first polythiophenes substituted with organoborane acceptor moieties on the side chains **15** have been reported by our group and the strong influence of the boryl groups on the electronic and photophysical properties has been established.[17e] The boron functionality was installed by B/Si exchange in a post-polymerization modification of the silylated polymer. The absorption of the side-chain-borylated polythiophene displays a strong bathochromic shift (ca. 60 nm) relative to that of the corresponding side-chain-silylated polymer indicating that the presence of electron-withdrawing boryl side groups leads to lowering of the optical gap from ca. 2.70 to 2.36 eV (Figure 10). The emission of PT-BMes$_2$ (617 nm) is also strongly red-shifted relatively to the orange emission of PT-SiMe$_3$ (554 nm), further confirming the presence of significantly lower LUMO energy levels upon side-chain borylation. According to a cyclic voltammetry study in THF, the first reduction of PT-BMes2 ($E_{1/2}(1)$ = -2.18 V) is much less negative than that of PT-SiMe3 ($E_{1/2}(1)$ = -2.35 V) which confirms the electron-accepting ability of side-chain-borylated polythiophenes.
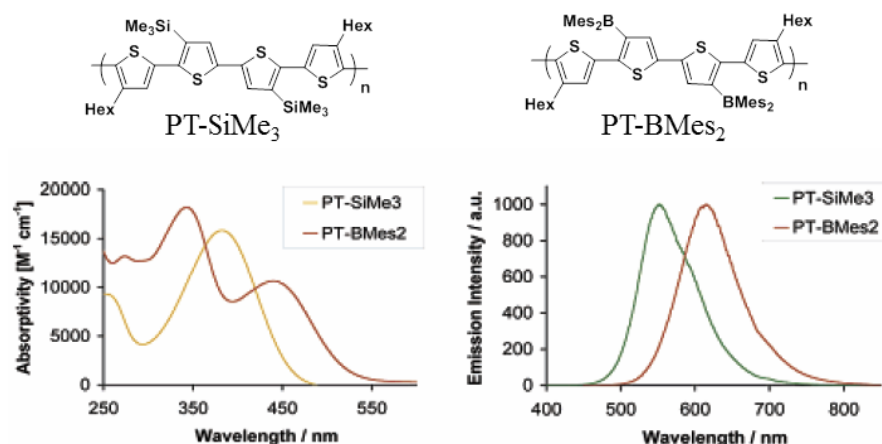
Figure 10. UV-vis absorption and emission spectra of PT-SiMe$_3$ and PT-BMes$_2$ in CH$_2$Cl$_2$ solution. (reproduced with permission from reference 17e).

Later on, our group investigated the possibility of preparing side-chain borylated polythiophenes **16** by GRIM polymerization of vinylborane-functionalized 2,5-dibromothiophene[17f] and an alternative approach was to polymerize alkynyl-substituted thiophene monomers followed by hydroboration.[17d] In both cases, the resulting side-chain borylated polymers showed drastically different optical properties from those of the non-borylated polymers, but a lack of regioregularity caused by the formation of isomers either in the hydroboration process or in the metathesis step in Grignard metathesis polymerization (GRIM) became an impetus for improvement.

In Chapter 1, we will introduce a series of new alkynylphenylborane-functionalized monomers and describe the development of regioregular borane acceptor-modified polythiophenes (*rr*-**P1**, *rr*-**P2**) using Stille-type polymerization. The optical and electronic properties of the polymers *rr*-**P1**, *rr*-**P2** are described in detail and a comparison of the optical properties to those related polymers prepared by Kumada polycondensation is provided.

1.3 Boronic Acid Functionality and Polythiophenes

Boronic acid moieties can form reversible covalent boron-oxygen links with concurrent conversion to tetracoordinate borates (Figure 11).[6b] For boronic acid-functionalized polymers, the dynamics of this equilibrium in the presence of polyols such as sugars, RNA, etc, can be associated with (i) a change in the solubility induced by the conversion of the neutral boronic acid sites to anionic borate moieties, (ii) a change in the absorption or emission color of the polymer due to the changes in the electronic structure, or (iii) a change in conductivity because of conformational or electronic changes in conjugated polymers.

Figure 11. Equilibrium of boronic acid in the presence of polyols.

The solubility change-associated sugar-responsive properties of boronic acid-functionalized polymersome systems have been widely investigated (Figure 12). A sugar responsive behavior of some systems (**18-21**) has been realized even under physiological pH (7.4) either by modification of the boronic acid moieties or by adjusting the structure of the polymer strands.
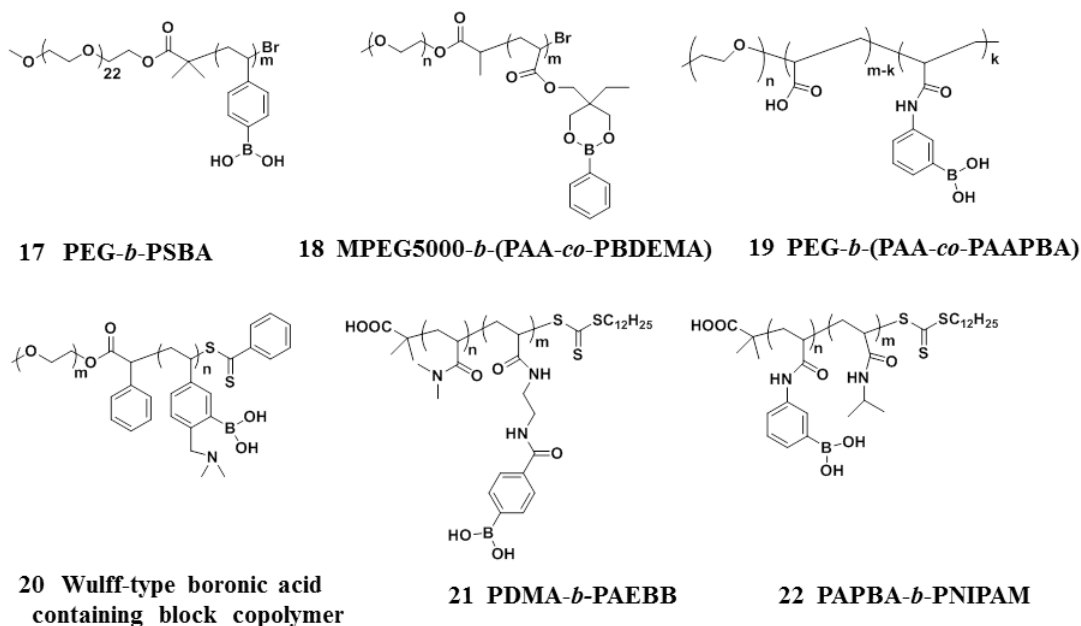
Figure 12. Boronic acid-functionalized sugar responsive amphiphilic block copolymers.

Most boronic acid-functionalized conjugated polymers developed so far have been prepared by chemical or electrochemical oxidative coupling reactions (Figure 13). The boronic acid functionalities in conjugated polymers have been used as doping sites to enhance the conductivity of the polymers[18], as a precursor for other functional groups[19], or to develop potentiometric chemical sensors.[20]
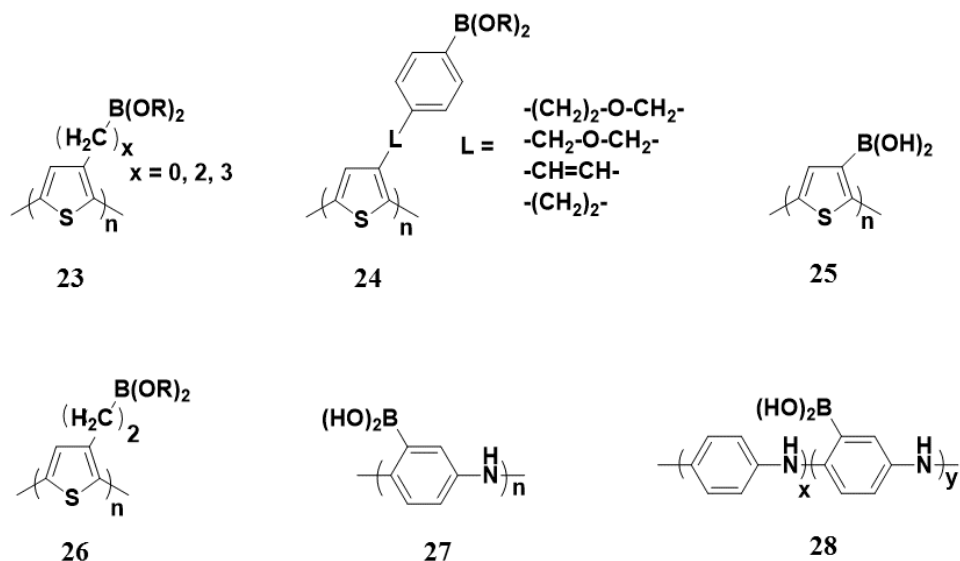
Figure 13. Examples of boronic acid-functionalized conjugated polymers.

Recently, the Liu group introduced water-soluble zwitterionic boronic acid-functionalized regioregular polythiophenes prepared by GRIM polymerization followed by modification with 3-pyridylboronic acid (Figure 14).[21] The resulting polymer showed ultrasensitive fluorescent response to carbohydrates through multivalent cooperative interaction at pH (7.4). An advantage of preparing the regioregular polythiophenes using the GRIM method is that the polymers obtained have controlled molecular weight and well defined structure. However, block copolymers that comprise polythiophene and boronic acid functionality have not been reported to date.
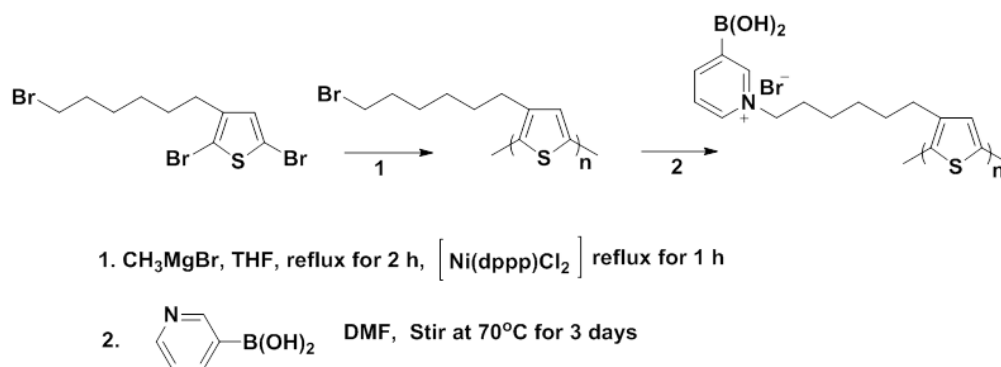
Figure 14. Preparation of zwitterionic boronic acid-functionalized PTs. (adapted with permission from reference 21)

In Chapter 2, the amphiphilic block copolymers poly(3-hexylthiophene)-block-polystyrene boronic acid (P3HT-*b*-PSBA) and poly(3-hexylthiophene)-block-poly (4-vinylpyridine-stat-styrene boronic acid) (P3HT-*b*-P(4VP-*stat*-SBA)) are prepared by combining controlled radical polymerization (CRP) and click chemistry. The resulting amphiphilic block copolymers are designed such that the photophysical property changes of the conjugated P3HT block that are associated with the sugar responsive properties of PSBA/P (4VP-*stat*-SBA) block can be monitored.

2. 1,2-Azaborines

Another emerging strategy to incorporate boron in conjugated organic structures is to substitute a C=C bond with an isoelectronic and isosteric B-N unit (BN/CC isosterism). Among the three possible C_4BN benzene isomers, the BN-benzene formed by adjacent BN substitution (1,2-azaborine) was found to be the most stable due to the complimentary π- and σ-donations from nitrogen and boron, respectively (Figure 15).[22]
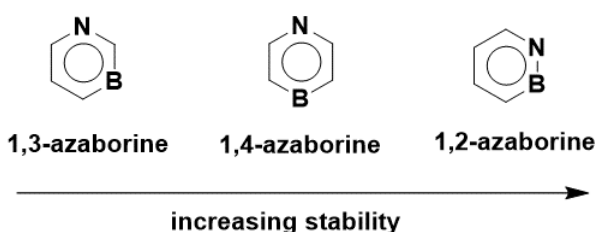
Figure 15. Azaborines and their relative stability.

In 1962, Dewar and co-workers synthesized derivatives of 1,2-azaborine using a desulfurization strategy[23] but thorough characterization was not obtained until Ashe,[24] and more recently Liu[25] investigated the aromaticity, reactivity, and optoelectronic properties. Despite the fact that the total valence electron count is the same, recent investigations have revealed that replacing a CC unit with a BN unit can induce significant property changes predicting potential applications in bioactive molecules (Figure 16, compound **29**),[26] hydrogen storage (compound **30**),[27] and organic electronic materials (compounds **31-33**, **35**).[22b,28] Fused polycyclic BN-containing compounds have been reported by different groups and significant progress has been made. The emissive properties of the fused polycyclic BN-containing compounds can be tuned by the position of the BN substitution and the substituents on the polycyclic moieties. For examples, compound **34** showed superior intrinsic hole mobility (0.07 $cm^2V^{-1}S^{-1}$), which is ten

times higher than its carbon analogue dibenzo [g,p]chrysene. The high hole mobility of compound **34** was attributed to BN substitution induced partial localization of the frontier orbitals.[28g] Perepichka and co-workers also accomplished the incorporation of 1, 2-azaborines into oligothiophene organic electronic materials (compound **35**). In comparison with fused polycyclic BN-containing compounds, conjugated monocyclic BN heterocycles have been underdeveloped. The Liu group has reported the synthesis of BN-tolans (compound **36**),[28e] which showed distinct absorption and emission properties from their carbonaceous analogue, tolan, an important building block in the structure of the carbon allotrope graphyne. Additionally, bis-BN-tolan exhibits unique N-H⋯π (C≡C) hydrogen bonding in the solid state. Yamaguchi and co-workers have pioneered the incorporation of 1, 2-dihydro-1, 2-azaborine into extended π-conjugated systems.[28f] The resulting compound **37** has a lower HOMO-LUMO energy gap compared to its carbon analogue and showed bathochromic shifts in both absorption and emission spectra while maintaining high fluorescence quantum yields in solution. In contrast to BN-containing fused polycyclic compounds, the theoretical calculations of compound **37** supported that the incorporation of the 1,2-dihydro-1,2-azaborine ring into the extended π-conjugated system decreased the aromatic character of the azaborine ring and made it more like a cyclohexadiene analogue instead of a benzene analogue.
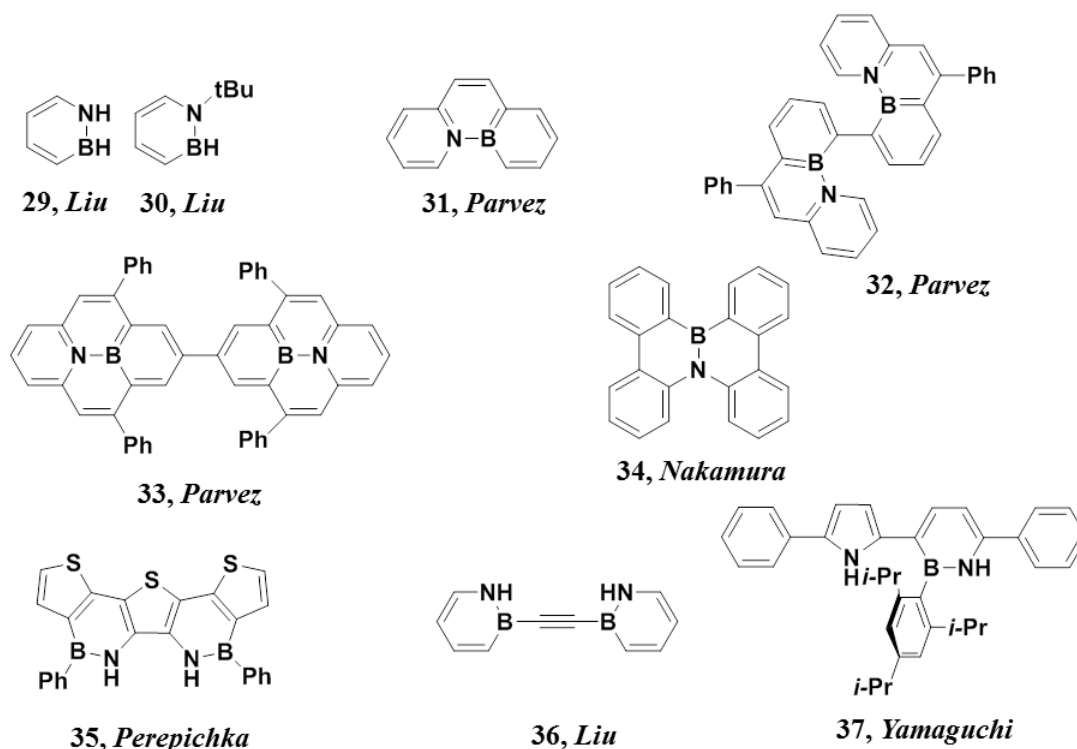
Figure 16. Examples of some 1, 2-azaborine derivatives.

Chapter 3 constitutes a collaborative effort with Prof. Liu's group at Boston College: Andrew Badget synthesized Suzuki-type functionalized AB-type monomers (**BN-M**) and regioregular model compounds (**BN1, BN2,** and **BN3**) with 1D NMR characterization, Bo Li solved the X-ray structure of **BN2** compound. We demonstrate the incorporation of the monocyclic 1, 2-azaborine into extended π-conjugated systems using the Suzuki-Miyaura coupling method. Photophysical and electrochemical studies on the resulting polymer and the corresponding model compounds, in combination with DFT calculations, offer detailed insights into the electronic structure and suggest intriguing applications as a new class of conjugated materials.

3. References

(1) Chiang, C. K.; Fincher, C. R.; Park, Y. W.; Heeger, A. J.; Shirakawa, H.; Louis, E. J.; Gau, S. C.; MacDiarmid, A. G. *Phys. Rev. Lett.* **1977**, *39*, 1098.

(2) Heeger, A. J. *Angew. Chem. Int. Ed.* **2001**, *40*, 2591.

(3) Salzner, U.; Lagowski, J. B.; Pickup, P. G.; Poirier, R. A. *Synth. Met.* **1998**, *96*, 177.

(4) (a) Zalar, P.; Henson, Z. B.; Welch, G. C.; Bazan, G. C.; Nguyen, T.-Q. *Angew. Chem. Int. Ed.* **2012**, *51*, 7495; (b) Ren, Y.; Kan, W. H.; Thangadurai, V.; Baumgartner, T. *Angew. Chem. Int. Ed.* **2012**, *51*, 3964; (c) Bruch, A.; Fukazawa, A.; Yamaguchi, E.; Yamaguchi, S.; Studer, A. *Angew. Chem. Int. Ed.* **2011**, *50*, 12094; (d) Grimsdale, A. C.; Müllen, K. *Macromol. Rap. Commun.* **2007**, *28*, 1676.

(5) (a) Wang, C.; Dong, H.; Hu, W.; Liu, Y.; Zhu, D. *Chem. Rev.* **2012**, *112*, 2208; (b) Dimitrakopoulos, C. D.; Malenfant, P. R. L. *Adv. Mater.* **2002**, *14*, 99; (c) Muccini, M. *Nature Mater.* **2006**, *5*, 605; (d) Li, C.; Liu, M.; Pschirer, N. G.; Baumgarten, M.; Müllen, K. *Chem. Rev.* **2010**, *110*, 6817; (e) Grimsdale, A. C.; Leok Chan, K.; Martin, R. E.; Jokisz, P. G.; Holmes, A. B. *Chem. Rev.* **2009**, *109*, 897; (f) Friend, R. H.; Gymer, R. W.; Holmes, A. B.; Burroughes, J. H.; Marks, R. N.; Taliani, C.; Bradley, D. D. C.; Santos, D. A. D.; Bredas, J. L.; Logdlund, M.; Salaneck, W. R. *Nature* **1999**, *397*, 121; (g) Wen, Y.; Liu, Y. *Adv. Mater.* **2010**, *22*, 1331.

(6) (a) Entwistle, C. D.; Marder, T. B. *Angew. Chem. Int. Ed.* **2002**, *41*, 2927; (b) Jäkle, F. *Chem. Rev.* **2010**, *110*, 3985.

(7) (a) Matsumi, N.; Naka, K.; Chujo, Y. *J. Am. Chem. Soc.* **1998**, *120*, 5112; (b) Matsumi, N.; Miyata, M.; Chujo, Y. *Macromolecules* **1999**, *32*, 4467; (c) Matsumi, N.; Chujo, Y.; Lavastre, O.; Dixneuf, P. H. *Organometallics* **2001**, *20*, 2425; (d) Matsumoto, F.; Matsumi, N.; Chujo, Y. *Polym. Bull.* **2001**, *46*, 257; (e) Matsumoto, F.; Chujo, Y. *Pure. Appl. Chem.* **2009**, *81*, 433.

(8) (a) Matsumi, N.; Umeyama, T.; Chujo, Y. *Polym. Bull.* **2000**, *44*, 431; (b) Matsumi, N.; Naka, K.; Chujo, Y. *J. Am. Chem. Soc.* **1998**, *120*, 10776.

(9) (a) Patil, A. O.; Heeger, A. J.; Wudl, F. *Chem. Rev.* **1988**, *88*, 183; (b) Yamamoto, T.; Sanechika, K.; Yamamoto, A. *J. Polym. Sci: Polym. Lett. Ed.* **1980**, *18*, 9; (c) Sato, M.-a.; Tanaka, S.; Kaeriyama, K. *J. Chem. Soc, Chem. Commun.* **1986**, 873; (d) Jen, K.-Y.; Miller, G. G.; Elsenbaumer, R. L. *J. Chem. Soc, Chem. Commun.* **1986**, 1346; (e) Berggren, M.; Inganas, O.; Gustafsson, G.; Rasmusson, J.; Andersson, M. R.; Hjertberg, T.; Wennerstrom, O. *Nature* **1994**, *372*, 444; (f) Inganäs, O.; Salaneck, W. R.; Österholm, J. E.; Laakso, J. *Synth. Met.* **1988**, *22*, 395; (g) Salaneck, W. R.; Inganäs, O.; Thémans, B.; Nilsson, J. O.; Sjögren, B.; Österholm, J. E.; Brédas, J. L.; Svensson, S. *J. Chem. Phys.* **1988**, *89*, 4613.

(10) Akcelrud, L. *Progress in Polym Sci.* **2003**, *28*, 875.

(11) (a) McCullough, R. D.; Tristram-Nagle, S.; Williams, S. P.; Lowe, R. D.; Jayaraman, M. *J. Am. Chem. Soc.* **1993**, *115*, 4910; (b) Adachi, T.; Brazard, J.; Ono, R. J.; Hanson, B.; Traub, M. C.; Wu, Z.-Q.; Li, Z.; Bolinger, J. C.; Ganesan, V.; Bielawski, C. W.; Vanden Bout, D. A.; Barbara, P. F. *J. Phys. Chem. Lett.* **2011**, *2*, 1400.

(12)   Xu, B.; Holdcroft, S. *Macromolecules* **1993**, *26*, 4457.

(13)   J.-P. Corriu, R.; Deforth, T.; E. Douglas, W.; Guerrero, G.; Deforth, T.; S. Siebert, W. *Chem. Commun.* **1998**, 963.

(14)   Sundararaman, A.; Victor, M.; Varughese, R.; Jäkle, F. *J. Am. Chem. Soc.* **2005**, *127*, 13748.

(15)   Yin, X.; Chen, J.; Lalancette, R. A.; Marder, T. B.; Jäkle, F. *Angew. Chem. Int. Ed.* **2014**, *53*, 9761.

(16)   Li, H.; Jäkle, F. *Angew. Chem. Int. Ed.* **2009**, *48*, 2313.

(17)   (a) Zhao, C.-H.; Wakamiya, A.; Yamaguchi, S. *Macromolecules* **2007**, *40*, 3898; (b) Reitzenstein, D.; Lambert, C. *Macromolecules* **2009**, *42*, 773; (c) Li, H.; Jakle, F. *Polym. Chem.* **2011**, *2*, 897; (d) Pammer, F.; Guo, F.; Lalancette, R. A.; Jäkle, F. *Macromolecules* **2012**, *45*, 6333; (e) Li, H.; Sundararaman, A.; Venkatasubbaiah, K.; Jäkle, F. *J. Am. Chem. Soc.* **2007**, *129*, 5792; (f) Pammer, F.; Jakle, F. *Chem. Sci* **2012**, *3*, 2598.

(18)   (a) Ma, Y.; Cheung, W.; Wei, D.; Bogozi, A.; Chiu, P. L.; Wang, L.; Pontoriero, F.; Mendelsohn, R.; He, H. *ACS Nano* **2008**, *2*, 1197; (b) Deore, B. A.; Yu, I.; Aguiar, P. M.; Recksiedler, C.; Kroeker, S.; Freund, M. S. *Chem. Mater.* **2005**, *17*, 3803.

(19)   Shoji, E.; Freund, M. S. *Langmuir* **2001**, *17*, 7183.

(20)   (a) Nicolas, M.; Fabre, B.; Marchand, G.; Simonet, J. *Eur. J. Org. Chem.* **2000**, 1703; (b) Shoji, E.; Freund, M. S. *J. Am. Chem. Soc.* **2001**, *123*, 3383; (c) Shoji, E.; Freund, M. S. *J. Am. Chem. Soc.* **2002**, *124*, 12486.

(21)   Xue, C.; Cai, F.; Liu, H. *Chem. -Eur. J.* **2008**, *14*, 1648.

(22)   (a) Campbell, P. G.; Marwitz, A. J. V.; Liu, S.-Y. *Angew. Chem. Int. Ed.* **2012**, *51*, 6074; (b) Bosdet, M. J. D.; Piers, W. E. *Can. J. Chem.* **2009**, *87*, 8.

(23)   Dewar, M. J. S.; Marr, P. A. *J. Am. Chem. Soc.* **1962**, *84*, 3782.

(24)   Ashe, A. J.; Fang, X.; Fang, X.; Kampf, J. W. *Organometallics* **2001**, *20*, 5413.

(25)   (a) Abbey, E. R.; Zakharov, L. N.; Liu, S.-Y. *J. Am. Chem. Soc.* **2008**, *130*, 7250; (b) Daly, A. M.; Tanjaroon, C.; Marwitz, A. J. V.; Liu, S.-Y.; Kukolich, S. G. *J. Am. Chem. Soc.* **2010**, *132*, 5501.

(26)   Liu, L.; Marwitz, A. J. V.; Matthews, B. W.; Liu, S.-Y. *Angew. Chem. Int. Ed.* **2009**, *48*, 6817.

(27)   Campbell, P. G.; Zakharov, L. N.; Grant, D. J.; Dixon, D. A.; Liu, S.-Y. *J. Am. Chem. Soc.* **2010**, *132*, 3289.

(28)   (a) Liu, Z.; Marder, T. B. *Angew. Chem. Int. Ed.* **2008**, *47*, 242; (b) Jaska, C. A.; Piers, W. E.; McDonald, R.; Parvez, M. *J. Org. Chem.* **2007**, *72*, 5234; (c) Bosdet, M. J. D.; Jaska, C. A.; Piers, W. E.; Sorensen, T. S.; Parvez, M. *Org. Lett.* **2007**, *9*, 1395; (d) Lepeltier, M.; Lukoyanova, O.; Jacobson, A.; Jeeva, S.; Perepichka, D. F. *Chem. Commun.* **2010**, *46*, 7007; (e) Marwitz, A. J. V.; Lamm, A. N.; Zakharov, L. N.; Vasiliu, M.; Dixon, D. A.; Liu, S.-Y. *Chem. Sci* **2012**, *3*, 825; (f) Taniguchi, T.; Yamaguchi, S. *Organometallics* **2010**, *29*, 5732; (g) Hatakeyama, T.; Hashimoto, S.; Seki, S.; Nakamura, M. *J. Am. Chem. Soc.* **2011**, *133*, 18614.

Chapter 1

Regioregular Organoborane-Functionalized Poly(3-alkynylthiophene)s[a]

1.1 Introduction

Polythiophenes have been extensively studied for chemical and biological sensing applications,[1] as battery components,[2] and as optical, electronic, and thermoelectric materials[3].[4] Recently, they have also attracted much interest as components of solar cells, typically in combination with fullerenes or other strong acceptor materials.[5] The properties of substituted polythiophenes are greatly affected by the regioregularity and, consequently, much effort has been devoted to developing methods that furnish control over head-to-tail coupling patterns.[6] Propagation of head-to-head defects in poly(3-alkylthiophene)s[4a,7] or poly(3-alkenylthiophene)s[8] is known to lead to twisted conformations of the thiophene rings due to steric repulsion of the pendent groups. The chain twisting in turn can have a detrimental effect on the extended conjugation along the polymer main chain. In contrast, Yamamoto and coworkers demonstrated that head-to-head placement of alkynyl groups in thiophene polymers results in favorable coplanarity as evidenced by X-ray scattering studies and the presence of strongly red-shifted bands in the absorption spectra.[9] Moreover, Li et al described the formation of a low molecular weight poly(3-(octyloxyphenylethynyl)thiophene) via Kumada coupling polycondensation and found the absorptions to be significantly red-shifted relative

---

[a]This chapter is adpated from "Regioregular Organoborane-Functionalized Poly(3-alkynylthiophne)s," Guo, F.; Yin, X.; Pammer, F.; Cheng, F.; Fernandez, D. ; Lalancette, R. A. ; Jäkle, F. *Macromolecules*, **2014**, 47, 7831.

to the corresponding alkenylthiophene polymer.[8c] However, poly(3-alkynylthiophene)s have received far less attention than poly(3-alkylthiophene)s, possibly due to a lack of controlled polymerization methods and the typically poor solubility[8c,9] of the products. Thus the development of functional poly(3-alkynylthiophene)s poses an interesting challenge as they have remained underdeveloped despite their promise.

Over the past several years, we[10] and others[11] have pursued the incorporation of electron-deficient borane moieties into the main and side chains of conjugated polymers as a means of tailoring the electronic properties and to develop new types of electronic and sensory materials.[12] Tricoordinate organoborane moieties exert a strong π-acceptor effect, while also acting as Lewis acids in the complexation of anions or other Lewis basic substrates.[13] Direct attachment of dimesitylborane moieties to the conjugated polythiophene backbone was accomplished by the replacement of silyl groups with the strong Lewis acid BBr_3 and subsequent installation of sterically hindered mesityl groups on boron (**A**).[10b,e,f] The resulting air-stable polymers exhibit significantly less cathodic reduction potentials due to the electronic coupling with the tricoordinate boryl groups. Polymers with a vinylene linker between the polymer backbone and the boryl groups (**B**) were obtained by hydroboration of the corresponding alkynyl-functionalized monomers or polymers.[14] Again, strong coupling of the borane moieties with the conjugated polymer chain was evident and utilized in the optical detection of fluoride anions. However, attempts to achieve regioregular high molecular weight polymers via Ni-catalyzed Kumada coupling were met with failure. Moreover, the presence of the

proton in α-position of the alkenyl group is known to results in a more twisted polythiophene main chain.

In this chapter we present a new class of alkynylphenylborane-functionalized thiophene monomers and their regioregular polymerization by Stille coupling methods. The alkyne motif favours coplanarity of the thiophene moieties in the conjugated polymer main chain, while at the same time promoting electronic coupling between the borane moieties and the conjugated polymer backbone. The optical and electronic properties of the resulting polymers (**C**) are described in detail and a comparison of the optical properties with those of related polymers prepared by Kumada polycondensation is provided.
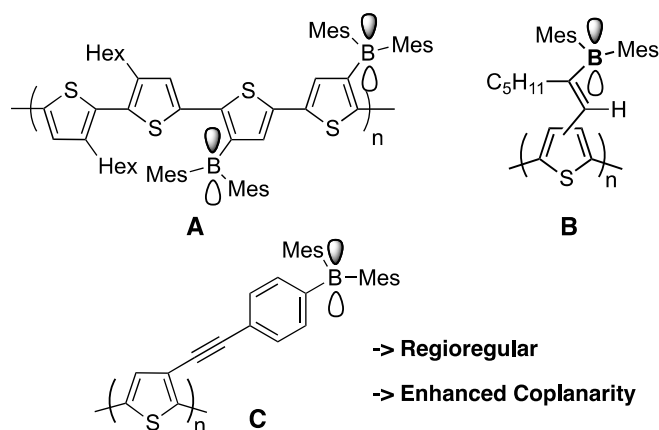
1.2 Results and discussion

Monomer Synthesis. The dibromothiophene species **1-Br2** was prepared by Sonogashira-Hagihara coupling of 2,5-dibromo-3-iodothiophene with (4-ethynylphenyl)-dimesitylborane, purified by column chromatography on silica gel with hexanes as the eluent and then isolated as a light yellow solid by addition of a CH_2Cl_2 solution into MeOH (Scheme 1-1). Using similar procedures, the

corresponding mono-brominated species **1-Br** was prepared from 2-bromo-3-iodothiophene and model compound **1** from 3-iodothiophene. The bifunctional 5-bromo-2-stannylthiophene monomer **1-BrSn** was obtained by highly regioselective lithiation of **1-Br2** with *n*-BuLi at −78 ℃, followed by treatment with Me₃SnCl. The product was isolated as a single regioisomer by precipitation from diethyl ether into MeOH. To prepare the corresponding bithiophene derivative **2-BrSn**, compound **1-Br** was first reacted with 2-trimethylstannyl-5-hexylthiophene in a Stille coupling to give **2**, which in turn was converted to **2-Br** by reaction with NBS in DMF. Lithiation of **2-Br** with LDA in THF, followed by treatment with Me₃SnCl resulted in selective formation of the desired 5'-bromo-2-stannylbithiophene monomer, **2-BrSn**, which was isolated as a light brown solid by precipitation from CH₂Cl₂ into MeOH. The successful synthesis of monomers **1-BrSn** and **2-BrSn** and the corresponding unfunctionalized model compounds **1** and **2** was confirmed by multinuclear NMR spectroscopy and high-resolution MALDI-MS analysis, which in all cases showed the expected isotopic pattern of the molecular ion peak or a fragment ion formed by loss of bromine. A broad signal in the ^{11}B NMR spectra at ca. 73 ppm is in the expected region for tricoordinate boron and confirms that the borane moiety was retained throughout the monomer syntheses. The substitution pattern of the thiophene and bithiophene species was ascertained based on the ^{1}H NMR patterns and the H,H and $^{117/119}$Sn,H coupling constants (Figure 1-1). For example, for species **1-Br** two doublets are observed for the thiophene protons at 7.05 and 7.24 ppm with a relatively large coupling constant of *J* = 5.5 Hz, which confirms the 3-alkynyl-2-bromo (rather

than 4-alkynyl-2-bromo) substitution pattern. For **1-BrSn**, the absence of tin satellites for the thiophene proton at 7.24 ppm indicates that the proton is not adjacent to the stannyl group, thus confirming the 3-alkynyl-5-bromo-2-stannylthiophene substitution pattern.
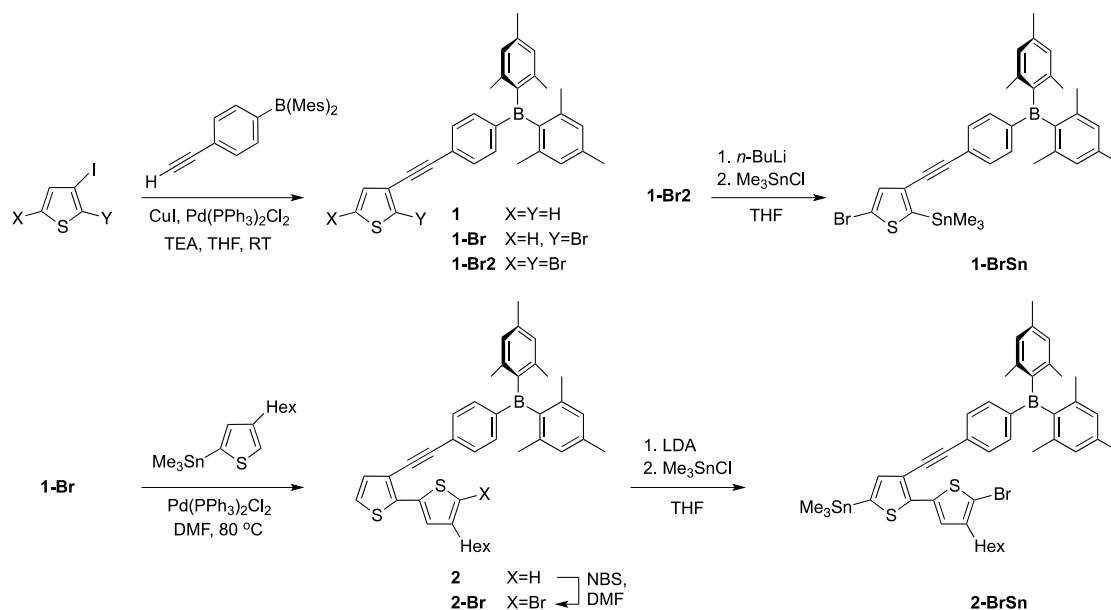
Scheme 1-1. Synthesis of monomers (**1-BrSn**, **2-BrSn**) for Stille-type polymerization and corresponding model compounds (**1** and **2**)
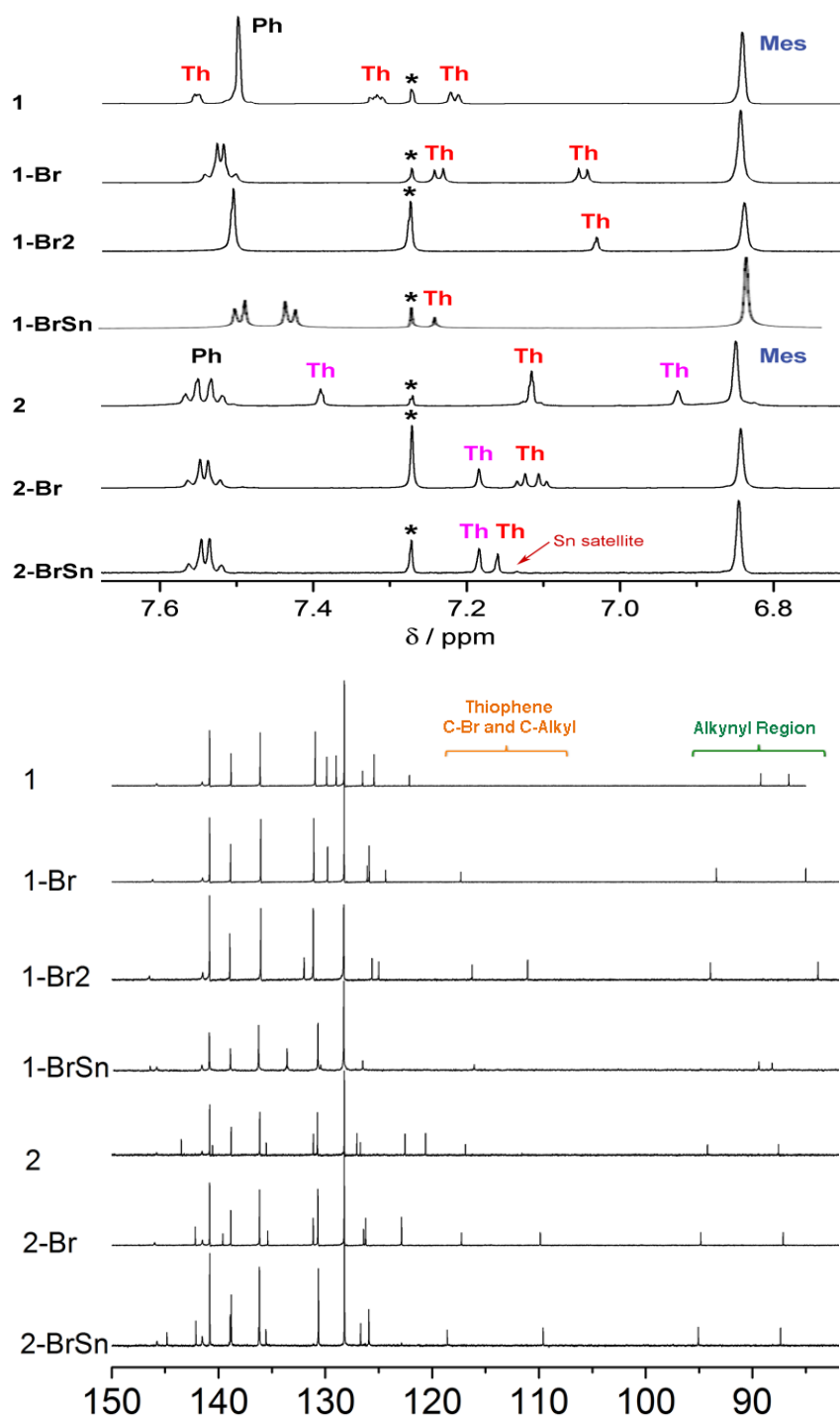
Figure 1-1. Comparison of the aromatic region of the ^{1}H NMR and ^{13}C NMR spectra of monomers and model compounds in CDCl$_3$ (**red**: alkynylthiophene; **purple**: hexylthiophene).

The structures of monomer **1-BrSn** and the bithiophene species **2-Br** were further investigated by X-ray diffraction analysis. The crystal structures of **1-BrSn** and **2-Br** were solved by Dr. Roger Lalancette. Single crystals of **1-BrSn** were obtained by slow solvent evaporation of a solution in diethyl ether and crystals of **2-Br** were grown by slow solvent evaporation of a solution in a mixture of hexanes/ether (1:1). The structure of **1-BrSn** confirms the regioselective lithiation in the 2-position next to the alkynyl group (Figure 1-2). The bond lengths and angles are in the expected range. Compound **2-Br** crystallized in the triclinic space group *P*-1 with two symmetry equivalent molecules in the unit cell. The thiophene rings assume a trans conformation with a small torsion angle of 2.8 ° (Figure 1-3), which is comparable to the perfectly coplanar arrangement in 3,3'-dialkynyl-2,2'-bithiophene reported by Yamamoto and coworkers.[9c] Inspection of the extended structure revealed the formation of slightly tilted (due to slippage) π-stacks along the crystallographic *a*-axis with short intermolecular distances between thiophene rings of ca. 3.5 Å, which is in the typical range of π-π interactions (Figure 1-3b).[15] The observed π -stacking is remarkable considering the presence of the very bulky borane moieties in the side chains. To minimize steric interactions the orientation of the individual molecules in the stack alternates so that the borane moieties are positioned on opposite sides. As a consequence, a ribbon-like structure is generated in the b-c and a-c planes, where strands of bithiophenes alternate with the dimesitylborane pendent groups (Figure 1-3c).
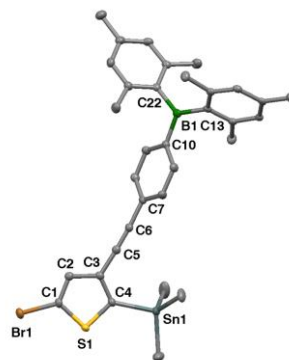
Figure 1-2. Thermal ellipsoid plots (50%) of **1-BrSn.** Hydrogen atoms are omitted for clarity. Selected bond lengths (Å) and angles (º) for **1-BrSn**: B1-C10 1.568(3), B1-C13 1.568(3), B1-C22 1.583(3), Br1-C1 1.876(2), Sn1-C4 2.148(2), Sn1-C31 2.125(3), Sn1-C32 2.140(2), Sn1-C33 2.129(2), S1-C1 1.723(2), S1-C4 1.724(2), C1-C2 1.349(3), C2-C3 1.428(3), C3-C4 1.382(3), C3-C5 1.438(3), C5-C6 1.201(3), C6-C7 1.438(3), C10-B1-C13 119.44(18), C10-B1-C22 118.28(18), C13-B1-C22 122.25(18).
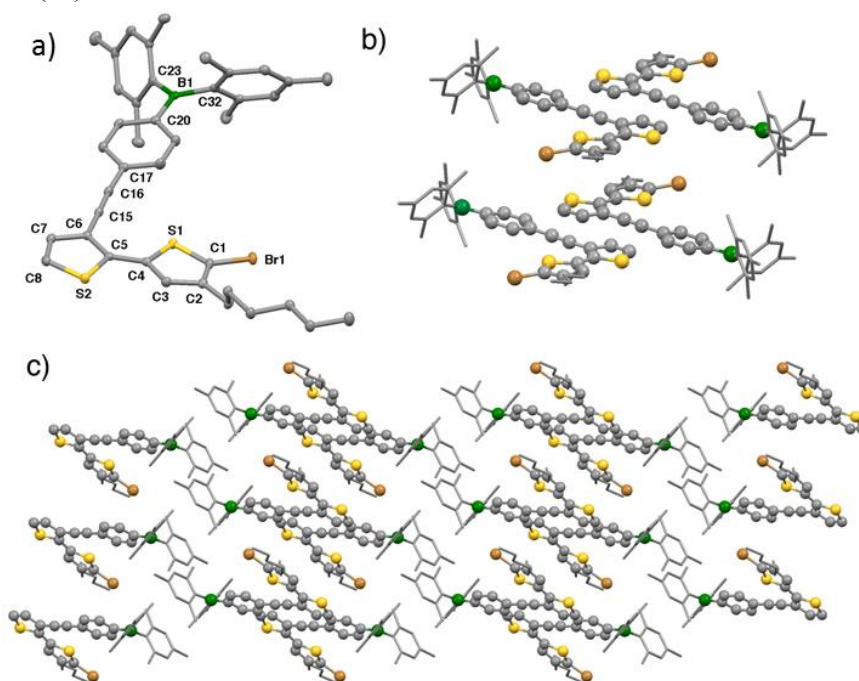
Figure 1-3. (a) X-ray structure plot of **2-Br** (thermal ellipsoids at 50%); (b) plot illustrating the slipped π-stacks of **2-Br** along the crystallographic *a*-axis; (c) view down the crystallographic *b*-axis illustrating the ribbon-like extended structure. Hydrogen atoms are omitted for clarity. Selected bond lengths (Å) and angles (º) for **2-Br**: B1-C20 1.567(2), B1-C23 1.576(2), B1-C32 1.588(2), Br1-C1 1.8844(16), S1-C1 1.7232(17), S1-C4 1.7392(16), S2-C5 1.7307(16), S2-C8 1.7163(17), C1-C2 1.360(2), C2-C3 1.424(2), C3-C4 1.370(2), C4-C5 1.447(2), C5-C6 1.391(2), C6-C7 1.428(2), C7-C8 1.354(2), C6-C15 1.424(2), C15-C16 1.201(2), C16-C17 1.432(2), C20-B1-C23 120.02(15), C20-B1-C32 117.95(14), C23-B1-C32 121.95(15).

Polymer Synthesis. The polymerization of **1-BrSn** and **2-BrSn** via Stille poly-condensation

was investigated, which is expected to provide polymers *rr*-**P1** and *rr*-**P2** with the desired

regioregularity conferred by the regiochemistry of the AB-type monomers. In both cases, polymerization was accomplished in DMF/toluene mixture at 115 ºC using $Pd_2(dba)_3$ / t-Bu_3P as the catalyst system (Scheme 1-2). The products were collected by precipitation into MeOH and in the case of rr-**P2** precipitated once more from THF into acetone. The polymers were further purified by preparative column chromatography on Biobeads™ (THF-eluent) to give the products as black solids in 27% (rr-**P1**) and 30% (rr-**P2**) yield, respectively.
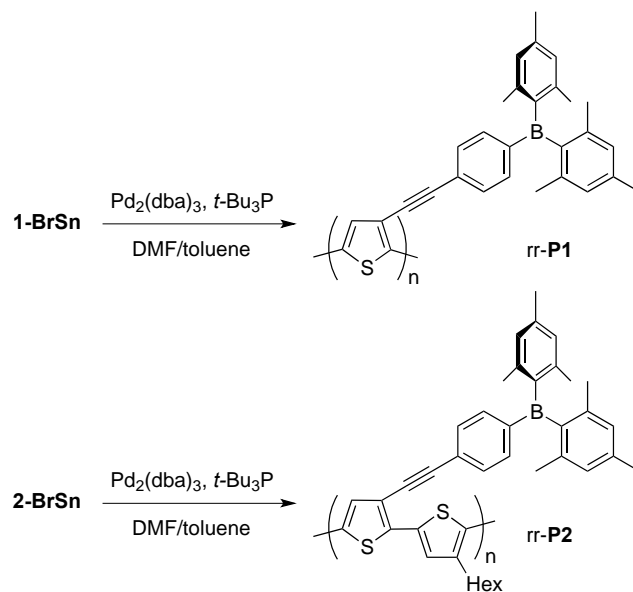
Scheme 1-2. Synthesis of rr-**P1** and rr-**P2** via Stille-type polycondensation of AB-type bromo-stannyl-thiophene monomers

The fractionated polymers gave rise to monomodal GPC traces corresponding to molecular weights of M_n = 4690 g/mol ($Đ$ = 1.30) for rr-**P1** and M_n = 8860 g/mol ($Đ$ = 1.73) for rr-**P2** relative to narrow PS standards. The somewhat lower molecular weight for rr-**P1** could be due to steric effects of the bulky dimesitylborane moieties attached to each of the thiophene repeating units. The presence of the intact borane moieties was confirmed by a single broad resonance in the ^{11}B NMR at ca. 73 ppm (rr-**P1**) and 66 ppm (rr-**P2**).[16] Two broad peaks were observed in the aromatic region of the ^{1}H NMR spectrum of rr-**P1**. By

comparison with data for the monomer **1-BrSn**, a signal at ca. 7.5 ppm is attributed to the phenylene group and a resonance at 6.8 ppm to the mesityl protons (Figure 1-4). Based on the relative integrals and the peak position in the monomer, the proton of the thiophene repeat unit likely overlaps with the phenylene protons.[17] Similar features were observed for *rr*-**P2**. Again, a signal at ca. 7.5 ppm is attributed to the phenylene group and a resonance at 6.8 ppm to the mesityl protons. An additional resonance at ca. 7.0-7.1 ppm is assigned to one of the distinct aromatic protons on the bithiophene repeat unit, while the second thiophene proton again overlaps with the other aromatic signals. For both *rr*-**P1** and *rr*-**P2**, the disappearance of the signal at ca. 0.4 ppm for the stannyl group further corroborates the successful polycondensation. In contrast to other alkynylthiophene polymers of similar molecular weight such as head-to-head *hh*-P3(C≡C-Dec)T (M_n = 7900 g/mol)[9] or poly(3-(octyloxyphenylethynyl)thiophene)[8c] (M_n = 3380 g/mol), *rr*-**P1** and *rr*-**P2** much more readily dissolve in organic solvents such as THF and chloroform even at room temperature. This effect, which is attributed to the presence of the bulky Mes_2B pendent groups, makes it much easier to purify and process the polymers into thin films.
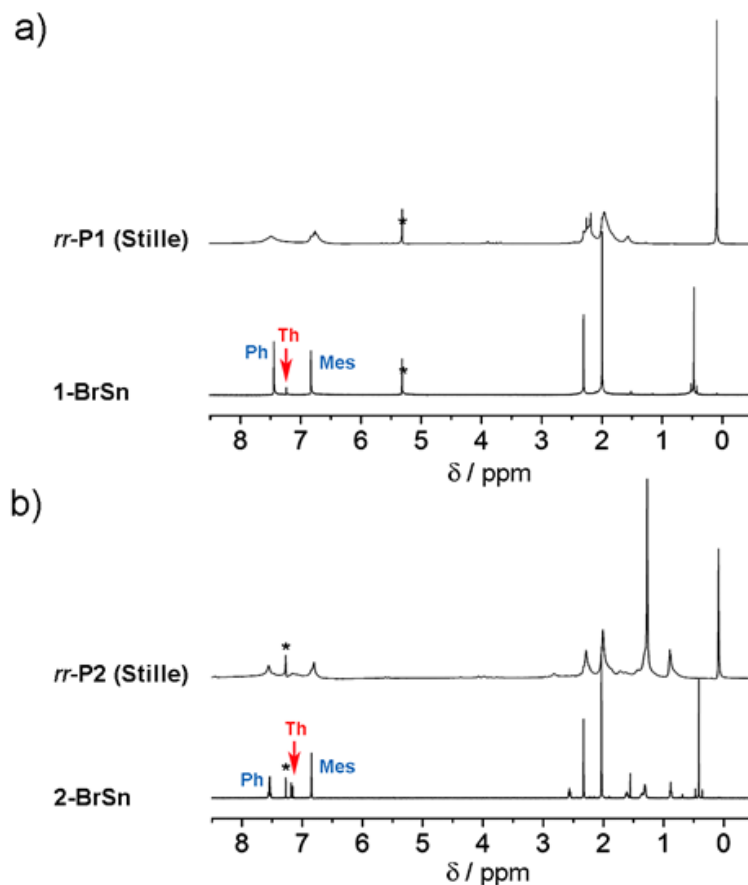
Figure 1-4. Comparison of ^{1}H NMR spectra of a) monomer **1-BrSn** and rr-**P1** in CD$_2$Cl$_2$, b) monomer **2-BrSn** and rr-**P2** in CDCl$_3$. Residual solvent peaks are indicated with an asterisk (*).

The Kumada coupling polymerization of **1-Br2** was also investigated, but a well-defined chain growth process could not be achieved. The resulting polymer (**P1**, M_n = 4910 g/mol, $Đ$ = 1.19) is therefore not expected to be regioregular, but valuable for comparison purposes. To develop the Kumada coupling polycondensation of monomer **1-Br2**, we first investigated the metal-halogen exchange of the monomer with different Grignard reagents (Scheme 1-3). A limiting factor in the polymerization of 3-substituted 2,5-dibromothiophenes in general is the formation of two isomeric magnesio species in the initial Grignard metathesis step.[18] As shown in Table 1-1, the selectivity and conversion for the

metathesis of **1-Br2** depends on the reaction temperature and the nature of the Grignard reagent. In most cases the selectivity was modest. Good selectivity for the 2-magnesiated isomer was observed in some cases when *t*-BuMgCl was used, but the conversion was relatively low and the results varied considerably. Excellent selectivity with essentially quantitative conversion to the 2-magnesiated species was achieved reproducibly when **1-Br2** was first lithiated with *t*-BuLi or *n*-BuLi and then converted *in-situ* to the Grignard reagent by addition of $MgCl_2$. The preferential formation of the (unexpected) 2-magnesiated isomer may be related to precoordination of the organolithium reagent to the alkynyl group. We also note that the steric demand of the alkynyl group is considerable lower than for alkyl groups, which may also influence the regioselectivity.
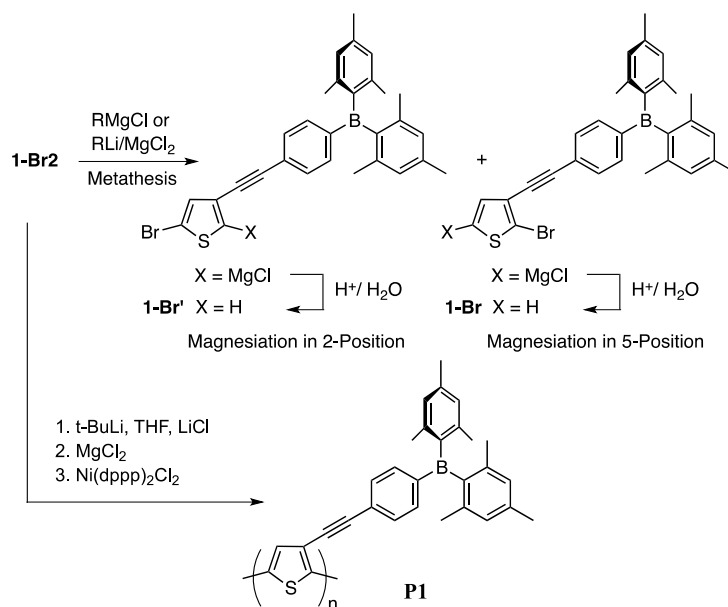
Scheme 1-3. Metathesis of **1-Br2** and subsequent coupling polymerization

Table 1-1. Results for metathesis of **1-Br2** with different Grignard reagents

Grignard Reagent [b] (equiv)	T (°C)	Time (h)	Conversion [a] (%)	2-MgCl: 5-MgCl [a]
i-PrMgCl (1)	RT	1	100	1.4:1
i-PrMgCl (1)	0	1	53	1:1
t-BuMgCl (1)	RT	1	47	5:1
t-BuMgCl (1)	0	1	50	>99:1
1. 2 t-BuLi; 2. 4 MgCl$_2$ [c]	−78→0	1	100	>99:1

[a] Determined by ^{1}H NMR integration after hydrolysis. Integrals for thiophene protons of hydrolyzed 2-magnesio species (**1-Br'**; δ 7.41, 7.46 ppm, J(H,H) = 1 Hz) and 5-magnesio species (**1-Br**; δ 7.24, 7.05 ppm, J(H,H) = 6 Hz) were compared with the precursor **1-Br2**. [b] 0.96 equiv of LiCl was added along with Grignard reagents except the in-situ generated Grignard reagent. [c] A similar result was obtained with n-BuLi (1 equiv)/MgCl$_2$.

After conversion of **1-Br2** to the corresponding 2-magnesiated Grignard reagent with *t*-BuLi and MgCl$_2$, the Kumada coupling polymerization was conducted at different polymerization temperatures and **1-Br2**:Ni(dppp)Cl$_2$ ratios (Scheme 1-3, Table 1-2**)**. The polymerization did not occur readily at room temperature. At elevated temperatures the molecular weight of the products was moderate even for large ratios of monomer to initiator, while the dispersity (*Đ*) proved to be reasonably narrow. However, the yields after preparative column separation on Biobeads^{TM} were low. This indicates that some control can be achieved, but the reaction is very sluggish. A likely reason is the formation of complexes between the Ni catalyst and the alkynyl groups[8a] that impede the polymerization, despite the presence of the bulky dimesitylborane moiety. MALDI-MS of the crude polymer showed multiple sets of peaks (Figure 1-5).The presence of Br/Br-terminated polymer is likely a result of chain-chain coupling at high temperature. The observation of a small amount of polymers that contain 3 Br atoms might be due to halogen dance processes[19] in the presence of *t*-BuLi. The ^{11}B NMR spectrum of the product showed a broad resonance at ca. 70 ppm, similar to the chemical shift of the corresponding monomer, which indicates that the borane functional groups remained

largely intact during polymerization. This was further confirmed by ^{1}H NMR analysis, which shows the expected signals for the phenylene and mesitylene groups, while the thiophene protons overlap with the other aromatic protons (Figure 1-6).

Table 1-2. Kumada coupling polymerization of **1-Br2** using *in-situ* generated Grignard reagent (*t*-BuLi / MgCl$_2$)

T (ºC)	% Ni cat.		M_n [a]	$Đ$ [b]	% Yield
25	2.5	crude	[d]	[d]	[d]
		purified[c]	[d]	[d]	[d]
80	2.5	crude	3010	1.24	30
		purified[c]	4720	1.19	18
110	1	crude	4210	1.25	31
		purified[c]	4910	1.19	21

[a] Determined by GPC-RI analysis in THF relative to narrow PS standards.
[b] Dispersity $Đ$ = M_w/M_n.
[c] After preparative GPC separation.
[d] No polymeric product could be isolated.
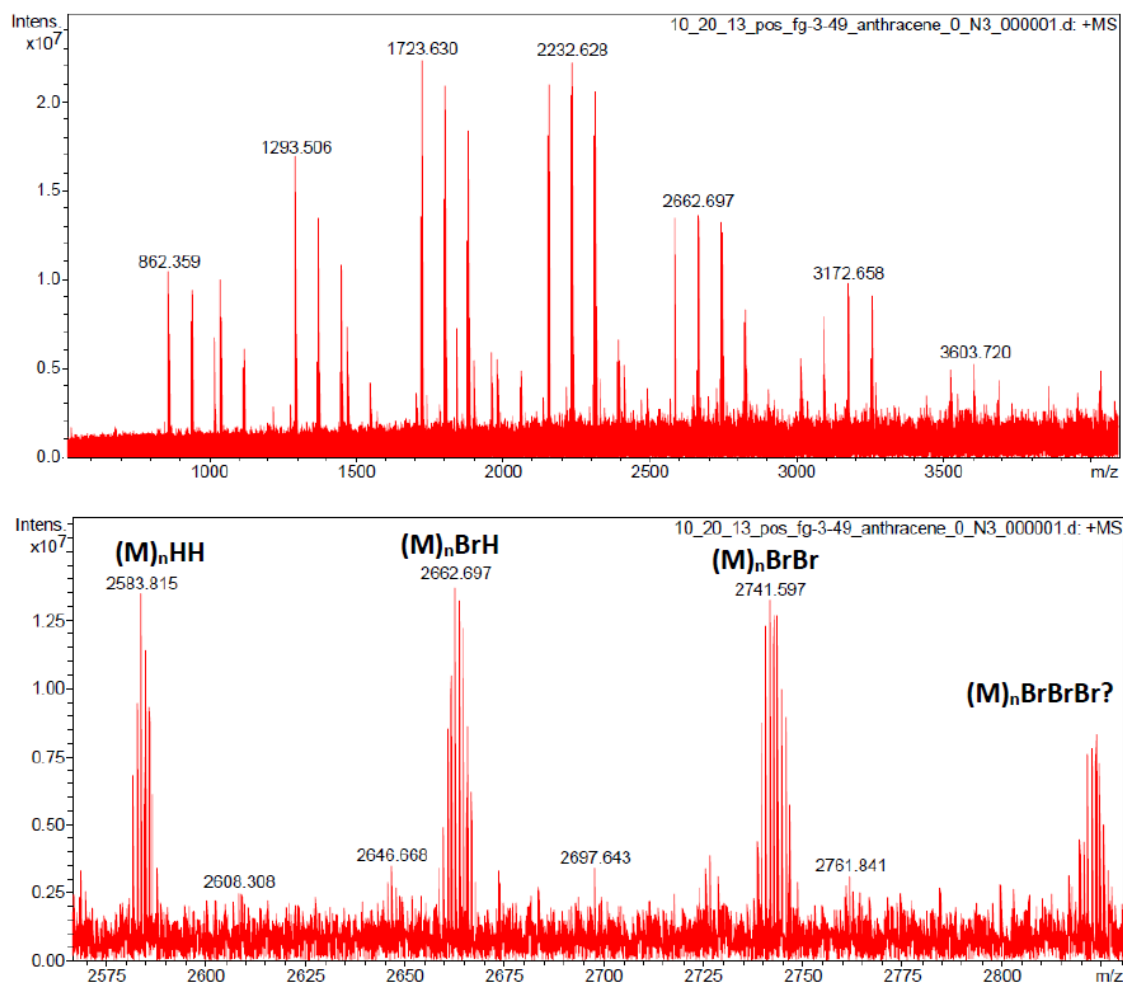
Figure 1-5. High resolution (pos. mode) MALDI-MS data of **P1** prior to preparative GPC separation.
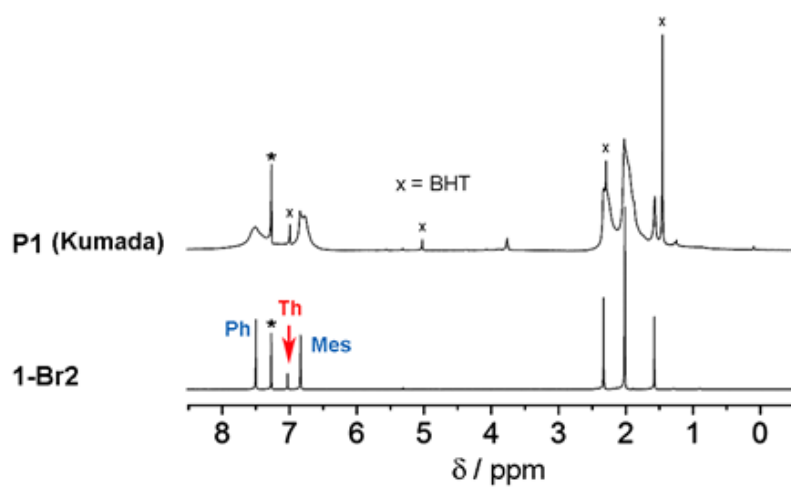
Figure 1-6. Comparison of ^{1}H NMR spectra of monomer **1-Br2** and **P1** in CDCl$_3$. Residual solvent peaks are indicated with an asterisk (*) and BHT with an (x).

Electronic Structure. The photophysical properties of the obtained polymers were examined by UV-vis absorption and fluorescence spectroscopy in THF solution (Figure 1-7 and Table 1-3). Both *rr*-**P1** and *rr*-**P2** show two absorption bands, one in the visible and one in the UV region (*rr*-**P1**: 338, 520 nm; *rr*-**P2**: 338, 480 nm). The longest wavelength absorption maximum of *rr*-**P1** is significantly red shifted compared to that of **P1** obtained by Kumada coupling polymerization (328, 485 nm). Given that the molecular weight of the polymers is comparable, this indicates improved extension of conjugation due to a more regioregular structure for the Stille-coupling product. While adjacent thiophene rings in **P1** likely assume a coplanar conformation even when head-to-head (HH) defects are present,[9] the alkynylphenylborane side-chains would clash with the side group of the next neighbour in a head-to-tail/head-to-head (HT-HH) sequence,[7] thereby reducing the effective conjugation length.

The band gaps were estimated from the solution UV-vis absorption onsets to be ca. 2.00 (*rr*-**P1**) and 2.07 eV (*rr*-**P2**). They are significantly lower compared to regioregular poly(3-alkylthiophene)s (*rr*-P3HT: λ_{max} = ~450 nm, onset ~560 nm, 2.20 eV, $CHCl_3$),[20] which is consistent with earlier results by Yamamoto et al. on a head-to-head coupled decyl-alkynylthiophene polymer (*hh*-P3(C≡C-Dec)T,[9] ca. 2.07 eV). Indeed, the optical band gap gradually decreases in the order of P3HT>*rr*-**P2**>*rr*-**P1**, which correlates with an increasing number of alkynyl instead of alkyl side chains. Similar absorption features were reported for poly(3-(octyloxyphenylethynyl)thiophene),[8c] indicating that the longest wavelength

absorption is primarily determined by the polythiophene main chain conformation

and not influenced to a great extent by the boryl pendent groups.
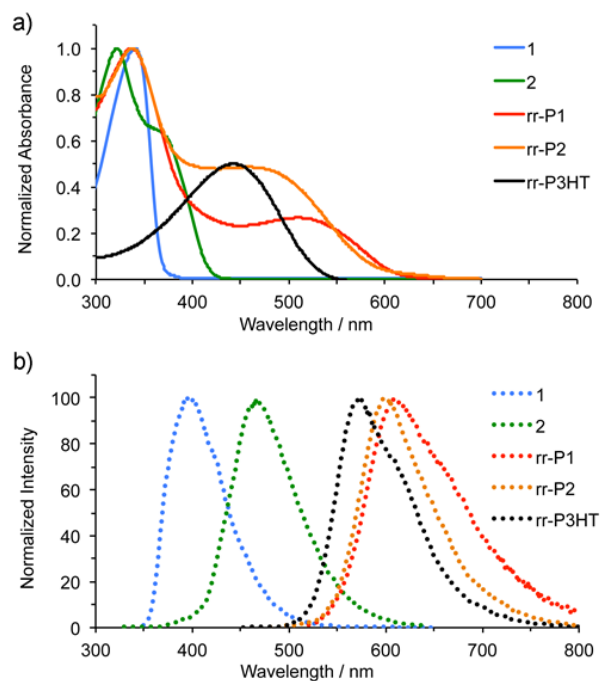
Figure 1-7. Comparison of a) UV-vis and b) fluorescence spectra of model compounds and polymers in THF solution (excited at the longest wavelength absorption maxima).

Table 1-3. Summary of photophysical and electrochemical data

	$\lambda_{abs,max}$[a]	$\lambda_{abs,onset}$	$E_{g,opt}$[b]	λ_{em}[c]	Φ_{fl}[c]	τ[d]	$E_{ox,CV}$[e]	$E_{red,CV}$[e]	HOMO[f]	LUMO[f]	$E_{g,CV}$
	(nm)	(nm)	(eV)	(nm)	(%)	(ns)	(V)	(V)	(eV)	(eV)	(eV)
1	340	--	3.65	392	10.8	2.12±0.01	--	-2.30	--	-2.50	--
P1 (Kumada)	328,485	600	2.07	590	4.0	0.64±0.01 [g]	--	--	--	--	--
rr-**P1** (Stille)	338,520	620	2.00	615	8.8	0.68±0.01 [g]	0.60	-1.63	-5.40	-3.17	2.23
2	321,370(sh)	--	3.35	465	8.2	0.70±0.01	--	-2.22	--	-2.58	--
rr-**P2** (Stille)	338,480	600	2.07	599	2.8	0.54±0.01 [g]	0.62	-1.78	-5.36	-3.02	2.40
P3HT	450	560	2.20 [h]	575 [h]	--	--	0.45 [i]	--	-5.25	--	--

[a] In THF solution. [b] Based on λ_{max} for molecular compounds, absorption onsets for polymers. [c] Quantum yield; excited at the longest wavelength absorption maximum; measurement error ca. 5%. [d] Fluorescence lifetime. [e] All data reported vs. Fc/Fc[+] . For polymers *rr*-**P1** and *rr*-**P2** recorded on thin films at scan rates of 500 mV/s with $CH_3CN/[(n-Bu)_4N]PF_6$ (0.1 M) as supporting electrolyte; E_{ox} and E_{red} were estimated from the oxidation and reduction peak onsets. For molecular compounds **1** and **2** recorded in solution at scan rates of 100 mV/s with $THF/[(n-Bu)_4N]PF_6$ (0.1 M) as supporting electrolyte; E_{red} was estimated from the maxima of the redox waves ($E_{1/2, red}$) for **1** ($\Delta E_p = 88$ mV) and **2** ($\Delta E_p = 70$ mV). [f] $E_{HOMO} = -(E_{ox} + 4.8)$ eV and $E_{LUMO} = -(E_{red} + 4.8)$ eV; ref. [18]. [g] For **P1**(Kumada): $\tau_1 = 0.64\pm0.01$ ns (96%), $\tau_2 = 2.63\pm0.09$ ns (4%); for *rr*-**P1**: $\tau_1 = 0.68\pm0.01$ ns (single exponential); for *rr*-**P2**: $\tau_1 = 0.54\pm0.01$ ns (96%), $\tau_2 = 1.65\pm0.13$ ns (4%). [h] UV-vis and fluorescence data in $CHCl_3$; refs. [20-21]. [i] Data acquired under similar conditions, ref. [22].

The shorter wavelength absorption in the UV-vis spectra at ca. 338 nm is assigned to charge transfer to the borane pendent groups based on a comparison with the optical properties of molecular model compounds. Compound **1** corresponds to one repeat unit in *rr*-**P1** and features a single thiophene ring linked via a phenylalkynyl bridge to the borane moiety. The absorption spectrum of **1** shows a maximum at 340 nm, a wavelength that is very similar to the high-energy absorption of the polymers. For the bithiophene derivative, **2**, which represents one repeat unit of *rr*-**P2**, two overlapping absorptions are observed: a shoulder at 370 nm, and another higher energy band at 321 nm. DFT calculations (B3LYP, 6-31g(d)) were conducted on the model compounds **1** and **2-th** (methyl instead of hexyl group in **2**), as well as an unsymmetrical diborylated bithiophene species (**3-th**), which represents two repeating units of the regioregular polymer *rr*-**P1** (Figure 1-8). In all three compounds, the HOMO orbital is localized on the (bi)thiophene moiety with some conjugation into the alkynylphenyl pendent group, but the LUMO orbital shows a strong contribution of the *p* orbital on boron with delocalization into the phenylethynyl group and to a lesser degree the thiophene moieties (Figure 1-8).[23] TD-DFT calculations (CAM-B3LYP, 6-31g(d)) in turn reveal that the lowest energy vertical transitions originate from HOMO-LUMO excitation and therefore involve significant charge transfer to boron (Table 1-4, Figure 1-9). When comparing the absorption data for the model compounds to those of the polymers (see Figure 1-7), it is clear that the absorptions at 340 nm for **1** and at 321/370(sh) nm for **2** are almost unchanged at ca. 328-338 nm in the

corresponding polymers **P1**(Kumada), *rr*-**P1** and *rr*-**P2**. The extension of the conjugated thiophene main chain leads to additional lower energy $\pi \rightarrow \pi^*$ transitions in the visible region at close to 500 nm, but has only a small effect on the charge transfer to the conjugated organoborane side chains. AM1 calculations were performed by Dr. F. Pammers on a longer sexithiophene segment of *rr*-**P1.** They are consistent as they show the HOMO and LUMO levels to be centered on the thiophene main chain, while contributions from the borylated side chains to higher energy orbitals are evident (Table 1-5).
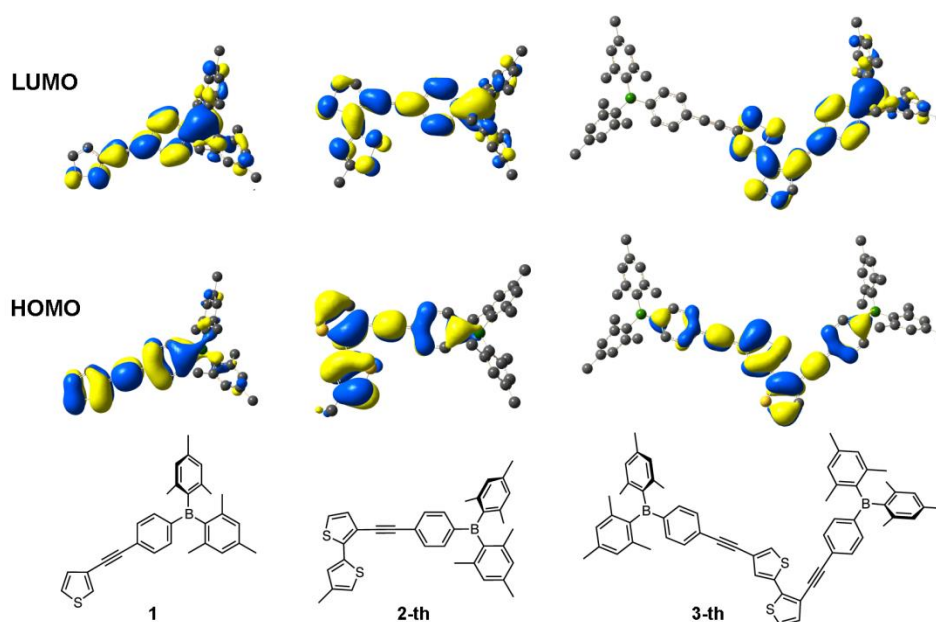
Figure 1-8. Calculated HOMO / LUMO orbital plots of **1**, **2-th** and **3-th** (B3LYP, 6-31g(d)).

Table 1-4. TD-DFT data for **1-th**, **2-th** and **3-th** (CAM-B3LYP/6-31g(d))

Compound	E_{ex} (eV)	λ (nm)	Oscillator strength f	Assignment (%)
1-th	3.91	**318**	**1.05**	**H → L (0.63)**
	3.98	311	0.11	H-1 → L (0.65)
	4.35	285	0.16	H-3 → L (0.13)
				H-2 → L (0.60)
2-th	3.51	**353**	**0.78**	**H → L (0.64)**
	3.98	311	0.11	H-1 → L (0.59)
				H-1 → L+1 (0.33)
	4.14	**299**	**0.35**	**H-2 → L (0.53)**
	4.41	281	0.28	H-3 → L (0.56)
				H-3 → L+1 (0.21)
3-th	3.48	**357**	**1.28**	H-1→L (0.24)
				H→L (0.59)
	3.89	**319**	**0.92**	**H-1 → L+1 (0.45)**
				H-4 → L+1 (0.18)
	3.96	313	0.09	H-3 → L (0.56)
				H-3 → L+2 (0.35)
	3.98	312	0.11	H-2→ L+1 (0.64)
				H-2 → L+2 (0.1)
	4.11	302	0.38	H-4 → L (0.33))
				H-4 → L+2 (0.18)
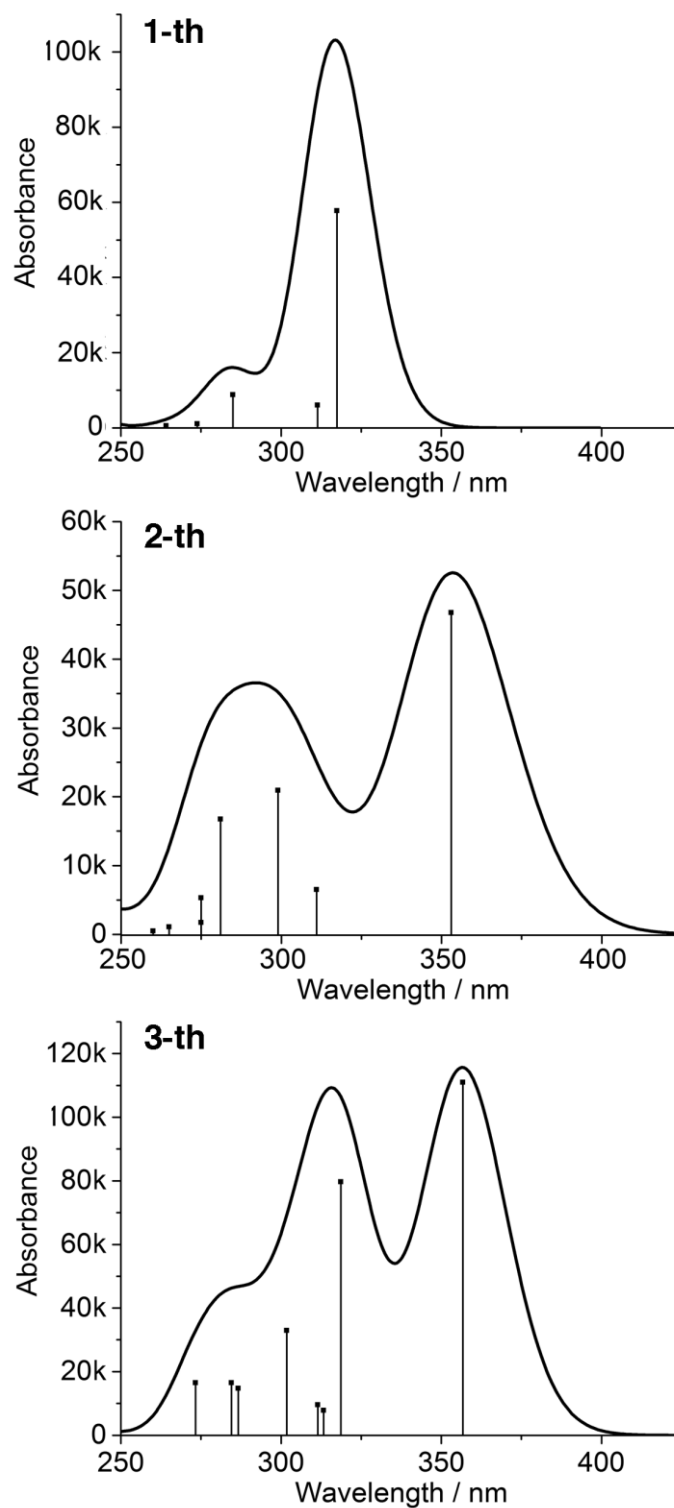
Figure 1-9. Calculated absorption spectra of **1-th**, **2-th**, **3-th** (TD-DFT, CAM-B3LYP/6-31g(d))

Table 1-5.   Calculated orbital plots for a *rr*-(3-alkynylphenylborane)-substituted sexithiophene. The molecular structure was optimized with Gaussian09, using the semi-empirical AM1-method. Color code: C grey, S yellow, B pink, H white. (Courtesy of Dr. F. Pammer)
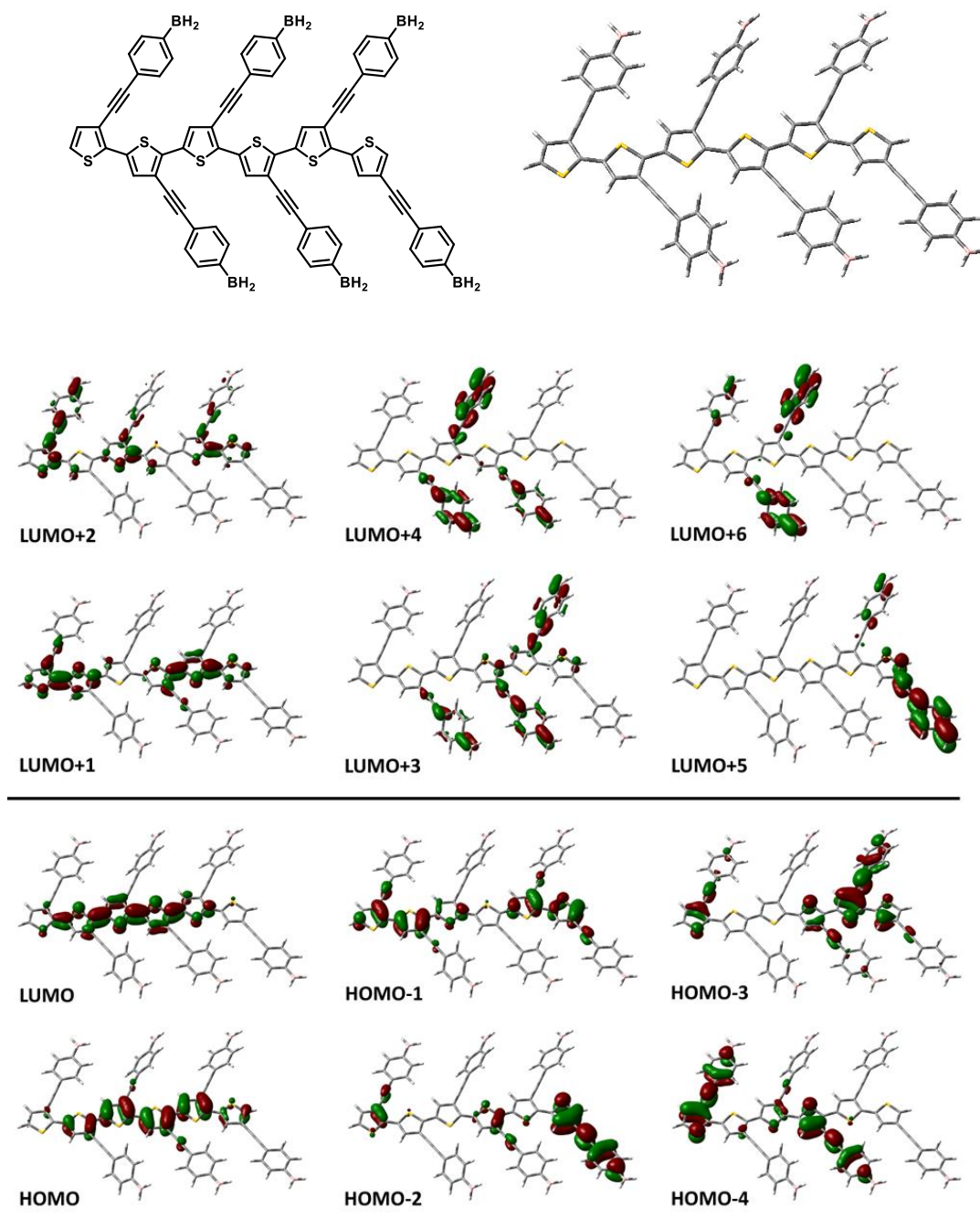
All the monomers and polymers are fluorescent in solution. When excited at the longest wavelength absorption maximum, the emission of *rr*-**P1** (615 nm) and *rr*-**P2** (599 nm) in THF is strongly red-

shifted relative to that of the molecular species **1** (392 nm) and **2** (465 nm). Overall similar quantum yields and lifetimes are measured for the polymers (**P1**(Kumada): $\Phi_F = 4.0\%$, $\tau_1 = 0.64\pm0.01$ ns (96%); *rr*-**P1**: $\Phi_F = 8.8\%$, $\tau_1 = 0.68\pm0.01$ ns (100%); *rr*-**P2**: $\Phi_F = 2.8\%$, $\tau_1 = 0.54\pm0.01$ ns (96%)) as for the molecular species (**1**: $\Phi_F = 10.8\%$, $\tau_1 = 2.12\pm0.01$ ns; **2**: $\Phi_F = 8.2\%$, $\tau_1 = 0.70\pm0.01$ ns). When the polymers *rr*-**P1** and *rr*-**P2** were excited at the higher energy absorption maximum, still only the low energy emission at ca. 600 nm was observed and no emission was detected in the region where the molecular organoborane chromophores **1** and **2** were found to emit (390-500 nm; Figure 1-10). No emission band is observed in the range of 350-500 nm (borane chromophore). Note also that the enhanced emission intensity upon excitation at shorter wavelength correlates well with the stronger absorbance at 330/338 nm.
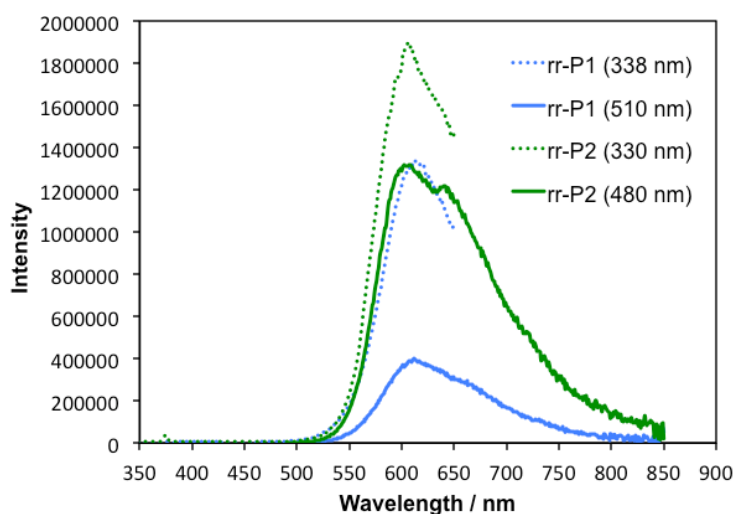
Figure 1-10.   Comparison of fluorescence spectra of rr-**P1** (blue) and rr-**P2** (green) in THF solution when excited at the longer wavelength absorption maxima (solid lines) and the shorter wavelength absorption maxima (dotted lines).

Given that the emission from the charge transfer states of the molecular species **1** and **2** effectively overlaps with the longest wavelength absorption of the polymers (Figure 1-11), a possibly explanation is that energy transfer occurs from the side chain chromophores to lower energy electronic states that are localized on the conjugated polymer backbone. However, since (1) the absorbance at the excitation

wavelength is not only due to the charge transfer transition but also higher energy polymer main chain-centered transitions and (2) the borane donor is covalently linked to the main chain it is difficult to obtain conclusive evidence.
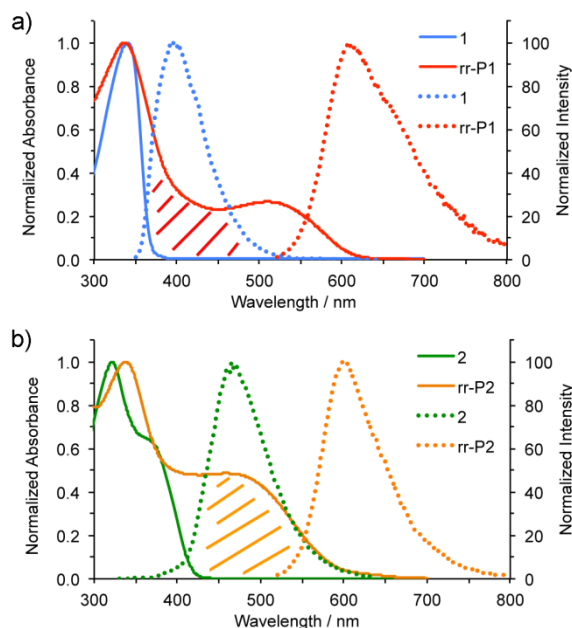
Figure 1-11. Illustration of overlap of borane monomer fluorescence spectra with polymer absorption spectra in THF solution (absorption: solid lines, fluorescence: dotted lines; excited at the longest wavelength absorption maxima).

We also examined the properties of spin-coated thin films of *rr*-**P1** and *rr*-**P2**. The absorption spectra were almost unchanged relative to those in solution. This is not unexpected given that a coplanar structure should be favourable not only in the solid but also in solution. However, the fluorescence maxima experienced a significant additional red shift compared to the solution data in THF (*rr*-**P1**: λ_{max} = 648 nm, Δ = 830 cm^{-1}; *rr*-**P2**: λ_{max} = 687 nm, Δ = 2140 cm^{-1}; Figure 1-12).
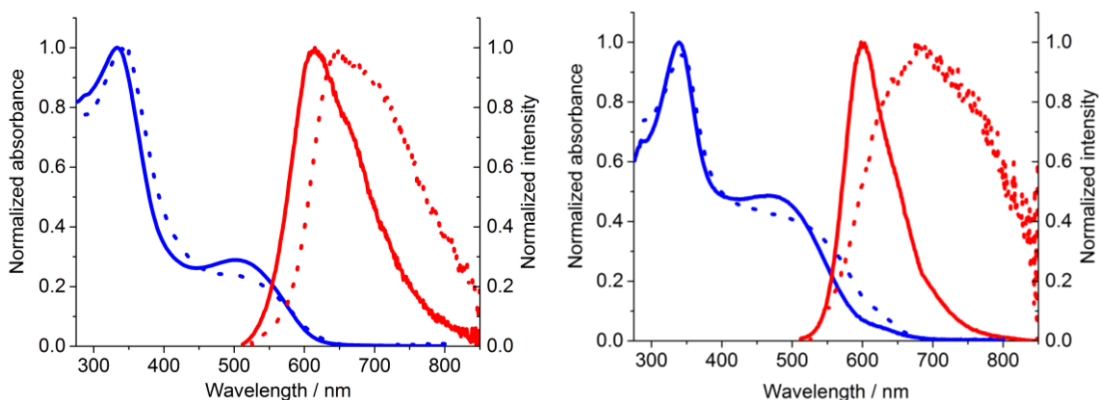
Figure 1-12. Comparison of UV-vis (blue) and fluorescence (red) spectra of (a) rr-**P1** and (b) rr-**P2** in THF solution (solid line) and in thin film (dotted line).

To further probe the charge transfer character of the excited state we studied the solvent-dependence of the emission of compounds **1** and **2**. For both compounds, a pronounced solvatochromic emission effect is evident, which is attributed to a more polar excited state upon charge transfer to the borane moiety (Figure 1-13). An increase in fluorescence lifetime with increasing solvent polarity (cyclohexane to DMF) from 0.9 ns to 3.4 ns for **1** and from 0.7 ns to 2.4 ns for **2** was also detected.[24] The first singlet-excited states of **1-th** and **2-th** were optimized using the TD-DFT method as implemented in Gaussian09 (CAM-B3LYP, 6-31g(d)). A comparison of the ground state and excited state geometry revealed that the dihedral angle of **2-th** decreases from 19.7 to 0.5 °upon excitation, resulting in an almost perfectly coplanar arrangement of the thiophene rings (Table 1-6). The C-C bond length alternation for the thiophenes is also reduced in the excited state, which is consistent with a more pronounced quinoid structure that favours π-conjugation. The calculated dipole moments for the first singlet-excited state (**1-th**: 3.3 D; **2-th**: 5.1 D) are significantly larger than for the ground state (**1-th**: 0.7 D; **2-**

th: 1.1 D). We conclude that in polar solvents the charge-separated species is stabilized and therefore emits at longer wavelength and shows a longer lifetime.
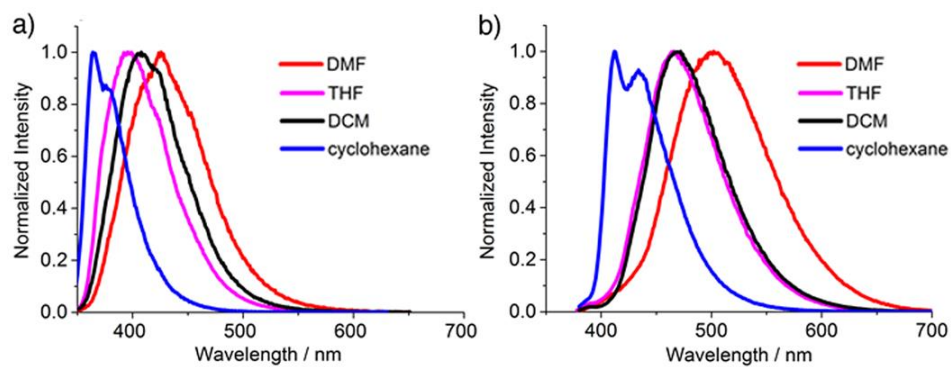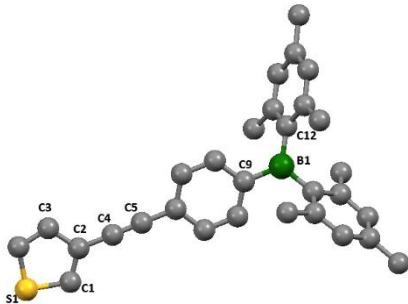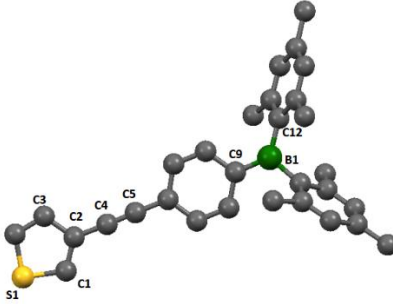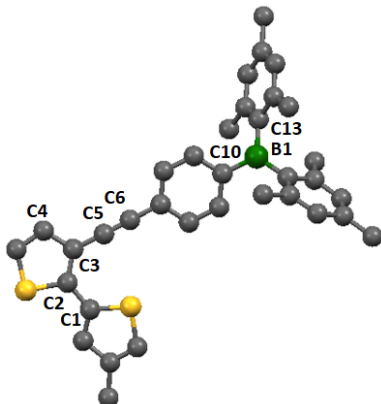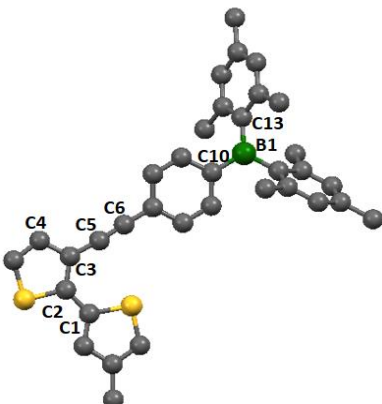
Figure 1-13. Fluorescence spectra of a) compound **1 (**excited at 340 nm) and b) compound **2** (excited at 370 nm) in solvents of different polarity.

Table 1-6. Comparison of calculated geometries in the ground state (GS; B3LYP/6 31g(d)) and excited state (ES; CAM-B3LYP/6-31g(d)). Bond distances in Å and dihedral angles in °. Color code: C black, S yellow, B deep green.

	Ground State		Excited State	
1-th				
	C1-C2	1.382	C1-C2	1.388
	C2-C3	1.443	C2-C3	1.445
	C2-C4	1.418	C2-C4	1.396
	C4-C5	1.217	C4-C5	1.230
	C9-B1	1.570	C9-B1	1.537
	C12-B1	1.585	C12-B1	1.586
	Dipole moment	0.70 D	Dipole moment	3.3 D

	Ground State		Excited State	
2-th				
	C1-C2	1.450	C1-C2	1.400
	C2-C3	1.398	C2-C3	1.444
	C3-C4	1.440	C3-C4	1.435
	C3-C5	1.416	C3-C5	1.375
	C5-C6	1.210	C5-C6	1.234
	C10-B1	1.571	C10-B1	1.551
	C13-B1	1.586	C13-B1	1.584
	Dihedral angle (Th//Th)	19.7	Dihedral angle (Th//Th)	0.5
	Dipole moment	1.1 D	Dipole moment	5.1 D

The electron-accepting properties of polymers *rr*-**P1** and *rr*-**P2** were studied by cyclic voltammetry on thin films and those of the corresponding model compounds **1** and **2** in THF solution (Figure 1-14). The polymers are more easily reduced than the molecular species, due to the attachment of the borane moiety to the more delocalized polythiophene backbone (see Table 1-3). Also, the onset of reduction for *rr*-**P1** ($E_{red, onset} = -1.79$ V vs Fc/Fc$^+$, THF/[(n-Bu)$_4$N]PF$_6$) is less negative than that for *rr*-**P2** ($E_{red, onset} = -1.93$ V vs Fc/Fc$^+$, THF/[(n-Bu)$_4$N]PF$_6$). A tentative explanation for the observed difference is that the electron-deficient borane moieties are present on each repeating unit of *rr*-**P1**,[25] but in *rr*-**P2** they alternate with hexyl groups, which exert an electron-donating effect.[26] Noteworthy is also that the onset of oxidation for *rr*-**P1** and *rr*-**P2** ($E_{ox, onset}$ ~0.6 V) is shifted to somewhat higher potential relative to *rr*-P3HT under similar experimental conditions ($E_{ox, onset} = 0.45$ V vs Fc/Fc$^+$, CH$_3$CN/[(n-Bu)$_4$N]PF$_6$),[22] again presumably due to the attachment of the electron-withdrawing side chains. A conversion to HOMO and LUMO orbital energy levels is shown in Table 1 using a value of 4.8 eV for the Fc/Fc$^+$ couple relative to vacuum, but we note the well-known difficulties associated with electrochemical determinations of orbital energy levels.[27] Nonetheless, a qualitative comparison indicates that the HOMO and LUMO energy levels are lower for *rr*-**P1** and *rr*-**P2** than for P3HT.

a)
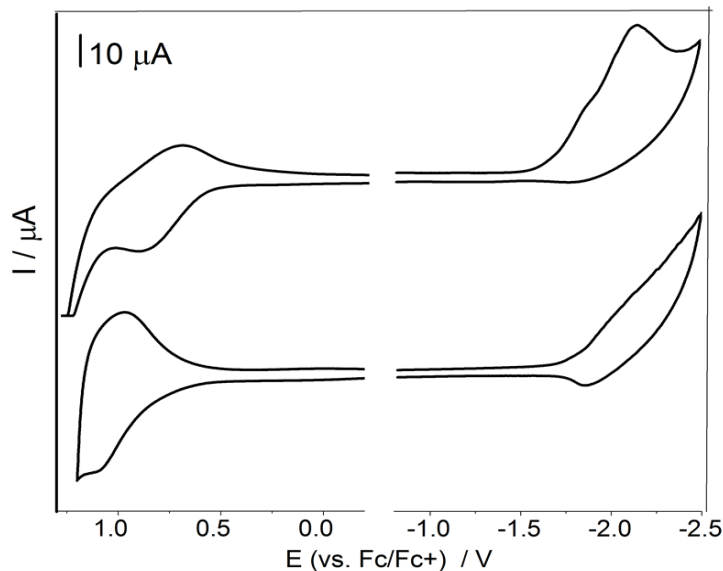
b)
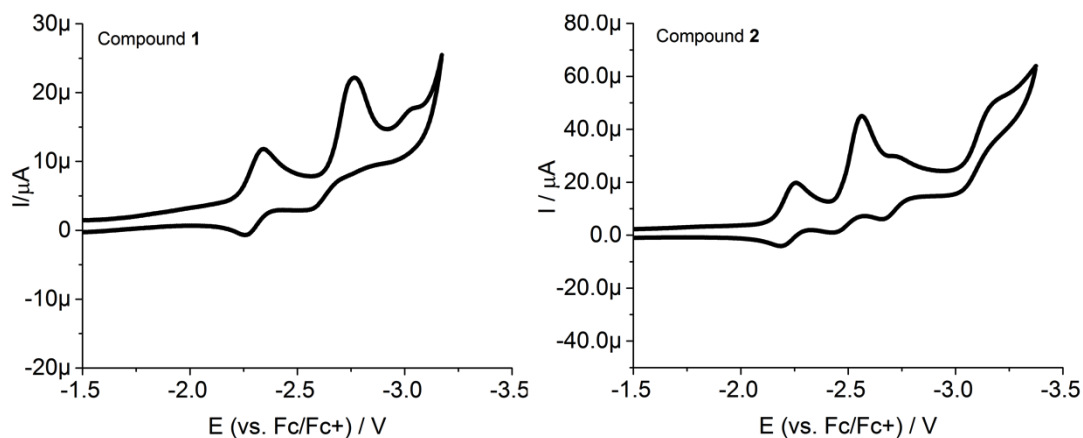
Figure 1-14. a) Cyclic voltammograms of rr-**P1** and rr-**P2** as thin films in CH$_3$CN/0.1M Bu$_4$N[PF$_6$] at a scan rate of 500 mV/s; referenced to Fc$^{0/+}$ couple (+480 mV vs. Ag/AgCl). b) Cyclic voltammograms of **1** and **2** in THF/0.1M Bu$_4$N[PF$_6$] at a scan rate of 100 mV/s; referenced internally to the Fc$^{0/+}$ couple.

Fluoride anion binding behaviour. Finally, we explored the possibility of influencing the polymer characteristics by anion binding[13e] to the borane acceptor sites. We first examined the effect of fluoride binding to the molecular model compounds (Figure 1-15a,b). Addition of F$^-$ to a THF solution of **1** led to a blue

shift of the absorption at 340 nm due to complexation to the borane atom, which strongly contributes to the LUMO orbital of the free acid as discussed above. Exposure of **2** to F⁻ triggered a comparable shift of the absorption at 321 nm and a more subtle blue shift of the lowest energy absorption at 370 nm. For the polymers *rr*-**P1** and *rr*-**P2**, addition of F⁻ resulted in the disappearance of the higher energy absorption band in the UV region, but the lowest energy band in the visible region only slightly shifted (*rr*-**P1**) or remained unchanged (*rr*-**P2**) (Figure 1-15c,d). This is consistent with our assignment of the longest wavelength absorption band to the π-conjugated polythiophene backbone. The emission band of the molecular species **1** was almost completely quenched and that of **2** experienced a distinct shift to higher energy upon F⁻ binding. In contrast, for the polymers *rr*-**P1** and *rr*-**P2**, the emission at ca. 600 nm decreased somewhat in intensity, but did not change its position. This further substantiates that the polymer backbone itself is the main source of the fluorescence in *rr*-**P1** and *rr*-**P2**.
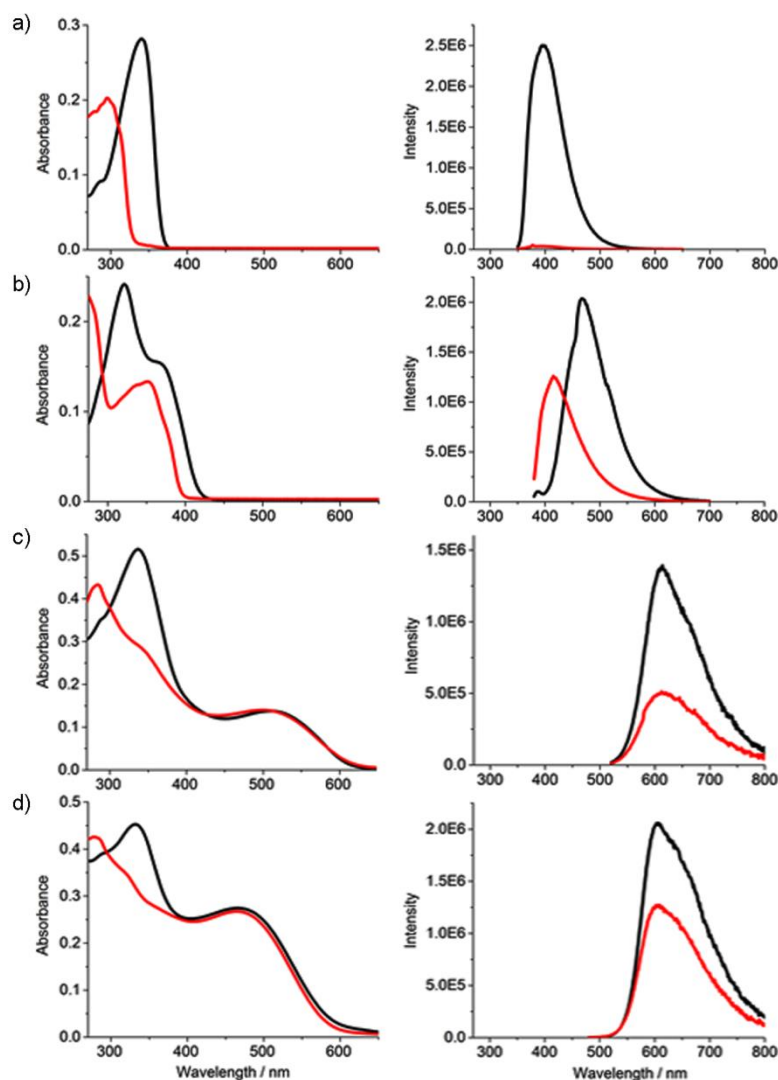
Figure 1-15. UV-vis and fluorescence spectra in THF before (black) and after addition of an excess of TBAF (red). a) **1**, λ_{exc} = 340 nm; b) **2**, λ_{exc} = 370 nm (similar result for λ_{exc} = 322 nm); c) *rr*-**P1**, λ_{exc} = 470 nm; d) *rr*-**P2**, λ_{exc} = 470 nm. [Borane] in the range of 5 × 10^{-5} to 5 x 10^{-6} M, [F$^-$] = 4 × 10^{-3} added until no more change in absorption data observed.

1.3 Conclusions

We have prepared a new class of 3-alkynylphenylborane-functionalized thiophene monomers and converted them to the corresponding regioregular

borane-functionalized poly(3-alkynylthiophene)s *rr*-**P1** and *rr*-**P2** via Stille-type protocols. The thiophene moieties in poly(3-alkynylthiophene)s are able to adopt an almost perfectly coplanar conformation, which favours extended conjugation along the polymer backbone. A single crystal X-ray analysis of the bithiophene species **2-Br** is consistent with a coplanar structure and demonstrates that the bulky boryl moieties do not interfere. Favourable coplanarity is also reflected in the optical band gaps of the polymeric products, which are significantly lower than for the corresponding poly(3-alkylthiophene)s. A comparison between polymer **P1** prepared by the Kumada technique with the regioregular polymer *rr*-**P1** of similar molecular weight derived from Stille-type coupling suggests that the higher regioregularity in *rr*-**P1** results in significant bathochromic shifts of both the longest wavelength absorption and the fluorescence. Theoretical calculations on model systems and fluoride anion binding studies confirm the assignment of the lowest energy absorption bands at ca. 500 nm to the polymer backbone (almost unchanged) and the higher energy bands at ca. 330-340 nm (quenched) to a charge transfer state that is localized on the borane moieties.

Our studies suggest that the little explored class of poly(3-alknynylthiophene)s are promising candidates for the development of new functional polymeric materials. Although the direct electronic effect of the borane pendent groups on the polythiophene main chain is not very pronounced, charge transfer to the borane side chains is apparent from the absorption data of polymers *rr*-**P1** and *rr*-**P2**, and the exposure to fluoride anions triggers changes in the absorption and to a lesser extent the emission spectra. We expect that stronger electronic communication can

be achieved by lowering the energy of the charge transfer states. A promising direction in this respect is to further tune the electronic structure of the borane group (e.g. the use of more electron-withdrawing fluorinated substituents) and the phenylene linker structure. Ultimately, we envision favorable properties and broad utility of regioregular borane-functionalized polymers for optical and sensory materials.

1.4 Experimental

Materials and Methods. Ether solvents and THF were distilled from Na/benzophenone prior to use. Hydrocarbon solvents were purified using a solvent purification system (Innovative Technologies; alumina/copper columns for hydrocarbon solvents). LDA,[7] dimesitylboron fluoride,[28] 2,5-dibromo-3-iodothiophene,[29] 2-bromo-3-iodothiophene,[29] and (4-ethynylphenyl)dimesityl-borane[30] were prepared according to literature procedures. All other reagents were commercially available (Aldrich, Acros, Strem) and either used as obtained or purified by standard procedures. All reactions and manipulations of air sensitive compounds were carried out under an atmosphere of prepurified nitrogen using either Schlenk techniques or an inert atmosphere glovebox (Innovative Technologies). All 499.9 MHz ^{1}H, 125.7 MHz ^{13}C, and 160.4 MHz ^{11}B NMR spectra were recorded at ambient temperature on a Varian INOVA 500 spectrometer and all 599.7 MHz ^{1}H, 150.8 MHz ^{13}C, and 192.4 MHz ^{11}B NMR spectra on a Varian INOVA 600 spectrometer equipped with a boron-free 5 mm dual broadband gradient probe (Nalorac, Varian Inc., Martinez, CA). Solution ^{1}H and ^{13}C NMR spectra were referenced internally to solvent signals. ^{11}B NMR spectra were acquired with boron-free

quartz NMR tubes and referenced externally to $BF_3 \cdot Et_2O$ (δ 0). GPC analyses were performed using a Viscotek GPCmax equipped with a VE 2001 GPC solvent/sample module, a 2600 PDA detector, a TDA 305 triple detector array and three columns, consisting of a PLgel 5 μm mixed-D and two PLgel 5 μm mixed-C columns. The system was calibrated against narrow polystyrene standards (10) in the molecular weight range of 580 to 371100 Da. MALDI-MS measurements were performed on an Apex-ultra 7T Hybrid FT-MS (Bruker Daltonics) in linear (+) and (-) mode. The samples (10 mg/mL in THF) were mixed with anthracene (10 mg/mL in THF) as the matrix in a 1:2 ratio and then spotted on the wells of a target plate.

UV-vis absorption data were acquired on a Varian Cary 5000 UV-Vis/NIR spectrophotometer. The fluorescence data and lifetimes were measured using a Horiba Fluorolog-3 spectrofluorometer equipped with a 350 nm nanoLED and a FluoroHub R-928 detector. Absolute quantum yields (Φ_F) were measured with a pre-calibrated Quanta-φ integrating sphere attached to the Fluorolog-3 instrument. Light from the sample compartment is directed into the sphere via a fiber-optic cable and then returned to the sample compartment (and ultimately the emission monochromator) via a second fiber-optic cable.

Cyclic voltammetry (CV) experiments were carried out on a CV-50W analyzer from BASi. For solution measurements, the three-electrode system consisted of an Au disk as working electrode, a Pt wire as counter electrode and an Ag wire as the reference electrode. The voltammograms were recorded with ca. 10^{-3} to 10^{-4} M solutions in THF containing $Bu_4N[PF_6]$ (0.1 M) as the supporting electrolyte. The scans were referenced after the addition of a small amount of decamethylferrocene

(Fc*) as internal standard. The potentials are reported relative to Fc/Fc$^+$ (Fc*/Fc^{*+} at –462 mV vs. Fc/Fc$^+$). Thin film voltammetric experiments were carried out in CH$_3$CN containing Bu$_4$N[PF$_6$] (0.1 M) as the supporting electrolyte. The Au working electrode was coated with a saturated polymer solution in THF followed by drying in air. The scans were referenced to Fc/Fc$^+$ as an internal reference.

X-ray diffraction intensities for **1-BrSn** (crystallized by slow solvent evaporation of a solution in diethyl ether) and **2-Br** (crystallized by slow solvent evaporation of a solution in a mixture of hexanes/ether (1:1)) were collected on a Bruker SMART APEX CCD diffractometer using Cu Kα (1.54178 Å) radiation at 100 K. The structures were refined by full-matrix least squares based on F2 with all reflections (G. M. Sheldrick, SHELXTL V5.10; Siemens XRD, Madison, WI). Non-hydrogen atoms were refined with anisotropic displacement coefficients, and hydrogen atoms were treated as idealized contribution. SADABS (G. M. Sheldrick, SADABS (2.01), Bruker/Siemens Area Detector Absorption Correction Program; Bruker AXS, Madison, WI, 1998) absorption correction was applied. Crystallographic data for the structures of **1-BrSn** and **2-Br** have been deposited with the Cambridge Crystallographic Data Center as supplementary publication CCDC 1015960-1015961. Copies of the data can be obtained free of charge on application to the CCDC, 12 Union Road, Cambridge CB2 1EZ, U.K. (fax, (+44) 1223-336-033; e-mail, deposit@ccdc.cam.ac.uk).

DFT calculations were performed with the Gaussian09 suite of programs. The input files were generated in Chem3D and then pre-optimized in Spartan10. Geometries were then optimized in Gaussian09 using the hybrid density functional

B3LYP with a 6-31g(d) basis set. Frequency calculations were performed to confirm the presence of local minima (only positive frequencies). Orbital representations were plotted with Gaussview 5.08 (scaling radii of 75%, isovalue of 0.02). Vertical excitations were then calculated using TD-DFT methods with the Coulomb-attenuated functional CAM-B3LYP/6-31g(d). Excited state optimization was also performed using the TD-DFT method.

(4-Iodophenyl)dimesitylborane. This compound was prepared in analogy to a literature procedure.[31] Under nitrogen protection, n-BuLi (31.5 mL, 1.6 M in hexanes) was added to a solution of 1,4-diiodobenzene (15.8 g, 48.0 mmol) in 300 mL THF at -78 ºC. After stirring for 1 h at that temperature, a solution of dimesitylboron fluoride (12.99 g, 48.44 mmol) in 50 mL THF was added. The mixture was stirred for 1 h at -78 ºC, allowed to warm to RT and then kept stirring for 12 h. The mixture was quenched by addition of a small amount of ethanol and was worked up with diethyl ether (130 mL) and brine (4×100 mL). The organic layer was dried over Na_2SO_4, filtered and reduced under vacuum. After re-crystallization from CH_2Cl_2/hexanes the product was dried under high vacuum to afford colorless crystals. Yield: 8.23 g, 38%. ^{1}H NMR ($CDCl_3$, 500 MHz) $\square$ = 7.73 (d, 2H, J = 8.1 Hz), 7.23 (d, 2H, J = 8.1 Hz), 6.84 (s, 4H), 2.33 (s, 6H), 2.01 (s, 12H).

((4-(Dimesitylboryl)phenyl)ethynyl)trimethylsilane. This compound was prepared in analogy to a literature procedure.[32] (4-Iodophenyl)dimesitylborane (6.60 g, 14.6 mmol), $PdCl_2(PPh_3)_2$ (512 mg, 0.73 mmol), CuI (278 mg, 1.46 mmol), and dry (i-Pr)$_2$NH (15 mL) were dissolved in THF (65 mL). Trimethylsilylacetylene (8.3 mL, 58 mmol) was then added dropwise. The mixture was stirred at RT for 24 h. After addition of water, the

mixture was extracted with Et$_2$O. The extract was washed with 1N HCl aqueous solution, water and brine, dried over Na$_2$SO$_4$, and concentrated under reduced pressure. The resulting mixture was subjected to column chromatography on silica gel (hexanes→20% of CH$_2$Cl$_2$ in hexanes→30% of CH$_2$Cl$_2$ in hexanes→50% of CH$_2$Cl$_2$ in hexanes) to give the product as white crystals. Yield: 5.00 g, 81%. ^{1}H NMR (CDCl$_3$, 500 MHz) □ = 7.45 (s, 4H), 6.83 (s, 4H), 2.32 (s, 6H), 1.99 (s, 12H), 0.27 (s, 9H).

(4-Ethynylphenyl)dimesitylborane. This compound was prepared in analogy to a literature procedure.[32] ((4-(Dimesitylboryl)phenyl)ethynyl)trimethylsilane (5.00 g, 11.8 mmol) was reacted with KOH (1.99 g, 35.5 mmol) in a CH$_3$OH/THF (100 mL/100 mL) solution for 5 hours at RT. After concentration under reduced pressure, water was added and the mixture was extracted with CH$_2$Cl$_2$. The extracts were washed with water (35 mL) and dried over Na$_2$SO$_4$ to afford (4-ethynylphenyl)dimesitylborane. Yield: 2.65 g, 64%. ^{1}H NMR (CDCl$_3$, 500 MHz) □ = 7.47 (s, 4H), 6.83 (s, 4H), 3.18 (s, 1H), 2.32 (s, 6H), 1.99 (s, 12H).

2-Trimethylstannyl-4-hexylthiophene. This compound was prepared in analogy to a literature procedure.[33] To a solution of 3-hexylthiophene (15.0 g, 89.1 mmol) in 200 mL of anhydrous THF was added n-BuLi (58.5 mL, 93.6 mmol, 1.6 M in hexanes) at -78 ºC under an N$_2$ atmosphere. After addition, the reaction mixture was stirred for 30 min at -78 ºC and then for an additional 1h at RT. The reaction mixture was cooled back to -78 ºC, a solution of Me$_3$SnCl (19.5 g, 98.0 mmol, 1.1 equiv) in 50 mL of THF was added slowly and the mixture slowly warmed to RT and stirred for 3h. The reaction mixture was worked up with distilled water / diethylether. Distillation under high vacuum gave the pure product as a colorless oil. Yield: 24 g, 81%. ^{1}H NMR (CDCl$_3$, 500 MHz) □ = 7.22

(s, 1H), 7.04 (s, 1H), 2.67 (t, $J = 7.5$ Hz, 2H), 1.66 (pentet, $J = 7.5$ Hz, 2H), 1.41-1.33 (m, 6H), 0.92 (t, $J = 6.5$ Hz, 3H).

Synthesis of 1. A solution of 3-iodo-thiophene (96 mg, 0.46 mmol), (4-ethynylphenyl)dimesitylborane (134 mg, 0.38 mmol), NEt_3 (5 mL) and THF (5 mL) was degassed by three freeze-pump-thaw cycles. CuI (7.0 mg, 0.037 mmol) and $PdCl_2(PPh_3)_2$ (13 mg, 0.019 mmol) were then added under N_2 atmosphere and the mixture was stirred for 24 h at RT. After addition of water, the mixture was extracted with CH_2Cl_2. The extracts were washed with 1N HCl aqueous solution, water, saturated $NaHCO_3$ and brine, and then dried over Na_2SO_4 and concentrated under reduced pressure. The residue was subjected to column chromatography on silica gel using hexanes-hexanes/DCM (10:1) as the eluent. The collected product fractions were reduced under vacuum, redissolved in CH_2Cl_2 and precipitated in MeOH to provide a light yellow solid. Yield: 34 mg, 21%. ^{1}H NMR (499.9 MHz, CDCl$_3$) $\delta = 7.55$ (m, 1H), 7.50 (s, 4H), 7.32 (m, 1H), 7.22 (d, $J = 5.0$ Hz, 1H), 6.84 (s, 4H), 2.33 (s, 6H), 2.02 (s, 12H). ^{13}C NMR (125.7 MHz, CDCl$_3$) $\delta = 145.78$ (br, B-C), 141.53 (br, B-C), 140.83, 138.83, 136.10, 130.95, 129.87, 128.98, 128.22, 126.51, 125.44, 122.13, 89.22, 86.60, 23.43, 21.23. ^{11}B NMR (160.4 MHz, CDCl$_3$) $\delta = 74$, $w_{1/2} = 2100$ Hz. High-res MALDI-MS (anthracene matrix, pos. mode): m/z = 864.4312 ($[M_2]^+$ (10%); calcd for $C_{60}H_{58}B_2S_2$ 864.4166), 610.2952 ($[M+anthracene]^+$ (10%); calcd for $C_{44}H_{39}BS$ 610.2866), 431.2047 ($[M-H]^+$ (100%); calcd for $C_{30}H_{28}BS$ 431.2005).

Synthesis of 1-Br. A solution of 2-bromo-3-iodo-thiophene (3.15 g, 10.90 mmol), (4-ethynylphenyl)dimesitylborane (3.47 g, 9.91 mmol), NEt_3 (60 mL) and

THF (60 mL) was degassed by three freeze-pump-thaw cycles. CuI (180 mg, 0.95 mmol) and $PdCl_2(PPh_3)_2$ (348 mg, 0.496 mmol) were then added under N_2 atmosphere and the mixture was stirred for 24 h at RT. After addition of water, the mixture was extracted with CH_2Cl_2. The extracts were washed with 1N HCl aqueous solution, water, saturated $NaHCO_3$ and brine, and then dried over Na_2SO_4 and concentrated under reduced pressure. The residue was subjected to column chromatography on silica gel using hexanes →hexanes/DCM (10:1) as the eluent. The collected product fractions were reduced under vacuum, redissolved in CH_2Cl_2 and precipitated in MeOH to provide a light yellow solid. Yield: 3.16 g, 62%. ^{1}H NMR (499.9 MHz, $CDCl_3$) δ = 7.53 (d, J = 8.0 Hz, 2H), 7.51 (d, J = 8.0 Hz, 2H), 7.24 (d, J = 5.5 Hz, 1H), 7.05 (d, J = 5.5 Hz, 1H), 6.84 (s, 4H), 2.33 (s, 6H), 2.02 (s, 12H). ^{13}C NMR (125.7 MHz, $CDCl_3$) δ = 144.25 (br, B-C), 139.58 (br, B-C), 138.92, 136.96, 134.14, 129.17, 127.88, 126.32, 124.17, 123.98, 122.44, 115.40, 91.48, 83.11, 21.53, 19.33. ^{11}B NMR (160.4 MHz, $CDCl_3$) δ = 74, $w_{1/2}$ = 2100 Hz. High-res MALDI-MS (without matrix, pos. mode): m/z = 511.1064 ([M][+] (100%); calcd for $C_{30}H_{28}BBrS$ 511.1086).

Synthesis of 1-Br2. A solution of 2,5-dibromo-3-iodothiophene (3.06 g, 8.32 mmol), (4-ethynylphenyl)dimesitylborane (2.65 g, 7.56 mmol), dry NEt_3 (45 mL) and THF (45 mL) was prepared and degassed by three freeze-pump-thaw cycles. CuI (139 mg, 7.30 mmol) and $PdCl_2(PPh_3)_2$ (265 mg, 0.378 mmol) were added under N_2 atmosphere. The mixture was stirred for 24 h. After addition of water, the mixture was extracted with CH_2Cl_2. The extracts were washed with 1N HCl aqueous solution, water, saturated $NaHCO_3$, and brine, and then dried over Na_2SO_4

and concentrated under reduced pressure. The residue was subjected to column chromatography on silica gel (hexanes). The collected product fractions were reduced under vacuum, redissolved in CH_2Cl_2 and precipitated in MeOH to provide **1-Br2** as a light yellow solid. Yield: 2.27 g, 51%. ^{1}H NMR (499.9 MHz, $CDCl_3$) δ = 7.52 (s, 4H), 7.04 (s, 1H), 6.85 (s, 4H), 2.34 (s, 6H), 2.03 (s, 12H). ^{13}C NMR (125.7 MHz, $CDCl_3$) δ = 146.47 (br, B-C), 141.48 (br, B-C), 140.84, 139.94, 136.05, 131.99, 131.13, 128.27, 125.63, 124.99, 116.26, 111.06, 93.94, 83.87, 23.47, 21.27. ^{11}B NMR (160.4 MHz, $CDCl_3$) δ = 74, $w_{1/2}$ = 2000 Hz. High-res MALDI-MS (without matrix, pos. mode): m/z = 589.0157 ([M-H]$^+$ (100%); calcd for $C_{30}H_{26}BBr_2S$ 589.0196).

Synthesis of 1-BrSn. To a solution of **1-Br2** (0.849 g, 1.44 mmol) in 20 mL of THF was added n-BuLi (0.90 mL, 1.44 mmol, 1.6 M in hexanes) at −78 ℃. The mixture was stirred for 1 h, followed by addition of a solution of Me_3SnCl (0.315 g, 1.58 mmol, 1.1 equiv) in 15 mL of THF. The reaction mixture was stirred overnight and then worked up using Et_2O/H_2O. The organic layer was reduced and precipitated into MeOH to give pure **1-BrSn** as a light yellow solid. Yield: 0.77 g, 79%. ^{1}H NMR (599.7 MHz, CD_2Cl_2) δ = 7.45 (s, 4H), 7.24 (s, 1H), 6.83 (s, 4H), 2.30 (s, 6H), 2.00 (s, 12H), 0.47 (s/d, $J(^{117/119}Sn,H)$ = 58 Hz, 9H). ^{1}H NMR (599.7 MHz, $CDCl_3$) δ = 7.49 (d, J = 8.0 Hz, 2H), 7.43 (d, J = 8.0 Hz, 2H), 7.24 (s, 1H), 6.83 (s, 4H), 2.62 (t, J = 8.5 Hz, 2H), 2.32 (s, 6H), 2.02 (s, 12H), 0.47 (s/d, $J(^{117/119}Sn,H)$ = 58 Hz, 9H). ^{13}C NMR (150.8 MHz, $CDCl_3$) δ = 146.55, 145.94 (br, B-C), 141.72 (br, B-C), 141.01, 139.04, 136.39, 133.73, 130.84, 130.58, 128.42, 126.65, 116.21, 89.55, 88.31, 23.65, 21.43, -7.81. ^{11}B NMR (192.4 MHz, $CDCl_3$) δ

= 74, $w_{1/2}$ = 2500 Hz. High-res MALDI-MS (anthracene matrix, pos. mode): *m/z* = 773.2617 ([M-Br+anthracene]$^+$ (100%); calcd for $C_{47}H_{46}BSSn$ 773.2445), 673.0911 ([M]$^+$ (30%); calcd for $C_{33}H_{36}BBrSSn$ 673.0752), 595.1800 ([M-Br]$^+$ (10%); calcd for $C_{33}H_{36}BSSn$ 595.1657).

Stille-type Polycondensation of 1-BrSn: Synthesis of *rr*-P1. A solution of **1-BrSn** (0.10 g, 0.15 mmol) in a mixture of 1 mL of DMF and 3 mL of toluene was degassed by three freeze-pump-thaw cycles. The reaction Schlenk flask was taken into the glove box and then $Pd_2(dba)_3$ (6.8 mg, 7.4 mol) and P(t-Bu)$_3$ (9.0 mg, 0.044 mmol) were added. The flask was then immersed in an oil bath that was set to 115 ℃. After 2 days, the reaction flask was cooled to RT and the mixture precipitated in MeOH. The precipitate was re-dissolved in THF and the solution was filtered through a short plug of alumina gel. The product was then further purified by preparative column chromatography on Biobeads^{TM} (THF-eluent) to give a black solid. Yield: 18 mg, 27%. GPC (THF, 1 mL/min): M_n = 4690 g/mol, Đ = 1.30. ^{1}H NMR (599.7 MHz, CD_2Cl_2) δ = 7.5 (br), 6.8 (br), 2.25 (br), 1.96 (br). ^{11}B NMR (192.4 MHz, $CDCl_3$) δ = 73, $w_{1/2}$ = 2700 Hz.

Synthesis of 2. A 50 mL Schlenk flask was charged with **1-Br** (1.00 g, 1.96 mmol), 2-trimethylstannyl-4-hexylthiophene (0.84 g, 2.54 mmol, 1.3 equiv), and 30 mL of DMF. The mixture was then degassed by three freeze-pump-thaw cycles and $Pd(PPh_3)_2Cl_2$ (0.069 g, 0.10 mmol) in DMF (5 mL) was added to the Schlenk flask. The reaction mixture was stirred at 80 ℃ overnight. After work up with DCM/H_2O, the crude material was purified using silica gel chromatography to give the product as a highly viscous yellow oil. Yield: 0.90 g, 77%. ^{1}H NMR (499.9

MHz, C$_6$D$_6$) δ = 7.63 (d, J = 8.0 Hz, 2H), 7.60 (d, J = 8.0 Hz, 2H), 7.47 (s, 1H), 6.93 (d, J = 5.0 Hz, 1H), 6.79 (s, 4H), 6.57 (s, 1H), 6.45 (d, J = 5 Hz, 1H), 2.36 (t, J = 7.5 Hz, 2H), 2.20 (s, 6H), 2.11 (s, 12H), 1.45 (m, J = 6.5 Hz, 2H), 1.23-1.18 (m, 6H), 0.86 (t, J = 6.5 Hz, 3H). ^{1}H NMR (499.9 MHz, CDCl$_3$) δ = 7.56 (d, J = 8.0 Hz, 2H), 7.53 (d, J = 8.0 Hz, 2H), 7.39 (s, 1H), 7.12 (s, 2H), 6.93 (s, 1H), 6.85 (s, 4H), 2.62 (t, J = 7.5 Hz, 2H), 2.33 (s, 6H), 2.04 (s, 12H), 1.66 (m, J = 7 Hz, 2H), 1.32-1.31 (m, 6H), 0.89 (t, J = 5.5 Hz, 3H). ^{13}C NMR (125.7 MHz, CDCl$_3$) δ = 145.80 (br, B-C), 143.49, 141.54 (br, B-C), 140.83, 140.57, 138.82, 136.14, 135.53, 131.12, 130.73, 128.22, 127.04, 126.72, 122.54, 120.62, 116.89, 94.22, 87.57, 31.68, 30.45 (2 signals), 28.99, 23.45, 22.61, 21.23, 14.09. ^{11}B NMR (160.4 MHz, CDCl$_3$) δ = 75, w$_{1/2}$ = 2100 Hz. High-res MALDI-MS (without matrix, pos. mode): m/z = 598.2858 ([M]$^+$ (100%); calcd for C$_{40}$H$_{43}$BS$_2$ 598.2901).

Synthesis of 2-Br. A 50 mL round bottom flask was charged with **2** (0.71 g, 1.19 mmol) and 10 mL of DMF. The flask was placed in an ice bath and then NBS (0.25 g, 1.40 mmol, 1.2 equiv) was added slowly. The reaction mixture was stirred at RT overnight, worked up with brine/DCM, and purified by silica gel column chromatography (hexanes→hexanes/DCM (10:1)). The product was obtained as a bright yellow solid. Yield: 339 mg, 42%. ^{1}H NMR (499.9 MHz, CDCl$_3$) δ = 7.56 (d, J = 8.0 Hz, 2H), 7.53 (d, J = 8.0 Hz, 2H), 7.19 (s, 1H), 7.13 (d, J = 5.5 Hz, 1H), 7.10 (d, 5.5 Hz, 1H), 6.84 (s, 4H), 2.57 (t, J = 7.5 Hz, 2H), 2.33 (s, 6H), 2.03 (s, 12H), 1.62 (m, J = 7.0 Hz, 2H), 1.38-1.29 (m, 6H), 0.88 (t, J = 5.5 Hz, 3H). ^{13}C NMR (125.7 MHz, CDCl$_3$) δ = 145.98 (br, B-C), 142.18, 141.51(br, B-C), 140.83, 139.60, 138.85, 136.16, 135.40, 131.14, 130.70, 128.23, 126.41, 126.22, 122.86,

117.25, 109.87, 94.85, 87.14, 31.61, 29.68, 29.51, 28.91, 23.46, 22.58, 21.23, 14.07. ^{11}B NMR (160.4 MHz, CDCl$_3$) δ = 74, w$_{1/2}$ = 2300 Hz. High-res MALDI-MS (anthracene matrix): m/z = 775.3525 ([M-Br+anthracene]$^+$ (60%); calcd for C$_{54}$H$_{52}$BS$_2$ 775.3603), 678.1922 ([M]$^+$ (100%); calcd for C$_{40}$H$_{42}$BBrS$_2$ 678.1982), 597.2779 ([M-Br]$^+$ (80%); calcd for C$_{40}$H$_{42}$BS$_2$ 597.2821).

Synthesis of 2-BrSn. To a solution of diisopropyl amine (179 mg, 1.77 mmol) in 6 mL of THF was added n-BuLi (1.11 mL, 1.79 mmol, 1.6 M in hexanes) at RT and the mixture was stirred at -40 ℃ for 40 min. The resulting LDA solution was added to a solution of **2-Br** (1.00 g, 1.48 mmol) in 9 mL of THF at -78 ℃ and the mixture was stirred for 30 min. The reaction mixture was then cooled to -78 ℃ and a solution of Me$_3$SnCl (382 mg, 1.92 mmol) in 10 mL of THF was added slowly. The mixture was allowed to slowly warm up to RT while stirring overnight. The reaction mixture was worked up with CH$_2$Cl$_2$/H$_2$O. A light brown oil was obtained, re-dissolved in CH$_2$Cl$_2$, and precipitated in MeOH to provide the product as a light brown solid. Yield: 520 mg, 42%. ^{1}H NMR (499.9 MHz, CDCl$_3$) δ = 7.55 (d, J = 7.5 Hz, 2H), 7.53 (d, J = 7.5 Hz, 2H), 7.18 (s, 1H), 7.16 (s/d, J($^{117/119}$Sn,H) = 20 Hz, 1H), 6.85 (s, 4H), 2.56 (t, J = 7.5 Hz, 2H), 2.33 (s, 6H), 2.03 (s, 12H), 1.61 (pentet, J = 7.0 Hz, 2H), 1.39-1.31 (m, 6H), 0.88 (t, J = 5.5 Hz, 3H), 0.41 (s/d, J($^{117/119}$Sn,H) = 57 Hz, 9H). ^{13}C NMR (125.7 MHz, CDCl$_3$) δ = 145.76, 144.83, 142.12, 141.53, 140.83, 138.91 (s/d, J($^{117/119}$Sn,^{13}C) = 25 Hz), 138.81, 136.25, 136.17, 135.56, 130.65, 128.21, 126.70, 125.92, 118.58, 109.61, 95.08, 87.38, 31.62, 29.66, 29.51, 28.90, 23.45, 22.57, 21.23, 14.07, -8.21 (s/d, J($^{117/119}$Sn,^{13}C) = 367 Hz). ^{11}B NMR (160.4 MHz, CDCl$_3$) δ = 73, w$_{1/2}$ = 2800 Hz.

High-res MALDI-MS (anthracene matrix, pos. mode): m/z = 939.3258 ([M-Br+anthracene]$^+$ (30%); calcd for $C_{57}H_{60}BS_2Sn$ 939.3251), 840.1654 ([M]$^+$ (100%); calcd for $C_{43}H_{50}BBrS_2Sn$ 840.1649), 761.2475 ([M-Br]$^+$ (40%); calcd for $C_{43}H_{50}BS_2Sn$ 761.2469).

Stille-type Polycondensation of 2-BrSn: Synthesis of *rr*-P2. A solution of **2-BrSn** (0.10 g, 0.12 mmol) in a mixture of 1 mL of DMF and 3 mL of toluene was degassed by three freeze-pump-thaw cycles. The reaction Schlenk flask was taken into the glove box and then $Pd_2(dba)_3$ (5.4 mg, 5.9 μmol) and $P(t\text{-Bu})_3$ (7.2 mg, 0.036 mmol) were added. The flask was then immersed in an oil bath that was set to 115 °C. After 2 d the reaction flask was cooled to RT and the mixture precipitated in MeOH. The precipitate was re-dissolved in THF and passed through a plug of alumina gel. The solution was then precipitated once more into acetone. The polymer was purified by preparative column chromatography on Biobeads^{TM} (THF-eluent) to give a black solid. Yield: 21.5 mg, 30%. GPC (THF, 1 mL/min): M_n = 8860 g/mol, $Đ$ = 1.73. ^{1}H NMR (499.9 MHz, CDCl$_3$) δ = 7.56 (br), 7.16 (br), 6.80 (br), 2.82 (br), 2.29 (br), 2.01 (br), 1.72 (br), 1.27 (br), 0.90 (br). ^{11}B NMR (160.4 MHz, CDCl$_3$) δ = 66, $w_{1/2}$ = 6400 Hz.

Metathesis of Monomer 1-Br2. A solution of **1-Br2** (50 mg, 0.085 mmol) and LiCl (3.4 mg, 0.080 mmol) in 1 mL of THF was stirred for 30 min. A solution of the selected Grignard reagent (*t*-BuMgCl or *i*-PrMgCl) in 1 mL of THF was added and the mixture was stirred for a predetermined time at different temperatures. The reaction was quenched by addition of dilute HCl, extracted with CHCl$_3$, the extracts were dried over Na$_2$SO$_4$ and reduced under vacuum. The NMR spectra of

the hydrolysis products of the 2-magesio and 5-magnesio species were then recorded. Hydrolysis of **2-magnesio species**: ^{1}H NMR (499.9 MHz, CDCl$_3$) δ = 7.50 (d, J = 8.0 Hz, 2H), 7.47 (d, J = 8.0 Hz, 2H), 7.41 (s, 1H), 7.16 (s, 1H), 6.84 (s, 4H), 2.32 (s, 6H), 2.01 (s, 12H). Hydrolysis of **5-magnesio species**: ^{1}H NMR (499.9 MHz, CDCl$_3$) δ = 7.50 (d, J = 8.0 Hz, 2H), 7.47 (d, J = 8.0 Hz, 2H), 7.24 (d, J = 5.5 Hz, 1H), 7.05 (d, J = 5.5 Hz, 1H), 6.84 (s, 4H), 2.33 (s, 6H), 2.02 (s, 12H). This compound was independently prepared in pure form as described above (synthesis of **1-Br**).

Metathesis of 1-Br2 by Treatment with t-BuLi and then MgCl$_2$. 1. Preparation of MgCl$_2$: To a suspension of Mg turnings (76 mg, 3.13 mmol) in THF (1.5 mL) were added dichloroethane (0.74 mL, 9.4 mmol) and the mixture was stirred at RT for 30 min. THF (1 mL) was added and the mixture was stirred for another 30 min. Additional THF (4 mL) was added to form a clear solution. 2. Metathesis: A solution of **1-Br2** (467 mg, 0.791 mmol) and LiCl (32.2 mg, 0.76 mmol) in 2 mL of THF was stirred for 30 min. t-BuLi (0.93 mL, 1.58 mmol, 1.7 M in pentane) was added at −78 ℃ and the mixture was stirred for 1h. The MgCl$_2$ solution prepared as described above was added and the reaction mixture stirred at 0 ℃ for 25 min. Then a sample of the mixture (0.5 mL) was quenched with dilute HCl, extracted with CHCl$_3$, dried over Na$_2$SO$_4$, reduced under vacuum, and subjected to ^{1}H NMR analysis. A similar result was obtained with n-BuLi (1 equiv).

Kumada Coupling Polymerization of 1-Br2 Using *in-situ* Generated Grignard Reagent (t-BuLi / MgCl$_2$): Synthesis of P1. A mixture of **1-Br2** (467

mg, 0.791 mmol) and LiCl (32.2 mg, 0.76 mmol) in 2 mL of THF was stirred for 30 min. t-BuLi (0.93 mL, 1.58 mmol, 1.7 M in pentane) was added at −78 ℃ and the mixture was stirred for 1h. A solution of $MgCl_2$ (6.5 mL, 0.5 M in THF) was added and the reaction mixture was stirred at 0 ℃ for 25 min. The ice bath was removed. A solution of Ni(dppp)Cl_2 (4.3 mg, 7.9 μmol) in 1 mL of THF was added, then 6 mL of toluene were added and the mixture was stirred overnight at 80 ℃. The reaction was quenched with a small amount of acidified MeOH and then precipitated in MeOH. A brownish red product was obtained and purified using preparative column chromatography on Biobeads[TM] (THF-eluent). Yield: 63 mg, 18%. GPC (THF, 1 mL/min): M_n = 4720, Đ = 1.19. ^{1}H NMR (499.9 MHz, CDCl$_3$) δ = 7.5 (br), 6.84-6.77 (br), 2.33 (br), 2.00 (br). ^{11}B NMR (160.4 MHz, CDCl$_3$) δ = 70, $w_{1/2}$ = 6100 Hz.
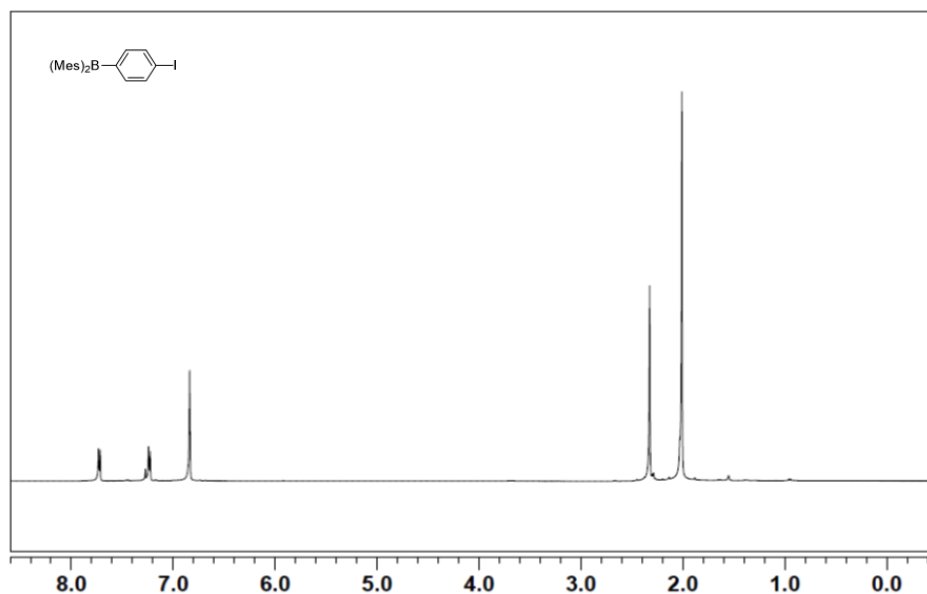
Figure 1-16. ^{1}H NMR spectrum of (4-iodophenyl)dimesitylborane in CDCl$_3$ (δ, ppm).
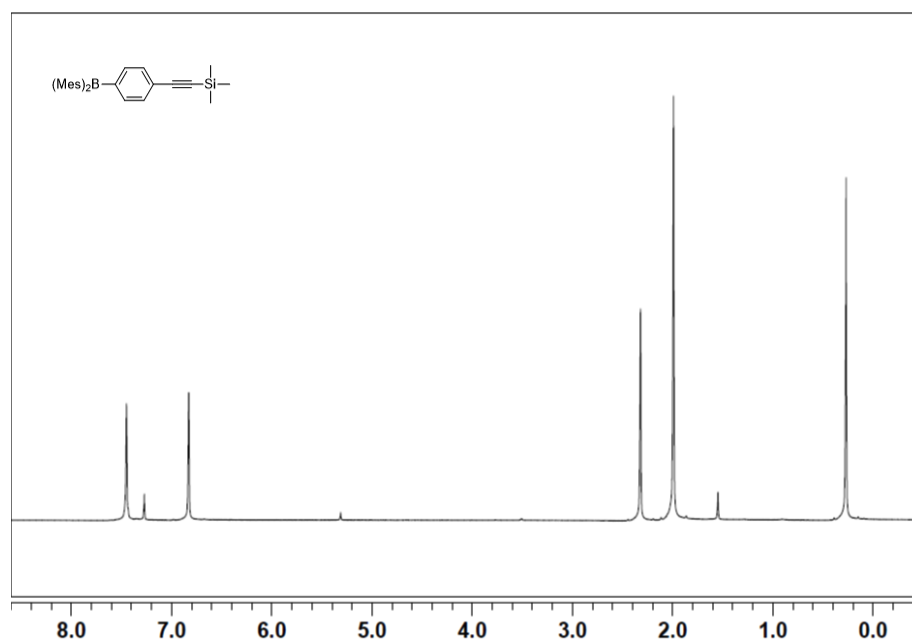
Figure 1-17. ^{1}H NMR spectrum of ((4-(dimesitylboryl)phenyl)ethynyl)trimethylsilane in CDCl$_3$ (δ, ppm).
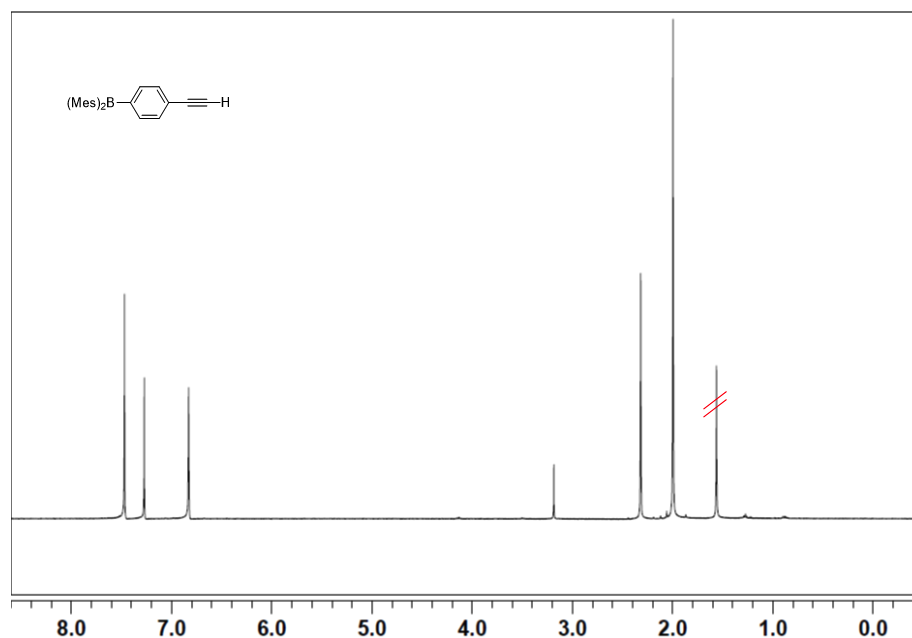
Figure 1-18. ^{1}H NMR spectrum of (4-ethynylphenyl)dimesitylborane in CDCl$_3$ (δ, ppm).
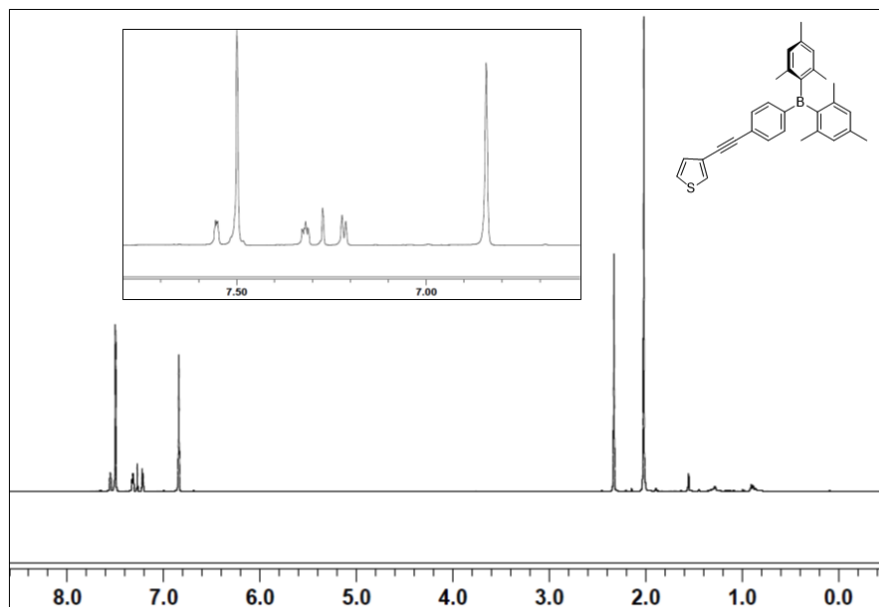
Figure 1-19. ^{1}H NMR spectrum of compound **1** in CDCl$_3$ (δ, ppm).
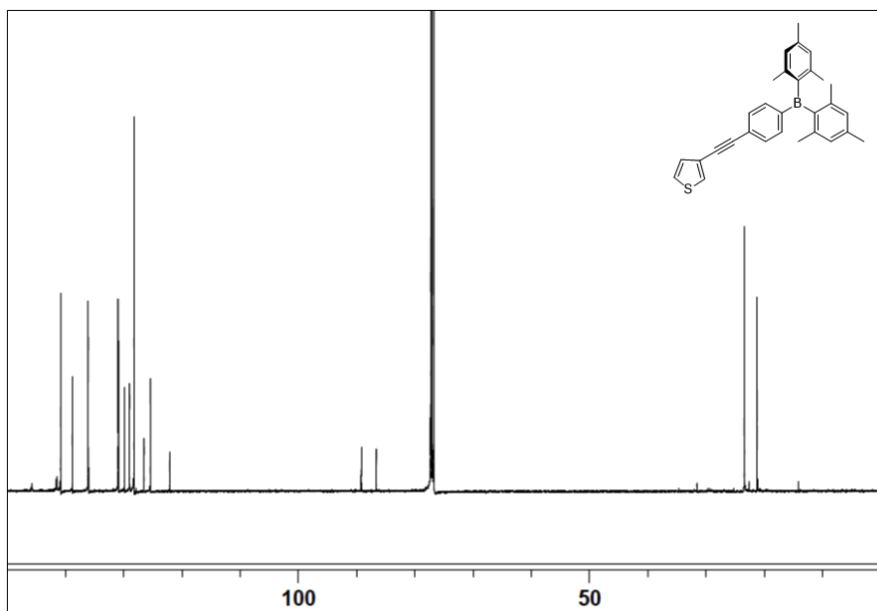
Figure 1-20. ^{13}C NMR spectrum of **1** in CDCl$_3$ (δ, ppm).
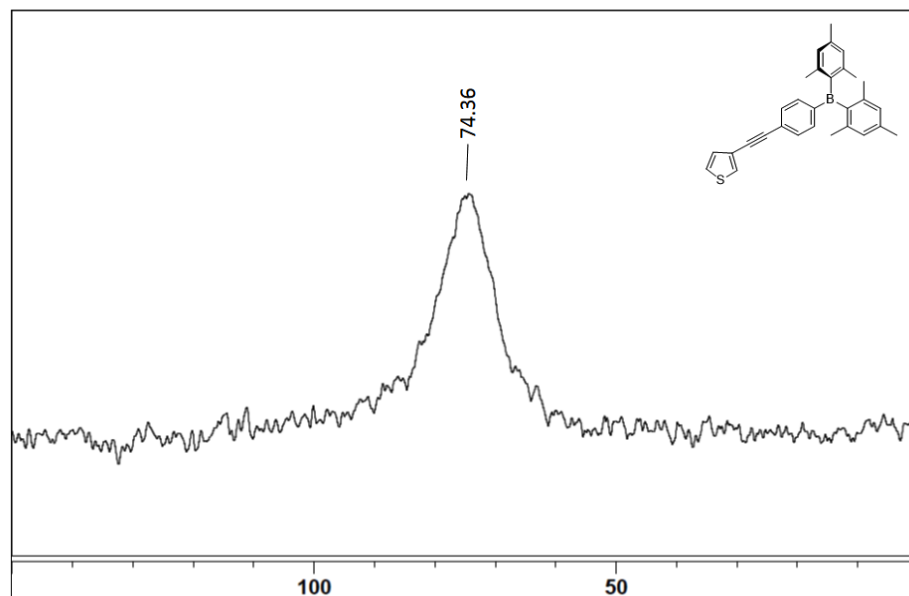
Figure 1-21. ^{11}B NMR spectrum of **1** in CDCl$_3$ (δ, ppm).
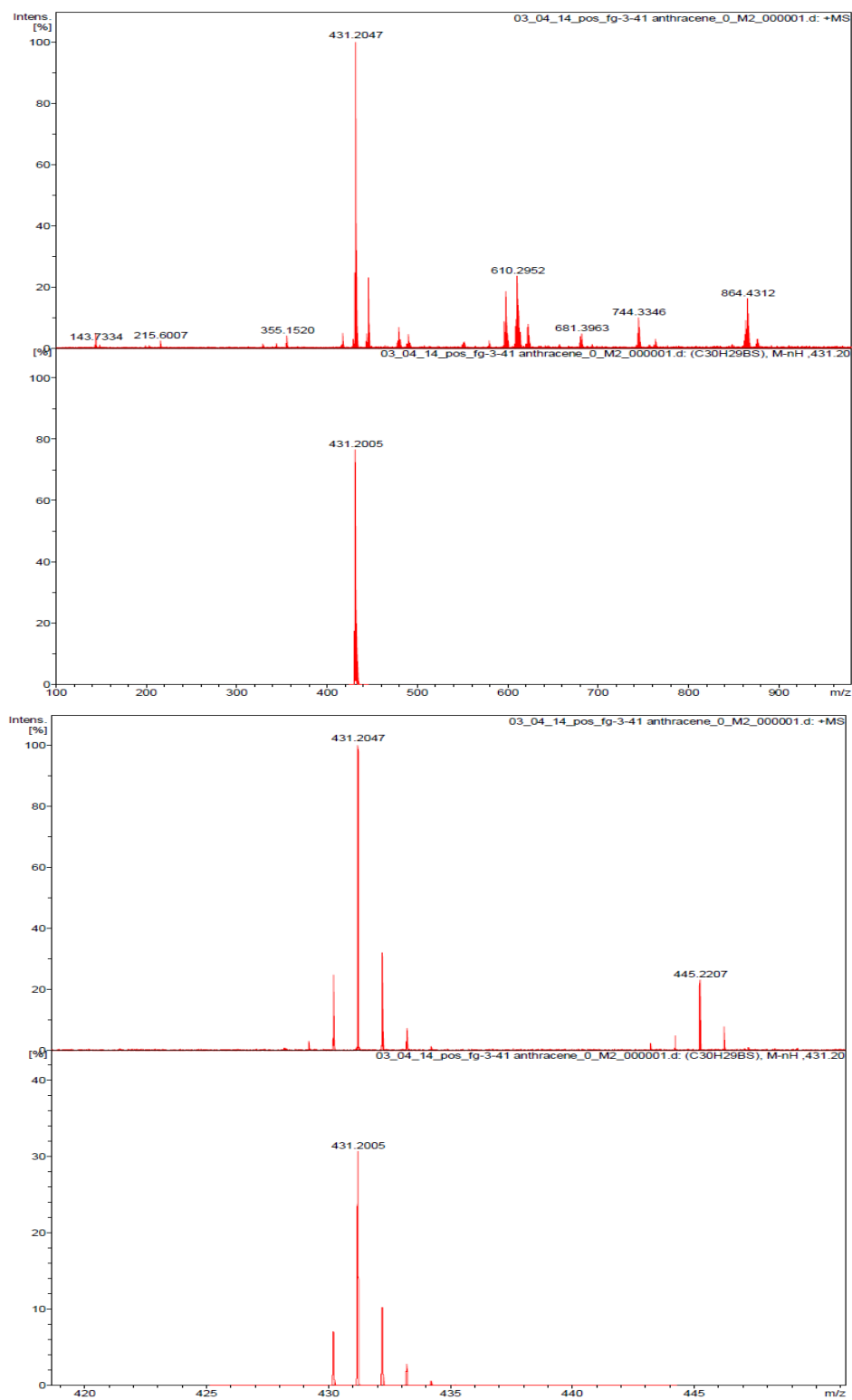
Figure 1-22. High resolution (pos. mode) MALDI-MS data of compound **1** (m/z, a.u.).
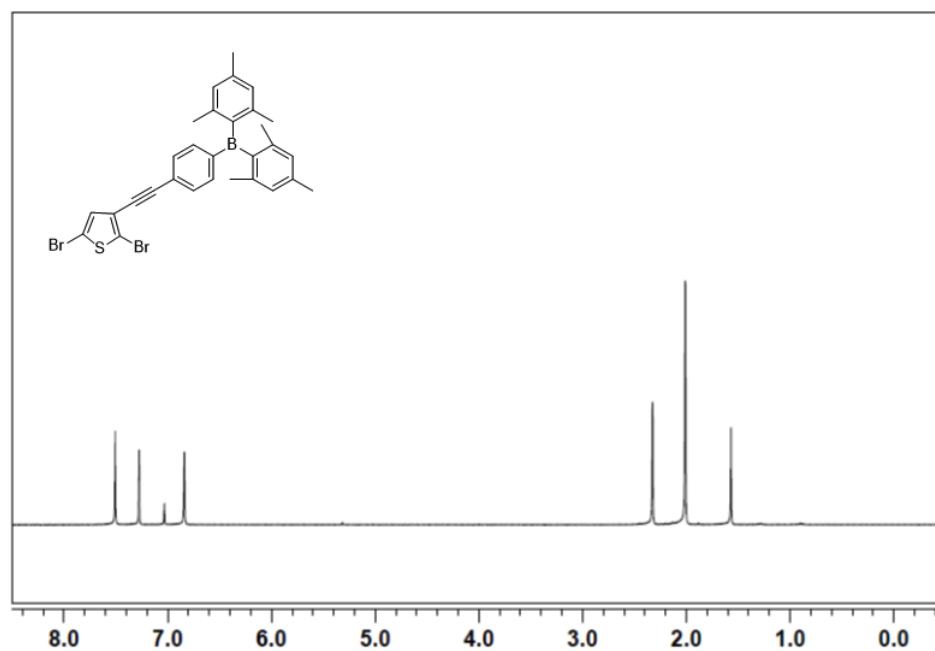
Figure 1-23. ^{1}H NMR spectrum of **1-Br2** in CDCl$_3$ (δ, ppm).
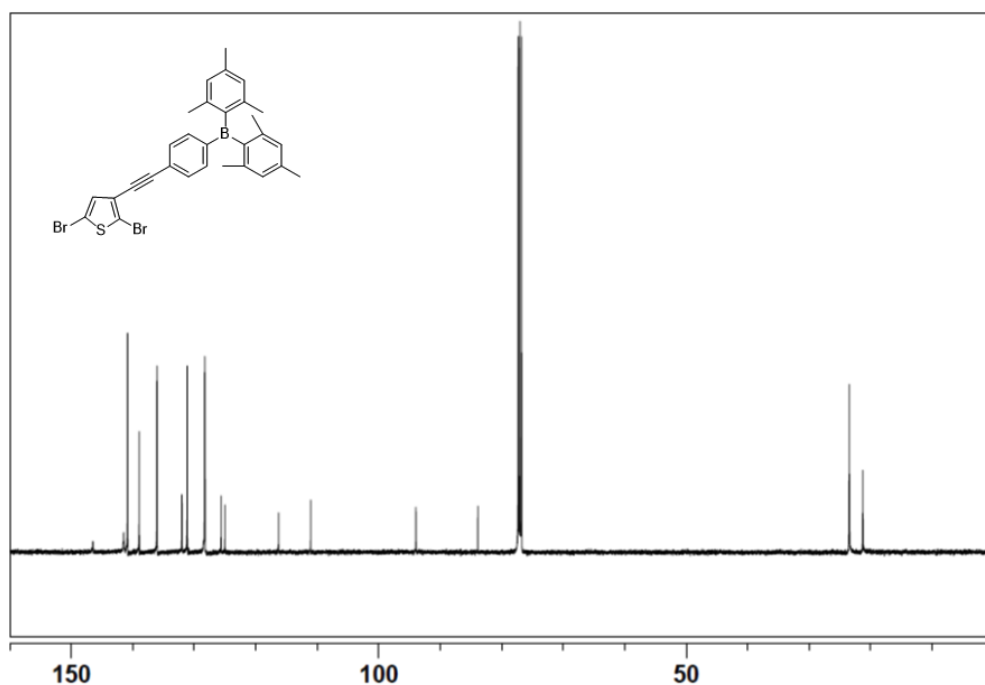
Figure 1-24. ^{13}C NMR spectrum of **1-Br2** in CDCl$_3$ (δ, ppm).

Figure 1-25. ^{11}B NMR spectrum of **1-Br2** in CDCl$_3$ (δ, ppm).
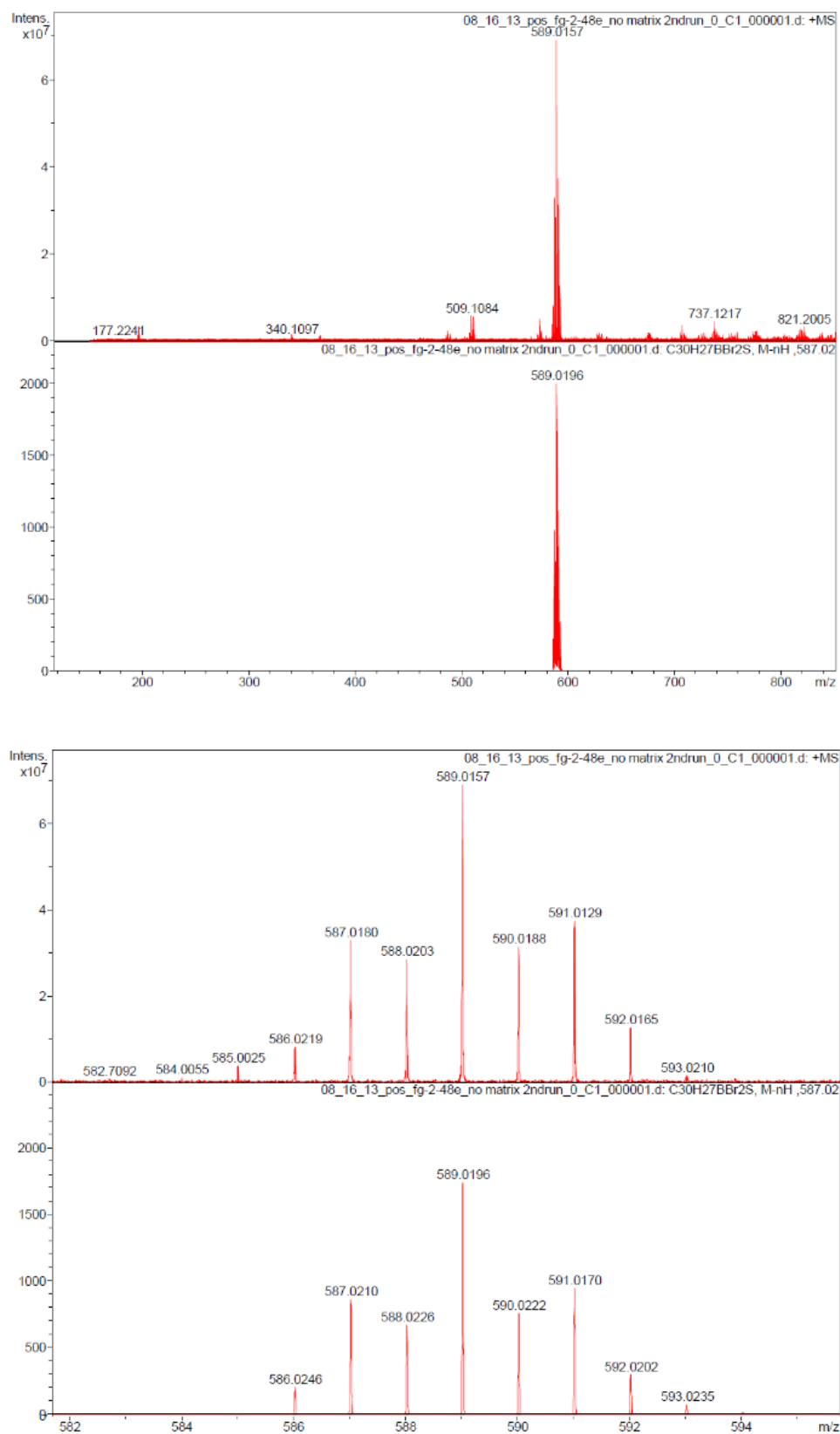
Figure 1-26. High resolution (pos. mode) MALDI-MS data of **1-Br2** (m/z, a.u.).
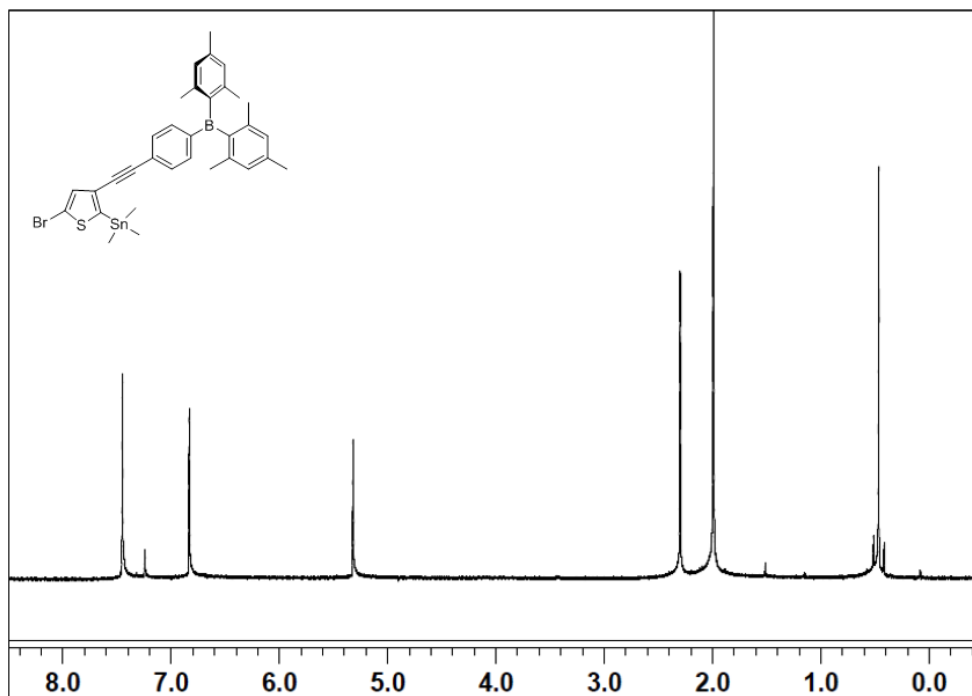
Figure 1-27. ^{1}H NMR spectrum of **1-BrSn** in CD$_2$Cl$_2$ (δ, ppm).
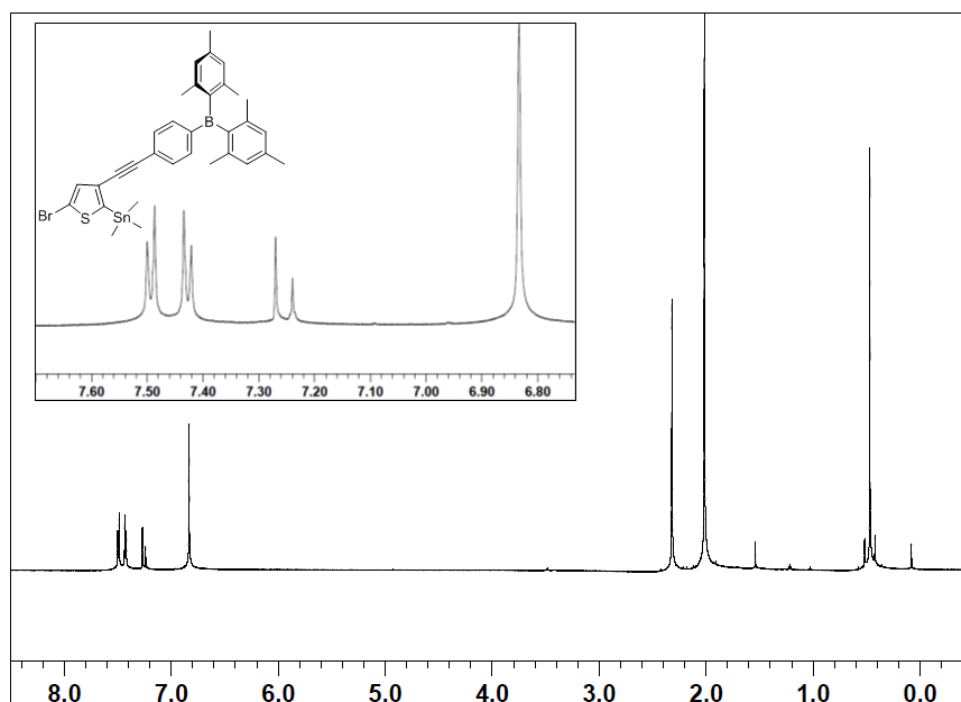
Figure 1-28. ^{1}H NMR spectrum of **1-BrSn** in CDCl$_3$ (δ, ppm).
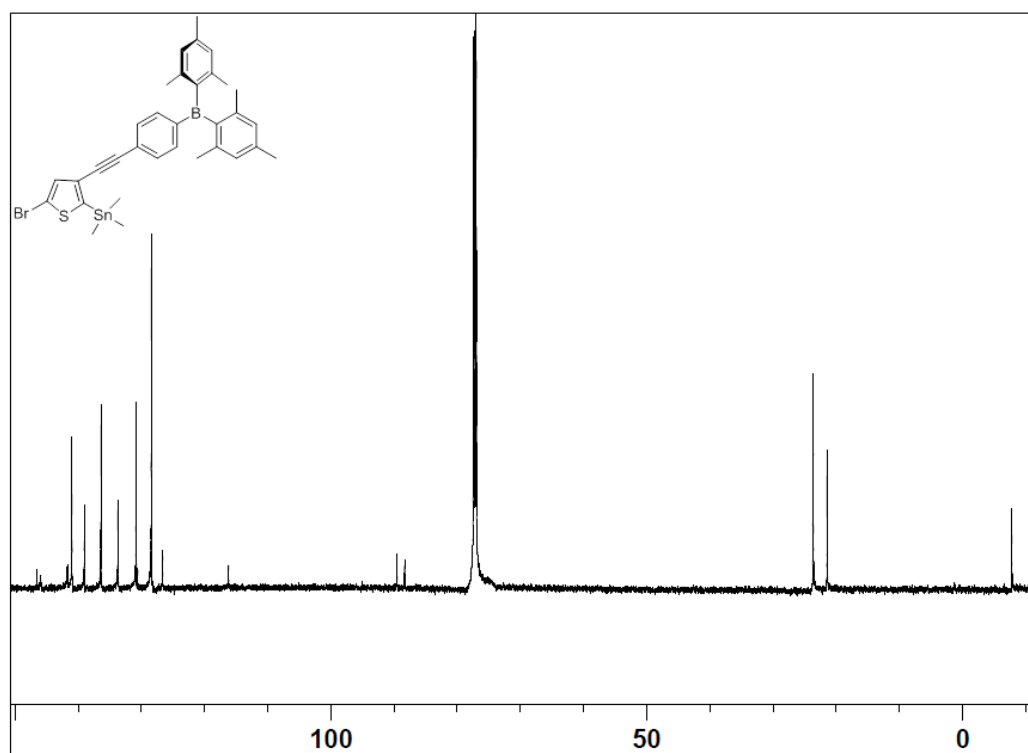
Figure 1-29. ^{13}C NMR spectrum of **1-BrSn** in CDCl$_3$ (δ, ppm).
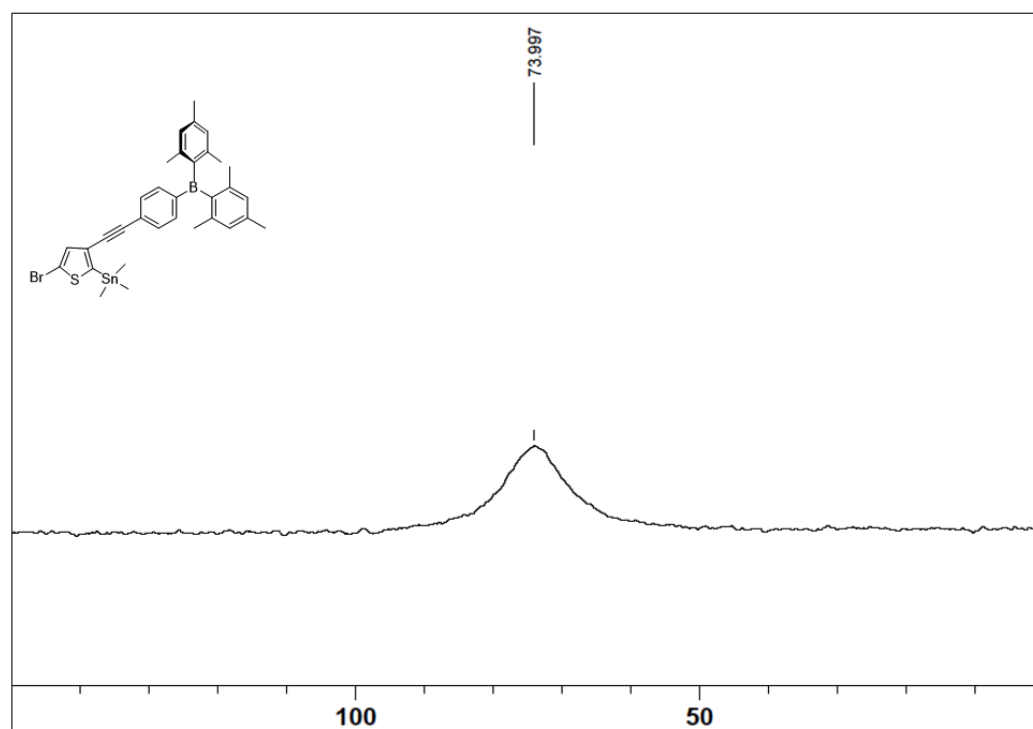
Figure 1-30. ^{11}B NMR spectrum of **1-BrSn** in CDCl$_3$ (δ, ppm).
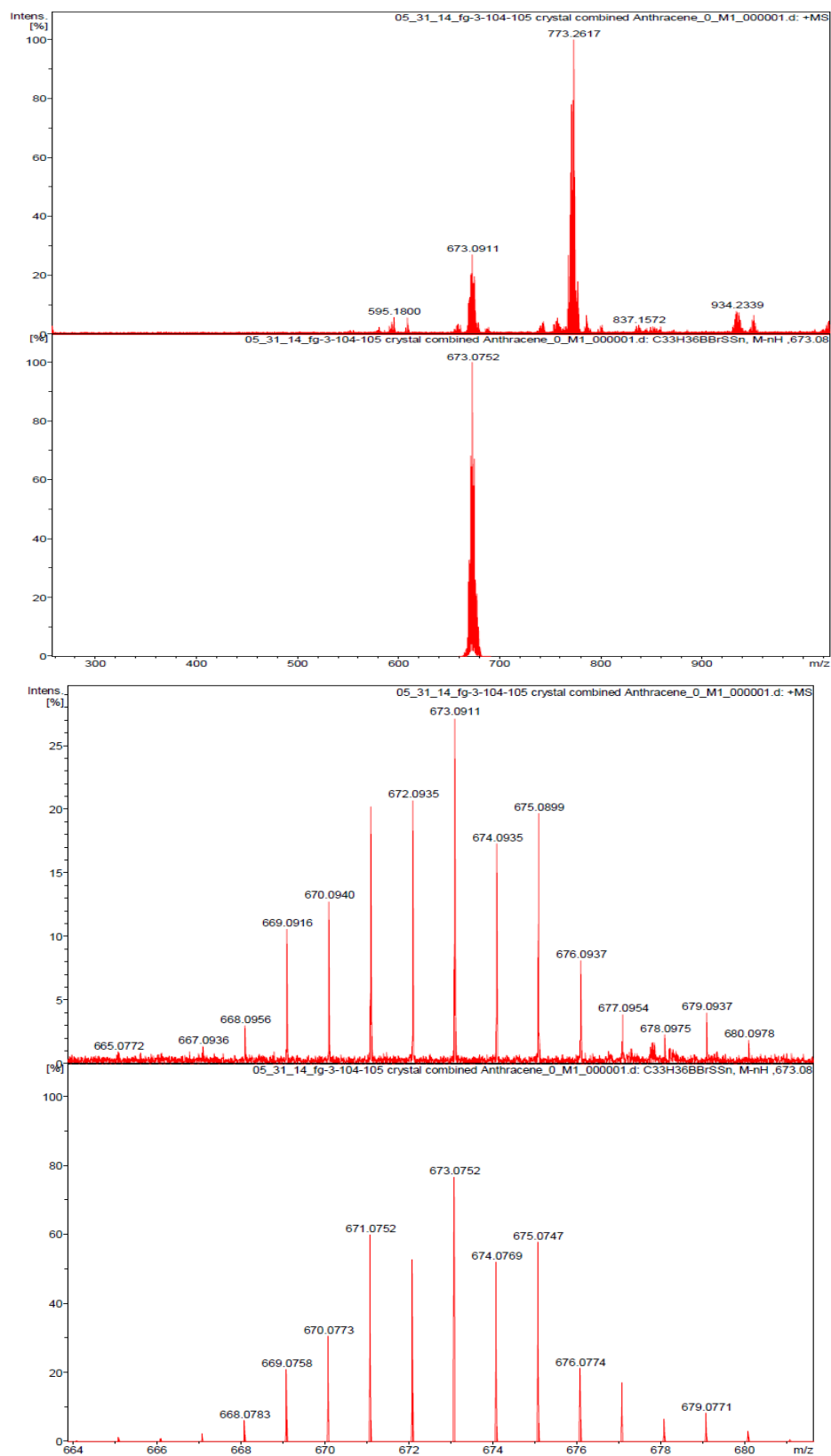
Figure 1-31. High resolution (pos. mode) MALDI-MS data of **1-BrSn** (m/z, a.u.).
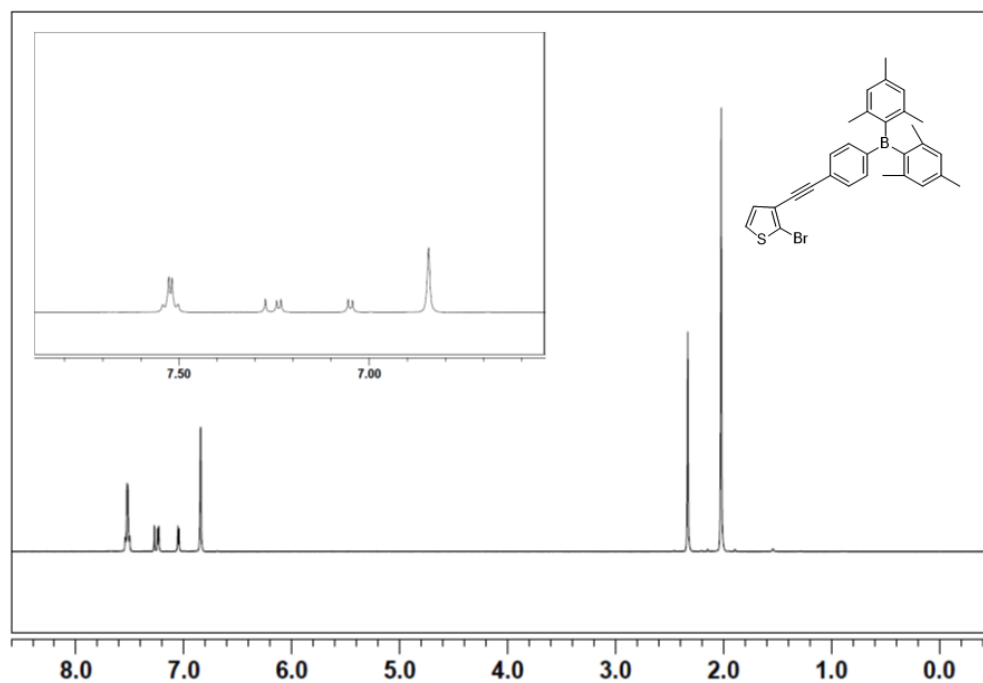
Figure 1-32 ^{1}H NMR spectrum of **1-Br** in CDCl$_3$ (δ, ppm).
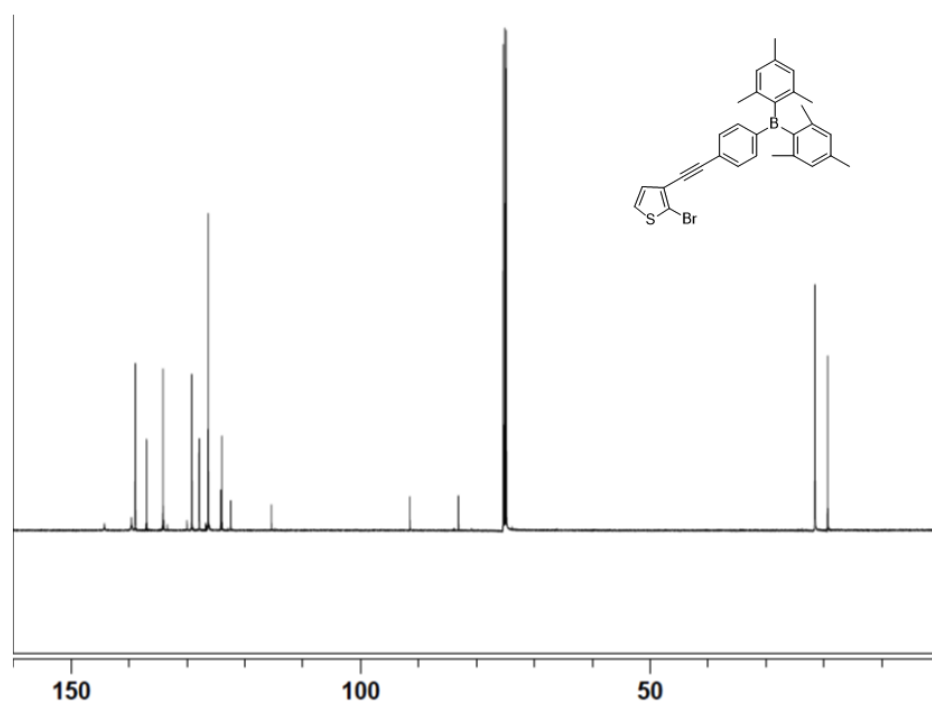
Figure 1-33. ^{13}C NMR spectrum of **1-Br** in CDCl$_3$ (δ, ppm).
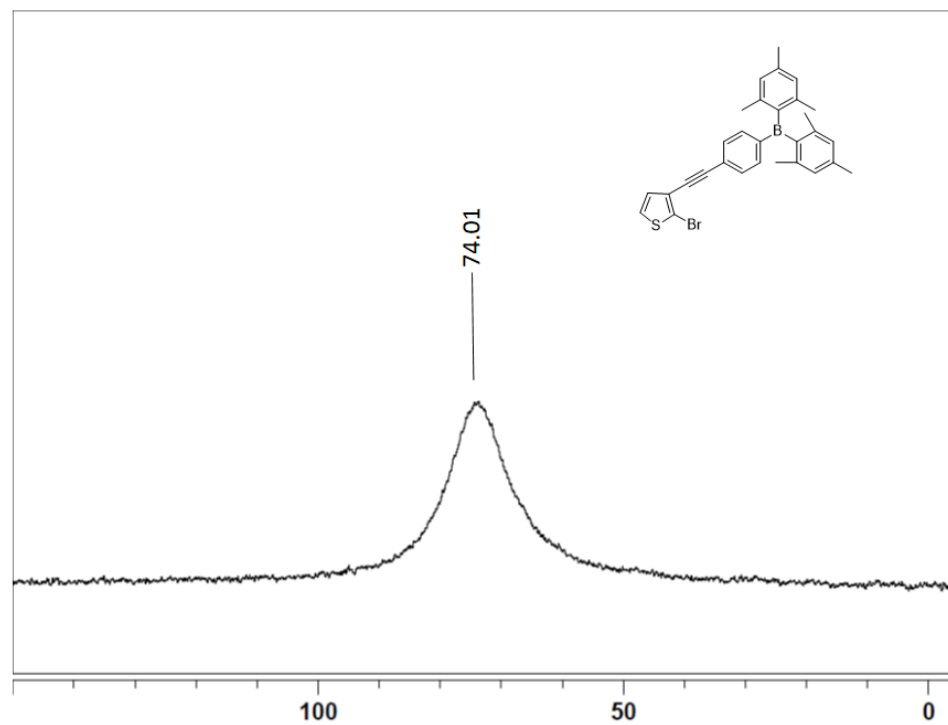
Figure 1-34. ^{11}B NMR spectrum of **1-Br** in CDCl$_3$ (δ, ppm).
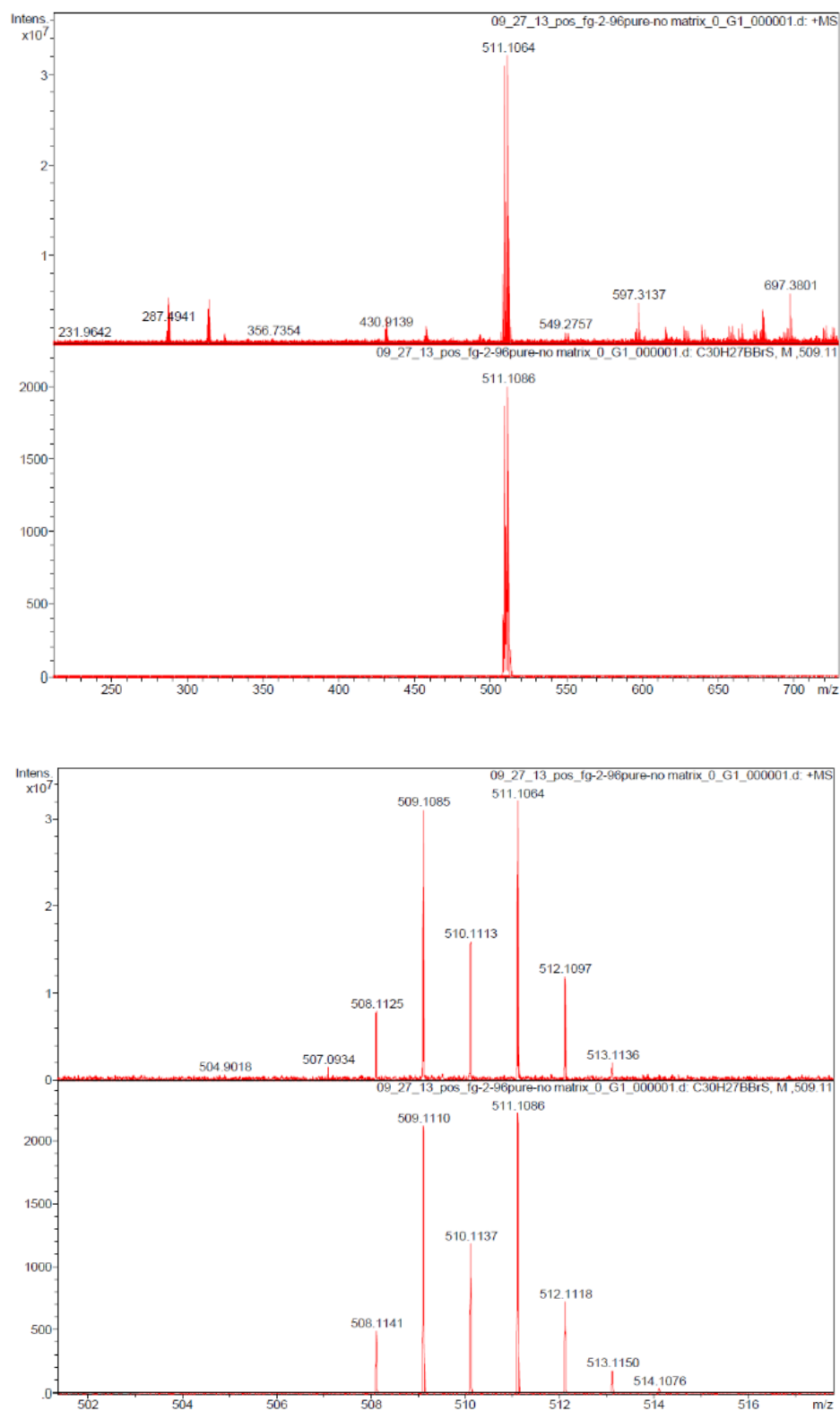
Figure 1-35. High resolution (pos. mode) MALDI-MS data of **1-Br** (m/z, a.u.).
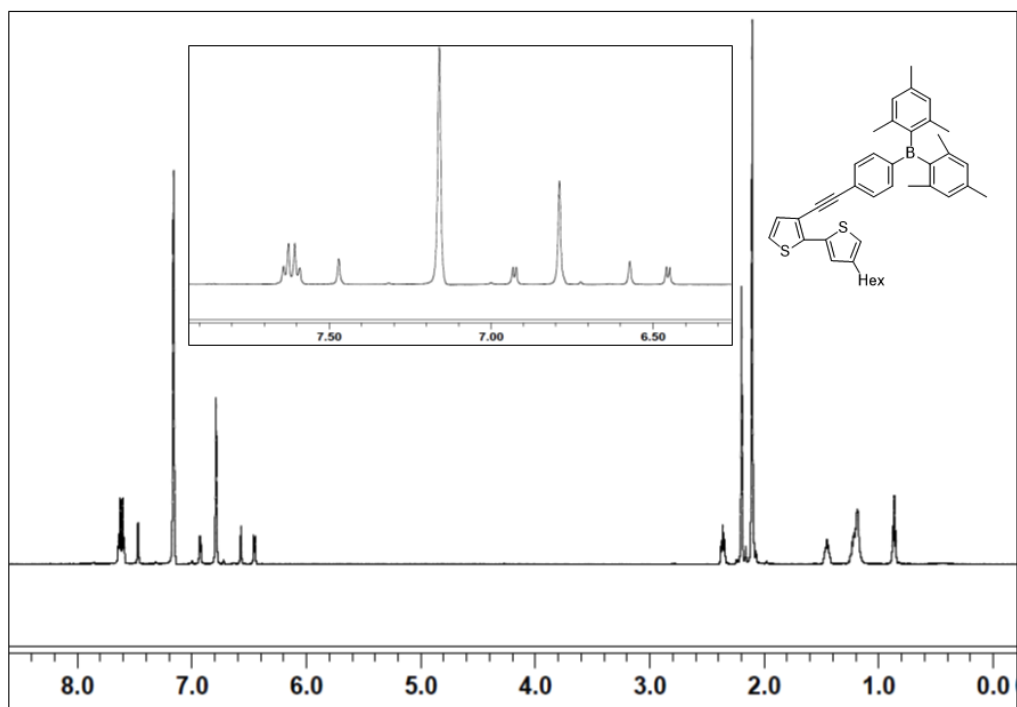
Figure 1-36. ^{1}H NMR spectrum of **2** in C$_6$D$_6$ (δ, ppm).
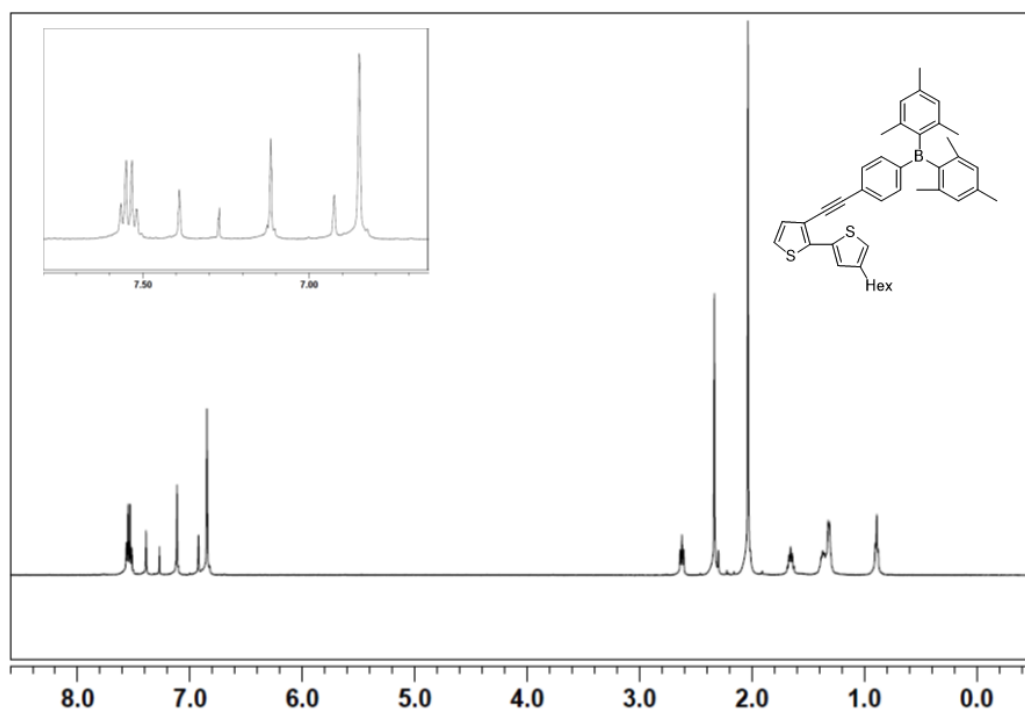
Figure 1-37. ^{1}H NMR spectrum of **2** in CDCl$_3$ (δ, ppm).
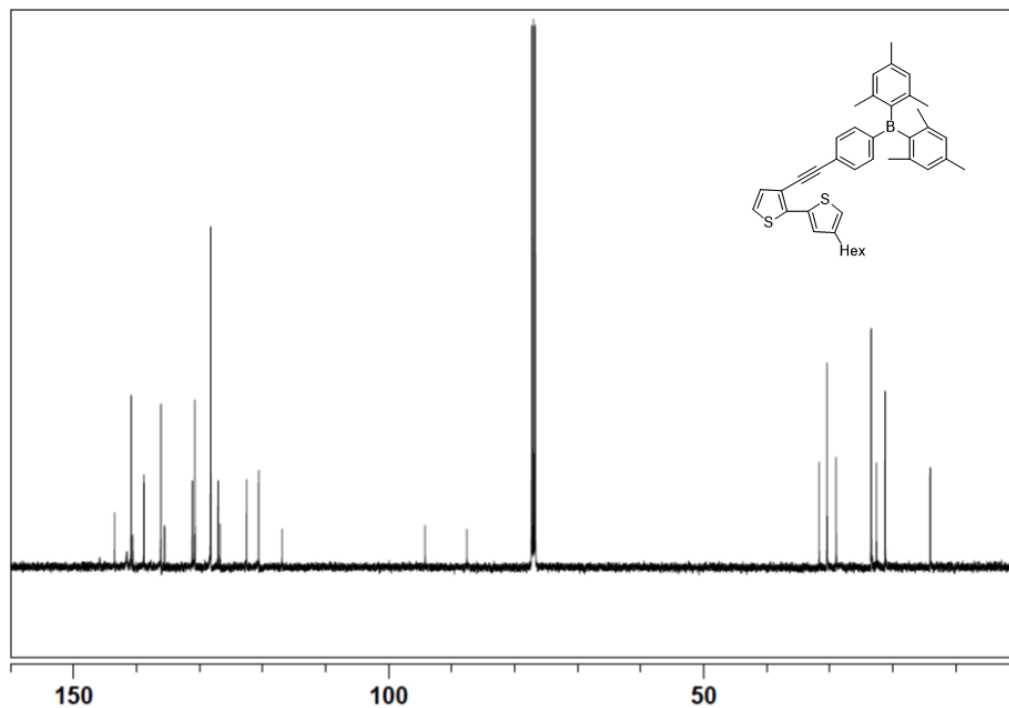
Figure 1-38. ^{13}C NMR spectrum of **2** in CDCl$_3$ (δ, ppm).
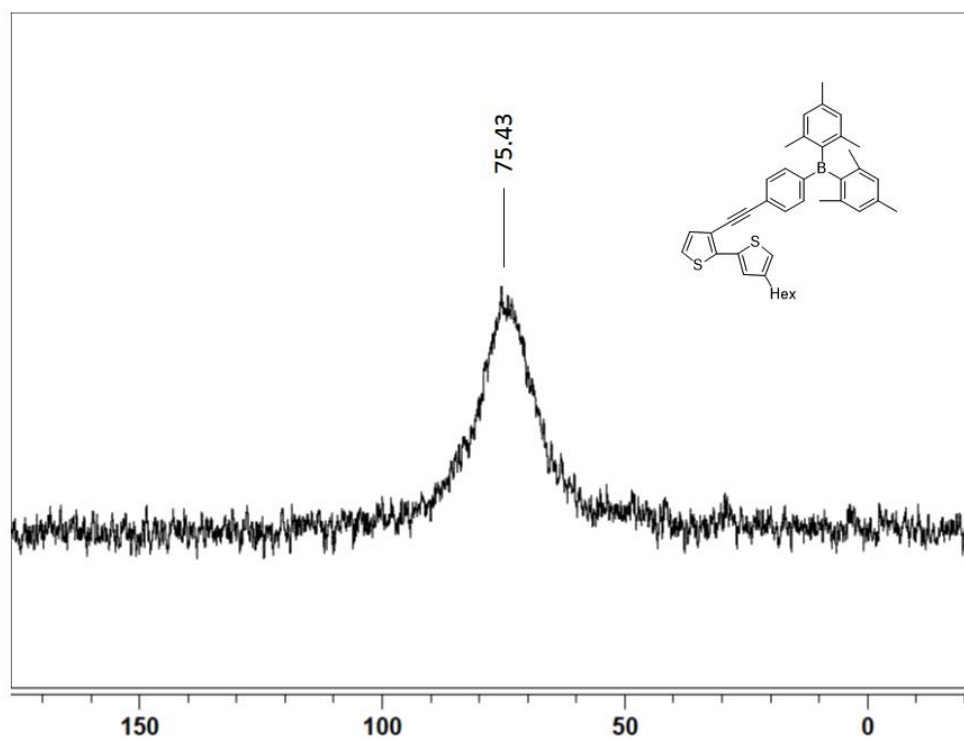
Figure 1-39. ^{11}B NMR spectrum of **2** in CDCl$_3$ (δ, ppm).
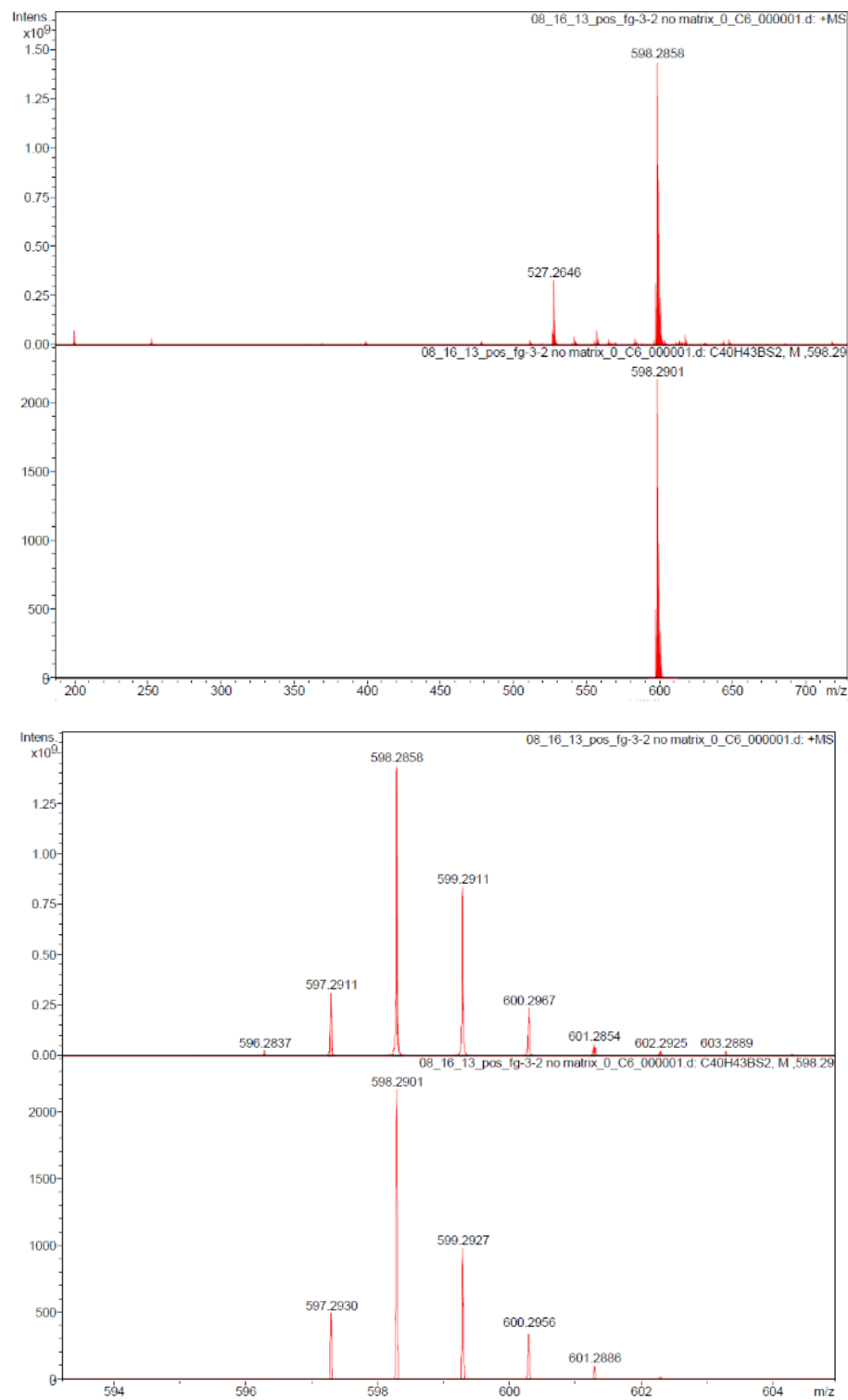
Figure 1-40. High resolution (pos. mode) MALDI-MS data of **2** (m/z, a.u.).
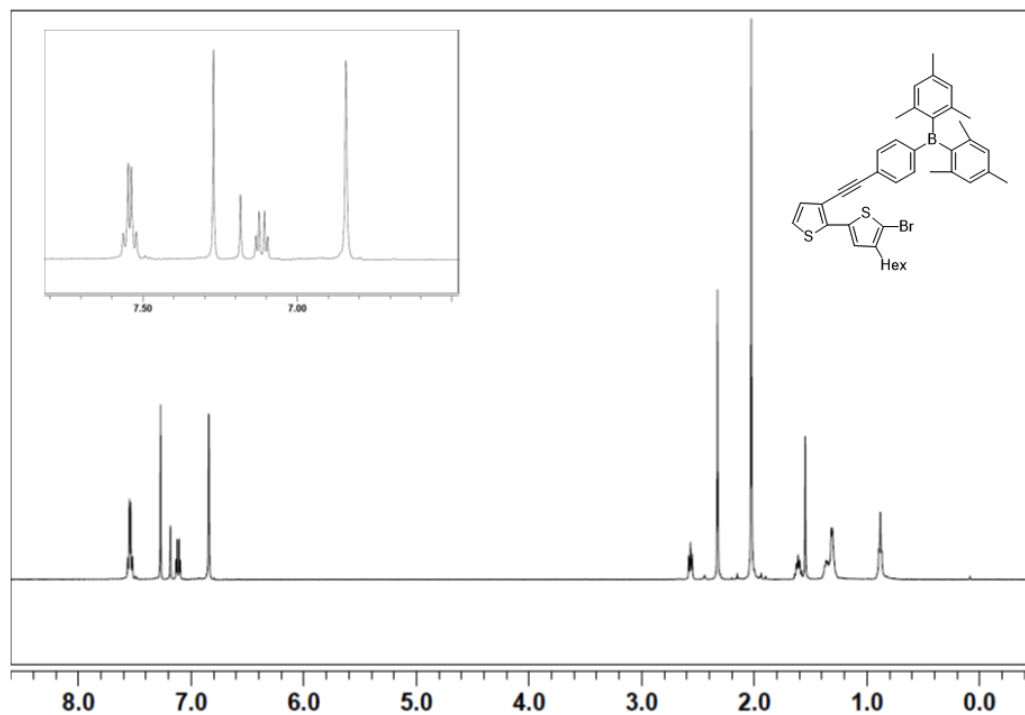
Figure 1-41. ¹H NMR spectrum of **2-Br** in CDCl₃ (δ, ppm).
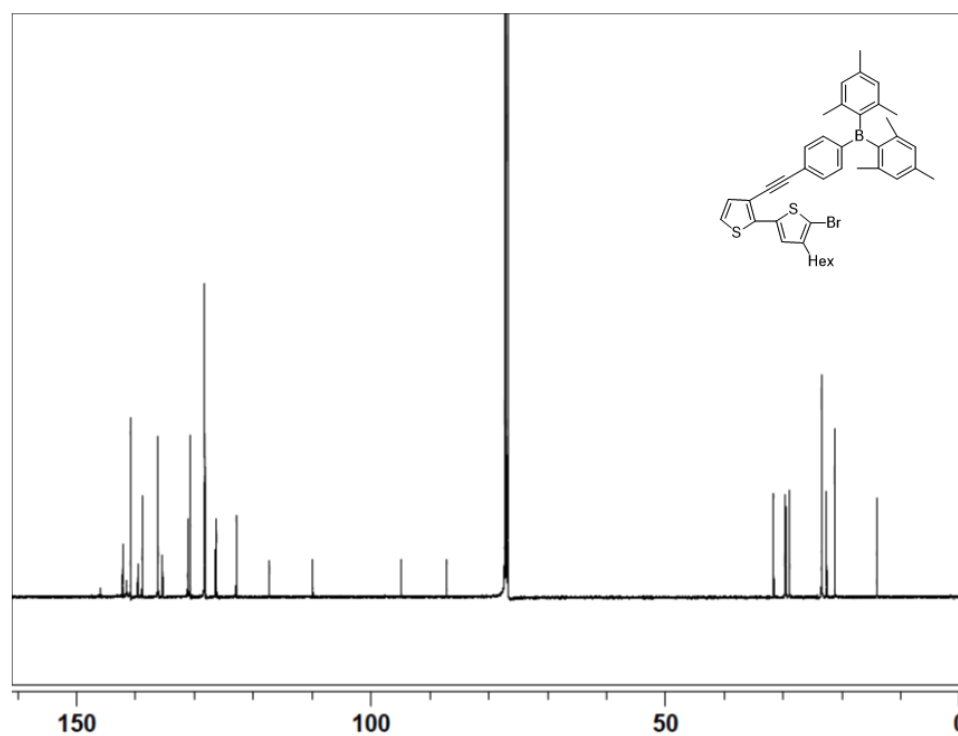
Figure 1-42. ¹³C NMR spectrum of **2-Br** in CDCl₃ (δ, ppm).
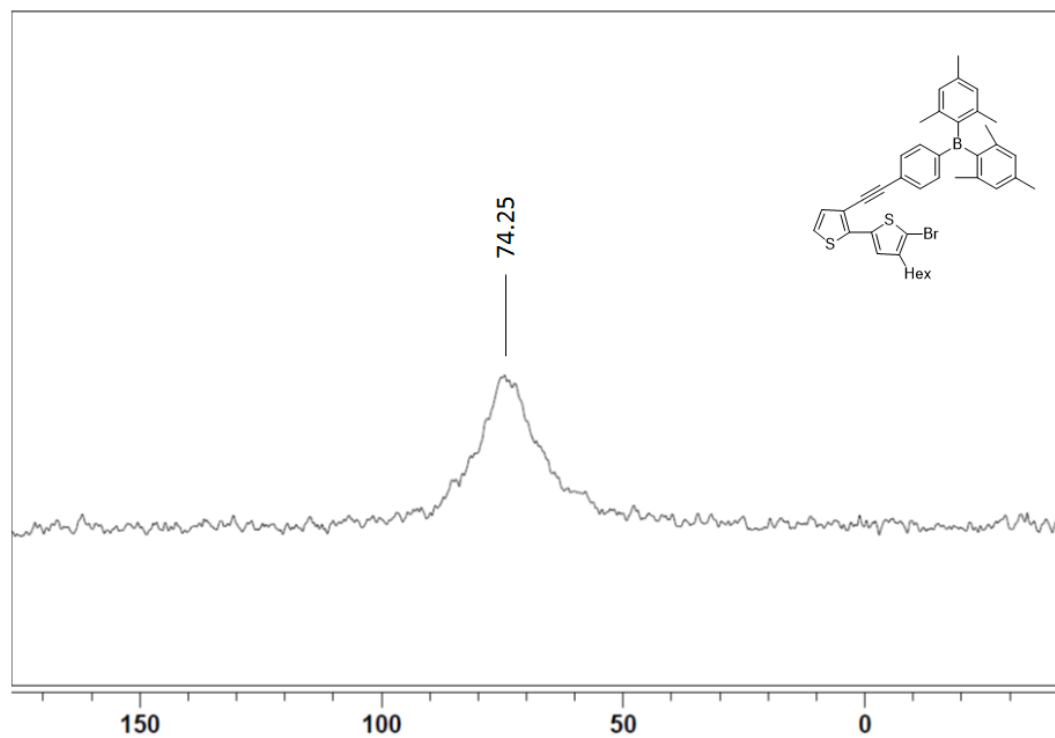
Figure 1-43. ^{11}B NMR spectrum of **2-Br** in CDCl$_3$ (δ, ppm).
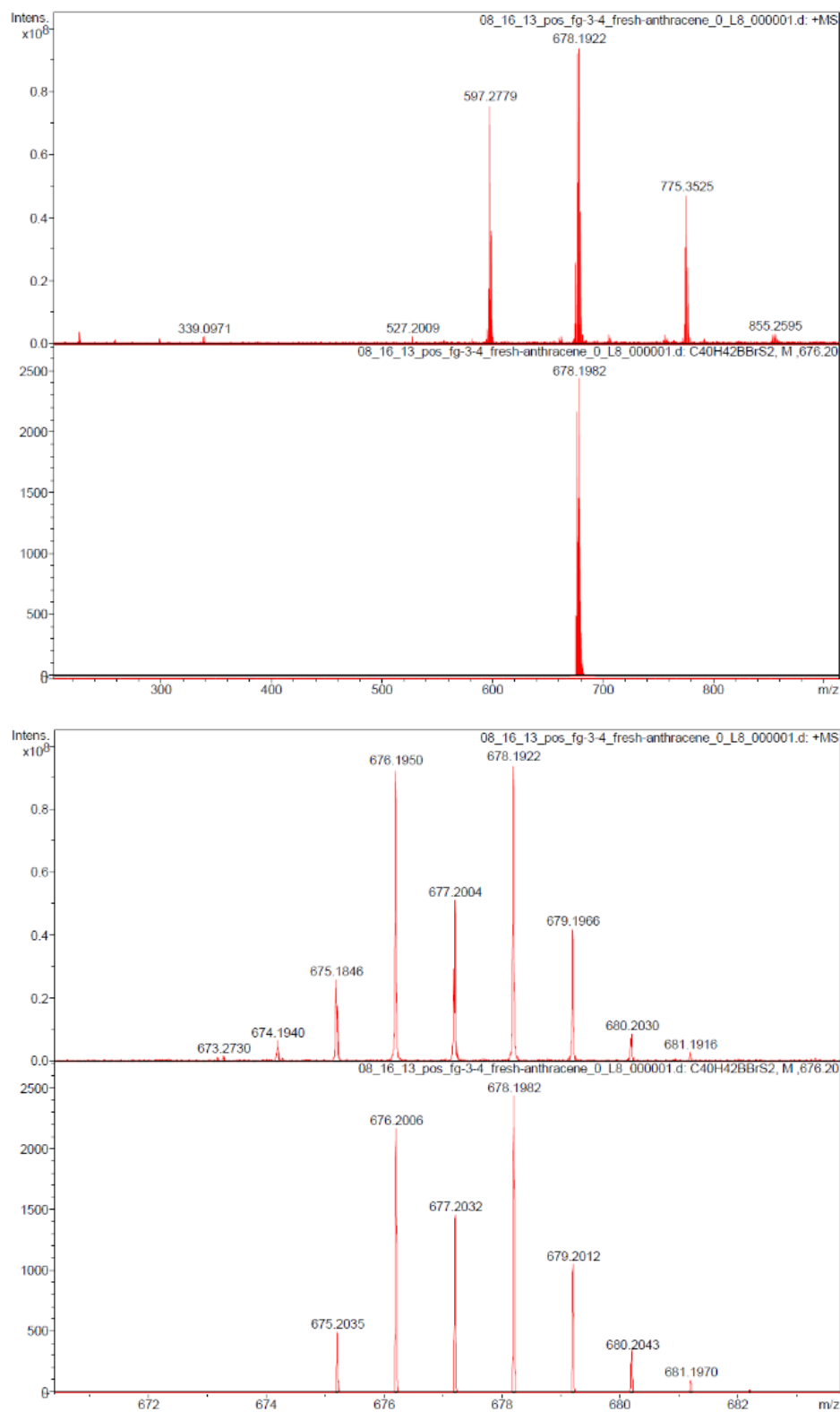
Figure 1-44. High resolution (pos. mode) MALDI-MS data of **2-Br** (m/z, a.u.).
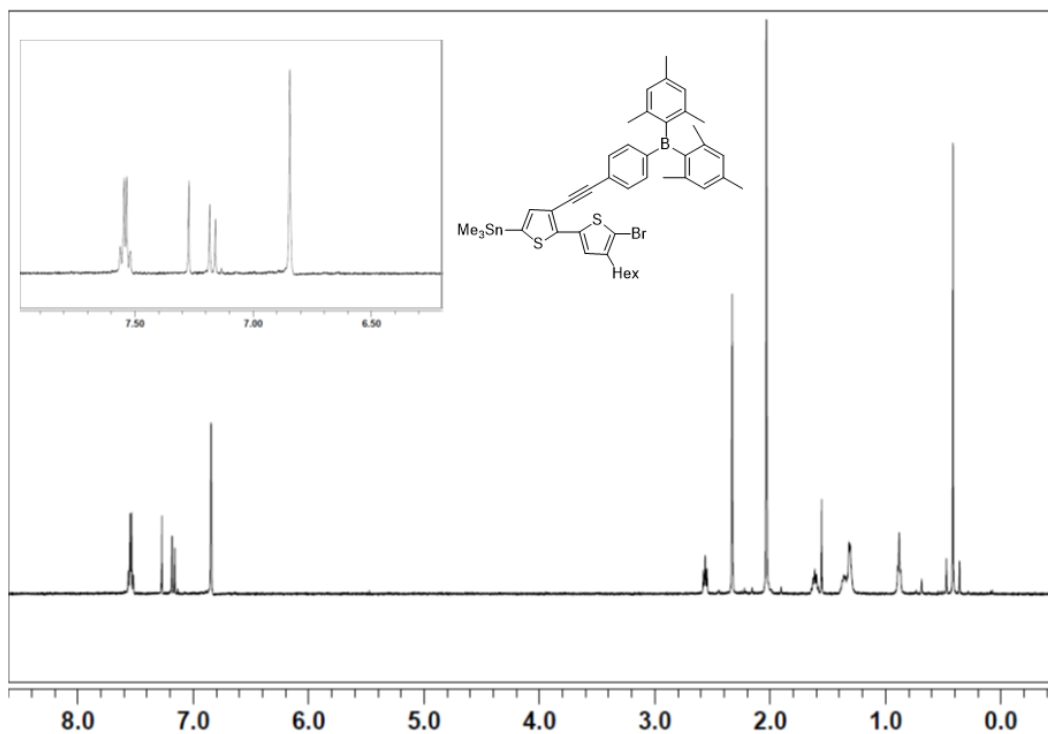
Figure 1-45. ^{1}H NMR spectrum of monomer **2-BrSn** in CDCl$_3$ (δ, ppm).
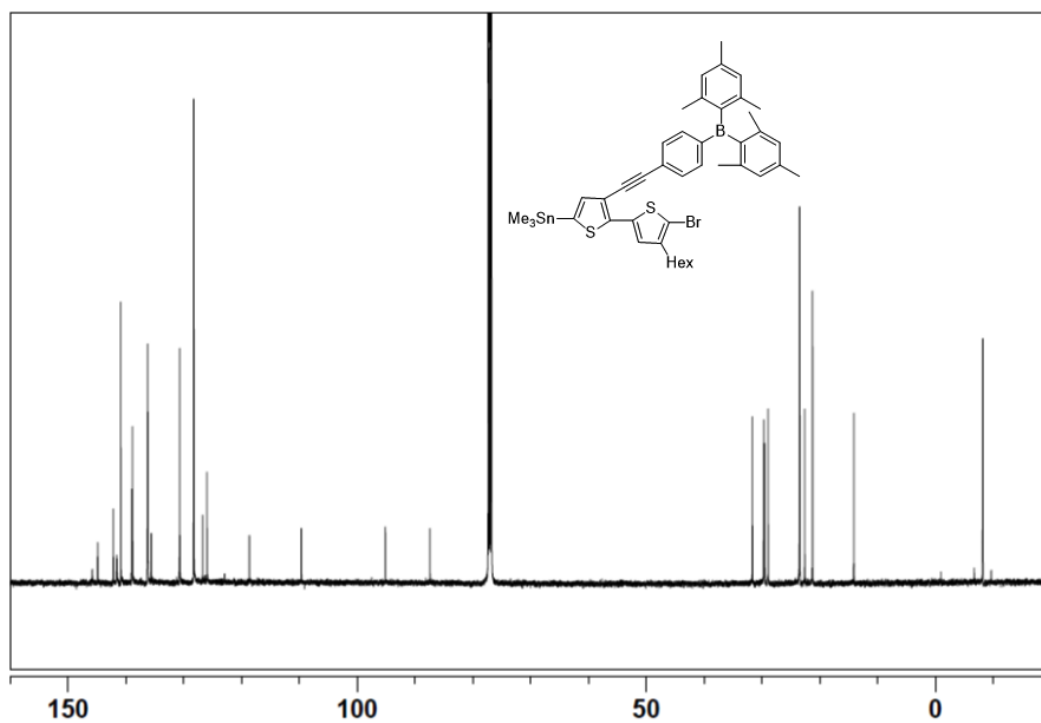
Figure 1-46. ^{13}C NMR spectrum of monomer **2-BrSn** in CDCl$_3$ (δ, ppm).
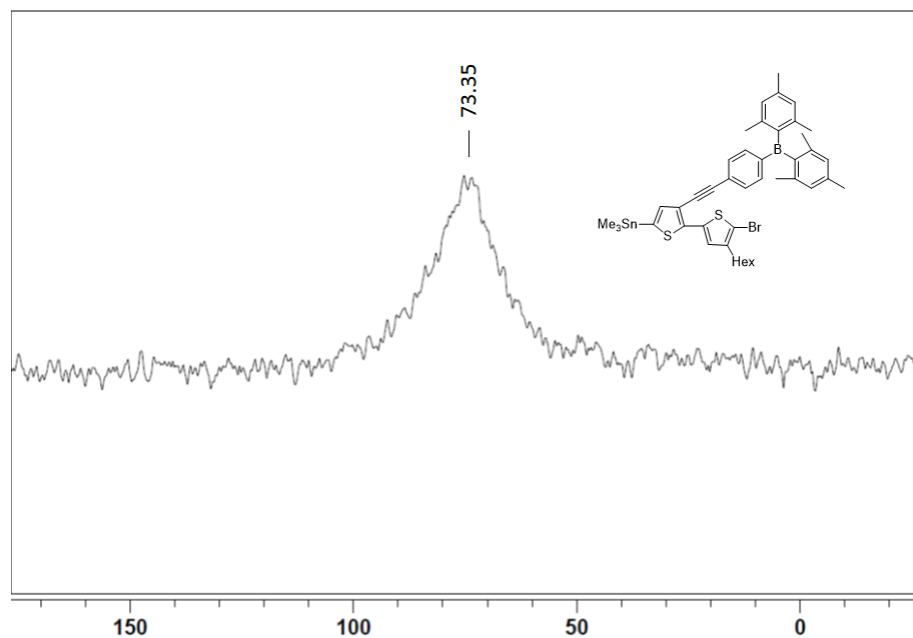
Figure 1-47. ^{11}B NMR spectrum of monomer **2-BrSn** in CDCl$_3$ (δ, ppm).
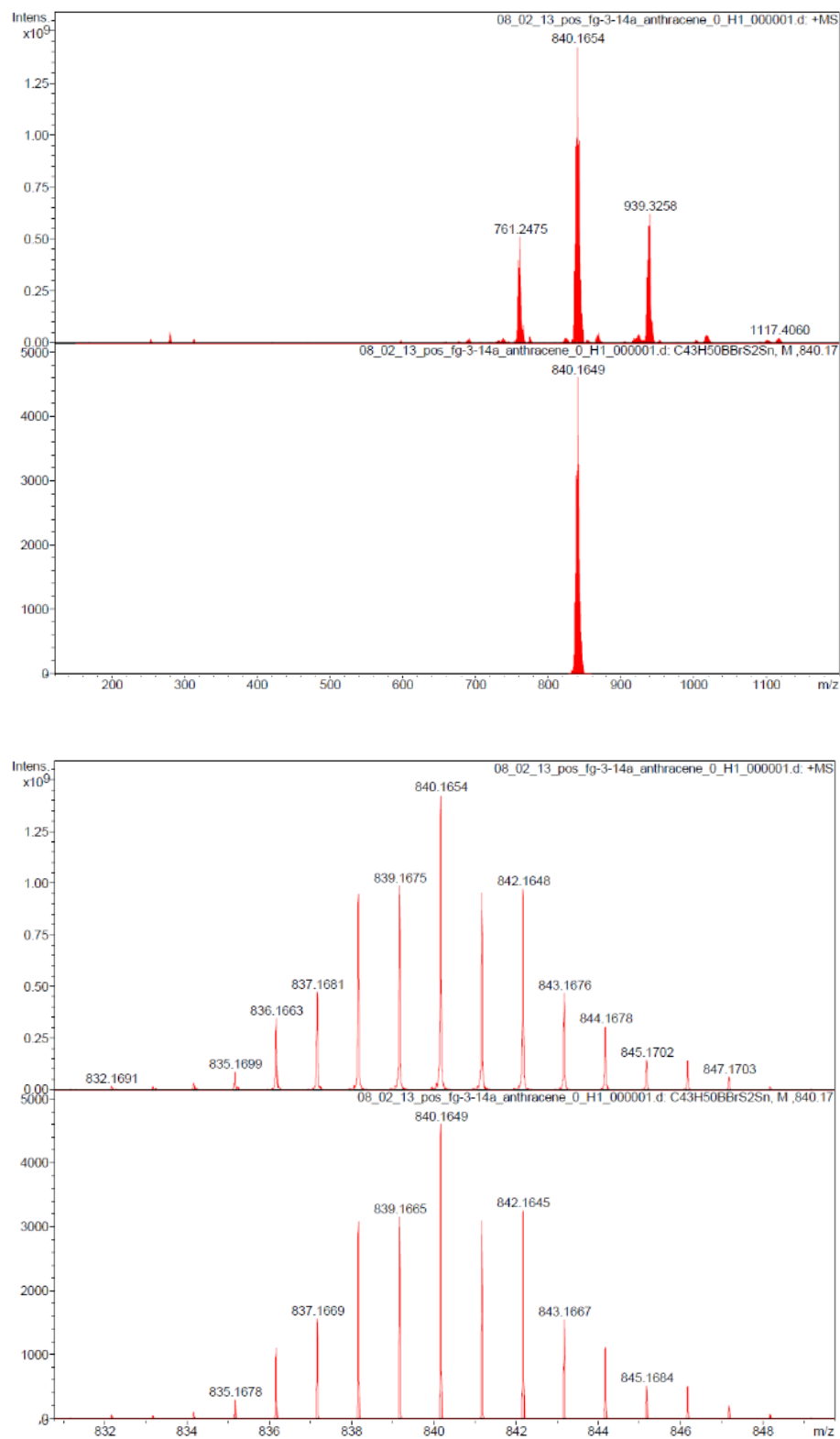
Figure 1-48. High resolution (pos. mode) MALDI-MS data of **2-BrSn** (m/z, a.u.).
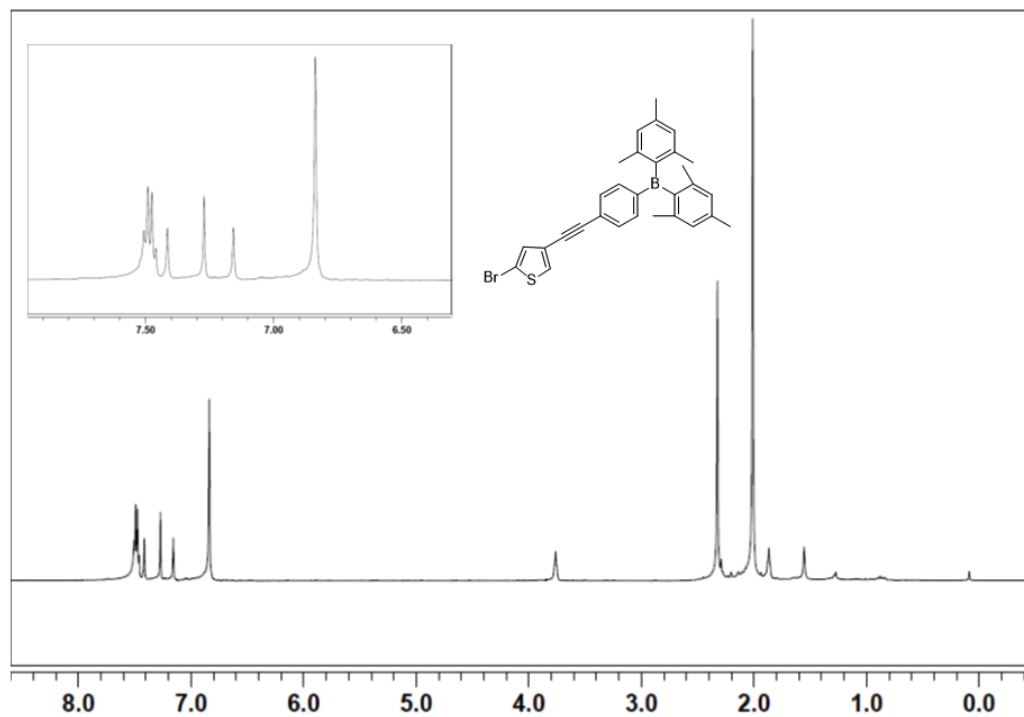
Figure 1-49. ^{1}H NMR spectrum of 4-alkynyl-2-bromothiophene isomer **1-Br'** in CDCl$_3$ (δ, ppm).
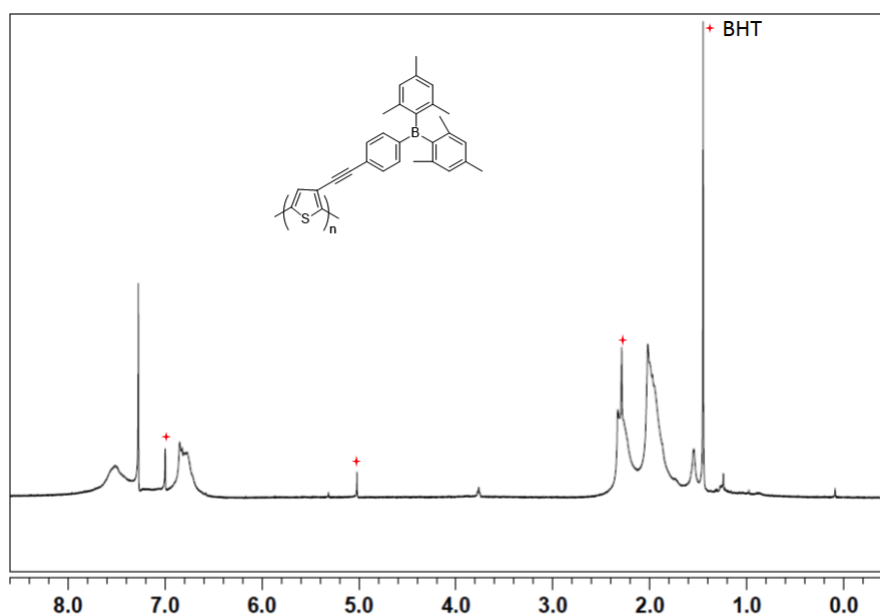
Figure 1-50. ^{1}H NMR spectrum of polymer **P1** (Kumada) in CDCl$_3$ (δ, ppm). The signals marked with red asterisks are due to BHT inhibitor introduced during preparative column separation on Biobeads ^{TM}.
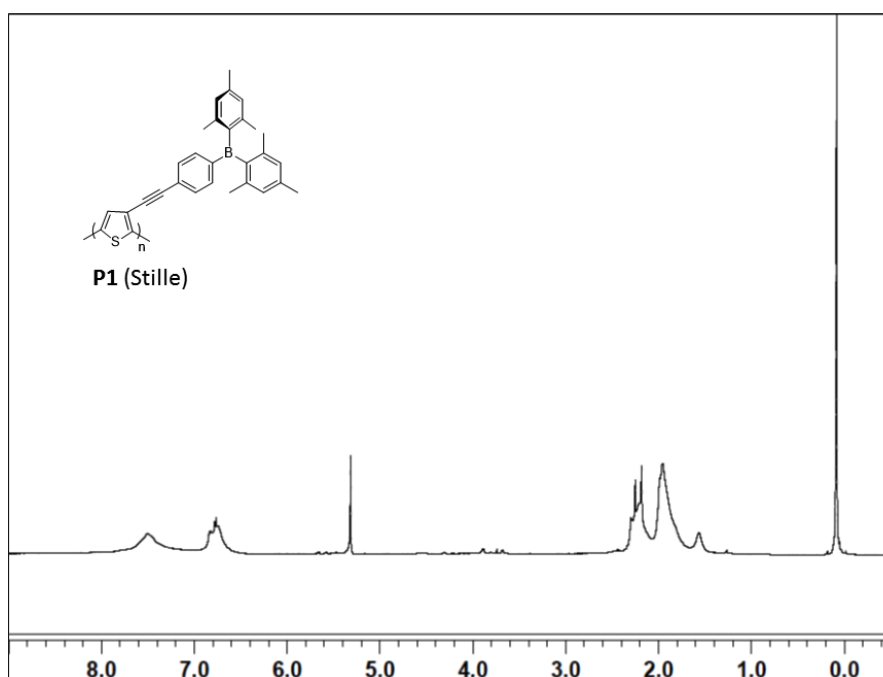
Figure 1-51. ^{1}H NMR spectrum of rr-**P1** (Stille) in CD$_2$Cl$_2$ (δ, ppm).
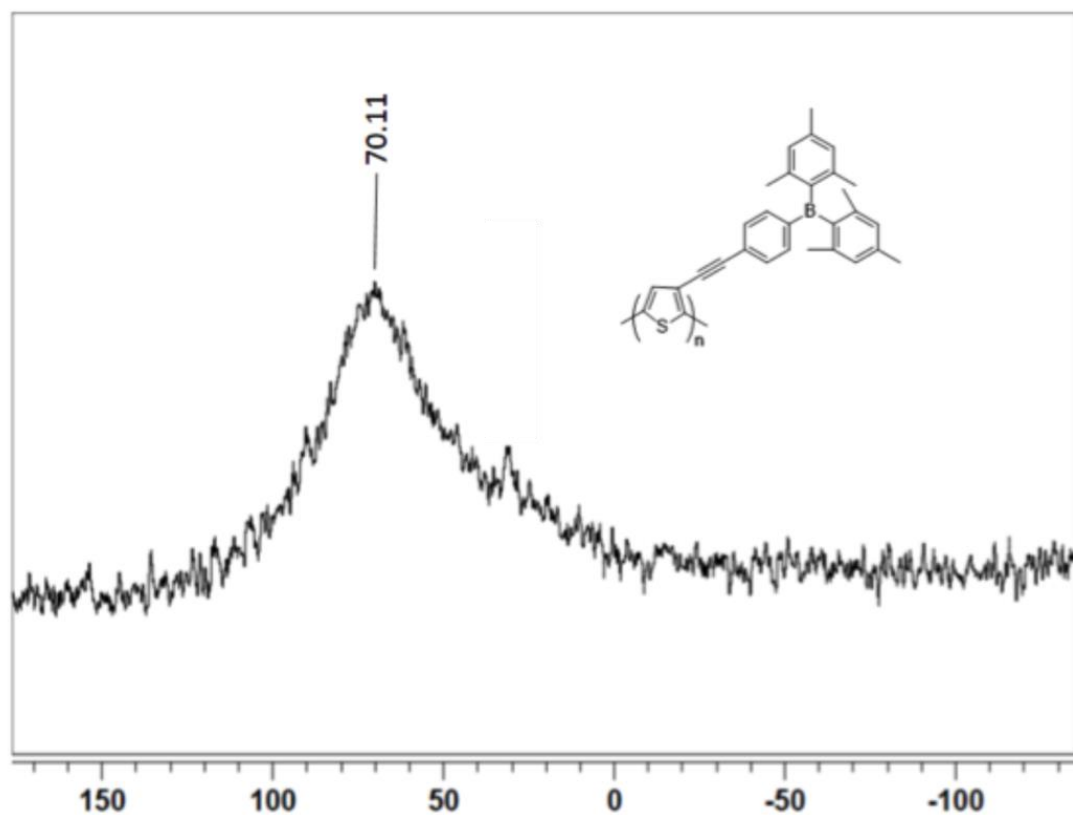
Figure 1-52. ^{11}B NMR spectrum of polymer **P1** (Kumada) in CDCl$_3$ (δ, ppm).
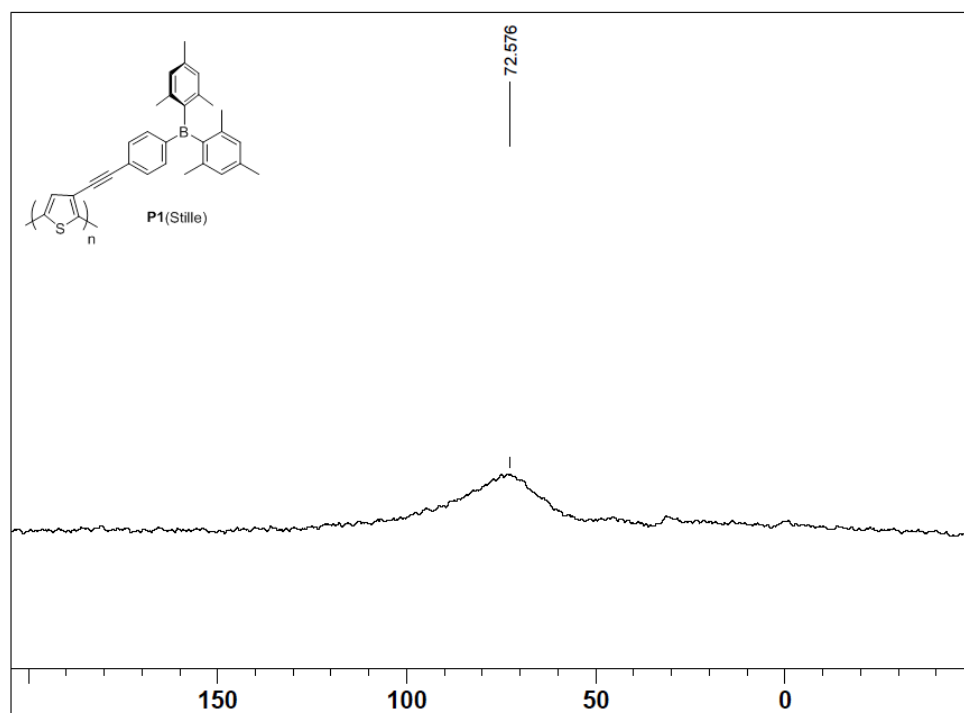
Figure 1-53. ^{11}B NMR spectrum of rr-**P1** (Stille) in CD$_2$Cl$_2$ (δ, ppm).
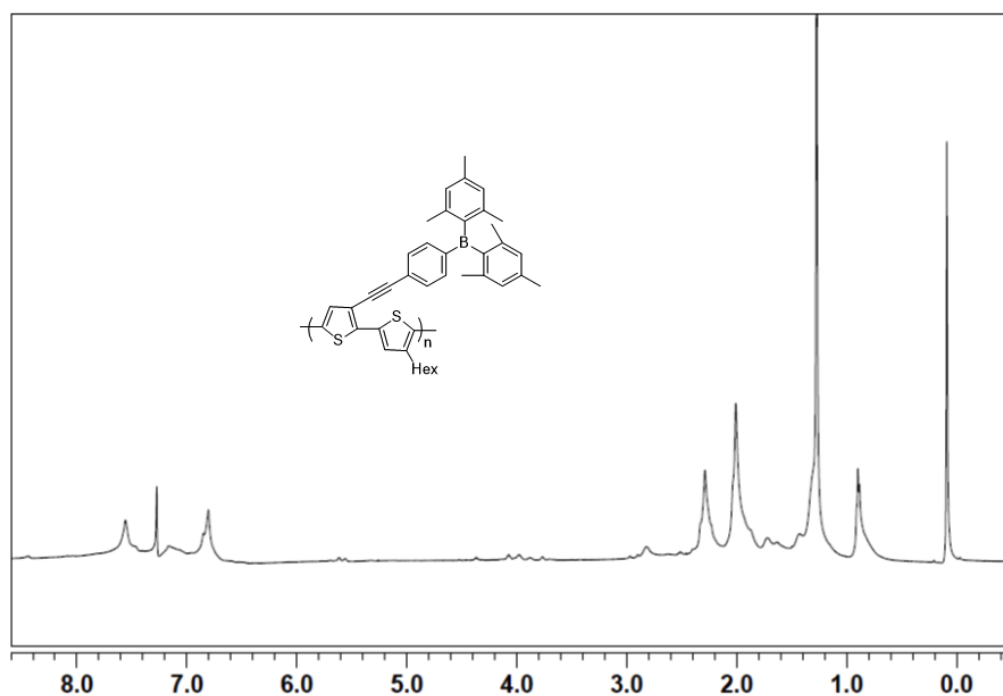
Figure 1-54.   ¹H NMR spectrum of polymer rr-**P2** in CDCl₃ (δ, ppm).
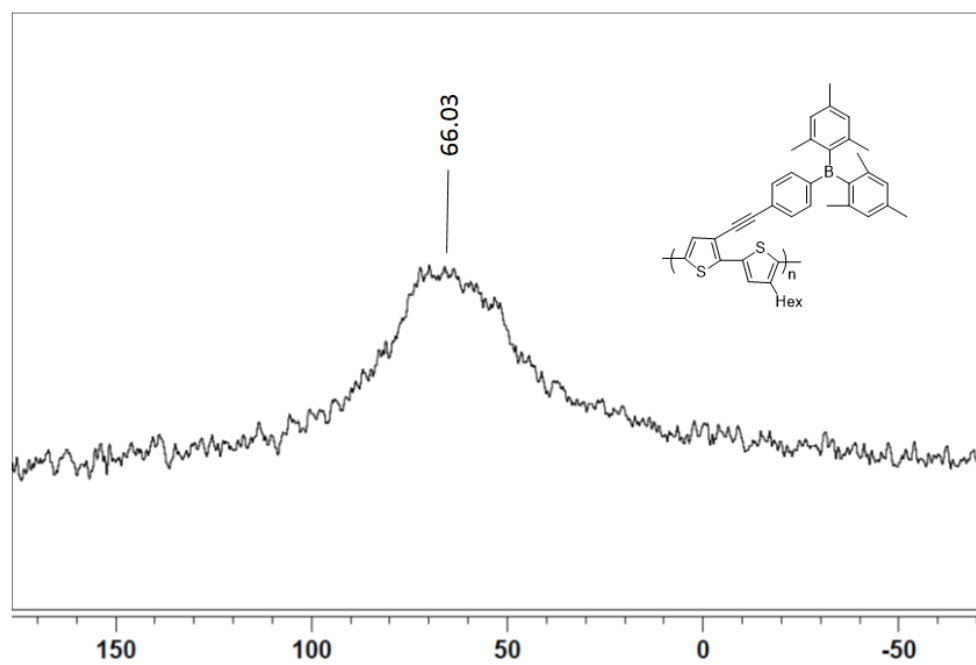
Figure 1-55   ¹¹B NMR spectrum of polymer rr-**P2** in CDCl₃ (δ, ppm).

a)

rr-**P1** (Stille)   **P1** (Kumada)

b)

rr-**P2** (Stille)
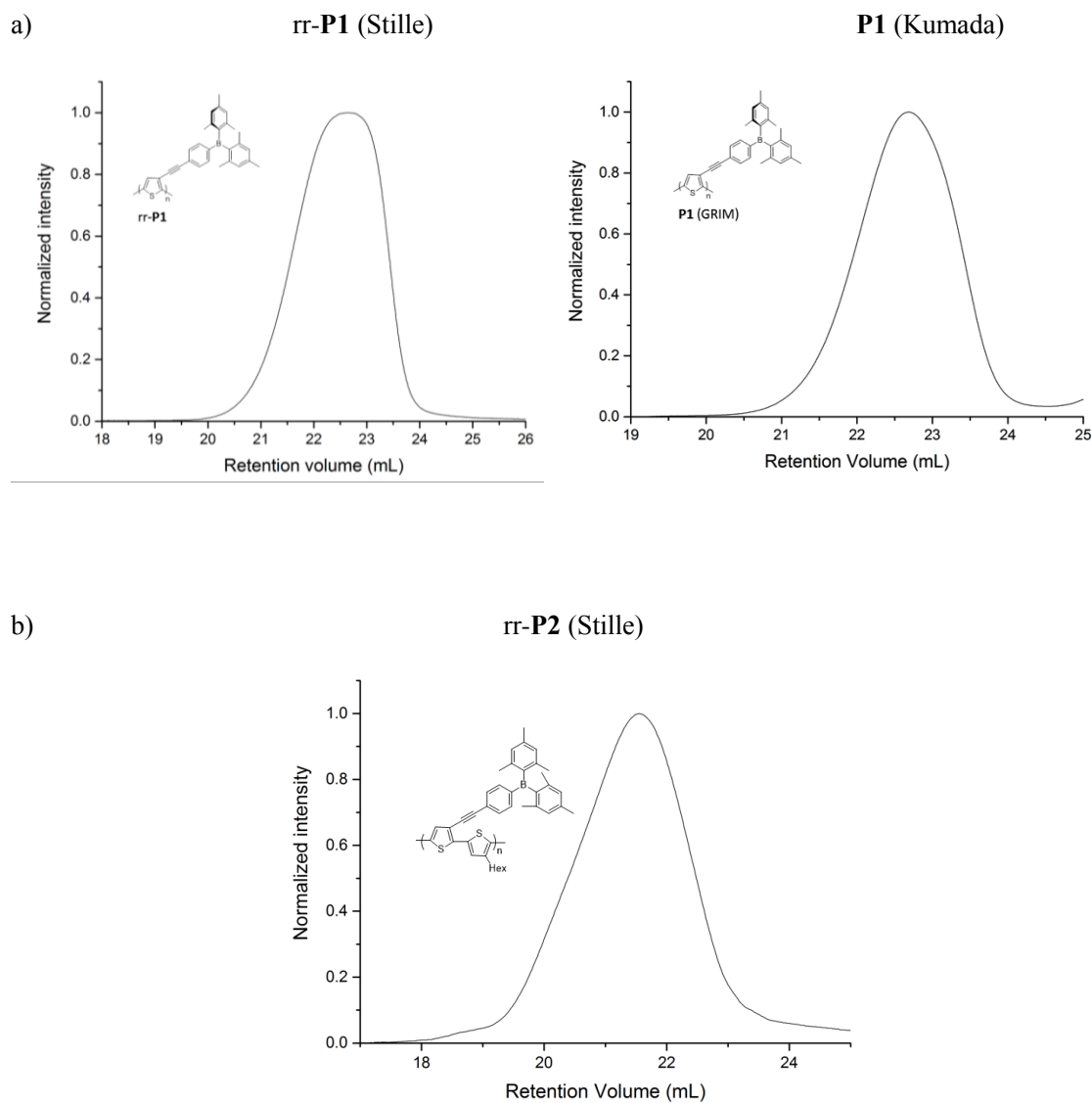
Figure 1-56. GPC-RI traces of (a) polymers **P1** and rr-**P1**; (b) polymer rr-**P2** in THF (1 mL/min).
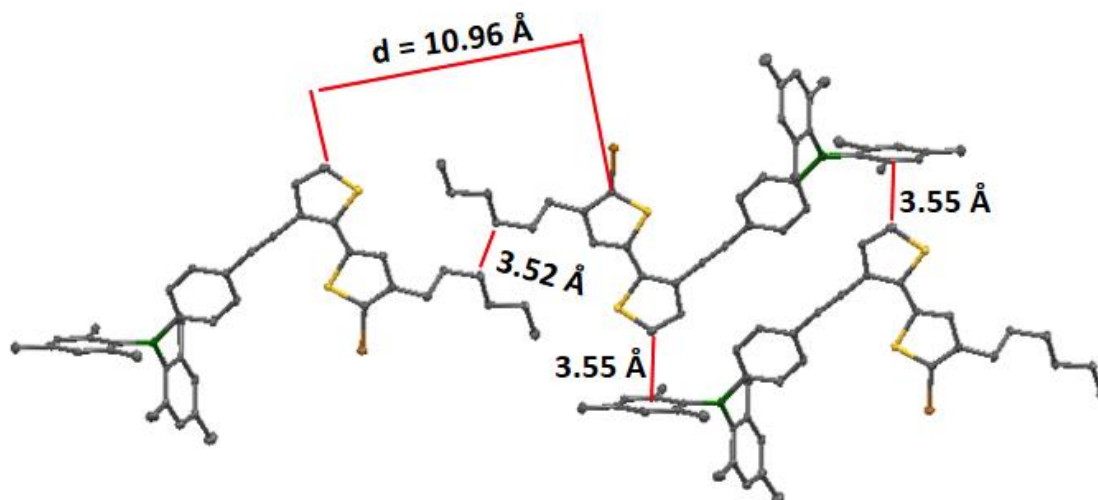
Figure 1-57. Extended structure of compound **2-Br** in the solid state. An intricate three-dimensional layered structure is observed that mimics a crystalline polymer with interdigitated side chains (3.52 Å) and features CH-π interactions (3.55 Å) between thiophene C-H and mesityl groups. The chain-chain distance (d) of 10.96 Å in **2-Br** is shorter than what is found for polymers with shorter side chains such as pBTTT-C6 (d = 13.5 Å)[32] and poly(3,6-dihexyl[2,2′]bi[thieno[3,2-b]thiophene]) (PDHTTC6) (d = 13 Å)[33] or non-interdigitating rr-P3HT (d = 14.4Å).[32] This suggests that the arrangement of the bithiophenes and the side chains resembles an interdigitated polymer, which allows maximum packing density of the pseudopolymer chains.
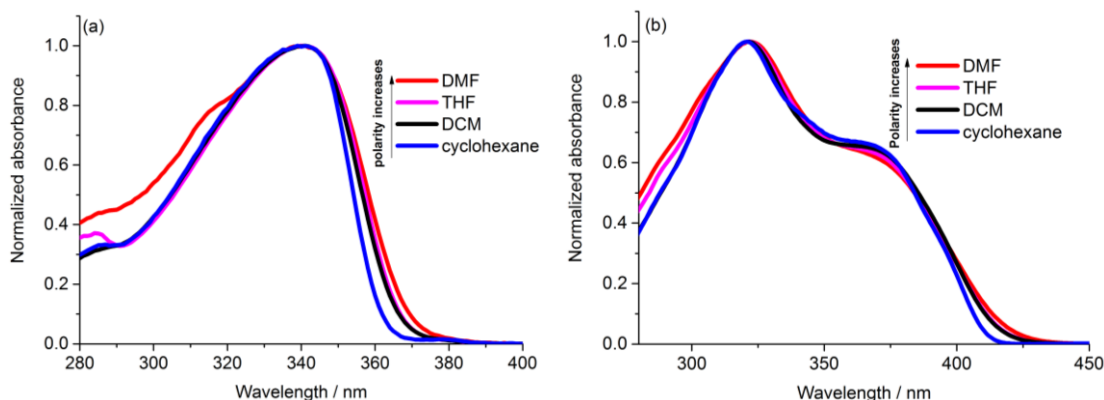
Figure 1-58. Normalized UV-vis spectra of (a) **1** and (b) **2** in different solvents.

Table 1-7. Comparison of experimental and calculated HOMO/LUMO energy levels.

	1 and **1-th** / eV	**2** and **2-th** / eV	**3-th** / eV
LUMO (exp) [a]	-2.50	-2.58	N/A
HOMO (exp) [a]	-6.15	-5.93	N/A
LUMO (calcd) [b]	-1.93	-2.26	-2.12
HOMO (calcd) [b]	-5.71	-5.59	-5.43

[a] LUMO energy determined using the equation $E_{LUMO} = -(4.8 + E_{vs.Fc})$, see ref. [34]; HOMO energy determined by $LUMO_{CV}$-$\Delta E_{opt\ gap}$

[b] Calculated orbital energies using DFT methods (B3LYP/6-31g(d)).

Table 1-8 Comparison of HOMO/LUMO orbital plots for compounds **1-th**, **2-th** and **3-th** (B3LYP/6-31g(d))

HOMO (-5.71 eV)	LUMO (-1.93 eV)
HOMO (-5.59 eV)	LUMO (-2.26 eV)
HOMO (-5.43 eV)	LUMO (-2.12 eV)
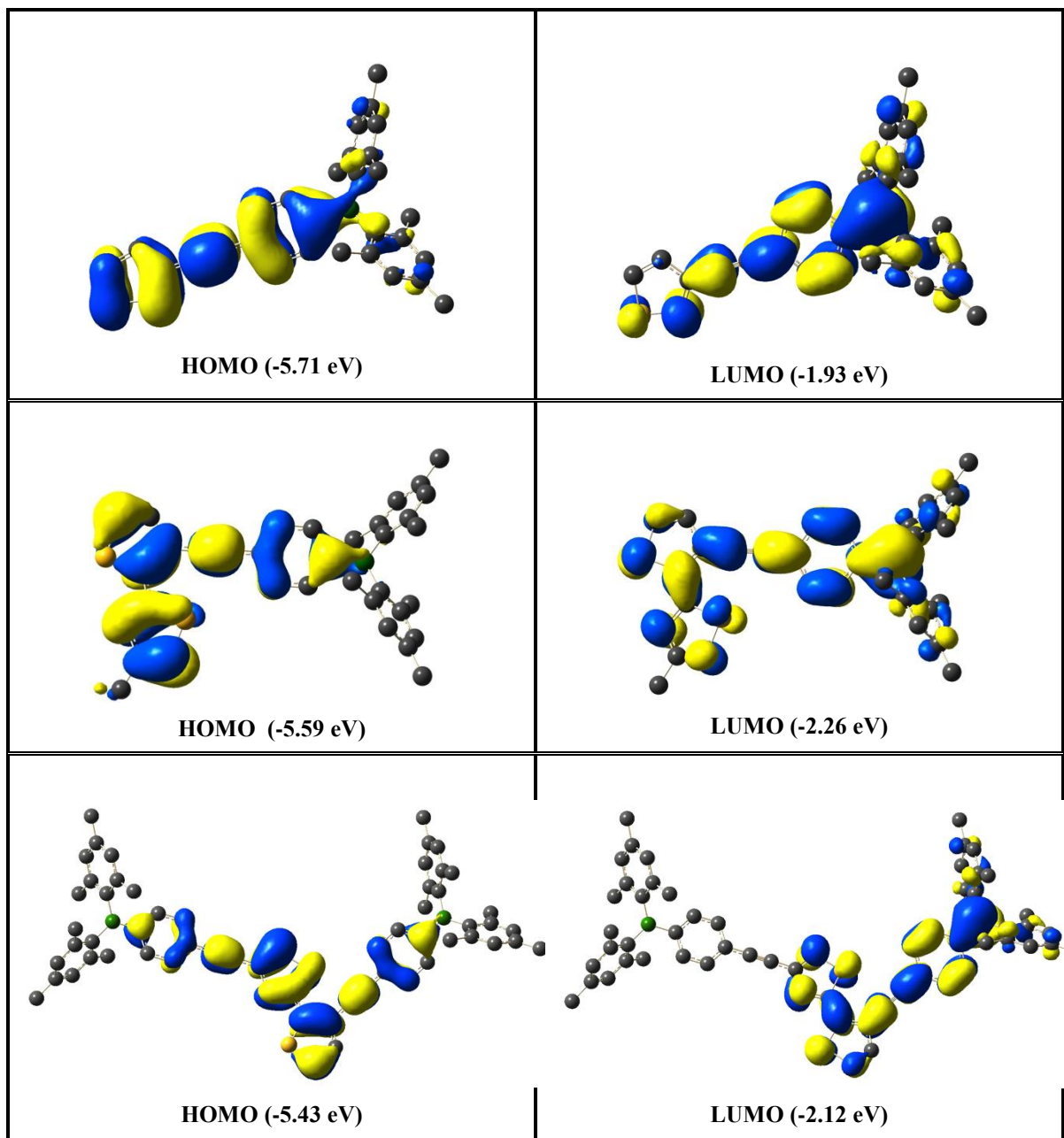
Table 1-9.   Additional orbital plots for compound **2-th** (B3LYP/6-31g(d))

LUMO (-2.26 eV)	**LUMO+1 (-1.57 eV)**
HOMO (-5.59 eV)	**HOMO-1 (-6.22 eV)**
HOMO-2 (-6.27 eV)	**HOMO-3 (-6.35 eV)**
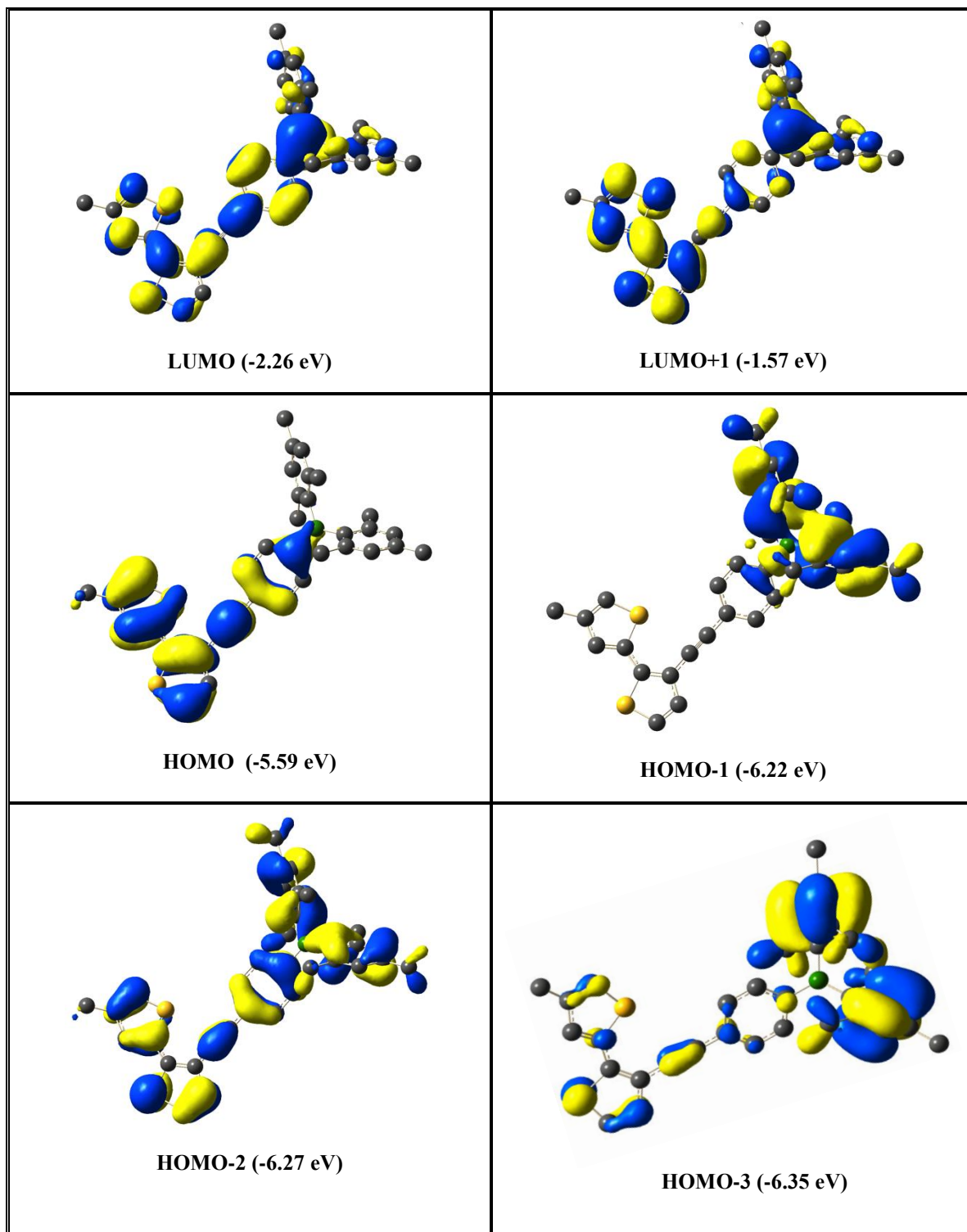
Table 1-10. Additional orbital plots for compound **3-th** (B3LYP/6-31g(d))

LUMO+1 (-1.93 eV)

LUMO+2 (-1.42 eV)

HOMO (-5.43 eV)

LUMO (-2.12 eV)

HOMO-2 (-6.27 eV)

HOMO-1 (-6.22 eV)
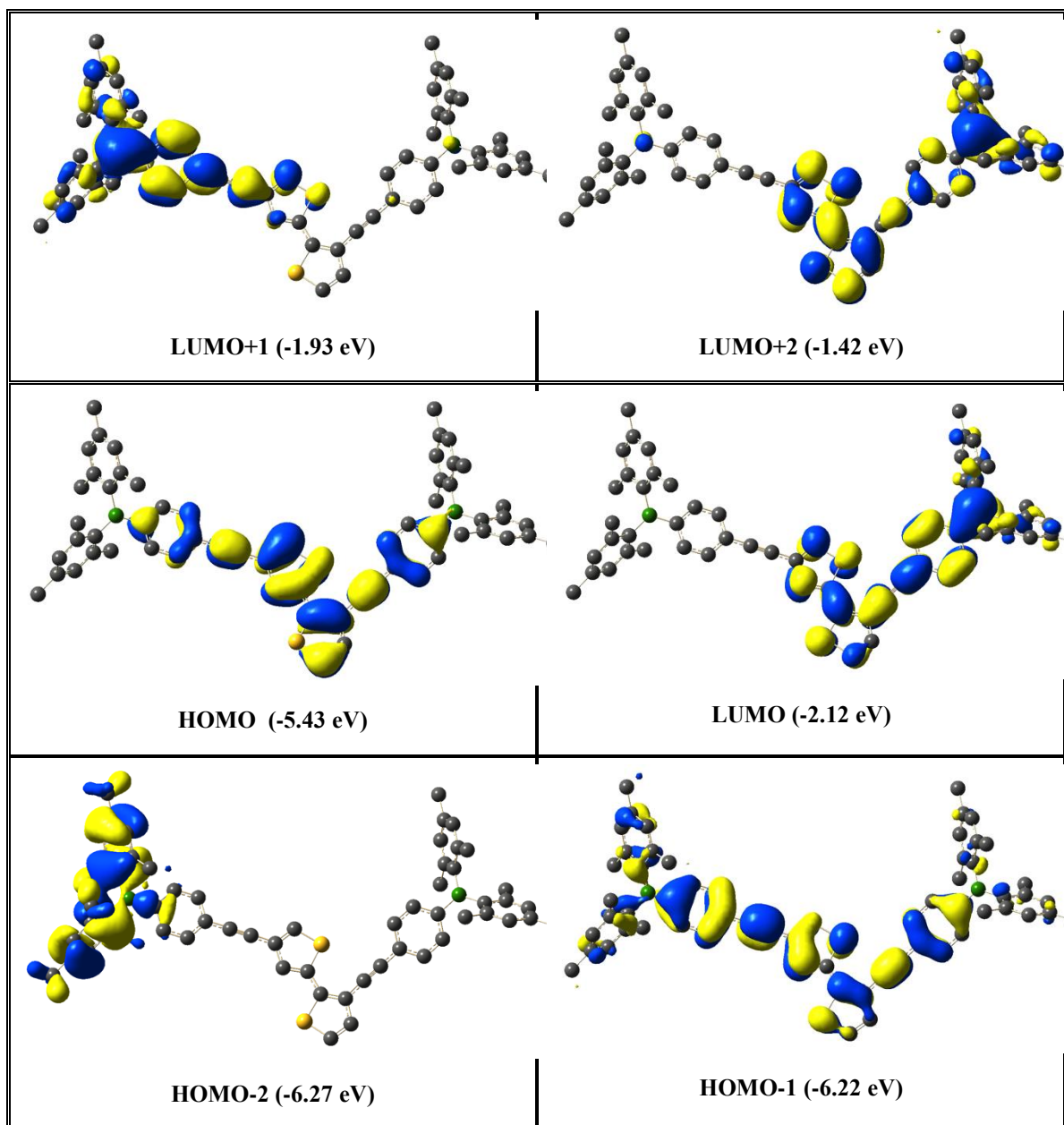
Table 1-11. DFT calculation of **1-th** (B3LYP/6-31g(d))
Standard orientation: (Ground State)

Center Number	Atomic Number	Atomic Type	Coordinates (Angstroms) X	Y	Z
1	6	0	6.577224	-0.086797	0.035859
2	6	0	7.361843	-1.163685	0.588131
3	6	0	8.703196	-0.954006	0.478014
4	16	0	9.055202	0.559649	-0.300551
5	6	0	5.159074	-0.060994	0.024779
6	6	0	3.942200	-0.057944	0.025004
7	6	0	2.519897	-0.043731	0.019651
8	6	0	1.812893	1.042980	-0.536813
9	6	0	0.424392	1.054236	-0.525330
10	6	0	-0.328805	-0.014561	0.008551
11	6	0	0.398072	-1.098531	0.548156
12	6	0	1.786449	-1.115608	0.570463
13	5	0	-1.898740	0.002288	0.002272
14	6	0	-2.676526	-1.378226	0.046421
15	6	0	-2.645006	1.399932	-0.049057
16	6	0	-3.582629	1.699216	-1.075463
17	6	0	-4.208553	2.948528	-1.114141
18	6	0	-3.966776	3.930057	-0.150171
19	6	0	-3.063091	3.627406	0.869010
20	6	0	-2.392529	2.400613	0.927073
21	6	0	-3.630593	-1.656693	1.063499
22	6	0	-4.285846	-2.891070	1.094660
23	6	0	-4.057905	-3.876957	0.131774
24	6	0	-3.137275	-3.594639	-0.878052
25	6	0	-2.437525	-2.383906	-0.928084
26	6	0	-4.768682	-5.207454	0.193893
27	6	0	-1.453258	-2.201823	-2.069379
28	6	0	-3.951337	-0.660006	2.158661
29	6	0	-1.424635	2.196178	2.078517
30	6	0	-4.645425	5.276794	-0.220828
31	6	0	-3.917098	0.708613	-2.172113
32	1	0	6.920039	-2.042826	1.040732
33	1	0	9.510459	-1.593701	0.805374
34	1	0	2.368971	1.870283	-0.966191
35	1	0	-0.099645	1.908040	-0.945887
36	1	0	-0.146543	-1.941303	0.964831
37	1	0	2.322033	-1.954116	1.004166
38	1	0	-4.913708	3.157244	-1.916100
39	1	0	-2.872130	4.366296	1.644990
40	1	0	-5.003290	-3.084008	1.889653

41	1	0	-2.955979	-4.337123	-1.652937
42	1	0	-4.211480	-5.925745	0.808709
43	1	0	-5.765140	-5.109238	0.635451
44	1	0	-4.879328	-5.649831	-0.800647
45	1	0	-1.385673	-1.167395	-2.413261
46	1	0	-0.440925	-2.500683	-1.775852
47	1	0	-1.742157	-2.819044	-2.925450
48	1	0	-3.074795	-0.439337	2.778788
49	1	0	-4.302570	0.291995	1.752512
50	1	0	-4.726140	-1.051660	2.823519
51	1	0	-0.401740	2.466507	1.794215
52	1	0	-1.705238	2.823848	2.929722
53	1	0	-1.388803	1.161416	2.426290
54	1	0	-4.748960	5.726242	0.771286
55	1	0	-4.069220	5.978746	-0.836999
56	1	0	-5.642400	5.200317	-0.665586
57	1	0	-4.300431	-0.231804	-1.767930
58	1	0	-4.672026	1.119991	-2.847833
59	1	0	-3.039451	0.461080	-2.780352
60	6	0	7.375507	0.915045	-0.480409
61	1	0	7.053218	1.832182	-0.951431

Table 1-12. TD-DFT calculation of **1-th** (CAM-B3LYP/6-31g(d))
Standard orientation: (Excited State)

Center Number	Atomic Number	Atomic Type	Coordinates (Angstroms) X	Y	Z
1	6	0	-6.573163	-0.097332	-0.033252
2	6	0	-7.369998	-1.200479	-0.518250
3	6	0	-8.699289	-0.972549	-0.417050
4	16	0	-9.037797	0.584123	0.267617
5	6	0	-5.177006	-0.078667	-0.026960
6	6	0	-3.947446	-0.072106	-0.025877
7	6	0	-2.559612	-0.055792	-0.020692
8	6	0	-1.839054	1.086949	0.445005
9	6	0	-0.472098	1.095351	0.442239
10	6	0	0.308611	-0.019295	-0.008333
11	6	0	-0.439905	-1.153332	-0.465929
12	6	0	-1.806588	-1.179572	-0.480310
13	5	0	1.845474	0.000987	-0.001233
14	6	0	2.663146	-1.357112	-0.042925
15	6	0	2.624490	1.381550	0.047613
16	6	0	3.626907	1.630513	1.025005
17	6	0	4.253738	2.868187	1.088710
18	6	0	3.960972	3.895629	0.191374
19	6	0	3.011139	3.644501	-0.791519
20	6	0	2.352483	2.421043	-0.883904
21	6	0	3.684367	-1.575977	-1.008226
22	6	0	4.344528	-2.796346	-1.067779
23	6	0	4.068282	-3.834153	-0.177108
24	6	0	3.100525	-3.611408	0.795083
25	6	0	2.408392	-2.406266	0.882963
26	6	0	4.792358	-5.149060	-0.275392
27	6	0	1.400949	-2.260543	1.995176
28	6	0	4.068777	-0.522836	-2.019265
29	6	0	1.361761	2.245936	-2.007026
30	6	0	4.648520	5.229684	0.294075
31	6	0	4.024926	0.591175	2.045046
32	1	0	-6.935015	-2.107759	-0.918041
33	1	0	-9.511451	-1.625515	-0.703971
34	1	0	-2.400279	1.946583	0.796984
35	1	0	0.053482	1.975195	0.801423
36	1	0	0.110872	-2.019431	-0.820790
37	1	0	-2.342695	-2.053120	-0.837140
38	1	0	4.997919	3.041986	1.863000
39	1	0	2.784603	4.421106	-1.518614
40	1	0	5.102512	-2.947713	-1.833359

41	1	0	2.886197	-4.396027	1.517238
42	1	0	4.401690	-5.754201	-1.102600
43	1	0	5.861447	-5.004657	-0.461269
44	1	0	4.682323	-5.735647	0.640808
45	1	0	1.467464	-1.286981	2.487054
46	1	0	0.374068	-2.348080	1.621840
47	1	0	1.543880	-3.037154	2.752112
48	1	0	3.192960	-0.121408	-2.536885
49	1	0	4.575910	0.324979	-1.550753
50	1	0	4.740375	-0.940907	-2.774389
51	1	0	0.328856	2.309317	-1.645600
52	1	0	1.493883	3.023152	-2.765305
53	1	0	1.457898	1.272559	-2.494481
54	1	0	4.539344	5.807882	-0.627570
55	1	0	4.227512	5.829219	1.110417
56	1	0	5.717555	5.114551	0.499539
57	1	0	4.552268	-0.249191	1.585633
58	1	0	4.682176	1.026926	2.802793
59	1	0	3.153129	0.175827	2.558707
60	6	0	-7.374143	0.940146	0.424047
61	1	0	-7.040923	1.880564	0.838265

Table 1-13. DFT calculation of **2-th** (B3LYP/6-31g(d))
Standard orientation: (Ground State)

Center Number	Atomic Number	Atomic Type	Coordinates (Angstroms) X	Y	Z
1	6	0	-6.118514	-1.054682	-0.191630
2	6	0	-5.054100	-1.933595	-0.412949
3	6	0	-5.496413	-3.272358	-0.709575
4	6	0	-6.852281	-3.404334	-0.711623
5	16	0	-7.644675	-1.897969	-0.371430
6	6	0	-6.127051	0.356157	0.142897
7	16	0	-4.774546	1.425892	-0.193366
8	6	0	-5.641598	2.791102	0.429843
9	6	0	-6.898839	2.466615	0.876719
10	6	0	-7.165086	1.074300	0.707423
11	6	0	-3.681449	-1.594072	-0.341942
12	6	0	-2.486146	-1.359336	-0.288992
13	6	0	-1.101758	-1.039028	-0.218644
14	6	0	-0.680774	0.208582	0.291889
15	6	0	0.672147	0.526879	0.335636
16	6	0	1.670064	-0.380282	-0.085454
17	6	0	1.228865	-1.631005	-0.572341

18	6	0	-0.120983	-1.955099	-0.657391
19	5	0	3.196398	-0.012806	-0.021592
20	6	0	4.259704	-1.178570	0.126928
21	6	0	3.615207	1.513616	-0.110493
22	6	0	4.420230	2.119680	0.895020
23	6	0	4.754868	3.475554	0.807674
24	6	0	4.346347	4.274446	-0.265514
25	6	0	3.576785	3.672309	-1.263018
26	6	0	3.193847	2.325737	-1.197864
27	6	0	5.327095	-1.326939	-0.803646
28	6	0	6.242785	-2.375277	-0.664036
29	6	0	6.169262	-3.290617	0.391727
30	6	0	5.134183	-3.130868	1.315012
31	6	0	4.178155	-2.112782	1.194165
32	6	0	-7.875946	3.442598	1.478457
33	6	0	7.169709	-4.416475	0.516375
34	6	0	3.098631	-2.049817	2.261406
35	6	0	5.502700	-0.389808	-1.983468
36	6	0	2.353249	1.793638	-2.346355
37	6	0	4.712701	5.739161	-0.331527
38	6	0	4.922195	1.347193	2.100251
39	1	0	-4.804815	-4.084968	-0.901348
40	1	0	-7.438790	-4.294592	-0.897427
41	1	0	-5.166175	3.764295	0.444543
42	1	0	-8.098696	0.610715	1.012801
43	1	0	-1.427534	0.916246	0.640331
44	1	0	0.970106	1.502532	0.712779
45	1	0	1.966247	-2.359956	-0.900753
46	1	0	-0.433391	-2.917117	-1.054221
47	1	0	5.361587	3.918473	1.596541
48	1	0	3.264857	4.265279	-2.122055
49	1	0	7.043466	-2.474149	-1.396120
50	1	0	5.066230	-3.816795	2.158521
51	1	0	-7.454831	4.452378	1.516917
52	1	0	-8.803785	3.488804	0.894158
53	1	0	6.966714	-5.209983	-0.215749
54	1	0	8.193067	-4.065821	0.336001
55	1	0	7.138292	-4.871655	1.512182
56	1	0	2.805789	-1.026506	2.513155
57	1	0	2.186316	-2.568258	1.942113
58	1	0	3.444114	-2.531707	3.182953
59	1	0	4.624042	-0.385809	-2.640078
60	1	0	5.666650	0.644034	-1.662655
61	1	0	6.360624	-0.693325	-2.592842
62	1	0	1.280815	1.868438	-2.127899
63	1	0	2.542488	2.372049	-3.257742

64	1	0	2.554824	0.743283	-2.573347
65	1	0	4.649528	6.122296	-1.355898
66	1	0	4.036190	6.344371	0.287652
67	1	0	5.730800	5.915536	0.035022
68	1	0	5.567257	0.511588	1.810062
69	1	0	5.496609	2.001201	2.764911
70	1	0	4.099404	0.926527	2.691002
71	1	0	-8.149196	3.154149	2.501433

Table 1-14. TD-DFT calculation of **2-th** (CAM-B3LYP/6-31g(d))
Standard orientation: (Excited State)

Center Number	Atomic Number	Atomic Type	X	Y	Z
1	6	0	-6.111486	-1.014740	-0.179118
2	6	0	-5.022847	-1.925374	-0.447574
3	6	0	-5.509421	-3.229707	-0.794730
4	6	0	-6.856627	-3.327519	-0.792268
5	16	0	-7.650045	-1.836859	-0.368051
6	6	0	-6.079026	0.338321	0.179946
7	16	0	-4.582305	1.256242	0.366703
8	6	0	-5.462613	2.674357	0.768610
9	6	0	-6.831268	2.492339	0.769962
10	6	0	-7.177735	1.174880	0.438504
11	6	0	-3.684637	-1.614694	-0.381967
12	6	0	-2.470826	-1.395829	-0.337803
13	6	0	-1.121295	-1.077998	-0.268521
14	6	0	-0.709857	0.235898	0.090432
15	6	0	0.626357	0.552514	0.147403
16	6	0	1.642739	-0.394804	-0.124496
17	6	0	1.212631	-1.701552	-0.469438
18	6	0	-0.115343	-2.042113	-0.551327
19	5	0	3.146454	-0.020701	-0.048065
20	6	0	4.223098	-1.170104	0.117123
21	6	0	3.566198	1.503798	-0.137028
22	6	0	4.348659	2.108465	0.875935
23	6	0	4.692422	3.453863	0.790248
24	6	0	4.309750	4.245517	-0.288907
25	6	0	3.561124	3.647245	-1.293720
26	6	0	3.176410	2.308067	-1.231082
27	6	0	5.291465	-1.309725	-0.801583
28	6	0	6.219983	-2.334080	-0.649763
29	6	0	6.155129	-3.237413	0.407855
30	6	0	5.119818	-3.088161	1.320468
31	6	0	4.155733	-2.088469	1.187754
32	6	0	-7.821190	3.574742	1.087567
33	6	0	7.169379	-4.342178	0.545153
34	6	0	3.073606	-2.032959	2.244406
35	6	0	5.453028	-0.380868	-1.982420
36	6	0	2.358348	1.773569	-2.386927
37	6	0	4.684843	5.702633	-0.353396
38	6	0	4.818162	1.337279	2.087671
39	1	0	-4.842655	-4.049002	-1.031637
40	1	0	-7.453374	-4.200792	-1.017012

41	1	0	-4.931760	3.590958	0.990337
42	1	0	-8.201420	0.821137	0.385581
43	1	0	-1.469171	0.977980	0.314534
44	1	0	0.918273	1.563043	0.418360
45	1	0	1.965252	-2.454408	-0.685024
46	1	0	-0.415895	-3.046923	-0.829918
47	1	0	5.284887	3.897080	1.587853
48	1	0	3.267385	4.238228	-2.158835
49	1	0	7.024907	-2.426099	-1.375982
50	1	0	5.057864	-3.768526	2.167295
51	1	0	-7.319026	4.515373	1.325413
52	1	0	-8.491915	3.756029	0.241335
53	1	0	6.975675	-5.149477	-0.170972
54	1	0	8.184295	-3.979424	0.353915
55	1	0	7.149577	-4.780070	1.546954
56	1	0	2.722181	-1.017491	2.437296
57	1	0	2.195204	-2.616505	1.948646
58	1	0	3.439400	-2.447481	3.188618
59	1	0	4.568105	-0.383443	-2.627280
60	1	0	5.613812	0.652975	-1.666286
61	1	0	6.305178	-0.682981	-2.597453
62	1	0	1.284140	1.869258	-2.195770
63	1	0	2.579207	2.331564	-3.301840
64	1	0	2.546649	0.716564	-2.584655
65	1	0	4.631482	6.083818	-1.377031
66	1	0	4.010605	6.312938	0.259309
67	1	0	5.699976	5.871387	0.019032
68	1	0	5.483470	0.514898	1.812501
69	1	0	5.357777	1.992817	2.776719
70	1	0	3.981583	0.898998	2.641490
71	1	0	-8.444601	3.299761	1.944592

Table 1-15.   DFT calculation of **3-th** (B3LYP/6-31g(d))
               Standard orientation: (Ground State)

Center Number	Atomic Number	Atomic Type	Coordinates (Angstroms) X	Y	Z
1	6	0	-0.795772	-3.019480	-0.266878
2	6	0	0.553751	-3.225896	-0.447571
3	16	0	1.325466	-1.733726	-0.979236
4	6	0	-0.173228	-0.882614	-0.949851
5	6	0	-1.227029	-1.682702	-0.551823
6	1	0	-1.477276	-3.790981	0.072767
7	1	0	-0.211174	0.166139	-1.210349
8	6	0	1.277938	-4.470453	-0.288713
9	6	0	2.646240	-4.715789	-0.157869
10	6	0	2.942956	-6.117029	-0.009924
11	6	0	1.836244	-6.907264	-0.027916
12	16	0	0.385719	-5.978677	-0.242855
13	1	0	3.954495	-6.486814	0.109783
14	1	0	1.778685	-7.983128	0.067220
15	6	0	-2.569305	-1.239855	-0.429959
16	6	0	3.659015	-3.728177	-0.146761
17	6	0	-3.727205	-0.882267	-0.321389
18	6	0	4.576780	-2.927364	-0.122398
19	6	0	-5.082303	-0.468199	-0.195545
20	6	0	-7.800414	0.350117	0.050914
21	6	0	-5.474624	0.841166	-0.544901
22	6	0	-6.063602	-1.362829	0.280794
23	6	0	-7.388199	-0.958680	0.384995
24	6	0	-6.799818	1.234646	-0.408697
25	1	0	-4.726826	1.535998	-0.915500
26	1	0	-5.769892	-2.371232	0.556749
27	1	0	-8.129681	-1.669680	0.740117
28	1	0	-7.077441	2.252410	-0.671191
29	6	0	5.628911	-1.971995	-0.092411
30	6	0	7.736216	-0.057766	-0.021975
31	6	0	5.344993	-0.592377	-0.008586
32	6	0	6.977310	-2.384263	-0.141788
33	6	0	7.998072	-1.443855	-0.092185
34	6	0	6.379781	0.333884	0.009866
35	1	0	4.309736	-0.268343	0.038435
36	1	0	7.204444	-3.443990	-0.210688
37	1	0	9.030338	-1.783836	-0.113313
38	1	0	6.138965	1.392635	0.061503
39	5	0	-9.301316	0.795144	0.175114
40	6	0	-10.428338	-0.317690	0.101492

41	6	0	-12.438211	-2.343667	-0.029176
42	6	0	-11.373702	-0.484872	1.150844
43	6	0	-10.520845	-1.189896	-1.015347
44	6	0	-11.523295	-2.165578	-1.066875
45	6	0	-12.341819	-1.489704	1.072750
46	1	0	-11.589644	-2.803487	-1.946920
47	1	0	-13.047907	-1.602575	1.893907
48	6	0	-9.631716	2.334096	0.361977
49	6	0	-10.197947	5.115457	0.688024
50	6	0	-9.062409	3.080615	1.429151
51	6	0	-10.499780	3.017950	-0.533068
52	6	0	-10.752929	4.382440	-0.363070
53	6	0	-9.365800	4.438102	1.580421
54	1	0	-11.412707	4.885620	-1.067905
55	1	0	-8.939207	4.980927	2.422508
56	6	0	-13.487787	-3.428278	-0.084408
57	1	0	-13.182877	-4.306970	0.499965
58	1	0	-13.663113	-3.764542	-1.111618
59	1	0	-14.443076	-3.084357	0.328163
60	6	0	-11.353372	0.378943	2.396148
61	1	0	-10.436610	0.228884	2.980680
62	1	0	-12.196236	0.134204	3.050347
63	1	0	-11.409043	1.444659	2.155940
64	6	0	-9.581272	-1.103174	-2.205423
65	1	0	-10.073795	-1.477093	-3.109622
66	1	0	-8.679295	-1.707454	-2.050632
67	1	0	-9.243974	-0.083472	-2.409389
68	6	0	-11.158339	2.323210	-1.708550
69	1	0	-10.420741	1.933603	-2.421075
70	1	0	-11.800421	3.019361	-2.257591
71	1	0	-11.773143	1.476197	-1.390061
72	6	0	-8.139007	2.458961	2.462397
73	1	0	-7.102997	2.418918	2.106317
74	1	0	-8.421033	1.434557	2.722203
75	1	0	-8.146443	3.048523	3.385344
76	6	0	-10.476567	6.591764	0.842688
77	1	0	-9.761531	7.193826	0.265520
78	1	0	-10.396401	6.908081	1.888232
79	1	0	-11.479034	6.850568	0.484542
80	5	0	8.899573	0.996392	0.029083
81	6	0	8.616454	2.468468	-0.484698
82	6	0	8.083434	5.116563	-1.413482
83	6	0	8.127115	2.702223	-1.798287
84	6	0	8.837000	3.598333	0.349697
85	6	0	8.556563	4.885009	-0.119777
86	6	0	7.889089	4.008581	-2.239305

87	1	0	8.723099	5.733164	0.542205
88	1	0	7.542147	4.163121	-3.259863
89	6	0	10.310405	0.547023	0.594187
90	6	0	12.846550	-0.289543	1.609121
91	6	0	11.495651	0.688460	-0.179503
92	6	0	10.431617	-0.024698	1.888816
93	6	0	11.685668	-0.415581	2.372316
94	6	0	12.724153	0.259057	0.329955
95	1	0	11.754577	-0.831264	3.376489
96	1	0	13.613836	0.362668	-0.289015
97	6	0	7.868103	1.580262	-2.788631
98	1	0	8.579847	0.755526	-2.693205
99	1	0	7.931048	1.954962	-3.815904
100	1	0	6.868346	1.149363	-2.657617
101	6	0	7.777658	6.515212	-1.894439
102	1	0	8.442601	7.253113	-1.432363
103	1	0	6.748307	6.805969	-1.643845
104	1	0	7.881771	6.597553	-2.981629
105	6	0	9.349071	3.463306	1.770168
106	1	0	8.668290	2.874948	2.397706
107	1	0	9.450872	4.447386	2.238616
108	1	0	10.324490	2.968807	1.807125
109	6	0	9.243959	-0.223740	2.814072
110	1	0	9.567834	-0.209890	3.860363
111	1	0	8.752816	-1.187979	2.636246
112	1	0	8.475850	0.545103	2.694913
113	6	0	11.476975	1.261649	-1.582747
114	1	0	12.490843	1.314628	-1.992119
115	1	0	11.049051	2.268088	-1.607902
116	1	0	10.883573	0.644159	-2.268758
117	6	0	14.193530	-0.699849	2.155490
118	1	0	14.093139	-1.438014	2.958138
119	1	0	14.734117	0.161778	2.570250
120	1	0	14.828778	-1.131828	1.374117

1.5 References

(1)   ThomasIII, S. W.; Joly, G. D.; Swager, T. M. *Chem. Rev.* **2007**, *107*, 1339.

(2)   Aradilla, D.; Estrany, F.; Casellas, F.; Iribarren, J. I.; Aleman, C. *Org. Electron.* **2014**, *15*, 40.

(3)   (a) Zhang, R.; Li, B.; Iovu, M. C.; Jeffries-El, M.; Sauve, G.; Cooper, J.; Jia, S.; Tristram-Nagle, S.; Smilgies, D. M.; Lambeth, D. N.; McCullough, R. D.; Kowalewski, T. *J. Am. Chem. Soc.* **2006**, *128*, 3480; (b) Bubnova, O.; Khan, Z. U.; Wang, H.; Braun, S.; Evans, D. R.; Fabretto, M.; Hojati-Talemi, P.; Dagnelund, D.; Arlin, J. B.; Geerts, Y. H.; Desbief, S.; Breiby, D. W.; Andreasen, J. W.; Lazzaroni, R.; Chen, W. M. M.; Zozoulenko, I.; Fahlman, M.; Murphy, P. J.; Berggren, M.; Crispin, X. *Nat Mater* **2014**, *13*, 190; (c) Qian, J. S.; Li, X. Y.; Lunn, D. J.; Gwyther, J.; Hudson, Z. M.; Kynaston, E.; Rupar, P. A.; Winnik, M. A.; Manners, I. *J. Am. Chem. Soc.* **2014**, *136*, 4121; (d) Oosterbaan, W. D.; Bolsee, J. C.; Wang, L. J.; Vrindts, V.; Lutsen, L. J.; Lemaur, V.; Beljonne, D.; McNeill, C. R.; Thomsen, L.; Manca, J. V.; Vanderzande, D. J. M. *Adv Funct Mater* **2014**, *24*, 1994.

(4)   (a) McCullough, R. D. *Adv. Mater.* **1998**, *10*, 93; (b) *Handbook of Oligo- and Polythiophenes*; Fichou, D., Ed.; Wiley-VCH, 1999; (c) *Handbook of Thiophene-based Materials: Applications in Organic Electronics and Photonics, Volume One: Synthesis and Theory*; 1 ed.; Perepichka, I. F.; Perepichka, D. F., Eds.; John Wiley & Sons, 2009.

(5)   (a) Friedel, B.; McNeill, C. R.; Greenham, N. C. *Chem Mater* **2010**, *22*, 3389; (b) Yang, L. Q.; Sontag, S. K.; LaJoie, T. W.; Li, W. T.; Huddleston, N. E.; Locklin, J.; You, W. *Acs Appl Mater Inter* **2012**, *4*, 5069; (c) Higashihara, T.; Ueda, M. *Macromolecular Research* **2013**, *21*, 257; (d) Mao, Z. H.; Vakhshouri, K.; Jaye, C.; Fischer, D. A.; Fernando, R.; DeLongchamp, D. M.; Gomez, E. D.; Sauve, G. *Macromolecules* **2013**, *46*, 103; (e) Chen, W. C.; Lee, Y. H.; Chen, C. Y.; Kau, K. C.; Lin, L. Y.; Dai, C. A.; Wu, C. G.; Ho, K. C.; Wang, J. K.; Wang, L. *Acs Nano* **2014**, *8*, 1254; (f) Feng, W.; Rangan, S.; Cao, Y.; Galoppini, E.; Bartynski, R. A.; Garfunkel, E. *J Mater Chem A* **2014**, *2*, 7034.

(6)   (a) Loewe, R. S.; Khersonsky, S. M.; McCullough, R. D. *Adv. Mater.* **1999**, *11*, 250; (b) Sheina, E. E.; Liu, J.; Iovu, M. C.; Laird, D. W.; McCullough, R. D. *Macromolecules* **2004**, *37*, 3526; (c) Yokoyama, A.; Miyakoshi, R.; Yokozawa, T. *Macromolecules* **2004**, *37*, 1169; (d) Jeffries-El, M.; Sauve, G.; McCullough, R. D. *Macromolecules* **2005**, *38*, 10346; (e) Osaka, I.; McCullough, R. D. *Acc. Chem. Res.* **2008**, *41*, 1202; (f) Yokozawa, T.; Yokoyama, A. *Chem. Rev.* **2009**, *109*, 5595; (g) Lohwasser, R. H.; Thelakkat, M. *Macromolecules* **2011**, *44*, 3388; (h) Okamoto, K.; Luscombe, C. K. *Polym Chem-Uk* **2011**, *2*, 2424; (i) Koch, F. P. V.; Heeney, M. *Synthesis of Polymers* **2012**, *1*, 155; (j) Bryan, Z. J.; McNeil, A. J. *Macromolecules* **2013**, *46*, 8395; (k) Ricciotti, L.; Borbone, F.; Carella, A.; Centore, R.; Roviello, A.; Barra, M.; Roviello, G.; Ferone, C.; Minarini, C.; Morvillo, P. *J Polym Sci Pol Chem* **2013**, *51*, 4351.

(7)   McCullough, R. D.; Lowe, R. D.; Jayaraman, M.; Anderson, D. L. *J. Org. Chem.* **1993**, *58*, 904.

(8)   (a) Hundt, N.; Palaniappan, K.; Sista, P.; Murphy, J. W.; Hao, J.; Nguyen, H.; Stein, E.; Biewer, M. C.; Gnade, B. E.; Stefan, M. C. *Polym Chem-Uk* **2010**, *1*,

1624; (b) Bhatt, M. P.; Huynh, M. K.; Sista, P.; Nguyen, H. Q.; Stefan, M. C. *J. Polym. Sci. A: Polym. Chem.* **2012**, *50*, 3086; (c) Zhou, E.; Hou, J.; Yang, C.; Li, Y. *J. Polym. Sci. A: Polym. Chem.* **2006**, *44*, 2206; (d) Kuo, C.-Y.; Huang, Y.-C.; Hsiow, C.-Y.; Yang, Y.-W.; Huang, C.-I.; Rwei, S.-P.; Wang, H.-L.; Wang, L. *Macromolecules* **2013**, *46*, 5985.

(9)   (a) Sato, T.; Cai, Z. G.; Shiono, T.; Yamamoto, T. *Polymer* **2006**, *47*, 37; (b) Sato, T.; Kishida, H.; Nakamura, A.; Fukuda, T.; Yamamoto, T. *Synth. Met.* **2007**, *157*, 318; (c) Yamamoto, T.; Sato, T.; Iijima, T.; Abe, M.; Fukumoto, H.; Koizumi, T.; Usui, M.; Nakamura, Y.; Yagi, T.; Tajima, H.; Okada, T.; Sasaki, S.; Kishida, H.; Nakamura, A.; Fukuda, T.; Emoto, A.; Ushijima, H.; Kurosaki, C.; Hirota, H. *Bull. Chem. Soc. Jpn.* **2009**, *82*, 896.

(10)   (a) Sundararaman, A.; Victor, M.; Varughese, R.; Jäkle, F. *J. Am. Chem. Soc.* **2005**, *127*, 13748; (b) Li, H.; Sundararaman, A.; Venkatasubbaiah, K.; Jäkle, F. *J. Am. Chem. Soc.* **2007**, *129*, 5792; (c) Li, H.; Jäkle, F. *Angewandte Chemie, International Edition* **2009**, *48*, 2313; (d) Li, H.; Jäkle, F. *Macromol. Rap. Commun.* **2010**, *31*, 915; (e) Li, H.; Jäkle, F. *Polym Chem-Uk* **2011**, *2*, 897; (f) Li, H.; Sundararaman, A.; Pakkirisamy, T.; Venkatasubbaiah, K.; Schödel, F.; Jäkle, F. *Macromolecules* **2011**, *44*, 95; (g) Chen, P. K.; Lalancette, R. A.; Jäkle, F. *J. Am. Chem. Soc.* **2011**, *133*, 8802; (h) Chen, P. K.; Jäkle, F. *J. Am. Chem. Soc.* **2011**, *133*, 20142; (i) Pammer, F.; Lalancette, R. A.; Jäkle, F. *Chem. -Eur. J.* **2011**, *17*, 11280; (j) Chen, P. K.; Lalancette, R. A.; Jäkle, F. *Angewandte Chemie, International Edition* **2012**, *51*, 7994; (k) Yin, X.; Chen, J.; Lalancette, R. A.; Marder, T. B.; Jäkle, F. *Angewandte Chemie, International Edition* **2014**, *53*, 9761.

(11)   (a) Matsumi, N.; Naka, K.; Chujo, Y. *J. Am. Chem. Soc.* **1998**, *120*, 10776; (b) Matsumi, N.; Naka, K.; Chujo, Y. *J. Am. Chem. Soc.* **1998**, *120*, 5112; (c) Heilmann, J. B.; Scheibitz, M.; Qin, Y.; Sundararaman, A.; Jäkle, F.; Kretz, T.; Bolte, M.; Lerner, H.-W.; Holthausen, M. C.; Wagner, M. *Angewandte Chemie, International Edition* **2006**, *45*, 920; (d) Yamaguchi, I.; Choi, B. J.; Koizumi, T. A.; Kubota, K.; Yamamoto, T. *Macromolecules* **2007**, *40*, 438; (e) Zhao, C.; Wakamiya, A.; Yamaguchi, S. *Macromolecules* **2007**, *40*, 3898; (f) Bonifãcio, V. D. B.; Morgado, J.; Scherf, U. *J. Polym. Sci. Part A, Polym. Chem.* **2008**, *46*, 2878; (g) Reitzenstein, D.; Lambert, C. *Macromolecules* **2009**, *42*, 773; (h) Nagai, A.; Murakami, T.; Nagata, Y.; Kokado, K.; Chujo, Y. *Macromolecules* **2009**, *42*, 7217; (i) Hoven, C. V.; Wang, H. P.; Elbing, M.; Garner, L.; Winkelhaus, D.; Bazan, G. C. *Nat Mater* **2010**, *9*, 249; (j) Cataldo, S.; Fabiano, S.; Ferrante, F.; Previti, F.; Patane, S.; Pignataro, B. *Macromol. Rap. Comm.* **2010**, *31*, 1281; (k) Hubner, A.; Qu, Z. W.; Englert, U.; Bolte, M.; Lerner, H. W.; Holthausen, M. C.; Wagner, M. *J. Am. Chem. Soc.* **2011**, *133*, 4596; (l) Welch, G. C.; Bazan, G. C. *J. Am. Chem. Soc.* **2011**, *133*, 4632; (m) Lukoyanova, O.; Lepeltier, M.; Laferriere, M.; Perepichka, D. F. *Macromolecules* **2011**, *44*, 4729; (n) Peterson, J. J.; Davis, A. R.; Werre, M.; Coughlin, E. B.; Carter, K. R. *ACS Appl. Mater. Interf.* **2011**, *3*, 1796; (o) Hinkens, D. M.; Chen, Q. L.; Siddiki, M. K.; Gosztola, D.; Tapsak, M. A.; Qiao, Q. Q.; Jeffries-EL, M.; Darling, S. B. *Polymer* **2013**, *54*, 3510; (p) Reus, C.; Weidlich, S.; Bolte, M.; Lerner, H. W.; Wagner, M. *J. Am. Chem. Soc.* **2013**, *135*, 12892; (q) Reus, C.; Guo, F.; John, A.; Winhold, M.; Lerner, H. W.; Jäkle,

F.; Wagner, M. *Macromolecules* **2014**, *47*, 3727; (r) Levine, D. R.; Siegler, M. A.; Tovar, J. D. *J. Am. Chem. Soc.* **2014**, *136*, 7132.

(12)   (a) Jäkle, F. *Coord. Chem. Rev.* **2006**, *250*, 1107; (b) Matsumi, N.; Chujo, Y. *Polym. J.* **2008**, *40*, 77; (c) Elbing, M.; Bazan, G. C. *Angew. Chem., Int. Ed.* **2008**, *47*, 834; (d) Jäkle, F. *Chem. Rev.* **2010**, *110*, 3985; (e) Nagai, A.; Chujo, Y. *Chem. Lett.* **2010**, *39*, 430; (f) Lorbach, A.; Hubner, A.; Wagner, M. *Dalton Trans.* **2012**, *41*, 6048.

(13)   (a) Entwistle, C. D.; Marder, T. B. *Angewandte Chemie, International Edition* **2002**, *41*, 2927; (b) Entwistle, C. D.; Marder, T. B. *Chem Mater* **2004**, *16*, 4574; (c) Yamaguchi, S.; Wakamiya, A. *Pure Appl Chem* **2006**, *78*, 1413; (d) Hudson, Z. M.; Wang, S. *Acc. Chem. Res.* **2009**, *42*, 1584; (e) Wade, C. R.; Broomsgrove, A. E. J.; Aldridge, S.; Gabbai, F. P. *Chem. Rev.* **2010**, *110*, 3958.

(14)   (a) Pammer, F.; Guo, F.; Lalancette, R. A.; Jäkle, F. *Macromolecules* **2012**, *45*, 6333; (b) Pammer, F.; Jäkle, F. *Chem Sci* **2012**, *3*, 2598.

(15)   Yamamoto, T.; Komarudin, D.; Arai, M.; Lee, B.-L.; Suganuma, H.; Asakawa, N.; Inoue, Y.; Kubota, K.; Sasaki, S.; Fukuda, T.; Matsuda, H. *J. Am. Chem. Soc.* **1998**, *120*, 2047.

(16)   11BNMRShifts, 2014.

(17)   SharpPeaks.

(18)   Ashraf, R. S.; Shahid, M.; Klemm, E.; Al-Ibrahim, M.; Sensfuss, S. *Macromol. Rap. Commun.* **2006**, *27*, 1454.

(19)   (a) Fröhlich, H.; Kalt, W. *J. Org. Chem.* **1990**, *55*, 2993; (b) Kojima, T.; Hiraoka, S. *Org. Lett.* **2014**, *16*, 1024.

(20)   Chen, T.-A.; Wu, X.; Rieke, R. D. *J. Am. Chem. Soc.* **1995**, *117*, 233.

(21)   Xie, Y.; Li, Y.; Xiao, L.; Qiao, Q.; Dhakal, R.; Zhang, Z.; Gong, Q.; Galipeau, D.; Yan, X. *J. Phys. Chem. C* **2010**, *114*, 14590.

(22)   Pammer, F.; Passlack, U. *ACS Macro Lett.* **2014**, *3*, 170.

(23)   3-thcomment.

(24)   PolymerSolventDependence_Solubility.

(25)   Sundararaman, A.; Venkatasubbaiah, K.; Victor, M.; Zakharov, L. N.; Rheingold, A. L.; Jäkle, F. *J. Am. Chem. Soc.* **2006**, *128*, 16554.

(26)   HexylthiopheneInfluence, 2014.

(27)   Cardona, C. M.; Li, W.; Kaifer, A. E.; Stockdale, D.; Bazan, G. C. *Adv. Mater.* **2011**, *23*, 2367.

(28)   Pelter, A.; Singaram, B.; Warren, L.; Wilson, J. W. *Tetrahedron* **1993**, *49*, 2965.

(29)   Nagarjuna, G.; Yurt, S.; Jadhav, K. G.; Venkataraman, D. *Macromolecules* **2010**, *43*, 8045.

(30)   Yamaguchi, S.; Shirasaka, T.; Tamao, K. *Org. Lett.* **2000**, *2*, 4129.

(31)   Kline, R. J.; DeLongchamp, D. M.; Fischer, D. A.; Lin, E. K.; Richter, L. J.; Chabinyc, M. L.; Toney, M. F.; Heeney, M.; McCulloch, I. *Macromolecules* **2007**, *40*, 7960.

(32)   Northrup, J. E.; Xie, W. Y.; Sun, Y. Y.; Zhang, S. B. *Appl. Phys. Express* **2013**, *6*.

(33)   Choi, D.; Jeong, B. S.; Ahn, B.; Chung, D. S.; Lim, K.; Kim, S. H.; Park, S. U.; Ree, M.; Ko, J.; Park, C. E. *ACS Applied Materials & Interfaces* **2012**, *4*, 702.

(34)   Ashraf, R. S.; Shahid, M.; Klemm, E.; Al-Ibrahim, M.; Sensfuss, S. *Macromolecular Rapid Communications* **2006**, *27*, 1454.

Chapter 2

Amphiphilic Polythiophene Block Copolymers
Containing Phenylboronic Acid Functionality

2.1 Introduction

Among various π-conjugated polymers, regioregular poly(3-hexylthiophene) (P3HT) has been one of the most extensively studied semiconducting polymer materials for applications in light-emitting diodes, field-effect transistors (OFET), solar cells owing to their excellent optoelectronic properties and processability.[1] The most used methods to synthesize regioregular P3HT are McCullough (organomagnesium-mediated),[2] Rieke (organozinc-mediated),[3] and Grignard metathesis (GRIM) methods.[4] Both McCullough and Rieke methods require cryogenic temperature during the metal halogen exchange step. GRIM polymerization, also referred to as Kumada catalyst-transfer polycondensation (KCTP) by Kiriy,[5] was developed by McCullough's group in 1999 to prepare regioregular P3HT in large scale at room temperature.[4] The *living* nature of GRIM polymerization allows *in situ* end-group functionalization of P3HT[6] which triggered the development of a diverse array of block copolymers containing regioregular P3HT. Amphiphilic rod-coil block copolymers containing regioregular polythiophenes are an important class of polymeric materials (**Figure 2-1**).[7] The crystalline nature of the polythiophene block plays an important role in the self-assemblies of the amphiphilic block copolymers as a variety of micellar morphologies including spheres, vesicles, fibers, etc, can be formed while varying the composition of hydrophobic and hydrophiphilic blocks, the selective solvent used, and preparation methods. A very common phenomena associated with polymer aggregation in amphiphilic polythiophene

block copolymers is red shift in absorption and significant drops in photoluminescence (PL) intensity. Recently, the Park group demonstrated that besides the different morphologies, a wide range of PL colors from blue to red can also be obtained just by altering the solvent composition without altering the molecular structure of P3OT-*b*-PEO and the emission colors can be further manipulated by other external stimuli.[7a]
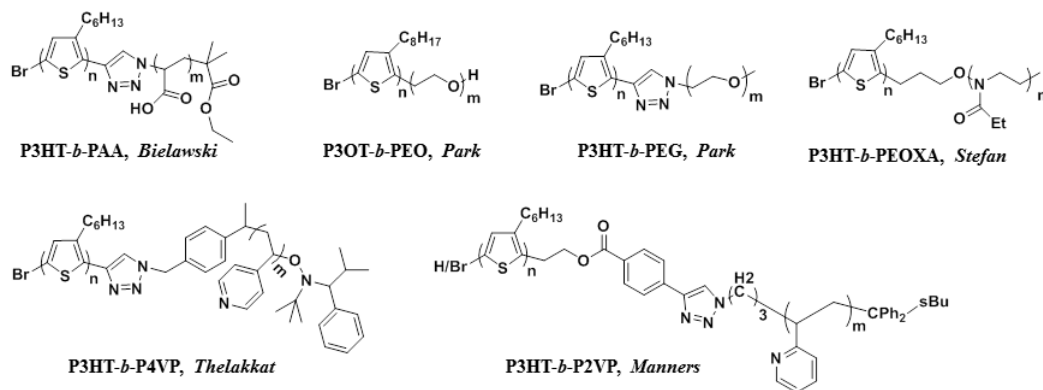
Figure 2-1. Examples of amphiphilic block copolymers containing polythiophenes (Examples are taken from reference 7).

Phenylboronic acid (PBA) and its derivatives are well known for their high affinity to diol species in aqueous solution. As shown in **Figure 2-2**, PBA compounds exist in equilibrium between the uncharged hydrophobic species and negatively charged hydrophilic boronate species. Both species can react reversibly with cis-1, 2 or 1, 3-diols
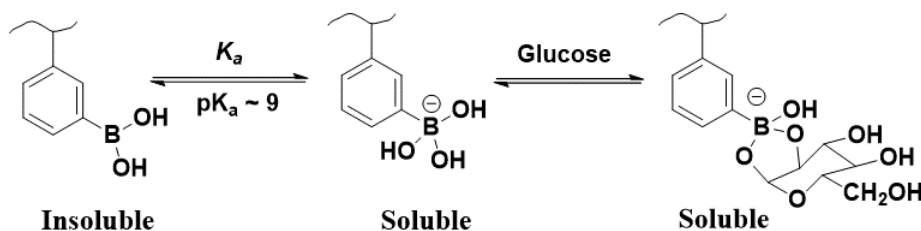
Figure 2-2.Equilibria of phenylboronic acid compounds in an aqueous solution in the presence of glucose.

of glucose, but the complex between the uncharged form and glucose is unstable due to its high susceptibility to hydrolysis. The charged form can make a stable cyclic boronic

ester with glucose which shifts the equilibrium to the charged form and improves the hydrophilicity of PBA compounds. Incorporation of PBA into amphiphilic polythiophene block copolymers is expected to provide highly sensitive fluorescent sensory materials for carbohydrates[8] in accordance with changes in the morphology that are anticipitated as the neutral polymer is converted to a water-soluble charged polymer. Recent developments in controlled/living radical polymerization (CRP/LRP) allow the preparation of well-defined polymers with predictable molecular weights, narrow molecular weight distributions, defined chain end functionalities, and controlled macromolecular architecture.[9] Among various CRP methods, atom transfer radical polymerization (ATRP)[10] and reversible addition-fragmentation chain transfer (RAFT)[11] have been widely used to prepare well-defined boronic acid-containing homo- and block copolymers mostly through postpolymerization modification.[12] "Click chemistry",[13] introduced by Sharpless and coworkers, proved to be a powerful tool to synthesize a range of functional polymeric architectures.[14] In this chapter, ATRP/RAFT, and copper (I)-catalyzed azide-alkyne cycloaddition (CUAAC) click chemistry were combined to prepare amphiphilic polythiophene block copolymers.

2.2 Results and Discussion

Two different approaches were used for the preparation of P3HT-b-PSBpin: (1) ATRP & click from ethynyl-P3HT, (2) RAFT & click from ethynyl-spacer-P3HT.

(1) ATRP & click from ethynyl-P3HT

Ethynyl-P3HT was prepared by KCTP using Ni(dppp)Cl$_2$ as the catalyst according to the procedure reported in the literature[6a] (**Scheme 2-1**). A mixture of mono- and di ethynyl-P3HT was obtained when high catalyst to monomer ratio was used as reported

elsewhere.[6a] This issue could be circumvented by using low catalyst to monomer ratio. Mono-functionalized ethynyl-P3HT was obtained with M_n = 7740 g/mol (GPC estimate against polystyrene standard) when 2.5% of Ni(dppp)Cl$_2$ was used. Homo polymers N$_3$-PSBpin of different molecular weights were synthesized using the ATRP method[15] followed by azidation with NaN$_3$ in DMF as the solvent. CuI and DBU (1, 8-diazabicycloundec-7-ene) were used to promote the click reaction of two functional homopolymers. N$_3$-PSBpin of lower molecular weight (M_n = 3760 g/mol) was used in excess to click with ethynyl-P3HT (M_n = 7740 g/mol) to ensure close to quantitative conversion of the ethynyl-P3HT. The excess of N$_3$-PSBpin was successfully removed by precipitation of the crude block copolymer in MeOH. GPC traces (**Figure 2-3**) of the clicked product shifted to shorter elution time compared to the functionalized homopolymers with a mono-modal distribution indicating successful click reaction (M_n = 11300, Đ = 1.23) . A comparison of the ^{1}H NMR spectra of homo and block copolymers further confirmed the incorporation of two blocks (**Figure 2-4**).
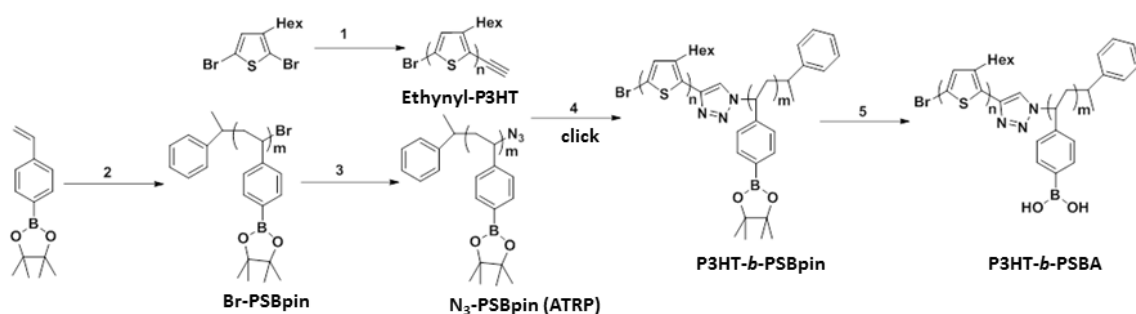
Scheme 1. Synthesis of amphiphilic block copolymer P3HT-*b*-PSBA using ATRP and click chemistry. 1. t-BuMgCl, LiCl; Ni(dppp)Cl$_2$, ethynylmagnesium chloride. 2. CuBr, PMDETA, PEB, anisole, 90°C. 3. NaN$_3$, DMF, RT. 4. CuI, DBU, THF, 40°C. 5. Polystyrene-supported boronic acid resin, THF/trifluoroacetic acid (2 vol. %), 65°C.

Figure 2-3. GPC traces of homopolymers and block copolymer.
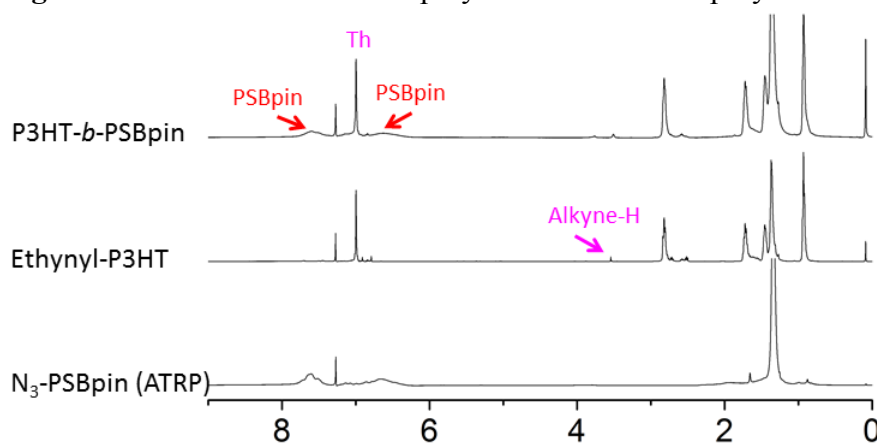
Figure 2-4. ^{1}H NMR spectra of homopolymers and the block copolymer recorded in CDCl$_3$ (δ, ppm).

In the IR spectra of the homopolymers and the block copolymer, the appearance of the signature azide peak at *ca*. 2100 cm^{-1} confirmed the conversion from Br- to N$_3$-end group functionalization of PSBpin (**Figure 2-5**). When comparing the data for the homopolymers and the block copolymer, the significantly reduced peak intensity at 2100 cm^{-1} after click reaction further indicated successful conversion to the product.
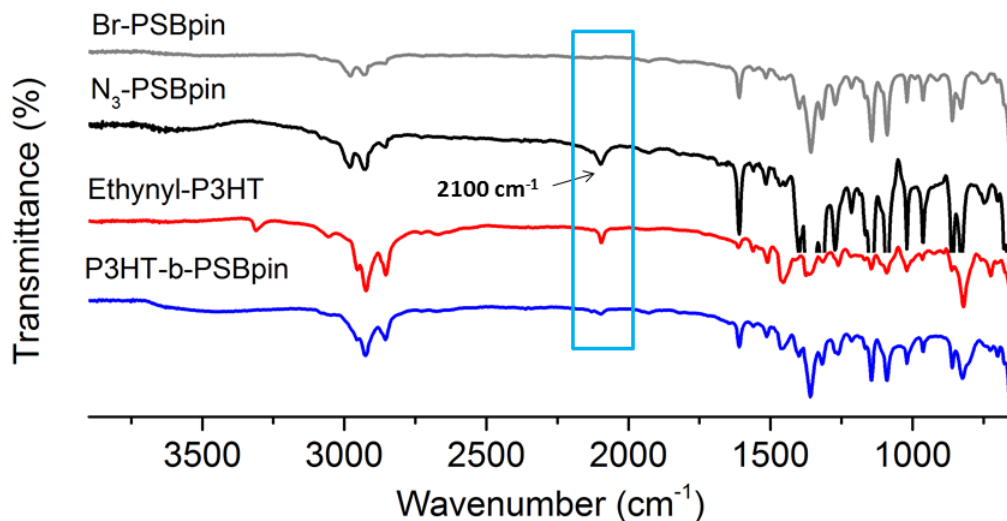
Figure 2-5. FT-IR spectra of homopolymers and the block copolymer.

We note that a major issue in the synthesis of P3HT-*b*-PSBpin (ATRP & click) using click chemistry turned out to be the removal of the excess of either of the homopolymers. When an excess of higher molecular weight N_3-PSBpin (M_n = 8000 g/mol) was used to couple with ethynyl-P3HT (M_n = 7740 g/mol), the relatively low solubility of high molecular weight N_3-PSBpin in MeOH jeopardized the successful removal of excess N_3-PSBpin. In an alternative approach, an excess of ethynyl-P3HT was used and expected to be removed by azide-functionalized Merrifield resin.[16] However, the homopolymer ethynyl-P3HT could not be completely removed by the resin based on GPC results. Thus, it proved to be imperative to use a PSBpin precursor of relatively low molecular weight to obtain the pure diblock copolymer.

Deprotection of P3HT-*b*-PSBpin (ATRP & click) was attempted using polystyrene-supported boronic acid resin in THF/ trifluoroacetic acid (2 vol %) at 65 °C. Before deprotection, P3HT-b-PSBpin (ATRP & click) readily dissolves in CDCl₃ with both blocks present in the ¹H NMR spectra (**Figure 2-6**). After deprotection, the proton signals of the P3HT block dominate in the spectra in CDCl₃ indicating micelle formation

with PSBA as the core and P3HT as corona. After a few drops of DMSO-d$_6$ were added, the PSBA block emerged as the addition of polar solvent favors dissolution of the PSBA block. The significantly reduced peak intensity at 1.36 ppm suggested efficient removal of the pinacol group though a weak signal of Bpin is still present in the ^{13}C NMR spectra (**Figure 2-7**). A peak at 115 ppm in the ^{13}C NMR spectra indicated partial deborylation of the polymer, possibly with Cu- catalyzed formation of C-Br groups.
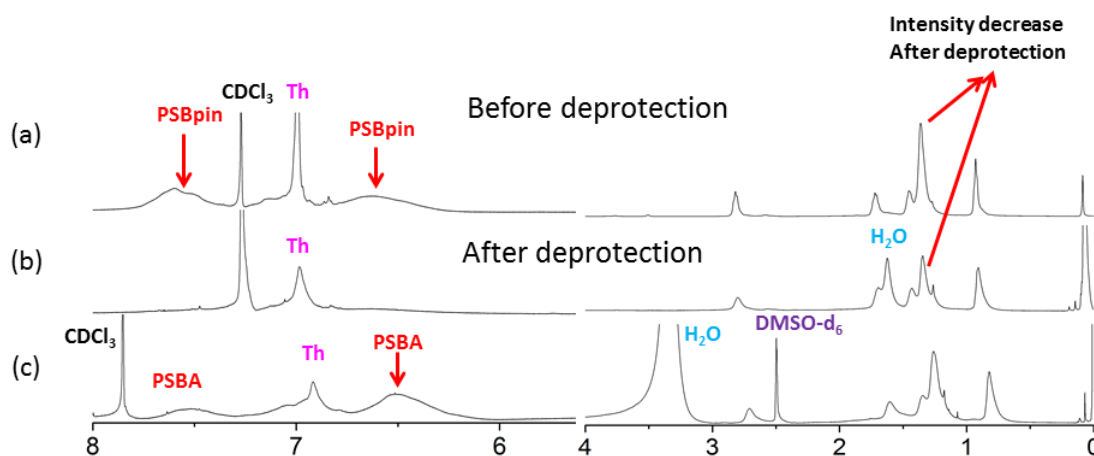
Figure 2-6. Comparison of ^{1}H NMR spectra of P3HT-*b*-PSBpin (ATRP & click) before (a) in CDCl$_3$, and after deprotection (b) in CDCl$_3$, (c) in CDCl$_3$/DMSO-d$_6$ mixture (20:3) (δ, ppm).
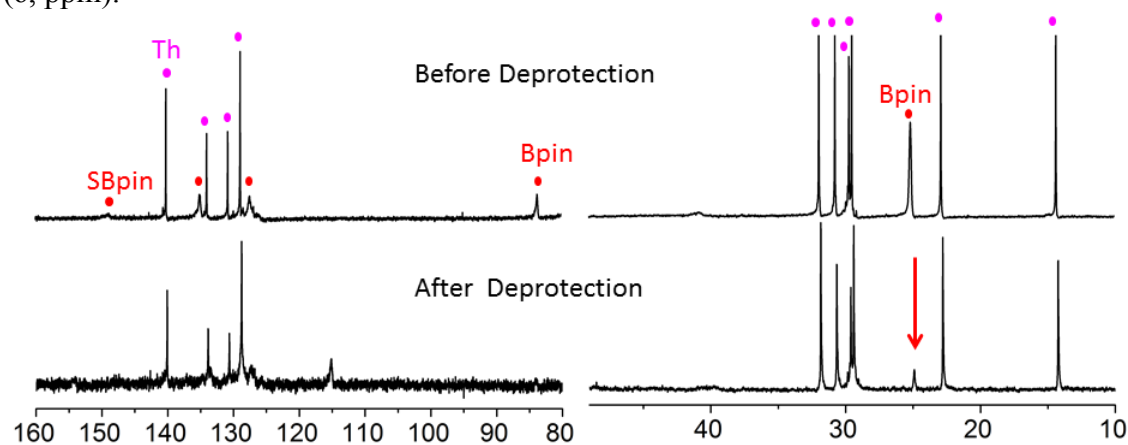
Figure 2-7. Comparison of ^{13}C NMR spectra of P3HT-*b*-PSBpin (ATRP & click) in CDCl$_3$ and P3HT-*b*-PSBA in CDCl$_3$/MeOH mixture (20:3) (δ, ppm).

The self-assembly of the amphiphilic block copolymer P3HT-*b*-PSBA (ATRP & click) was investigated by dynamic light scattering (DLS). Upon addition of 1 mL of 0.001 M

NaOH to a solution of the amphiphilic block copolymer P3HT-*b*-PSBA (ATRP & click) (0.3 mg) in 3 mL THF, significantly reduced fluorescence intensity indicates formation of aggregates which were detected by DLS with a number average hydrodynamic diameter of 18 nm (**Figure 2-8**). When an additional 2 mL NaOH solution was added to the block copolymer solution, the hydrodynamic diameter changed to 420 nm. The size changed further to a bimodal distribution of 187 nm (91% number) and 842 nm (9% number) when keeping the solution overnight. This indicates that the micelle structure formed is not stable, possibly due to the relatively long hydrophobic rigid rod P3HT core or the partial deborylation during attempted pinacol deprotection.
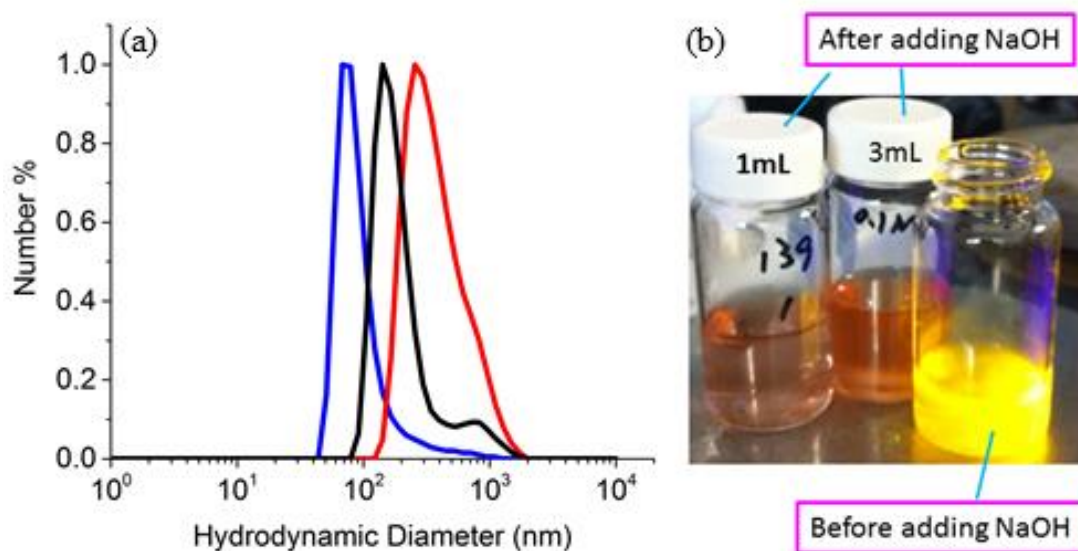
Figure 2-8. (a) DLS study of micelle formation of P3HT-*b*-PSBA (ATRP & click), the block copolymer solution in 1 mL of NaOH solution-blue, the block copolymer solution in 3 mL of NaOH solution-red, the block copolymer solution in 3 mL of NaOH solution overnight-black. (b) Emission of the block copolymer solution under UV lamp illumination before and after adding NaOH solution.

(2) RAFT & click from ethynyl-spacer-P3HT

To avoid the limitation of the previous route to low molecular weight PSBpin, an alternate route was explored that allows for incorporation of a P3HT block and a longer

hydrophilic PSBA block. In addition, we decided to pursue the incorporation of 4-vinylpyridine as a comonomer into the PSBA block. The rational for vinylpyridine incorporation is that quaternization of pyridine would lower the pK_a of the adjacent boronic acid moieties and thereby facilitate sugar binding to the amphiphilic block copolymer under physiological condition. To accomplish these goals, we turned to an alternative approach that installs the alkyne functionality separated from P3HT by a linker (**Scheme 2-2**). As mentioned earlier, the synthesis of ethynyl-P3HT of low molecular weight directly from KCTP provides a mixture of mono and di ethynyl functionalized P3HT. According to the literature, mono allyl-P3HT of low molecular weight is readily obtained by KCTP and can be converted to hydroxyl-P3HT quantitatively through hydroboration. The later can be further converted to ethynyl-spacer-P3HT through esterification.[7d,17] A similar procedure was adopted to synthesize low molecular weight ethynyl-spacer-P3HT (M_n = 7090 g/moL, $Đ$ = 1.13) and its high end-group integrity was confirmed by MALDI-TOF MS (**Figure 2-9**).
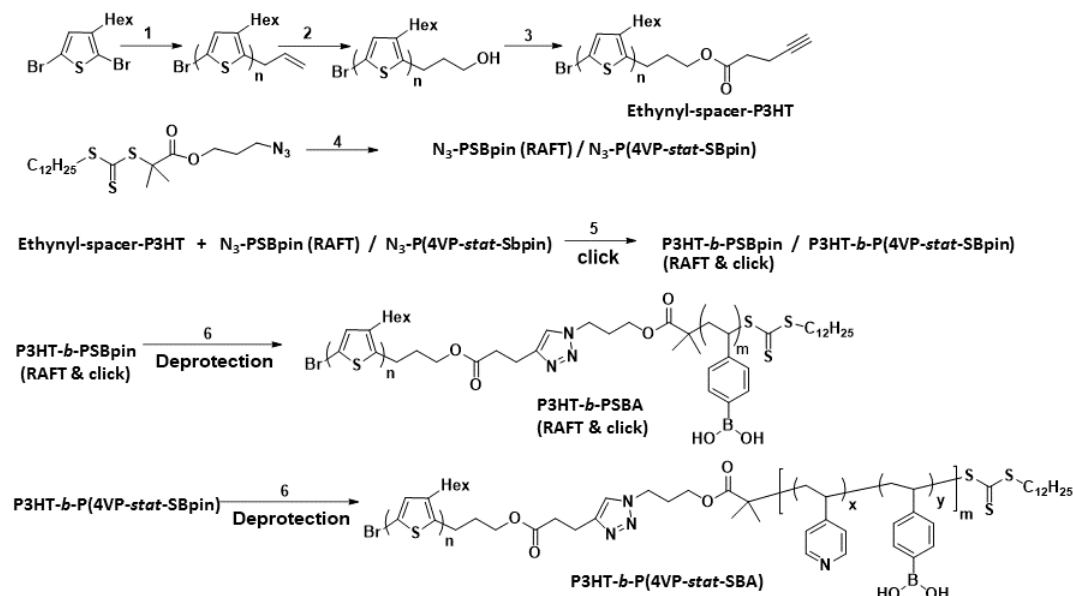
Scheme 2-2. Synthesis of amphiphilic block copolymer P3HT-*b*-PSBA/P3HT-*b*-P(4VP-*stat*-SBA) using RAFT and click chemistry. 1. t-BuMgCl, LiCl; Ni(dppp)Cl$_2$, allylmagnesium chloride. 2. 9-BBN, NaOH, H$_2$O$_2$, 40°C. 3. Pentynoic acid, DCC, DMAP, THF, RT. 4. Styrene boronic acid pinacol ester (4-vinylpyridine), AIBN, dioxane, 70 °C. 5. CuBr, PMDETA, THF, 50 °C. 6. Phenylboronic acid, THF, 1 drop of concentrated HCl, RT.
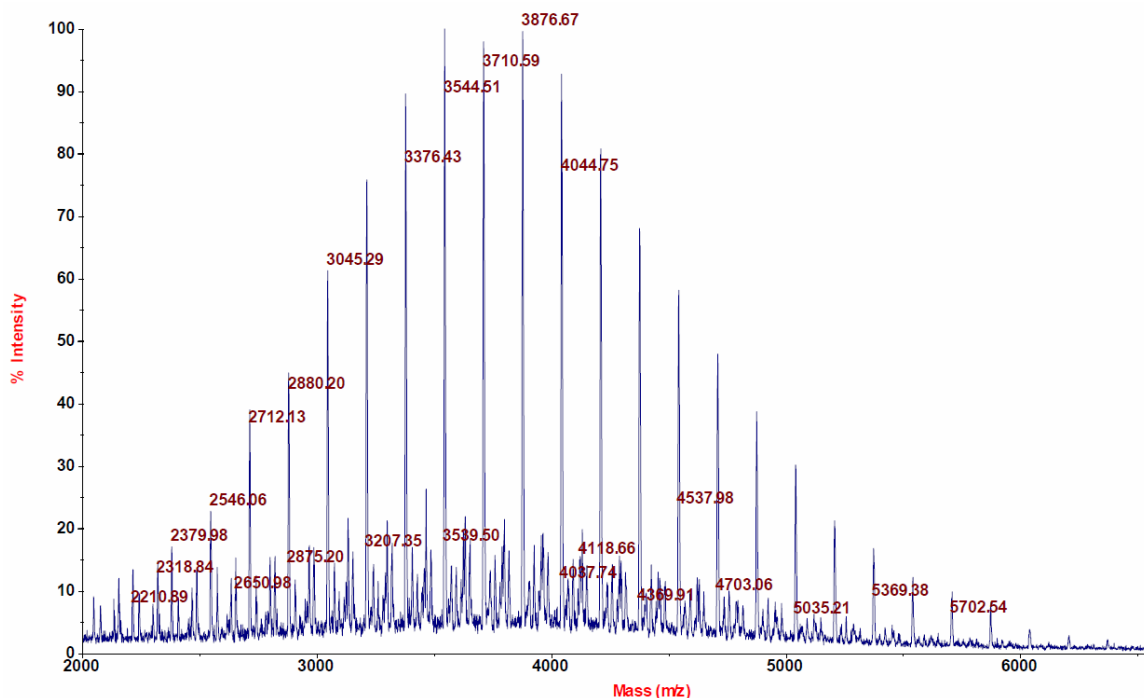
Figure 2-9. MALDI-TOF MS (pos. mode) of ethynyl-spacer-P3HT (matrix-dithranol).

The RAFT technique is well known for its tolerance to a variety of functional monomers which made the incorporation of comonomer 4-vinylpyridine more straightforward compared to the ATRP approach. Another consideration was the possibility of losing the Br- end group when synthesizing high molecular weight PSBpin in the ATRP approach. Hence, an azide functionalized RAFT agent was synthesized and utilized to prepare high molecular weight N_3-PSBpin (RAFT) (M_n = 7930, Đ = 1.20) and N_3-P(4VP-*stat*-SBpin) (Mn = 14100, Đ = 1.13, 4VP/SBpin = 4:5 (feed ratio); 4VP/SBpin = 1:1 (NMR integration)).[18] Both polymers of relatively higher molecular weight were obtained smoothly after 140 min of polymerization for N_3-PSBpin and 300 min for N_3-P(4VP-*stat*-SBpin). In the ^{1}H NMR spectra of N_3-P(4VP-*stat*-SBpin), the appearance of the peaks at 8.24 ppm and 6.39 ppm (overlap with PSBpin) confirmed the successful incorporation of 4VP into the PSBpin block. The polymers were clicked with ethynyl-spacer-P3HT using CuBr and PMDETA at 50°C in THF. The GPC traces of both clicked products shifted to shorter elution time with mono-modal distributions indicating successful click reaction (**Figure 2-10**). The GPC estimated molecular weight of block copolymers (against polystyrene standard) were 12400 g/moL for P3HT-*b*-PSBpin (RAFT & click) and 16300 g/moL for P3HT-*b*-P(4VP-*stat*-SBpin), which are reasonable considering the molecular weight of the homopolymers involved in the click reaction. A comparison of the ^{1}H NMR spectra of the homo and block copolymers further corroborated incorporation of both blocks (**Figure 2-11**).
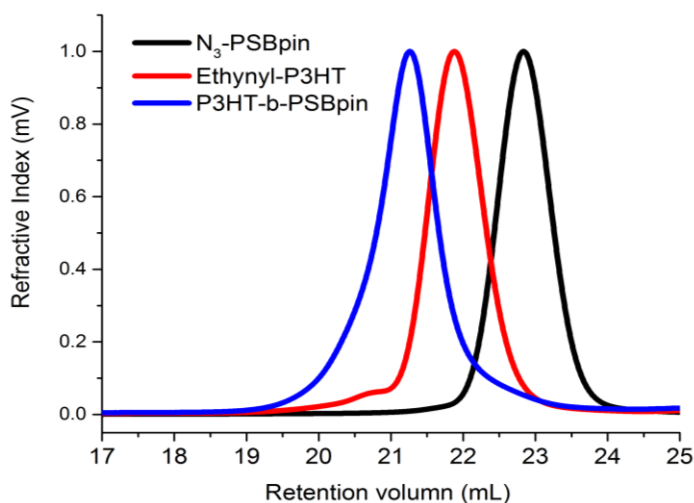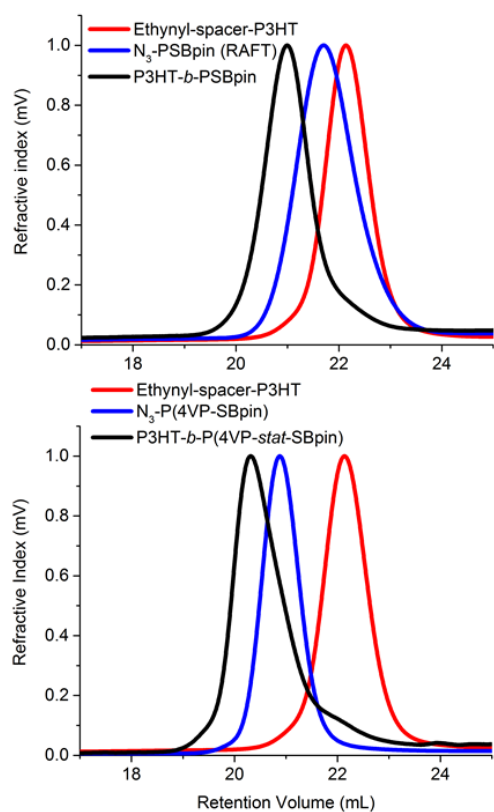
Figure 2-10. GPC traces of homopolymers and block copolymers.
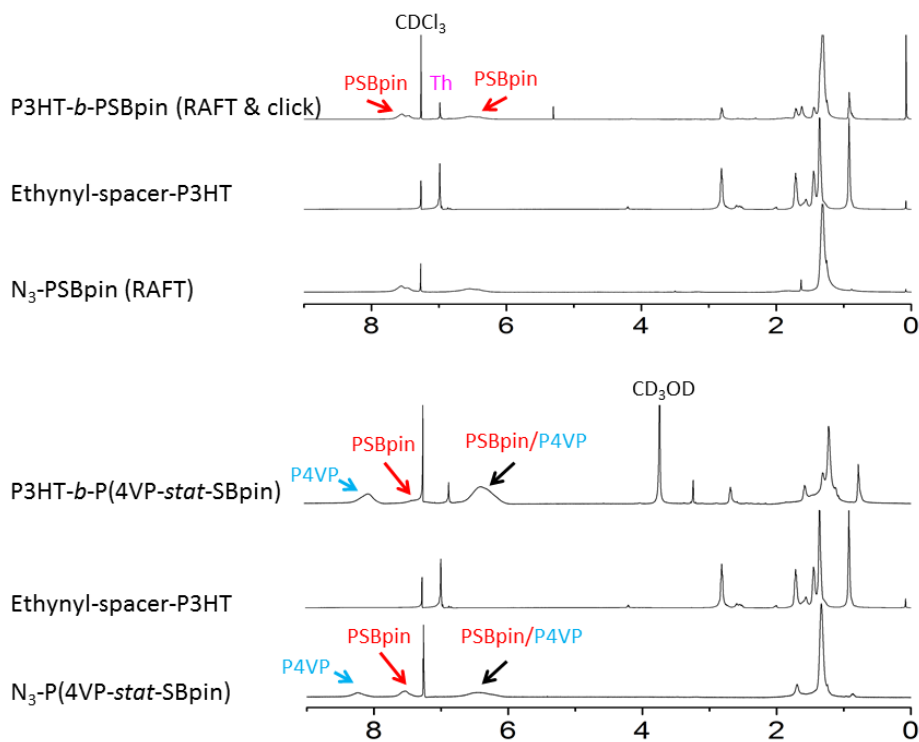
Figure 2-11. ^{1}H NMR spectra of homo and block copolymers recorded in CDCl$_3$ (δ-ppm).

When comparing the IR spectra of the homopolymers and block copolymers, the disappearance of the azide- signature peak at 2100 cm^{-1} further proved that the click reaction is highly efficient (**Figure 2-12**).
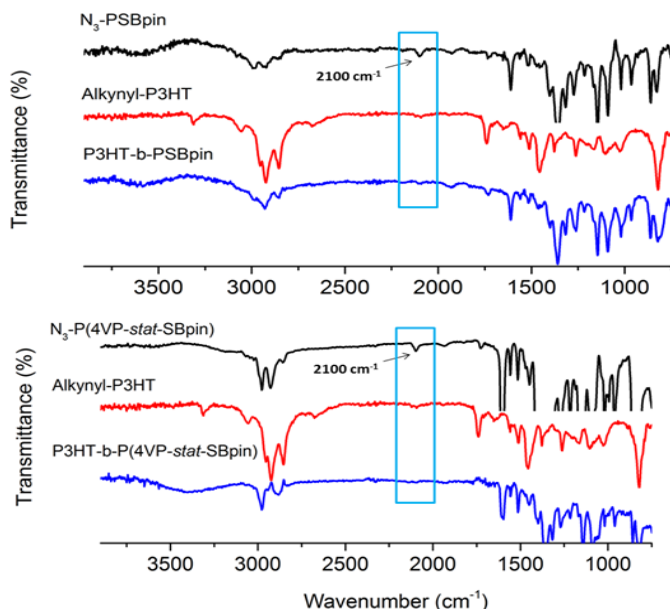
Figure 2-12. FT-IR spectra of homopolymers and block copolymer.

Deprotection of P3HT-*b*-PSBpin (RAFT & click) using phenylboronic acid and concentrated HCl generated the fully deprotected block copolymer P3HT-*b*-PSBA (RAFT & click) which was evidenced by the disappearance of the Bpin- signals at around 84 ppm and 25 ppm in the ^{13}C NMR spectra (**Figure 2-13**). However, deprotection of P3HT-*b*-P(4VP-*stat*-SBpin) under the same conditions only provided a partially deprotected block copolymer P3HT-*b*-P(4VP-*stat*-SBA/SBpin) which is evidenced by the still present but reduced intensity of the Bpin- signals in the ^{13}C NMR spectra. The partial deprotection of P3HT-*b*-P(4VP-*stat*-SBpin) might be due to quaternization of the pyridine with the acid which could play an important role in the Bpin deprotection (transesterification) process. An excess of concentrated HCl was added into a solution of partially deprotected block copolymer P3HT-b-P(4VP-*stat*-SBA/SBpin) in an attempt to

complete the deprotection process but the ^{1}H NMR and ^{13}C NMR spectra of the product indicated degradation in the presence of excess concentrated HCl. For both fully deprotected P3HT-b-PSBA and partially deprotected P3HT-*b*-P(4VP-*stat*-SBA/SBpin), the solubility of the block copolymers in chloroform and THF solvent decreased significantly. NMR samples of the block copolymers were prepared in a mixture of CDCl$_3$ and MeOH.
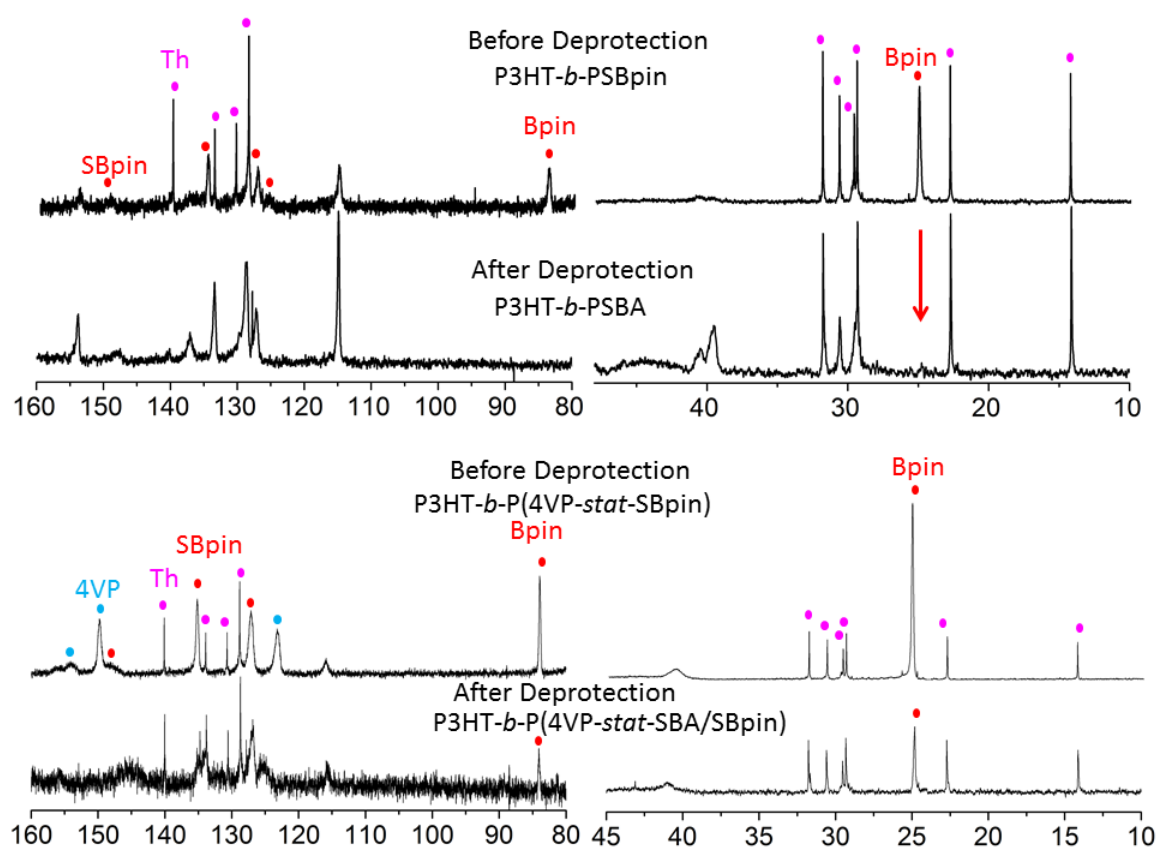
Figure 2-13. ^{13}C NMR spectra of block copolymers recorded in a mixture of CDCl$_3$ and MeOH (20:1) before and after deprotection (δ, ppm).

2.3 Conclusion

The polythiophene block copolymer P3HT-*b*-P-SBpin was successfully prepared by combining ATRP/RAFT & click chemistry and P3HT-*b*-P(4VP-*stat*-SBpin) was

prepared by combining RAFT & click chemistry. The results from GPC traces, ^{1}H NMR and ^{13}C NMR spectra, and FT-IR spectra of the homo polymers and the block copolymers proved that the combination of CRP and click chemistry indeed is a powerful tool to prepare well-defined block copolymers. Amphiphilic polythiophene block copolymers P3HT-*b*-PSBA were prepared by deprotection of the pinacol group using either polystyrene supported resin or concentrated HCl. A self-assembly study of P3HT-*b*-PSBA (ATRP&click) indicated that the micelle structure formed is not stable, possibly due to the relatively long hydrophobic rigid rod P3HT or the partial deborylation. Amphiphilic block copolymer P3HT-*b*-PSBA (RAFT & click)/P3HT-*b*-P(4VP-*stat*-SBpin/SBA) with a relatively longer PSBA block were also prepared but possible deborylation (evidenced by ^{13}C NMR spectra) during the click procedure prevented self-assembly studies of the products. In addition, deprotection of P3HT-*b*-P(4VP-*stat*-SBpin) only provided partially deprotected product which might be attributed to possible quarternization of pyridine with acid. An investigation of the effect of the Cu-catalyst on the deborylation of PSBpin and the effect of the quarternization of pyridine on the deprotection procedure would be necessary for a thorough understanding of the issues that are encountered and is expected to provide insights on possible modification for future work.

2.4 Experimental

Materials and Methods. Ether solvents and THF were distilled from Na/benzophenone prior to use. Hydrocarbon solvents were purified using a solvent purification system (Innovative Technologies; alumina/copper columns for hydrocarbon solvents). 2, 5-dibromo-3-hexylthiophene,[4b] styrene boronic acid pinacol ester,[15] and 3-

azidopropanol[18] were prepared according to literature procedures. All other reagents were commercially available (Aldrich, Acros, Strem) and either used as obtained or purified by standard procedures. All reactions and manipulations of air sensitive compounds were carried out under an atmosphere of prepurified nitrogen using either Schlenk techniques or an inert atmosphere glovebox (Innovative Technologies). All 499.9 MHz ^{1}H, 125.7 MHz ^{13}C, and 160.4 MHz ^{11}B NMR spectra were recorded at ambient temperature on a Varian INOVA 500 spectrometer and all 599.7 MHz ^{1}H, 150.8 MHz ^{13}C, and 192.4 MHz ^{11}B NMR spectra on a Varian INOVA 600 spectrometer equipped with a boron-free 5 mm dual broadband gradient probe (Nalorac, Varian Inc., Martinez, CA). Solution ^{1}H and ^{13}C NMR spectra were referenced internally to solvent signals. ^{11}B NMR spectra were acquired with boron-free quartz NMR tubes and referenced externally to BF$_3$·Et$_2$O (δ 0). GPC analyses were performed using a Viscotek GPCmax equipped with a VE 2001 GPC solvent/sample module, a 2600 PDA detector, a TDA 305 triple detector array and three columns, consisting of a PLgel 5 μm mixed-D and two PLgel 5 μm mixed-C columns. The system was calibrated against narrow polystyrene standards (10) in the molecular weight range of 580 to 371100 Da. MALDI-MS measurement of ethynyl-spacer-P3HT was performed on an AB SCIEX TOF/TOF^{TM} 5800 system (Shimaduzu) in (+) mode. The sample (10 mg/mL in THF) was mixed with dithranol (10 mg/mL in THF) as the matrix in a 1:2 ratio and then spotted on the wells of a target plate. MALDI-MS measurements of other compounds were performed on an Apex-ultra 7T Hybrid FT-MS (Bruker Daltonics) in (+) mode. The samples (10 mg/mL in THF) were mixed with anthracene or dithranol (10 mg/mL in THF) as the matrix in a 1:2 ratio and then spotted on the wells of a target plate. Dynamic light scattering (DLS) was conducted with a

Malvern Zetasizer Nano-S equipped with a 4 mV, 633 nm He-Ne laser and an Avalanche photodiode detector at an angle of 173°. Single Fourier transform infrared attenuated total reflectance (FTIR-ATR) spectra were performed on a Thermo Electron Corporation Nicolet 6700 FTIR (ZnSe crystal, with the number of spectra averaged of 128 and a resolution of 4 cm^{-1}).

Synthesis of Ethynyl-P3HT. All reactions were performed in a glove box or on a Schlenk line under N_2 atmosphere. The ethynyl-terminated poly(3-hexylthiophene) (ethynyl-P3HT) was prepared according to a literature procedure.[6a,7c,e,19] A solution of monomer **1** (3.00 g, 9.20 mmol) and LiCl (0.39 g, 9.20 mmol) in 40 mL of THF was stirred for 30 min. *t*-BuMgCl·1.44Et$_2$O (2.06 g, 9.20 mmol) in 40 mL of THF was added at RT and the mixture was stirred overnight. The reaction mixture (11.5 mL, 1.15 mmol) was added to a solution of Ni(dppp)Cl$_2$ (0.13 g, 0.23 mmol) in 10 mL of THF and stirred for 10 min until homogeneous to pre-initiate the catalyst as reported in the literature.[20] The pre-initiated Ni(dppp)Cl$_2$ catalyst was combined with the rest of the reaction mixture and stirred for 20 min before quenching with ethynylmagnesium chloride (4.6 mL, 2.3 mmol, 0.5 M) in an ice-bath. After 15 min the reaction mixture was precipitated by adding MeOH. The polymer was re-dissolved in THF, filtered through a short silica gel and precipitated in MeOH. After filtration and drying under vacuum, a black solid was obtained. Yield: 1.10 g, 37%. GPC (THF, 1 mL/min): M$_n$ = 7740 g/mol, Đ = 1.16. ^{1}H NMR (499.9 MHz, CDCl$_3$) δ = 7.00, 3.54, 2.82 (br), 1.72 (br), 1.45 (br), 1.36 (br), 0.93 (br).

Synthesis of Br-PSBpin[15] using ATRP. To a 25 ml Schlenk flask were added styrene boronic acid pinacol ester (4.0 g, 17.4 mmol), 1-phenylethylbromide (PEB) (32 mg,

0.174 mmol), CuBr (50 mg, 0.348 mmol), PMDETA (0.121 g, 0.696 mmol) and anisole (4.0 g) in a glove box. The reaction mixture was immersed into an oil bath that was preset to 90 ℃. After 40 min, the flask was cooled to RT. **Br-PSBpin** was recovered as a white solid by precipitation into MeOH/H_2O mixture (80/20). The solid was redissolved in THF, passed through a short plug of alumina, and precipitated once again into a MeOH/H_2O mixture (60:10). The polymer was filtered and dried under high vacuum to provide a white solid. Yield: 0.72 g, 18%. GPC (THF, 1 mL/min): Mn = 3530 g/mol, $Đ$ = 1.08.

Synthesis of N_3-PSBpin. [14a] **Br-PSBpin** (0.67 g, 0.19 mmol) and NaN_3 (122 mg, 1.80 mmol) were dissolved in DMF (15 mL) in a 25 mL round-bottom flask. The mixture was stirred at RT overnight, and the resulting polymer was isolated by repeated precipitation into a MeOH/H_2O mixture (60:10) and dried under vacuum to provide a white solid. Yield: 410 mg, 61%. GPC (THF, 1 mL/min): M_n = 3760 g/mol, $Đ$ = 1.10. ^{1}H NMR (499.9 MHz, $CDCl_3$) δ = 7.60 (br), 6.66 (br), 1.66, 1.34, 0.85. ^{13}C NMR (150.8 MHz, $CDCl_3$) δ = 148.77 (br), 134.91, 127.34, 126.13 (br), 83.49, 40.68 (br), 25.10. IR: 2097 cm^{-1}($-N_3$).

Synthesis of P3HT-*b*-PSBpin Block Copolymers (ATRP & click).[7c] Ethynyl- P3HT (Mn = 7740 g/mol, 192 mg, 2.6×10^{-2} mmol), **N_3-PSBpin** (350 mg, 9.9×10^{-2} mmol), and CuI (3.6 mg, 1.9×10^{-2} mmol, 38 equiv) were added to a Schlenk flask, evacuated for 15 min and backfilled with nitrogen. A solution of DBU (286.9 mg, 1.88 mmol, 37.5 equiv) in THF (50mL) was added and the flask was placed in a preset oil bath at 40℃ for 3 days. The reaction mixture was cooled to RT and passed through a short plug of alumina. The block copolymer was recovered by precipitation in MeOH/H_2O mixture (300 mL : 50 mL), filtered and dried under high vacuum overnight to provide a black solid. Yield:

250 mg, 89%. GPC (THF, 1 mL/min): M_n = 11300 g/mol, $Đ$ =1.23. ^{1}H NMR (599.7 MHz, CDCl$_3$) δ = 7.60 (br), 6.99, 6.60 (br), 2.82, 1.72, 1.45, 1.36, 0.93. ^{13}C NMR (150.8 MHz, CDCl$_3$) δ = 140.09, 135.15 (br), 133.90, 130.69, 128.81, 127.19 (br), 40.81 (br), 31.91, 30.72, 29.68, 29.47, 25.12, 22.86. ^{11}B NMR (160.4 MHz, CDCl$_3$) δ = 27.3, $w_{1/2}$ = 2700 Hz.

Deprotection of P3HT-*b*-PSBpin (ATRP and Click) Block Copolymers [21] using Polystyrene-supported Boronic Acid. In a 25 mL of round bottom flask, **P3HT-*b*-PSBpin** block copolymers (50 mg, 0.0044 mmol) and PS-supported boronic acid (50 mg, 0.15 mmol, ~3 mmol/g loading) were added 6 mL of THF and 0.2 mL of trifluoacetic acid. The reaction mixture was refluxed at 65 °C overnight and cooled to RT, filtered, washed with THF, reduced and dialyzed against distilled water. The block copolymer precipitated and was filtered. The block copolymer after deprotection reaction was analyzed by ^{1}H NMR (499.9 MHz, CDCl$_3$) δ = 7.00, 2.82, 1.70-1.63, 1.43-1.26, 0.91. ^{1}H NMR (499.9 MHz, CDCl$_3$ and DMSO) δ = 7.52 (br), 6.93, 6.49 (br), 2.71, 1.59, 1.36-1.27, 0.83. ^{13}C NMR (150.8 MHz, CDCl$_3$ and MeOH) δ = 140.07, 133.85, 130.63, 128.76, 127.38 (br), 115.21, 31.84, 30.66, 29.61, 29.40, 24.91, 22.80, 14.24.

Synthesis of Ethynyl-spacer-P3HT using RAFT.[17a] Hydroxypropyl-terminated P3HT[22] (0.285 g, 0.092 mmol, DP$_n$ (NMR) = 14), pentynoic acid (90 mg, 0.92 mmol), and 4-dimethylaminopyridine (DMAP) (6.0 mg, 0.047 mmol) were dissolved in anhydrous THF (7 mL) under nitrogen. To this reaction mixture, *N,N'*−dicyclohexylcarbodiimide (DCC) (0.228 g, 1.10 mmol) in 3 mL of THF was slowly added at RT and the mixture was stirred overnight. After filtration, the reaction mixture was precipitated in MeOH. A black solid was obtained after filtration and drying under

high vacuum. Yield: 155 mg, 54%. GPC (THF, 1 mL/min): M_n = 7090, $Đ$ = 1.13, DP_n = 42. ^{1}H NMR (599.7 MHz, CDCl$_3$, DP_n = 14) δ = 7.00, 4.19, 2.81, 2.55, 1.99, 1.71, 1.45-1.36, 0.92. ^{13}C NMR (150.8 MHz, CDCl$_3$ and MeOH-d$_4$) δ = 140.08, 133.87, 130.65, 128.78, 69.29, 64.08, 31.87, 30.68, 29.64, 29.43, 22.83, 14.28.

Synthesis of 2-Dodecylsulfanylthiocarbonylsulfanyl-2-methylpropionic Acid 3-Azidopropyl Ester.[18] A solution of 2-dodecylsulfanylthiocarbonylsulfanyl-2-methyl-propionic acid (1.50 g, 4.11 mmol), 3-azidopropanol (0.72 g, 7.16 mmol), and DMAP (0.025 g, 0.21 mmol) in 10 mL of dry DCM was brought to 0 °C. A solution of DCC (1.02 g, 4.93 mmol) in 10 mL of DCM was added slowly and the mixture was stirred overnight. After filtration, the reaction mixture was extracted with DCM/0.5 N HCl, the organic layers were combined and washed with saturated NaHCO$_3$ solution and dried over sodium sulfate. The product was obtained as a yellow oil after purification by silica gel chromatography (eluent: Hexanes/EtOAC = 9:1). Yield: 1.3 g, 71%. ^{1}H NMR (599.7 MHz, CDCl$_3$): 4.19 (t, 2H, J = 6.0 Hz,-CH$_2$-CH$_2$-O-C≡O), 3.36 (t, 2H, J = 6.9 Hz, -CH$_2$-CH$_2$-N$_3$), 3.28 (t, 2H, J= 7.6 Hz, -CH$_2$-CH$_2$-S-C=S), 1.91 (p, 2H, J = 6.3 Hz, -CH$_2$-CH$_2$-N$_3$), 1.71-1.62 (m, 8H, -CH$_2$-CH$_2$-S-C=S and -S-C(CH$_3$)$_2$-CO), 1.38-1.25 (m, 18H, CH$_3$-C$_9$H$_{18}$-CH$_2$-CH$_2$S-C=S), 0.89 (t, 3H, J = 5.9 Hz, CH$_3$-C$_9$H$_{18}$-CH$_2$-CH$_2$S-C=S).

Synthesis of Polymer N$_3$-PSBpin using RAFT.[18] A solution of 2-dodecylsulfanylthiocarbonylsulfanyl-2-methylpropionic acid 3-azidopropyl ester (38 mg, 0.086 mmol), 4,4,5,5-tetramethyl-2-(4-vinylphenyl)-1,3,2-dioxaborolane (SBpin) (3.98 g, 17.3 mmol), and AIBN (2.82 mg, 0.0172 mmol) in 2 mL of dioxane was subjected to three freeze-pump-thaw cycles and then heated at 70 °C for 140 mins. The polymerization was quenched by immersing the reaction tube in liquid nitrogen. After

diluting with THF the product was precipitated twice in MeOH. The polymer was obtained as a white solid after filtration and drying under high vacuum. Yield: 0.60 g, 18%.   GPC (THF, 1 mL/min): M_n = 7930, $Đ$ = 1.20, DP_n = 35. ^{1}H NMR (599.7 MHz, CDCl$_3$) δ = 7.57 (br), 6.56 (br), 1.31, 0.87. ^{11}B NMR (192.4 MHz, CDCl$_3$) δ = 27.3 (br), $w_{1/2}$ = 1850 Hz.

Synthesis of Copolymer N$_3$-P(4VP-*stat*-SBpin) using RAFT.[18]   A solution of 2-dodecylsulfanylthiocarbonylsulfanyl-2-methylpropionic acid 3-azidopropyl ester (45 mg, 0.10 mmol), 4-vinylpyridine (4VP) (0.80 g, 7.6 mmol), 4,4,5,5-tetramethyl-2-(4-vinylphenyl)-1,3,2-dioxaborolane (SBpin) (2.313 g, 10.05 mmol), and AIBN (3.3 mg, 0.020 mmol) in 1 mL of dioxane were subjected to three freeze-pump-thaw cycles and then heated at 70 °C for 5 hours. The polymerization was quenched by immersing the reaction tube in liquid nitrogen. After diluting with THF the product was precipitated twice in hexanes. The polymer was obtained as a beige white solid after filtration and drying under high vacuum. Yield: 1.3 g, 42%. GPC (THF, 1 mL/min): M_n = 14100, $Đ$ =1.13. ^{1}H NMR (599.7 MHz, CDCl$_3$) δ = 8.24 (br), 7.54 (br), 6.39 (br), 1.70, 1.33, 0.87. ^{13}C NMR (150.8 MHz, CDCl$_3$) δ = 153.50 (br), 149.89, 147.70 (br), 135.11, 127.23, 123.02, 83.88, 44.71-40.61 (br), 25.14.

Synthesis of P3HT-*b*-PSBpin Block Copolymer (RAFT & click). [7d] **Ethynyl-spacer-P3HT** (M_n = 7090 g/mol, 30 mg, 4.23 μmol), **N$_3$-PSBpin** (M_n = 7930 g/mol, 134 mg, 16.92 μmol) were added to a Schlenk flask, which was evacuated for 15 min and backfilled with nitrogen. Then 10 mL of THF, PMDETA (50 mg, 2.89 μmol, 68 equiv), and CuBr (13 mg, 90.6 μmol, 21 equiv) were added under N$_2$ flow. The flask was placed in a preset oil bath at 50 °C for 2 days. The reaction mixture was cooled to RT and passed

through a short plug of alumina. The block copolymer was recovered as a black solid by precipitation in MeOH, filtered and dried under high vacuum overnight. Yield: 86.6 mg, 61%. GPC (THF, 1 mL/min): M_n = 12400 g/mol, $Đ$ =1.24 g/mol. ^{1}H NMR (599.7 MHz, CDCl$_3$) δ = 7.51 (br), 6.99, 6.48 (br), 2.81, 1.71, 1.31, 0.92. ^{13}C NMR (150.8 MHz, CDCl$_3$) δ = 140.09, 134.76, 133.79, 130.66, 128.79, 127.38, 115.14, 83.97, 40.26 (br), 31.77, 30.62, 29.65, 29.44, 25.01, 22.83. ^{11}B NMR (192.4 MHz, CDCl$_3$) δ = 26.7 (br), 21.9 (sharp), $w_{1/2}$ = 1430 Hz.

Synthesis of P3HT-*b*-P(4VP-*stat*-SBpin) Block Copolymer.[7d] Ethynyl-spacer-P3HT (M_n = 7090 g/mol, 30 mg, 4.23 µmol), **N$_3$-P(4VP-*stat*-SBpin)** (M_n = 14100 g/mol, 134 mg, 14.2 µmol) were added to a Schlenk flask, which was evacuated for 15 min and backfilled with nitrogen. Then 10 mL of THF, PMDETA (50 mg, 289 µmol, 68 equiv), and CuBr (11 mg, 76.7 µmol, 18 equiv) were added under N$_2$ flow. The flask was placed in a preset oil bath at 50 °C for 2 days. The reaction mixture was cooled to RT and passed through a short plug of alumina. The block copolymer was recovered as a black solid by precipitation in MeOH, filtered and dried under high vacuum overnight. Yield: 93.0 mg, 74%. GPC (THF, 1 mL/min): M_n = 16300 g/mol, $Đ$ = 1.29 g/mol. ^{1}H NMR (599.7 MHz, CDCl$_3$) δ = 8.31 (br), 7.59 (br), 6.99, 6.50 (br), 2.80, 1.70, 1.35, 0.92. ^{13}C NMR (150.8 MHz, CDCl$_3$) δ = 149.74, 140.10, 135.17, 133.90, 130.70, 128.81, 127.14, 123.21, 115.83, 83.95, 40.54 (br), 31.90, 30.72, 29.68, 29.47, 25.14, 22.86, 14.33. ^{11}B NMR (192.4 MHz, CDCl$_3$) δ = 26.8 (br), $w_{1/2}$ = 1150 Hz.

Deprotection of P3HT-*b*-PSBpin (RAFT & click)/P3HT-*b*-P(4VP-*stat*-PSBpin) Block Copolymers using Phenylboronic Acid and Concentrated HCl.[12a,23] In a 20 mL of vial, to 30 mg of block copolymer in 1 mL of THF were slowly added 50 mg of

phenylboronic acid in 0.2 mL of MeOH. Then one drop of concentrated HCl was added and the mixture was stirred overnight. The reaction mixture was precipitated into hexanes, and washed thoroughly with MeOH/H$_2$O mixure. The precipitate was isolated and dried to provide a purple solid. Yield: P3HT-b-PSBA, 10.3 mg, 34%; P3HT-*b*-P(4VP-*stat*-PSBA), 9.5 mg, 32%. The deprotected amphiphilic block copolymer was characterized by ^{1}H NMR and ^{13}C NMR spectroscopy.
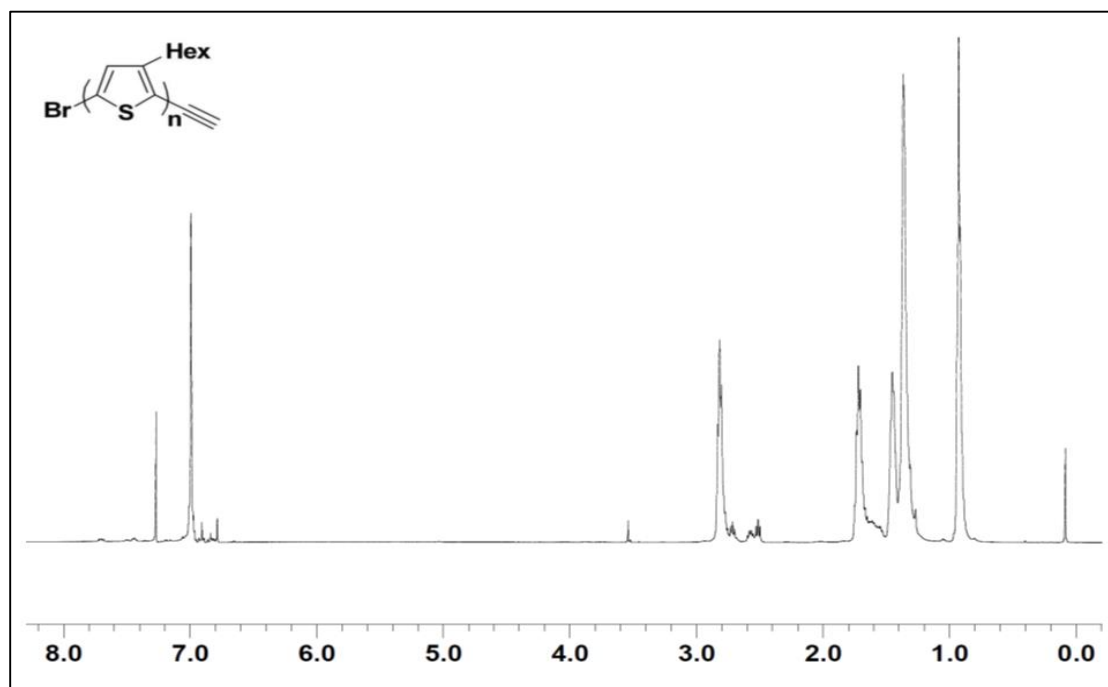
Figure 2-14. ^{1}H NMR of **Ethynyl-P3HT** recorded in CDCl$_3$ (δ, ppm).
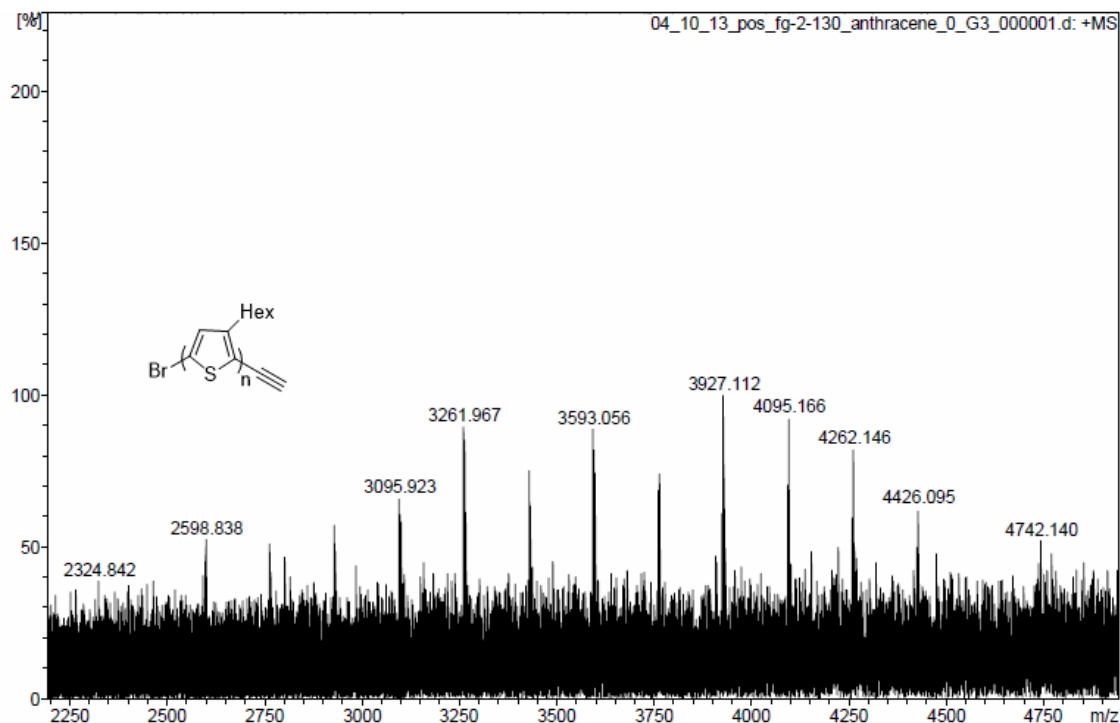
Figure 2-15. High resolution (pos. mode) MALDI-MS data of **Ethynyl-P3HT** (matrix-anthracene).
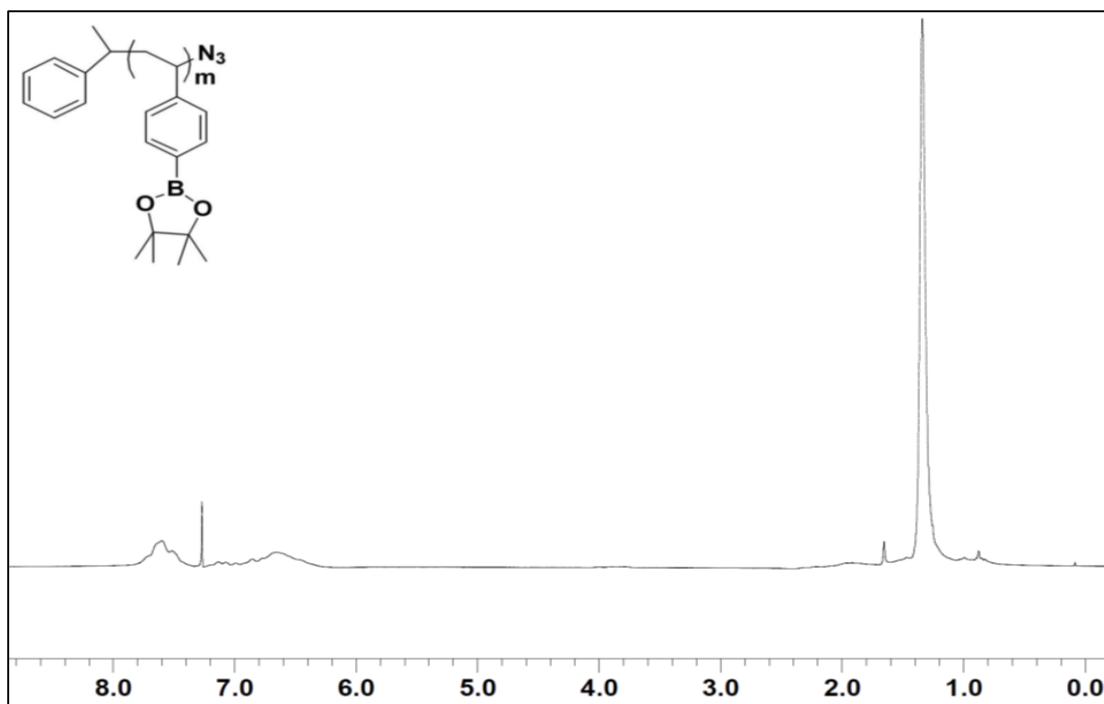
Figure 2-16. ^{1}H NMR of **N$_3$-PSBpin** recorded in CDCl$_3$ (δ, ppm).
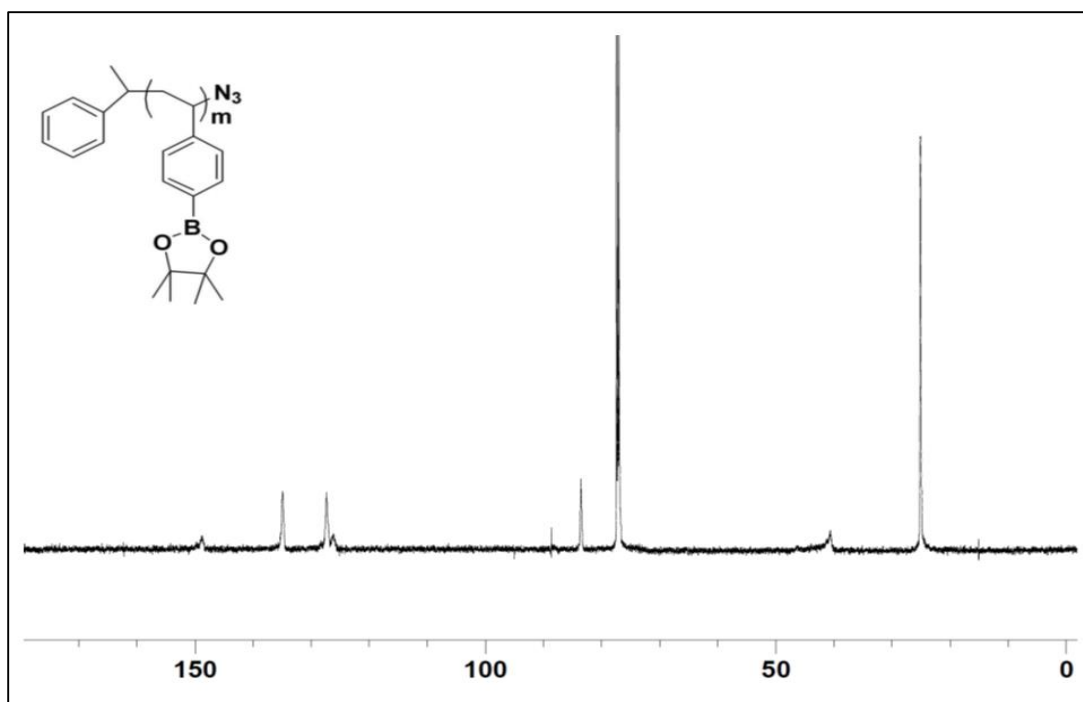
Figure 2-17. ^{13}C NMR of **N₃-PSBpin** recorded in CDCl₃ (δ, ppm).
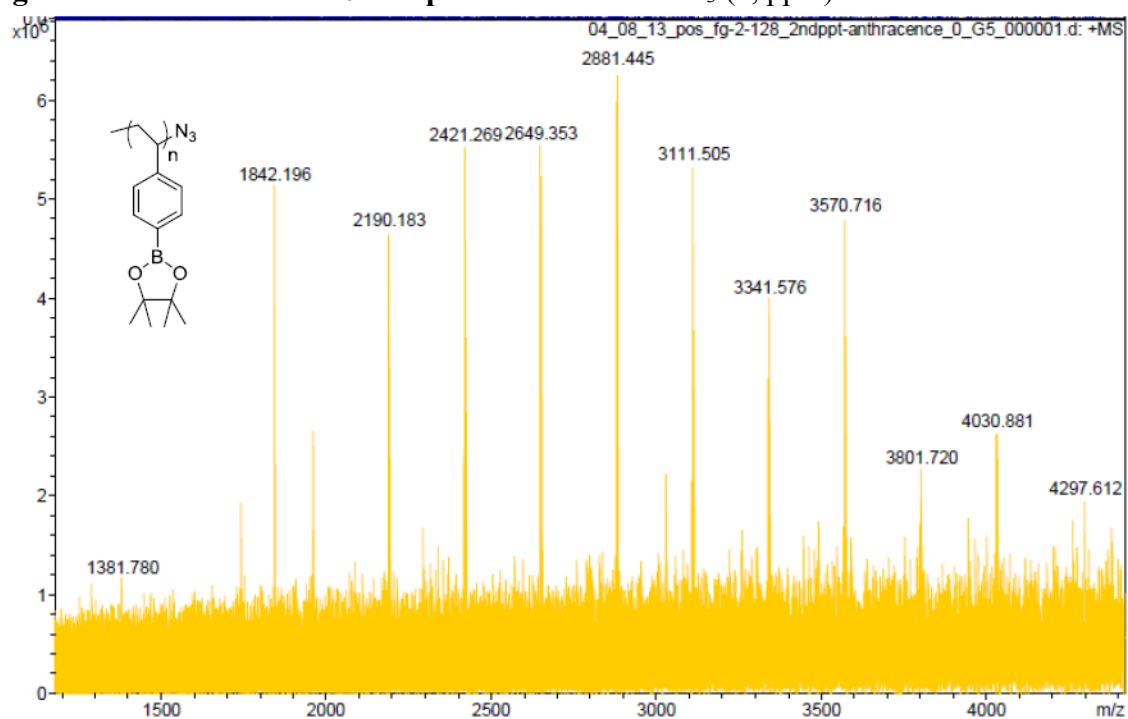
Figure 2-18. High resolution MALDI-MS (pos. mode) data of **N₃-PSBpin (ATRP)** (matrix-dithranol)
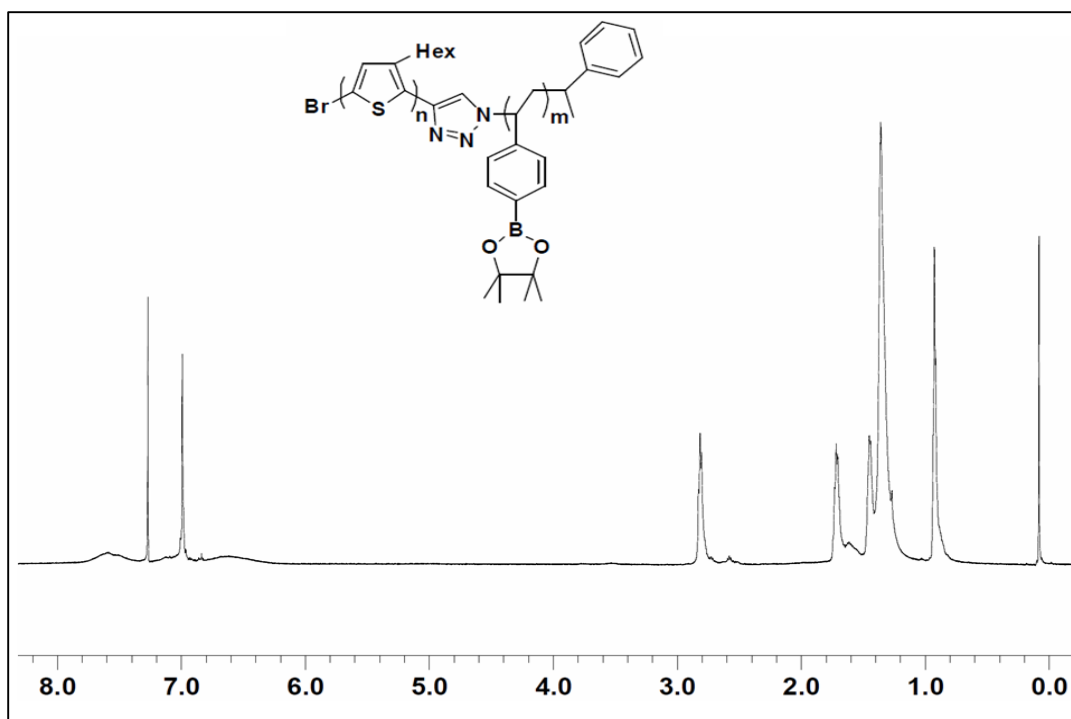
Figure 2-19. ^{1}H NMR of **P3HT-*b*-PSBpin (ATRP & click)** recorded in CDCl$_3$ (δ, ppm).
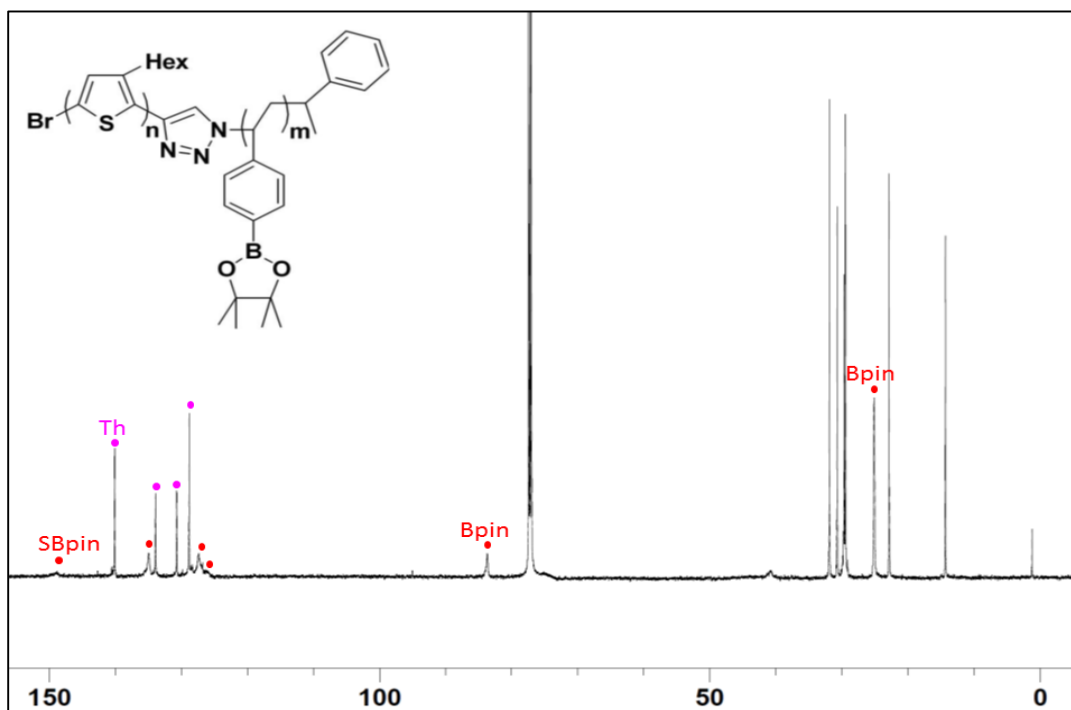
Figure 2-20. ^{13}C NMR of **P3HT-*b*-PSBpin (ATRP & click)** recorded in CDCl$_3$ (δ, ppm).
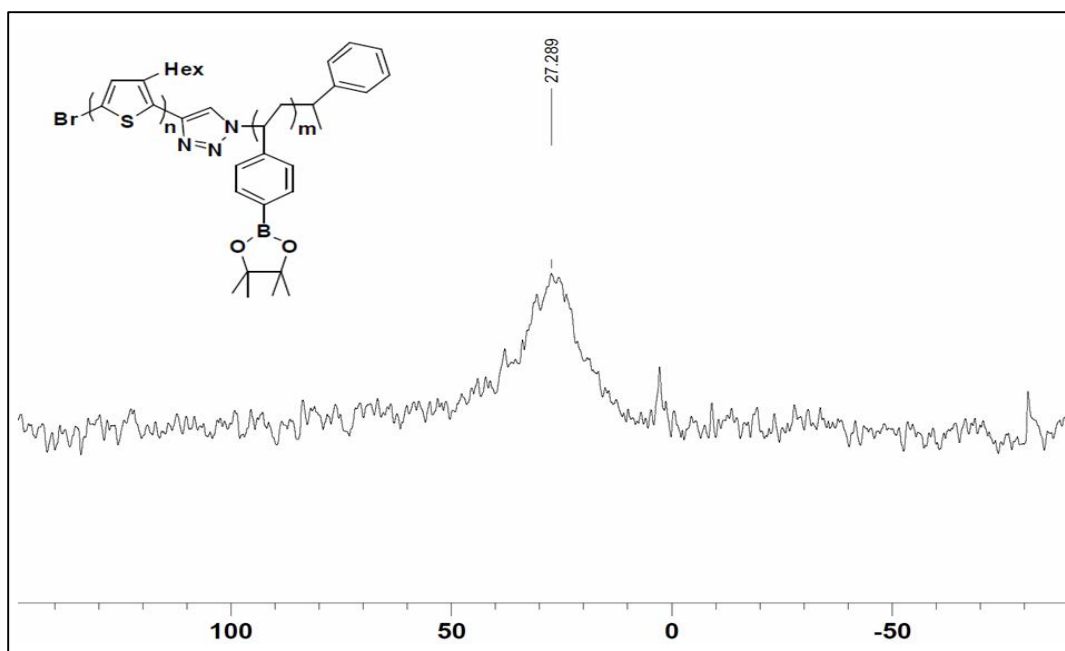
Figure 2-21. ^{11}B NMR of **P3HT-*b*-PSBpin (ATRP & click)** recorded in CDCl$_3$ (δ, ppm).
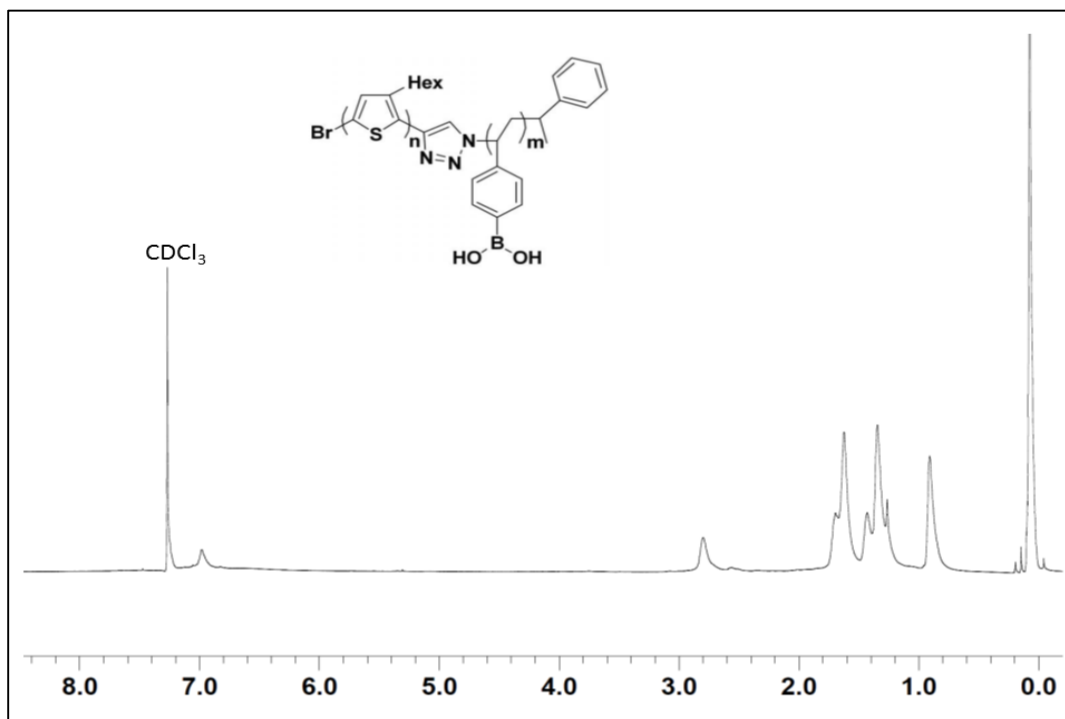
Figure 2-22. ^{1}H NMR of **P3HT-*b*-PSBA (ATRP & click)** recorded in CDCl$_3$ (δ, ppm)
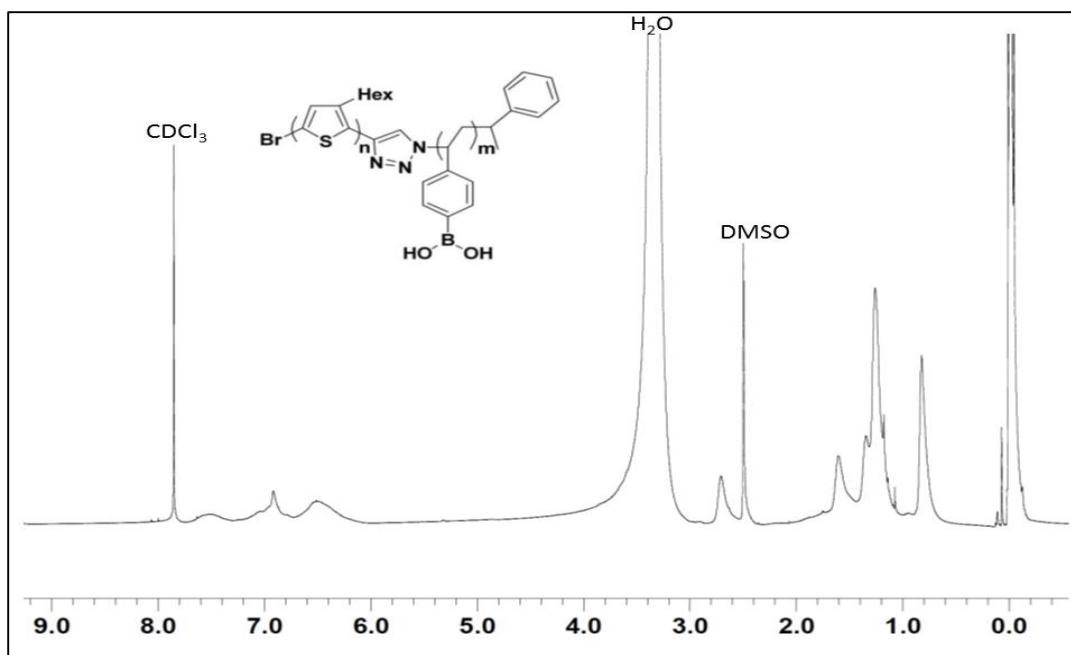
Figure 2-23. ^{1}H NMR of **P3HT-*b*-PSBA (ATRP & click)** recorded in a CDCl$_3$/ DMSO-d$_6$ (20:3) (δ, ppm).
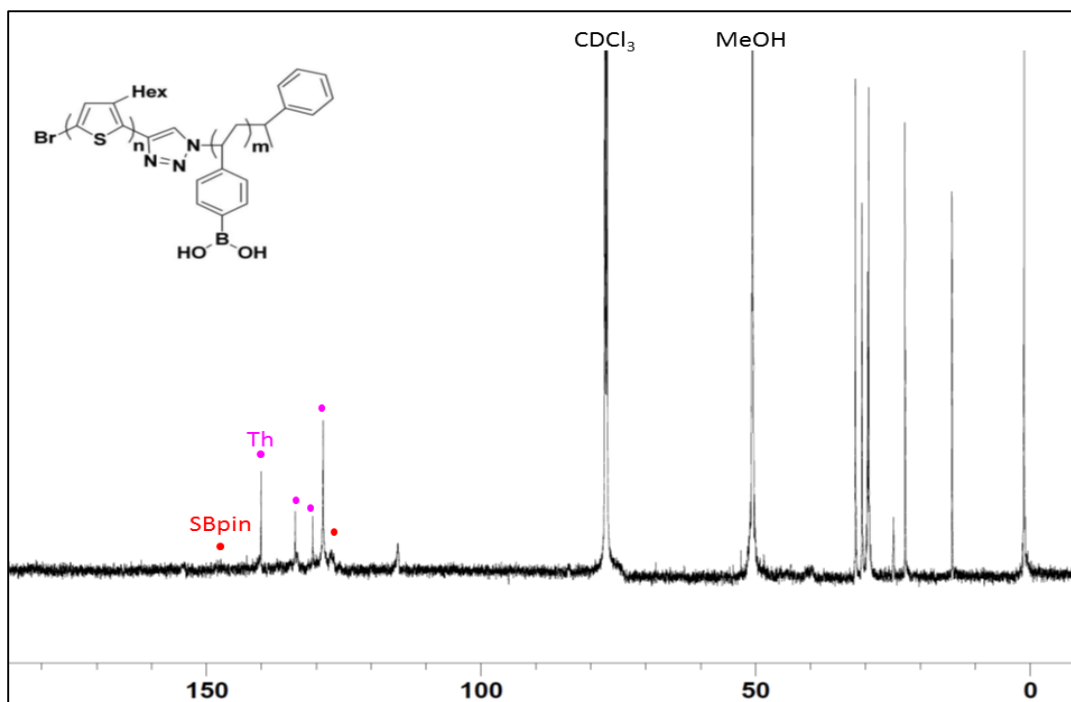
Figure 2-24. ^{13}C NMR of **P3HT-*b*-PSBA (ATRP & click)** recorded in a CDCl$_3$/MeOH mixture (5:1) (δ, ppm).
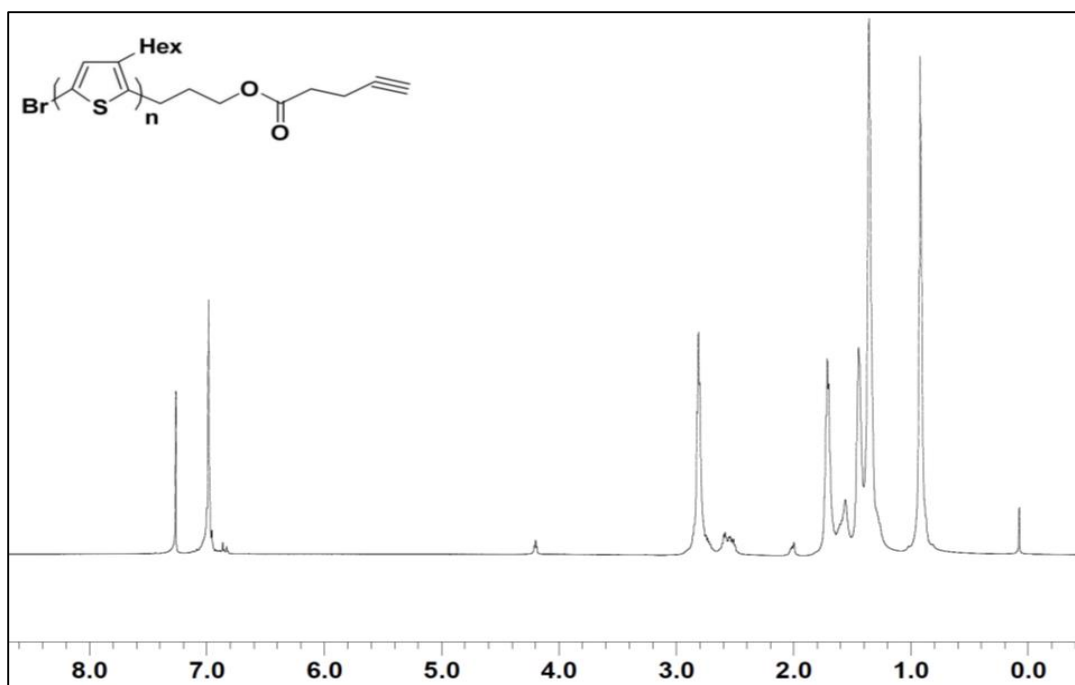
Figure 2-25. ^{1}H NMR of **Ethynyl-spacer-P3HT** recorded in CDCl$_3$ (δ, ppm).
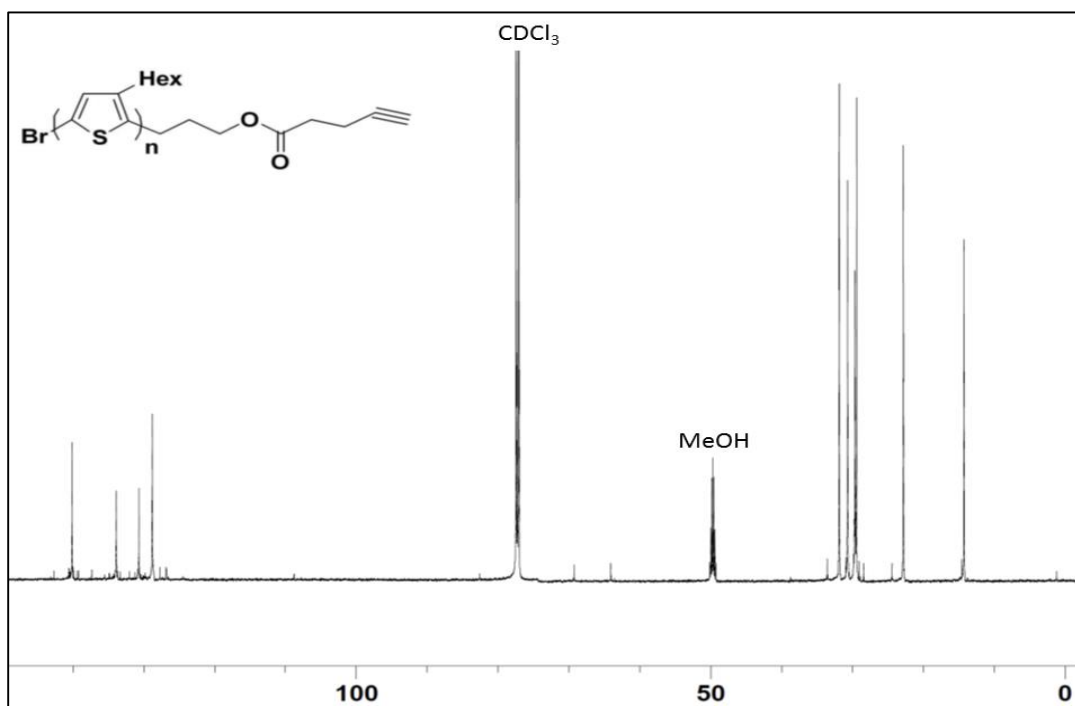
Figure 2-26. ^{13}C NMR of **Ethynyl-spacer-P3HT** recorded in a CDCl$_3$/MeOH-d$_4$ mixture (20:1) (δ, ppm)
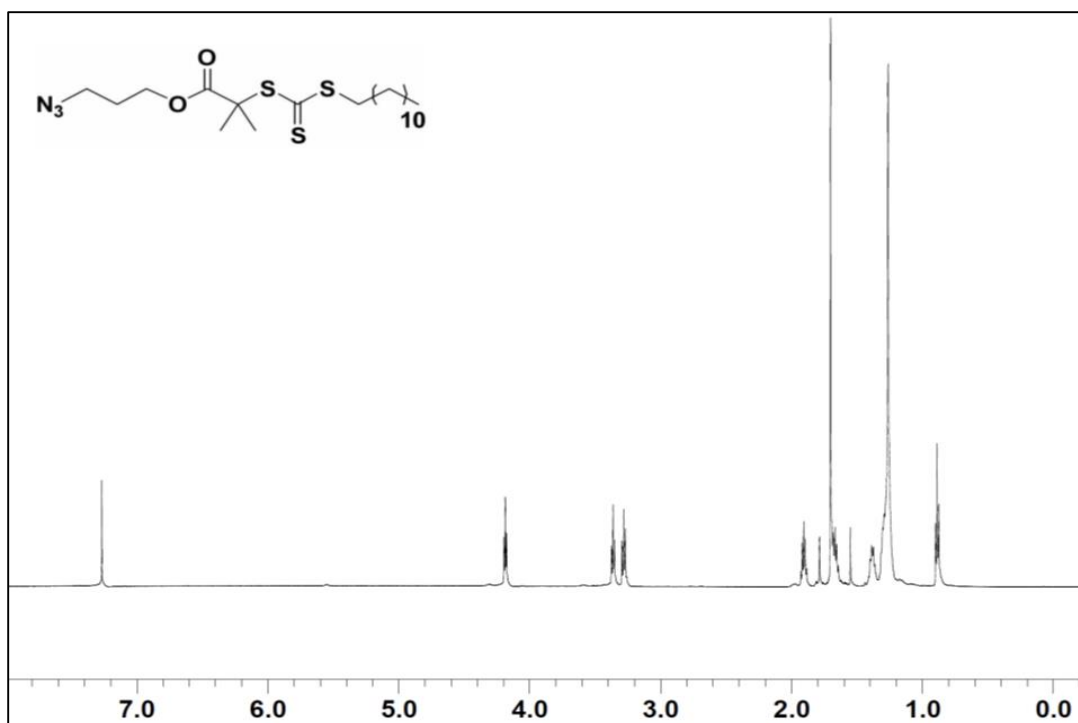
Figure 2-27. ^{1}H NMR of **2-Dodecylsulfanylthiocarbonylsulfanyl-2-methylpropionic Acid 3-Azidopropyl Ester** recorded in CDCl$_3$ (δ, ppm).
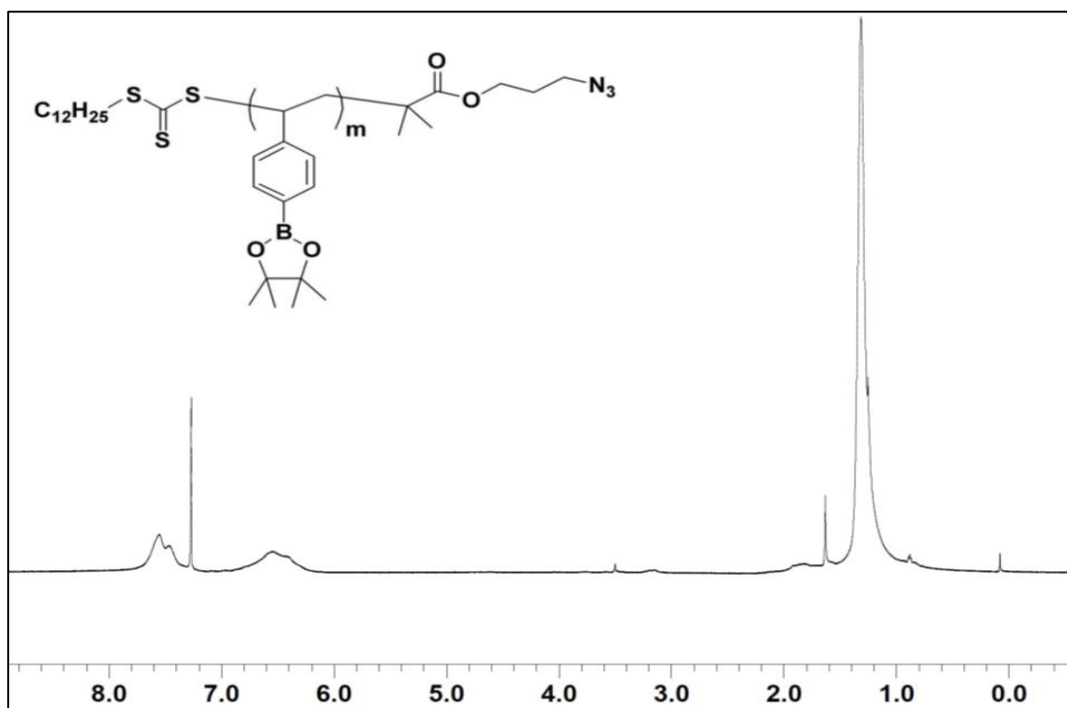
Figure 2-28. ^{1}H NMR of **N$_3$-PSBpin (RAFT)** recorded in CDCl$_3$ (δ, ppm).
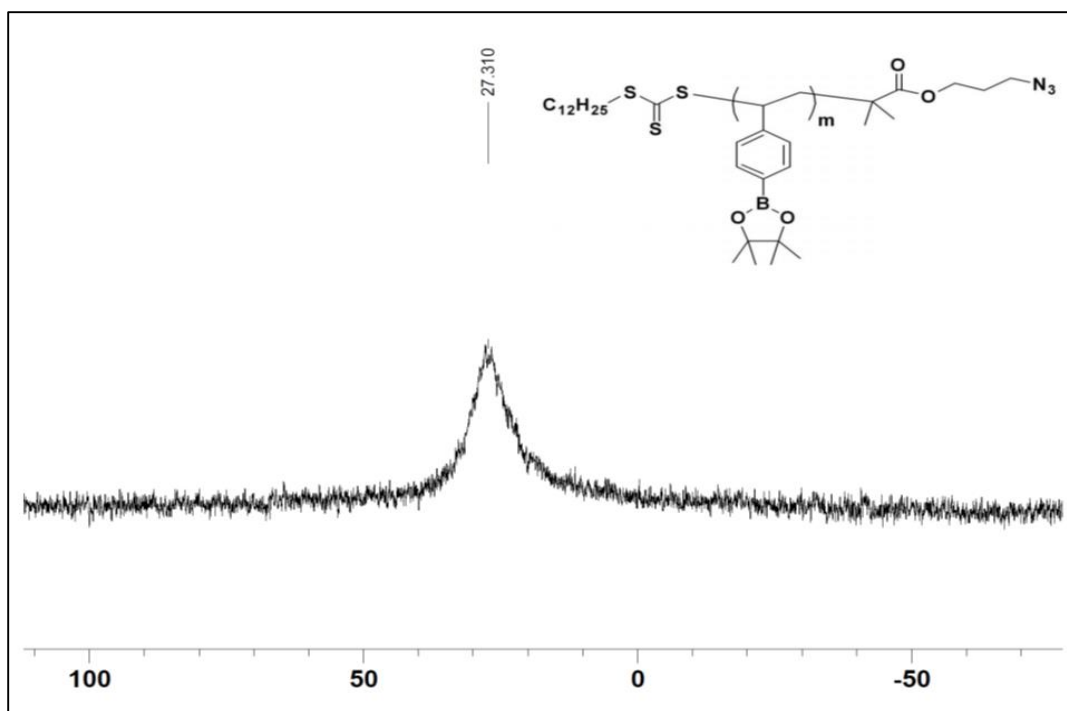
Figure 2-29. ^{11}B NMR of **N₃-PSBpin (RAFT)** recorded in CDCl₃ (δ, ppm).
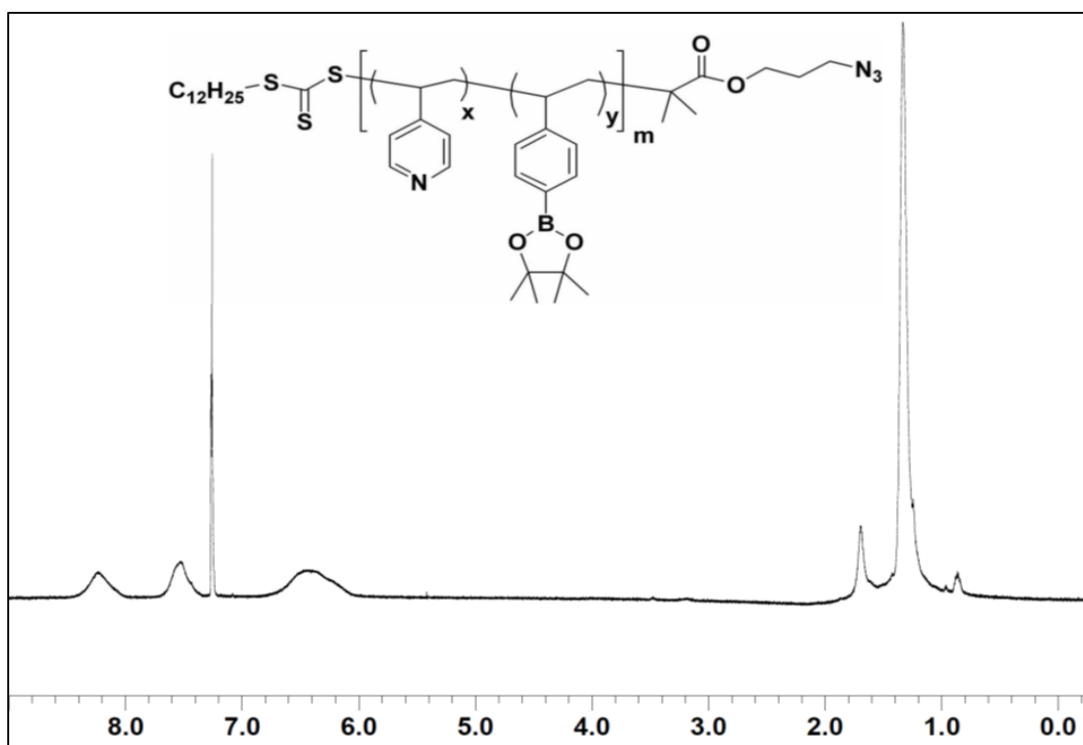
Figure 2-30. ^{1}H NMR of **N₃-P(4VP-*stat*-SBpin)** recorded in CDCl₃ (δ, ppm).
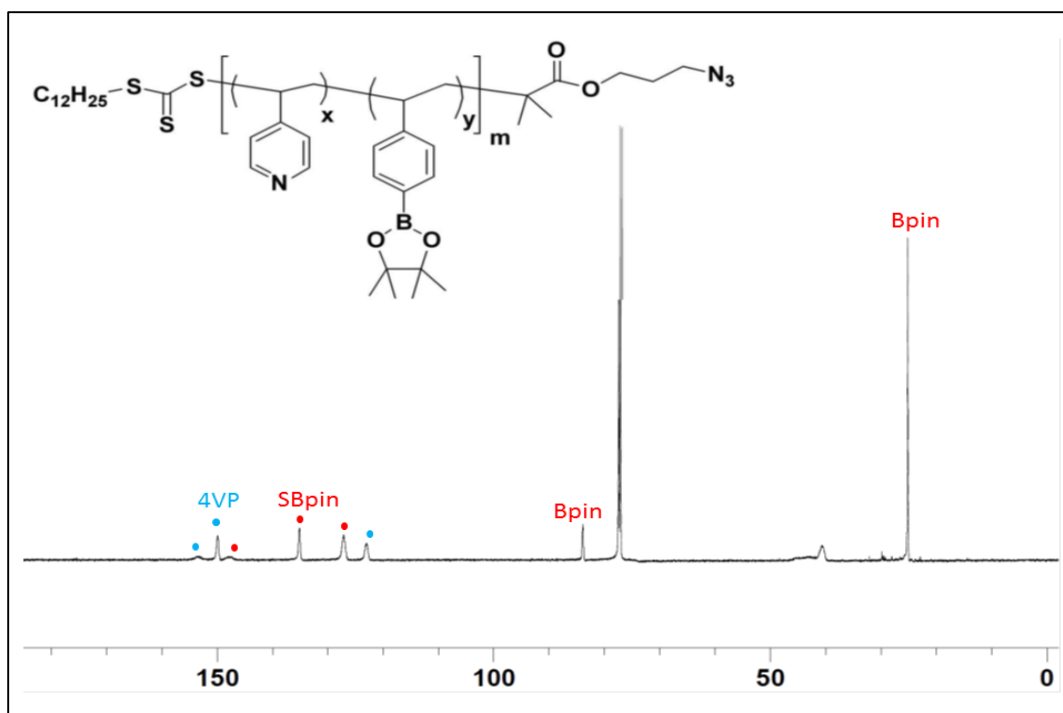
Figure 2-31. ^{13}C NMR of **N$_3$-P(4VP-*stat*-SBpin)** recorded in CDCl$_3$ (δ, ppm).
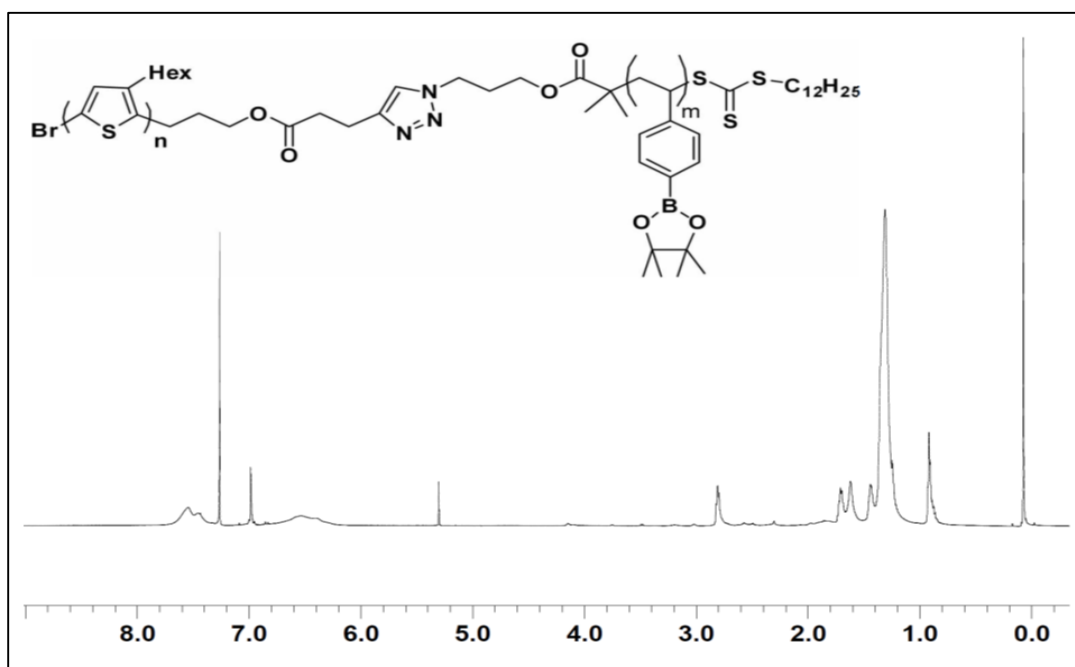
Figure 2-32. ^{1}H NMR of **P3HT-*b*-PSBpin (RAFT & click)** recorded in CDCl$_3$ (δ, ppm).
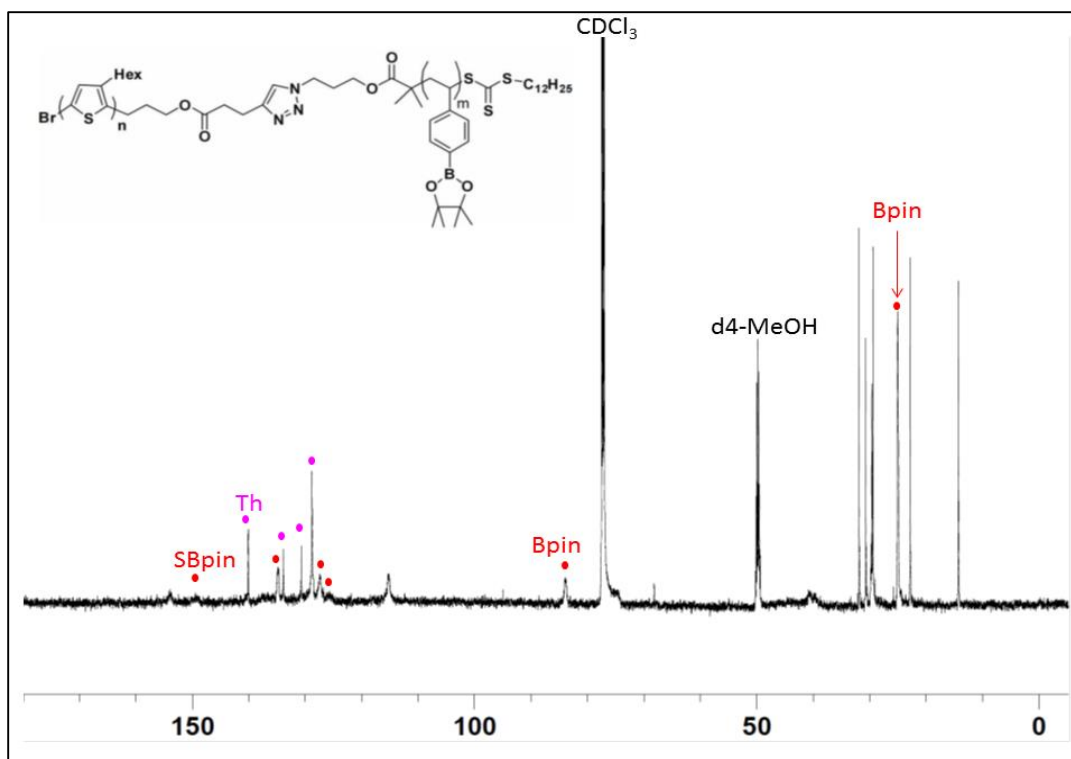
Figure 2-33. ^{13}C NMR of **P3HT-*b*-PSBpin (RAFT & click)** recorded in CDCl$_3$/MeOH-d$_4$ mixture (20:1) (δ, ppm).
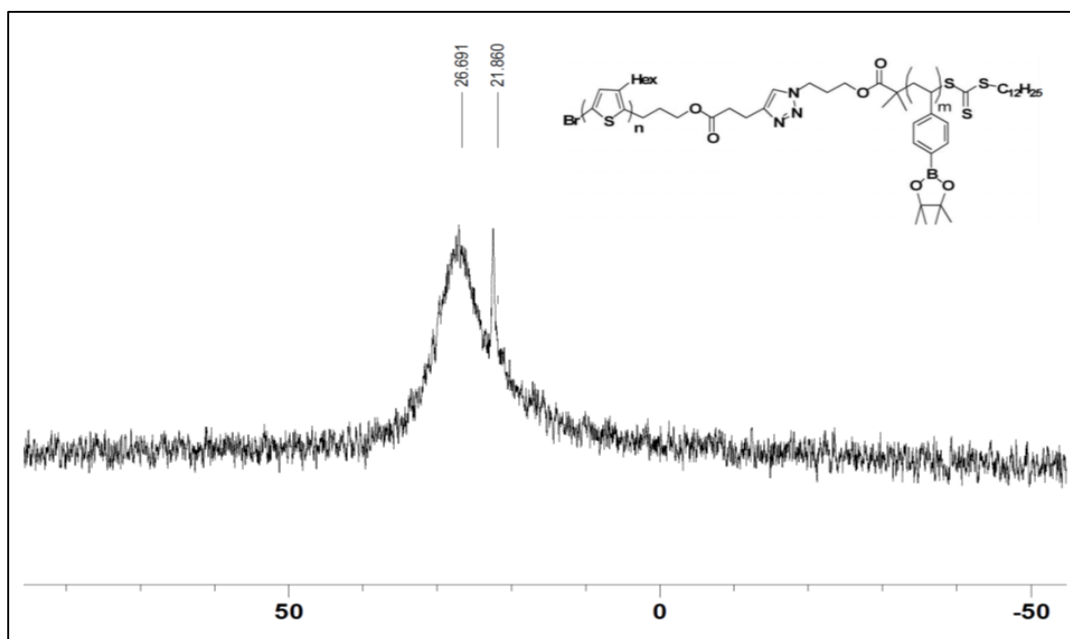
Figure 2-34. ^{11}B NMR of **P3HT-*b*-PSBpin (RAFT & click)** recorded in CDCl$_3$ (δ, ppm).
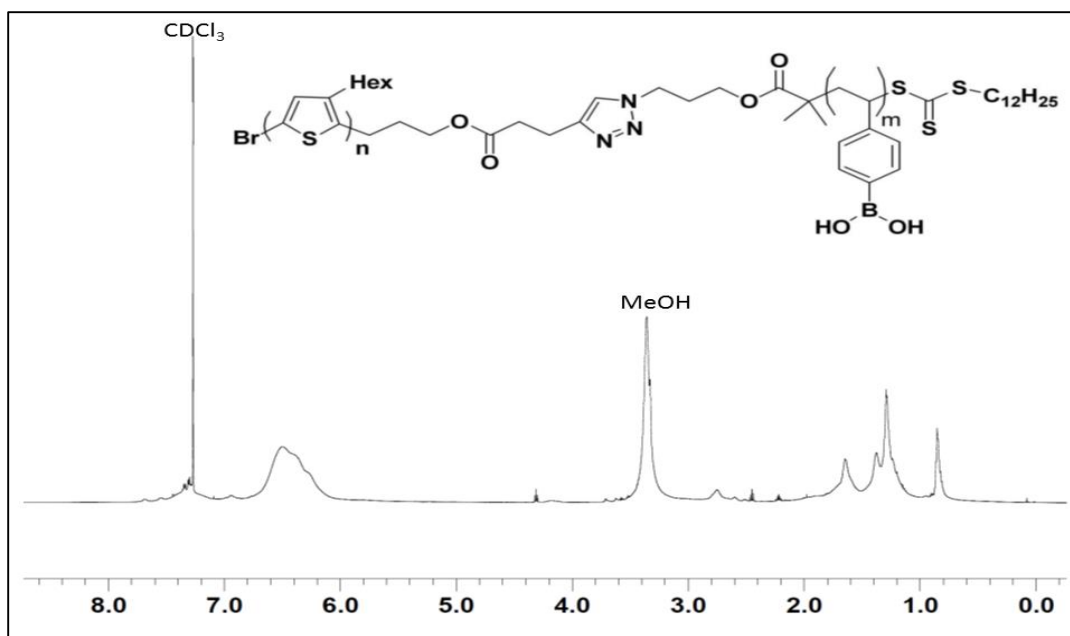
Figure 2-35. ^{1}H NMR of **P3HT-*b*-PSBA (RAFT & click)** recorded in CDCl$_3$ and MeOH (δ, ppm).
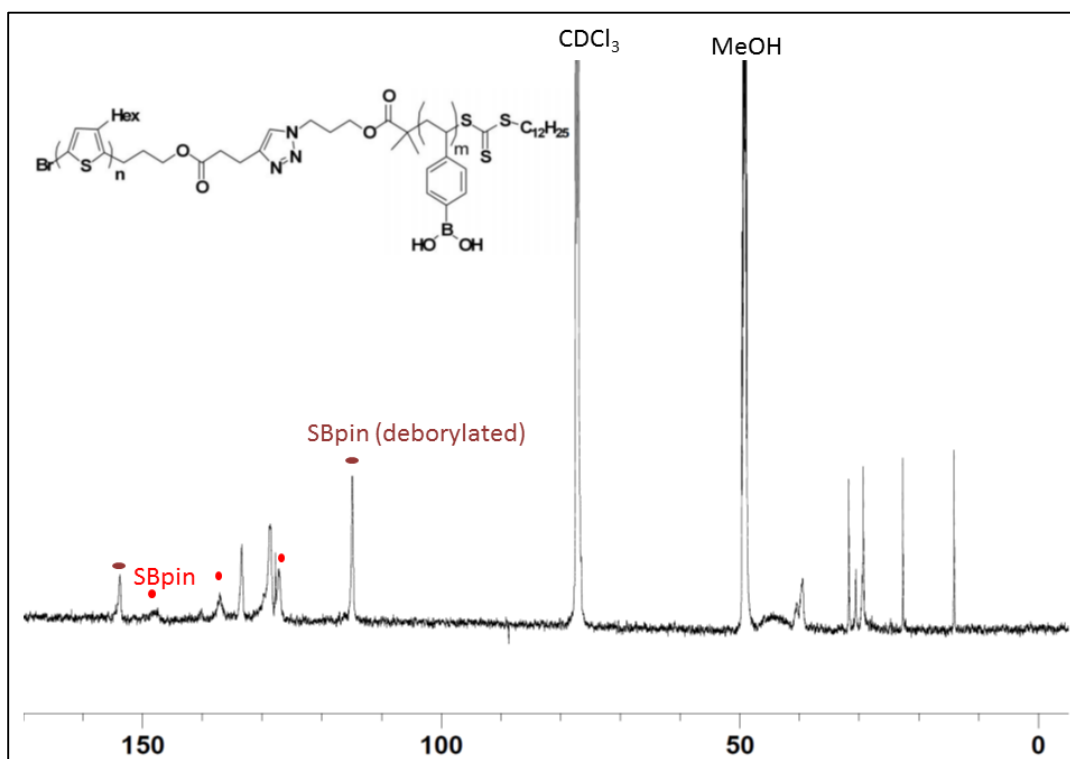
Figure 2-36. ^{13}C NMR of **P3HT-*b*-PSBA (RAFT & click)** recorded in CDCl$_3$/MeOH mixture (20:3) (δ, ppm).
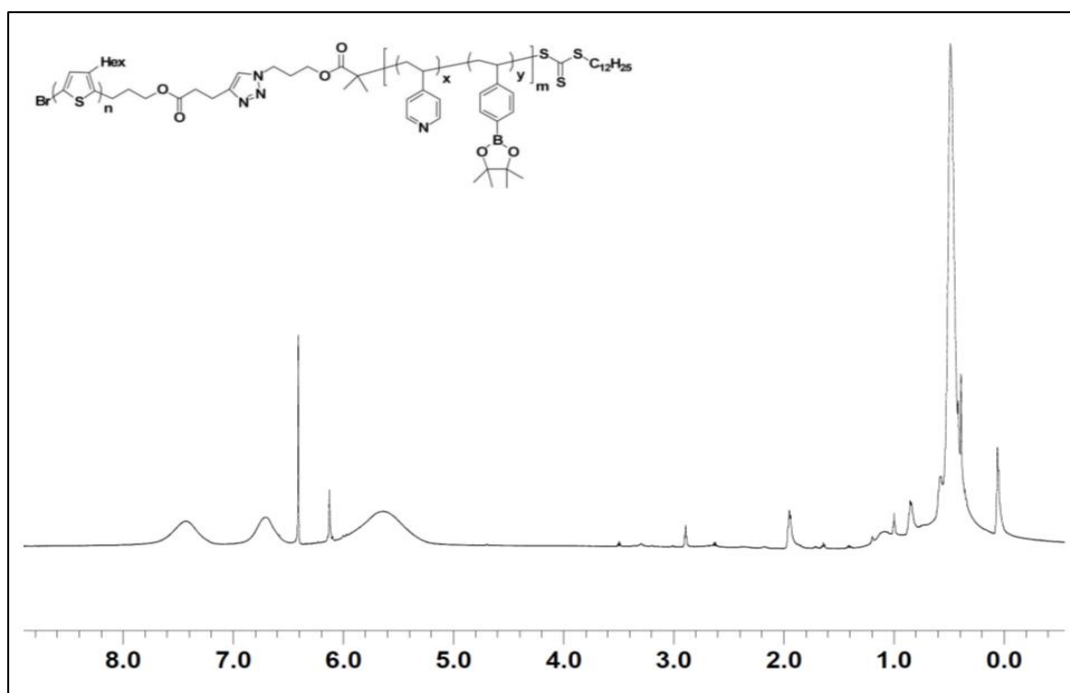
Figure 2-37. ^{1}H NMR of **P3HT-*b*-P(4VP-*stat*-SBpin)** recorded in CDCl$_3$ (δ, ppm).
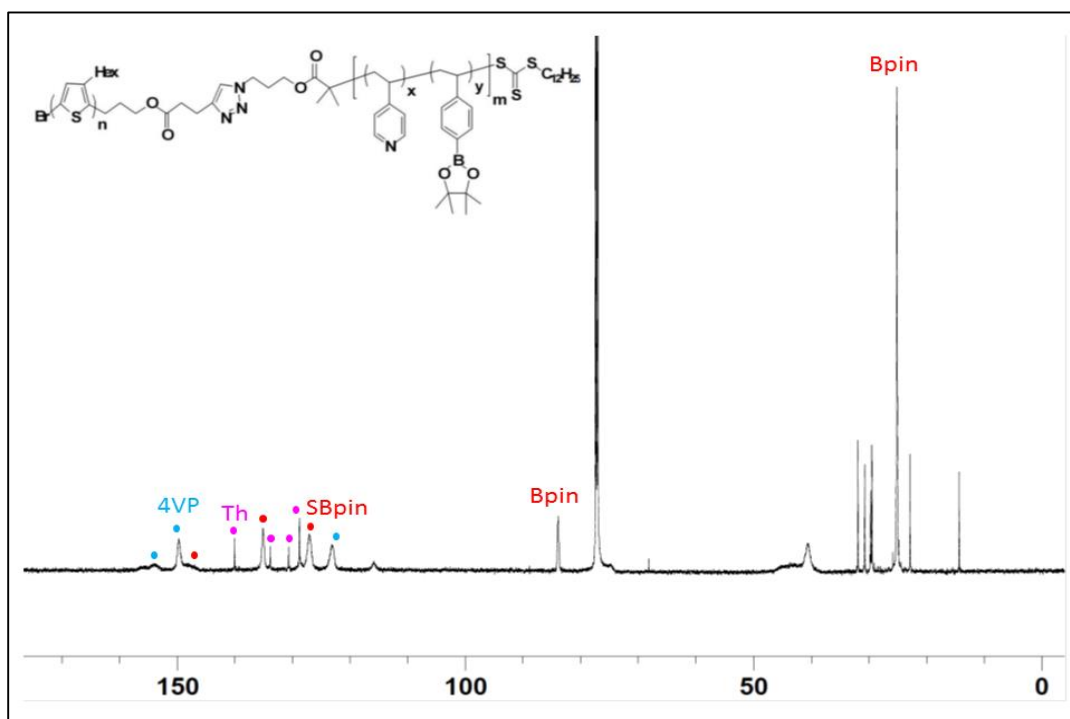
Figure 2-38. ^{13}C NMR of **P3HT-*b*-P(4VP-*stat*-SBpin)** recorded in CDCl$_3$ (δ, ppm).
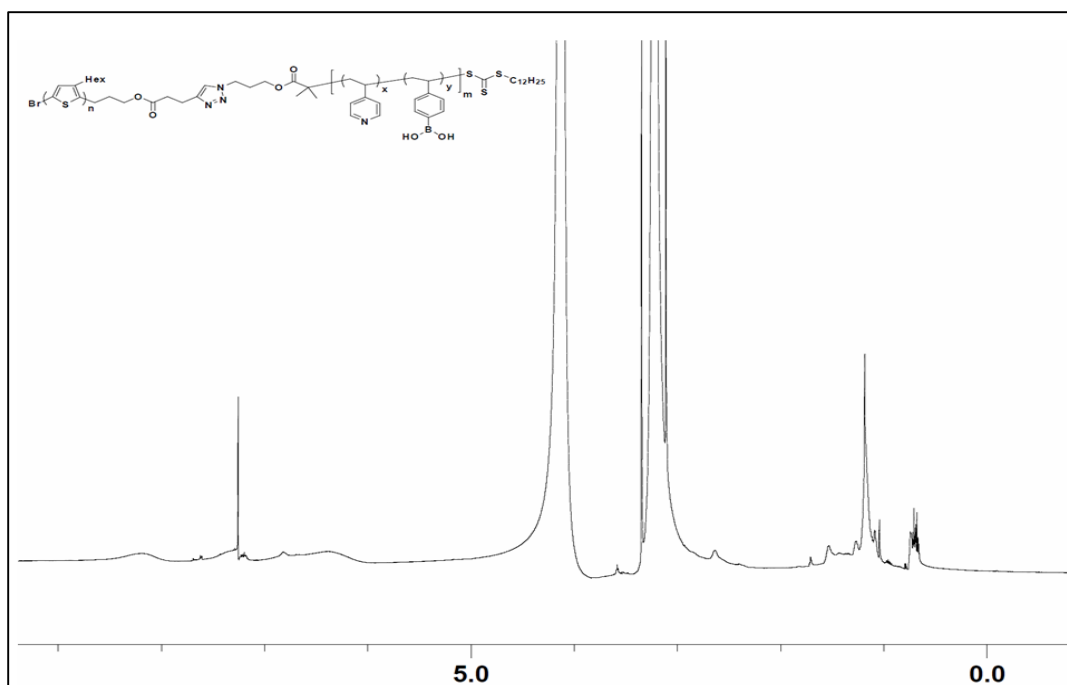
Figure 2-39. ^{1}H NMR of partially deprotected **P3HT-*b*-P(4VP-*stat*-SBA)** recorded in CDCl$_3$ and MeOH (δ, ppm).
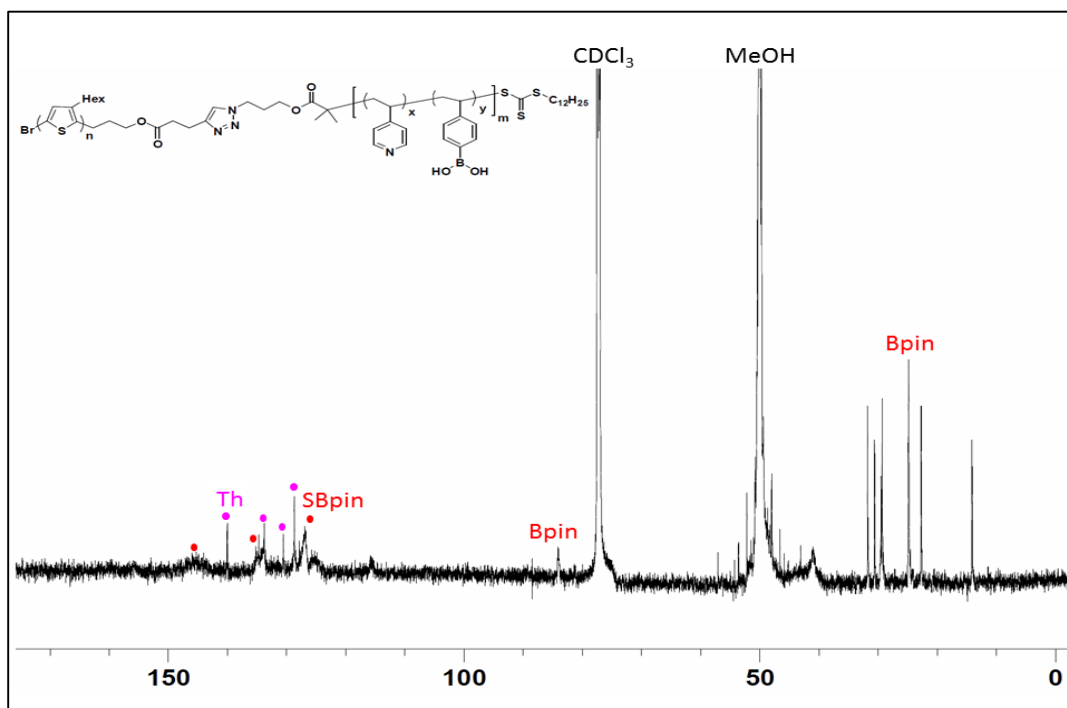
Figure 2-40. ^{13}C NMR of partially deprotected **P3HT-*b*-P(4VP-*stat*-SBA)** recorded in CDCl$_3$/MeOH (20:3) (δ, ppm).

2.5 References

(1)   (a) Yu, X.; Xiao, K.; Chen, J.; Lavrik, N. V.; Hong, K.; Sumpter, B. G.; Geohegan, D. B. *ACS Nano* **2011**, *5*, 3559; (b) Joseph Kline, R.; McGehee, M. D.; Toney, M. F. *Nat Mater* **2006**, *5*, 222; (c) Yang, C.; Lee, J. K.; Heeger, A. J.; Wudl, F. *J. Mater. Chem.* **2009**, *19*, 5416; (d) Sivula, K.; Ball, Z. T.; Watanabe, N.; Frechet, J. M. J. *Adv. Mater.* **2006**, *18*, 206; (e) Zhang, Q.; Cirpan, A.; Russell, T. P.; Emrick, T. *Macromolecules* **2009**, *42*, 1079; (f) Tsai, J.-H.; Lai, Y.-C.; Higashihara, T.; Lin, C.-J.; Ueda, M.; Chen, W.-C. *Macromolecules* **2010**, *43*, 6085; (g) Heeger, A. J. *Angew. Chem. Int. Ed.* **2001**, *40*, 2591.

(2)   (a) McCullough, R. D.; Lowe, R. D. *J. Chem. Soc. -Chem. Commun.* **1992**, 70; (b) McCullough, R. D.; Lowe, R. D.; Jayaraman, M.; Anderson, D. L. *J. Org. Chem.* **1993**, *58*, 904; (c) Sheina, E. E.; Liu, J.; Iovu, M. C.; Laird, D. W.; McCullough, R. D. *Macromolecules* **2004**, *37*, 3526.

(3)   (a) Chen, T. A.; Rieke, R. D. *J. Am. Chem. Soc.* **1992**, *114*, 10087; (b) Chen, T.-A.; Wu, X.; Rieke, R. D. *J. Am. Chem. Soc.* **1995**, *117*, 233.

(4)   (a) Loewe, R. S.; Ewbank, P. C.; Liu, J.; Zhai, L.; McCullough, R. D. *Macromolecules* **2001**, *34*, 4324; (b) Loewe, R. S.; Khersonsky, S. M.; McCullough, R. D. *Adv. Mater.* **1999**, *11*, 250.

(5)   (a) Beryozkina, T.; Senkovskyy, V.; Kaul, E.; Kiriy, A. *Macromolecules* **2008**, *41*, 7817; (b) Senkovskyy, V.; Sommer, M.; Tkachov, R.; Komber, H.; Huck, W. T. S.; Kiriy, A. *Macromolecules* **2010**, *43*, 10157; (c) Kiriy, A.; Senkovskyy, V.; Sommer, M. *Macromol. Rap. Commun.* **2011**, *32*, 1503.

(6)   (a) Jeffries-El, M.; Sauvé, G.; McCullough, R. D. *Macromolecules* **2005**, *38*, 10346; (b) Jeffries-El, M.; Sauve, G.; McCullough, R. D. *Adv. Mater.* **2004**, *16*, 1017.

(7)   (a) Park, S.-J.; Kang, S.-G.; Fryd, M.; Saven, J. G.; Park, S.-J. *J. Am. Chem. Soc.* **2010**, *132*, 9931; (b) Li, Z. C.; Ono, R. J.; Wu, Z. Q.; Bielawski, C. W. *Chem. Commun.* **2011**, *47*, 197; (c) Kamps, A. C.; Fryd, M.; Park, S.-J. *ACS Nano* **2012**, *6*, 2844; (d) Gwyther, J.; Gilroy, J. B.; Rupar, P. A.; Lunn, D. J.; Kynaston, E.; Patra, S. K.; Whittell, G. R.; Winnik, M. A.; Manners, I. *Chem. -Eur. J.* **2013**, *19*, 9186; (e) Lohwasser, R. H.; Thelakkat, M. *Macromolecules* **2012**, *45*, 3070; (f) Alemseghed, M. G.; Servello, J.; Hundt, N.; Sista, P.; Biewer, M. C.; Stefan, M. C. *Macromol. Chem. and Phys.* **2010**, *211*, 1291.

(8)   Ma, R.; Shi, L. *Polym. Chem.* **2014**, *5*, 1503.

(9)   Lutz, J.-F. *Polym. Int.* **2006**, *55*, 979.

(10)   (a) Wang, J.-S.; Matyjaszewski, K. *J. Am. Chem. Soc.* **1995**, *117*, 5614; (b) Kato, M.; Kamigaito, M.; Sawamoto, M.; Higashimura, T. *Macromolecules* **1995**, *28*, 1721; (c) Vogt, A. P.; Sumerlin, B. S. *Macromolecules* **2006**, *39*, 5286.

(11)   (a) Chiefari, J.; Chong, Y. K.; Ercole, F.; Krstina, J.; Jeffery, J.; Le, T. P. T.; Mayadunne, R. T. A.; Meijs, G. F.; Moad, C. L.; Moad, G.; Rizzardo, E.; Thang, S. H. *Macromolecules* **1998**, *31*, 5559; (b) Perrier, S.; Takolpuckdee, P. *J. Polym. Sci. A: Poym. Chem.* **2005**, *43*, 5347; (c) Moad, G.; Rizzardo, E.; Thang, S. H. *Austra. J. Chem* **2005**, *58*, 379; (d) Krasia, T.; Soula, R.; Borner, H. G.; Schlaad, H. *Chem. Commun.* **2003**, 538; (e) De, P.; Gondi, S. R.; Sumerlin, B. S. *Biomacromolecules* **2008**, *9*, 1064.

(12)   (a) Kim, K. T.; Cornelissen, J. J. L. M.; Nolte, R. J. M.; van Hest, J. C. M. *Adv. Mater.* **2009**, *21*, 2787; (b) Wang, B.; Ma, R.; Liu, G.; Liu, X.; Gao, Y.; Shen, J.; An, Y.; Shi, L. *Macromol. Rap. Commun.* **2010**, *31*, 1628; (c) Tang, Y. C.; Wu, J. H.; Duan, J. X. *Exp. Polym. Lett.* **2012**, *6*, 647; (d) Yao, Y.; Zhao, L.; Yang, J.; Yang, J. *Biomacromolecules* **2012**, *13*, 1837; (e) Wang, B.; Ma, R.; Liu, G.; Li, Y.; Liu, X.; An, Y.; Shi, L. *Langmuir* **2009**, *25*, 12522; (f) Ma, R.; Yang, H.; Li, Z.; Liu, G.; Sun, X.; Liu, X.; An, Y.; Shi, L. *Biomacromolecules* **2012**, *13*, 3409; (g) Kim, K. T.; Cornelissen, J. J. L. M.; Nolte, R. J. M.; Hest, J. C. M. v. *J. Am. Chem. Soc.* **2009**, *131*, 13908; (h) Roy, D.; Sumerlin, B. S. *ACS Macro Letters* **2012**, *1*, 529; (i) Roy, D.; Cambre, J. N.; Sumerlin, B. S. *Chem. Commun.* **2008**, 2477.

(13)   Kolb, H. C.; Finn, M. G.; Sharpless, K. B. *Angew. Chem. Int. Ed.* **2001**, *40*, 2004.

(14)   (a) Tsarevsky, N. V.; Sumerlin, B. S.; Matyjaszewski, K. *Macromolecules* **2005**, *38*, 3558; (b) van Dijk, M.; Rijkers, D. T. S.; Liskamp, R. M. J.; van Nostrum, C. F.; Hennink, W. E. *Bioconj. Chem.* **2009**, *20*, 2001; (c) Wu, P.; Feldman, A. K.; Nugent, A. K.; Hawker, C. J.; Scheel, A.; Voit, B.; Pyun, J.; Fréchet, J. M. J.; Sharpless, K. B.; Fokin, V. V. *Angew. Chem. Int. Ed.* **2004**, *43*, 3928; (d) Hawker, C. J.; Wooley, K. L. *Science* **2005**, *309*, 1200; (e) Sumerlin, B. S.; Vogt, A. P. *Macromolecules* **2010**, *43*, 1.

(15)   Qin, Y.; Sukul, V.; Pagakos, D.; Cui, C.; Jäkle, F. *Macromolecules* **2005**, *38*, 8987.

(16)   Han, D.; Tong, X.; Zhao, Y. *J. Polym. Sci. A: Poym. Chem.* **2012**, *50*, 4198.

(17)   (a) Gao, H.; Matyjaszewski, K. *J. Am. Chem. Soc.* **2007**, *129*, 6633; (b) Han, D. H.; Tong, X.; Zhao, Y. *J. Polym. Sci. Part A Polym. Chem.* **2012**, *50*, 4198.

(18)   Gondi, S. R.; Vogt, A. P.; Sumerlin, B. S. *Macromolecules* **2007**, *40*, 474.

(19)   (a) Iovu, M. C.; Jeffries-El, M.; Sheina, E. E.; Cooper, J. R.; McCullough, R. D. *Polymer* **2005**, *46*, 8582; (b) Urien, M.; Erothu, H.; Cloutet, E.; Hiorns, R. C.; Vignau, L.; Cramail, H. *Macromolecules* **2008**, *41*, 7033.

(20)   Lanni, E. L.; McNeil, A. J. *J. Am. Chem. Soc.* **2009**, *131*, 16573.

(21)   Cambre, J. N.; Roy, D.; Gondi, S. R.; Sumerlin, B. S. *J. Am. Chem. Soc.* **2007**, *129*, 10348.

(22)   Iovu, M. C.; Craley, C. R.; Jeffries-El, M.; Krankowski, A. B.; Zhang, R.; Kowalewski, T.; McCullough, R. D. *Macromolecules* **2007**, *40*, 4733.

(23)   Coutts, S. J.; Adams, J.; Krolikowski, D.; Snow, R. J. *Tetrahedron Lett.* **1994**, *35*, 5109.

Chapter 3. The First 1, 2-Azaborine Polymer[a]

3.1 Introduction

Azaborines are a unique class of heterocycles that are isosteric and isoelectronic to the benzene-based all-carbon congeners.[1] Oligomers and polymers that contain benzene as building blocks such as poly(p-phenylene)s, poly(p-phenylenevinylene)s and polyfluorenes are touted for their high stability and excellent luminescent properties and have been widely applied in organic light emitting devices.[2] However, efforts at utilizing azaborines as building blocks of conjugated oligomers and polymers remain scarce (Figure 1).[3] Yamaguchi et al[4] reported a diene-like character of the pyrrolyl-azaborine dyad **A**; Piers et al and Perepichka et al[5] introduced fused azaborine systems such as bis-BN phenanthrene **B** that displays low energy absorptions and emissions in comparison to corresponding polyaromatic hydrocarbons and Liu et al[6] showed that the bis(azaborine) **C** displays vastly different photophysical properties from its carbonaceous analog, tolan.

Much recent effort has been devoted to the development of new heterocyclic polymers. While polythiophenes and polypyrroles are most prominent, selenophenes, tellurophenes, boroles, phospholes, siloles, disilahexadiene, and stannoles have been explored as alternative components.[7] Oxidation of thiophene as a means to reduce the aromatic character of the heterocycles has attracted much recent attention,[8] but quantitative oxidation of polythiophenes[9] remains a challenge.[10] All these polymers are

---

typically assumed to preferentially adopt an anti (trans-cisoid trans-transoid) structure as depicted in Figure 1. Recent advances in the selective functionalization of 1, 2-azaborines provide a foundation for their use as building blocks of new conjugated oligomers and polymers. Specifically, the regioselective introduction of halogens and boronic ester moieties[11] can be exploited for Suzuki-Miyaura coupling reactions, which have proven to be an excellent tool for the preparation of polyphenylene-type materials.[12]
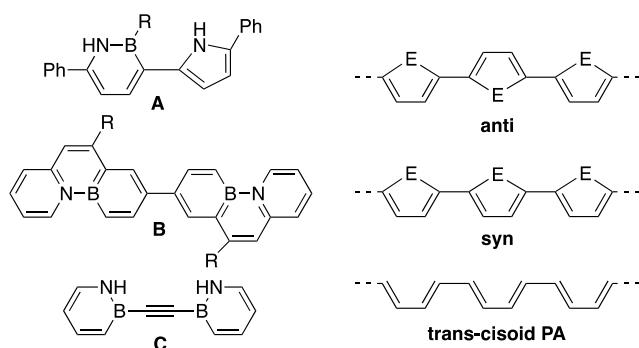
Figure 3-1. Examples 1, 2-Azaborines and possible confirmations adopted.

This Chapter constitutes a collaborative work with Prof. Shih-Yuan Liu's group at Boston College: Andrew W. Baggett synthesized Bpin/Br-functionalized AB-type monomers (**BN-M**) and regioregular model compounds (**BN1, BN2, BN3**) with 1D NMR characterization (Figure 2). Bo Li solved the crystal structure for **BN2**. In this Chapter, we demonstrate the incorporation of the monocyclic 1, 2-Azaborine into extended π-conjugated systems (**BN-P**) using the Suzuki-Miyaura coupling method. Photophysical and electrochemical studies on the resulting polymer and the corresponding model compounds, in combination with DFT calculations, offer detailed insight into the electronic structure. **BN1**, **BN2**, **BN3** and **BN-P** are designed to be regioregular to minimize steric interactions between side chains and ensure optimal π-conjugation along the conjugated backbone. We discuss the discovery of an unexpected strong preference

for a syn-arrangement, which is reminiscent of that of the elusive trans-cisoid form of poly(acetylene) (PA).[13] The importance of N-H…π interactions as a conformation-defining element is discussed and a detailed analysis of the electronic structure is offered.
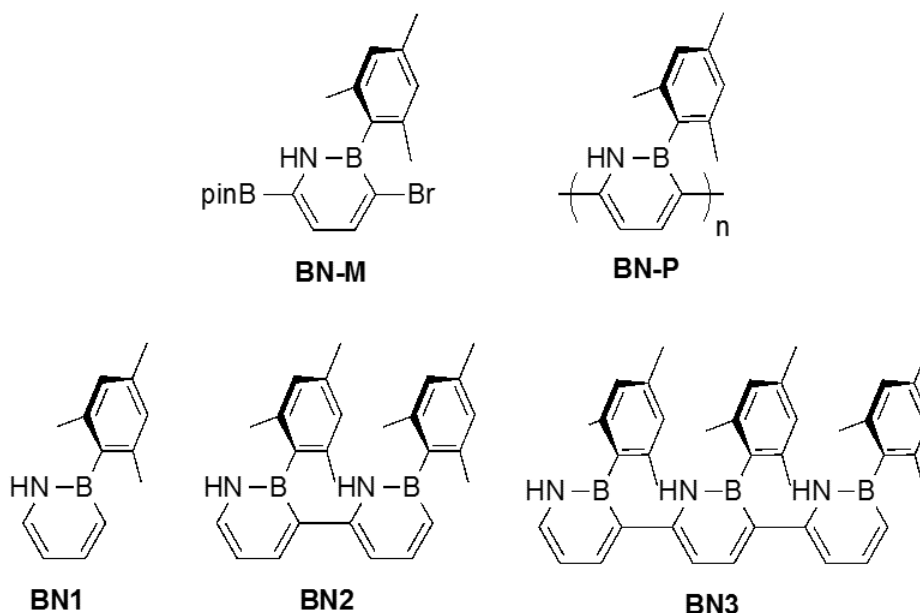
Figure 3-2. BN-compounds investigated in this Chapter.

3.2 Results and Discussion

The correct regiochemistry for **BN2**, **BN3** was ascertained by H, H-COSY and H, H-NOESY NMR studies (Figures 3-4) and that of **BN2** further confirmed by a single crystal X-ray structure.[14] The H, H COSY NMR of **BN2** establishes the connectivity within the azaborine rings. The a,b,c,d and f,g,k show the expected coupling paths and the coupling patterns for each of the mesityl groups are also evident (Figure 3-3a). The NOESY spectrum of **BN2** confirms the connectivity between the azaborine rings. The expected NOE signal for d/f is clearly observed. NOE peaks between ortho-methyl groups and NH protons further confirm the assignments. The Me group p shows only one

NOE peak with the NH proton e, whereas the other methyl group o shows two NOE peaks to NH protons (o to a, e) (Figure 3-3b). The H, H COSY NMR of **BN3** establishes the connectivity within the azaborine rings. Note that protons f and g only couple with each other, whereas a,b,c,d and i,j,k show the expected coupling paths. The expected coupling patterns for each of the mesityl groups are also evident (Figure 3-4a). The NOESY spectrum of **BN3** confirms the connectivity between azaborine rings. The expected NOE signals for d/f and g/i are clearly observed. NOE peaks between ortho-methyl groups and NH protons further confirm the assignments. The Me group q shows only one NOE peak with the NH proton h, whereas the other methyl groups (o, p) each show two NOE peaks to NH protons (o to a,e; p to e,h) (Figure 3-4b).
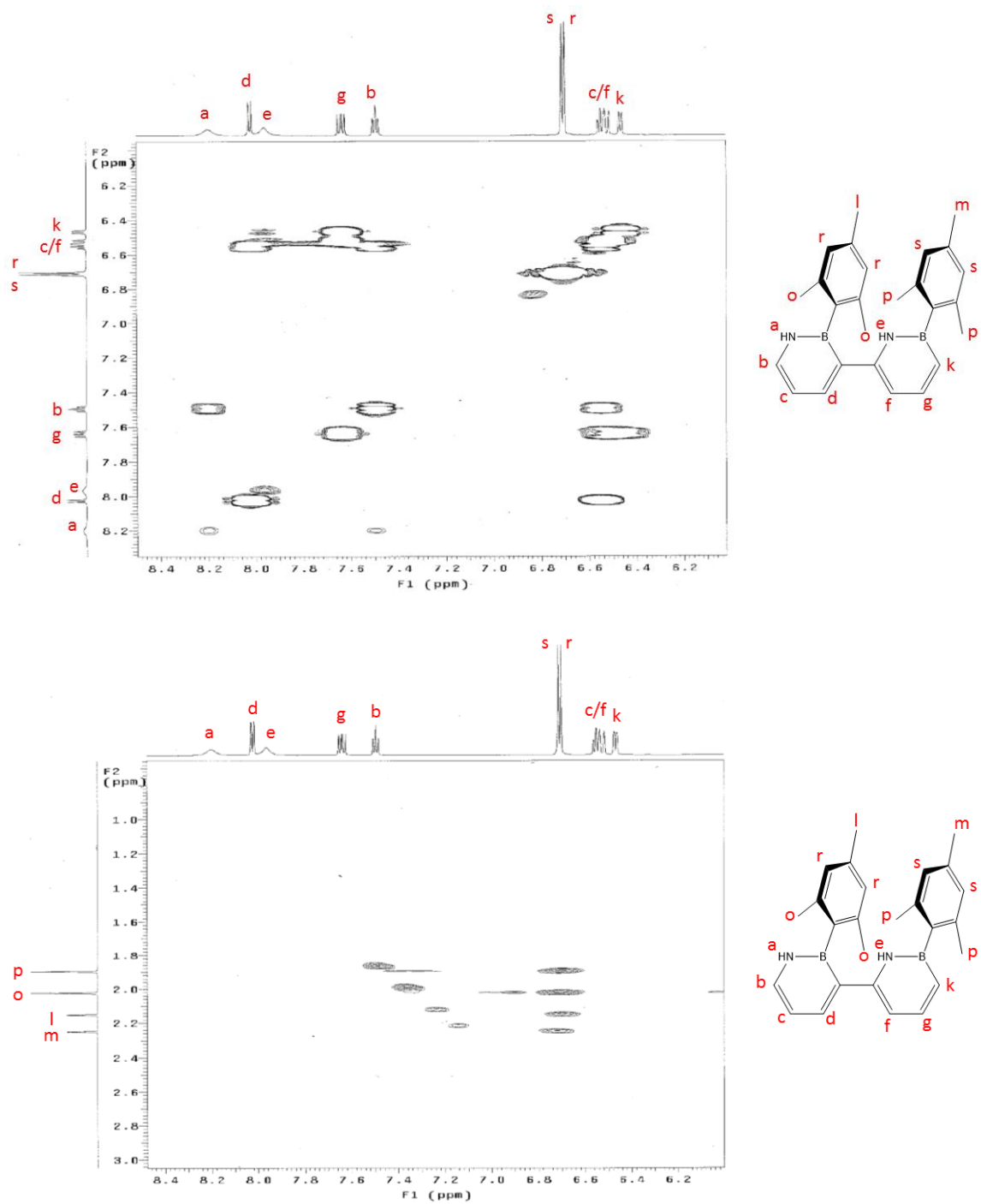
Figure 3-3a. H, H COSY NMR spectrum of dimer **BN2** in CD₂Cl₂.
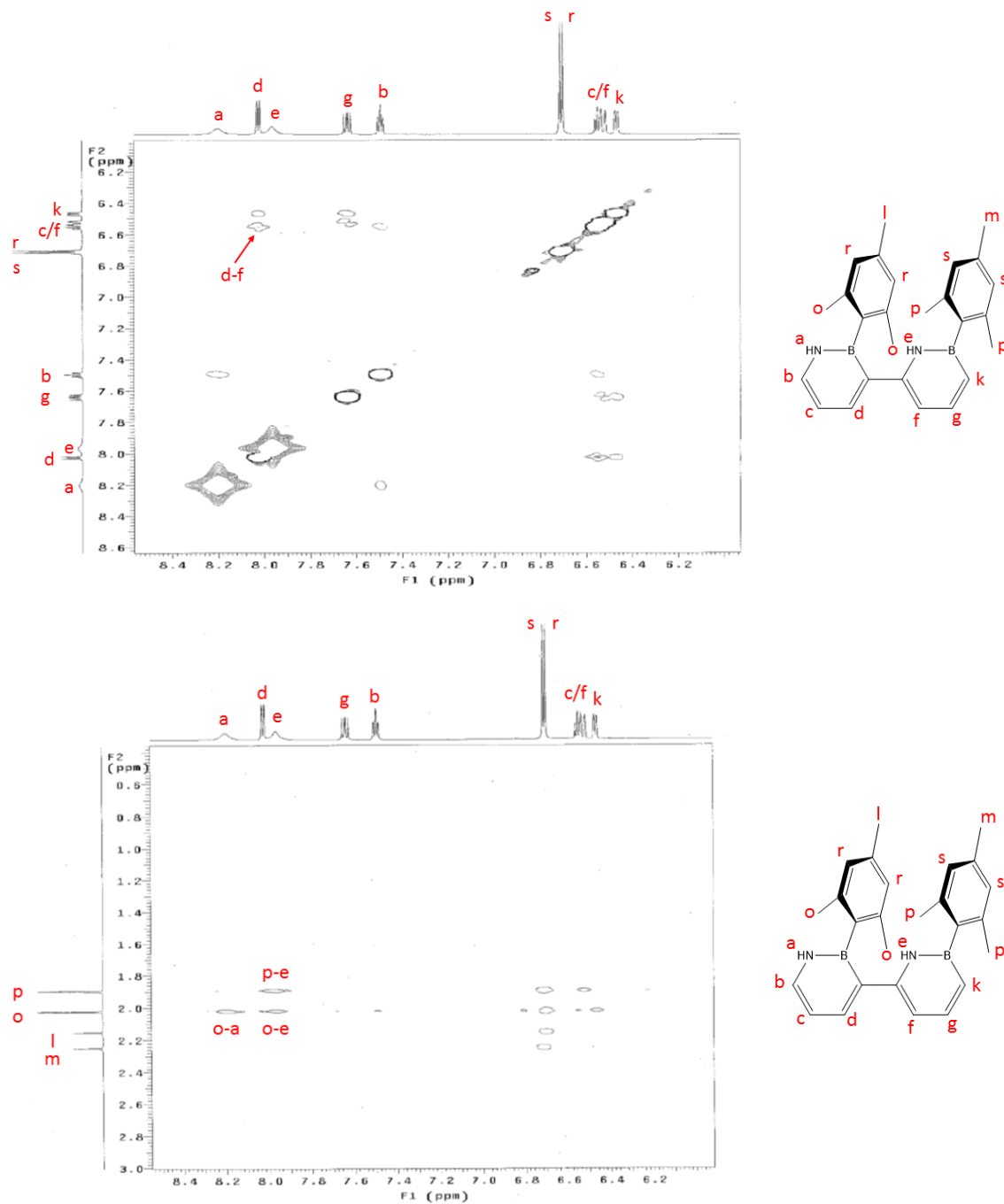
Figure 3-3b. H, H NOESY NMR spectrum of dimer **BN2** in CD_2Cl_2.
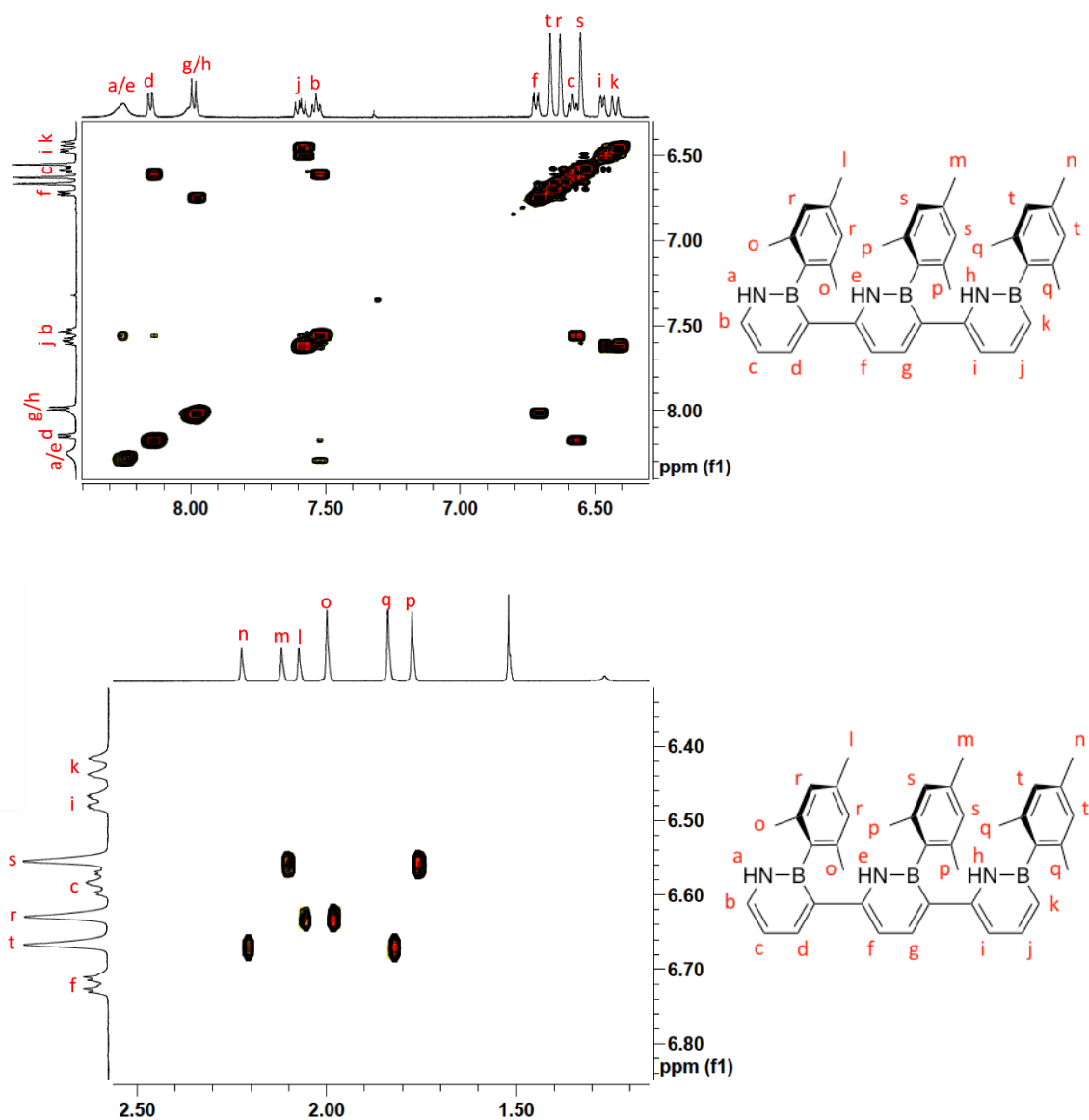
Figure 3-4a. H, H COSY NMR spectrum of trimer **BN3** in CD_2Cl_2.
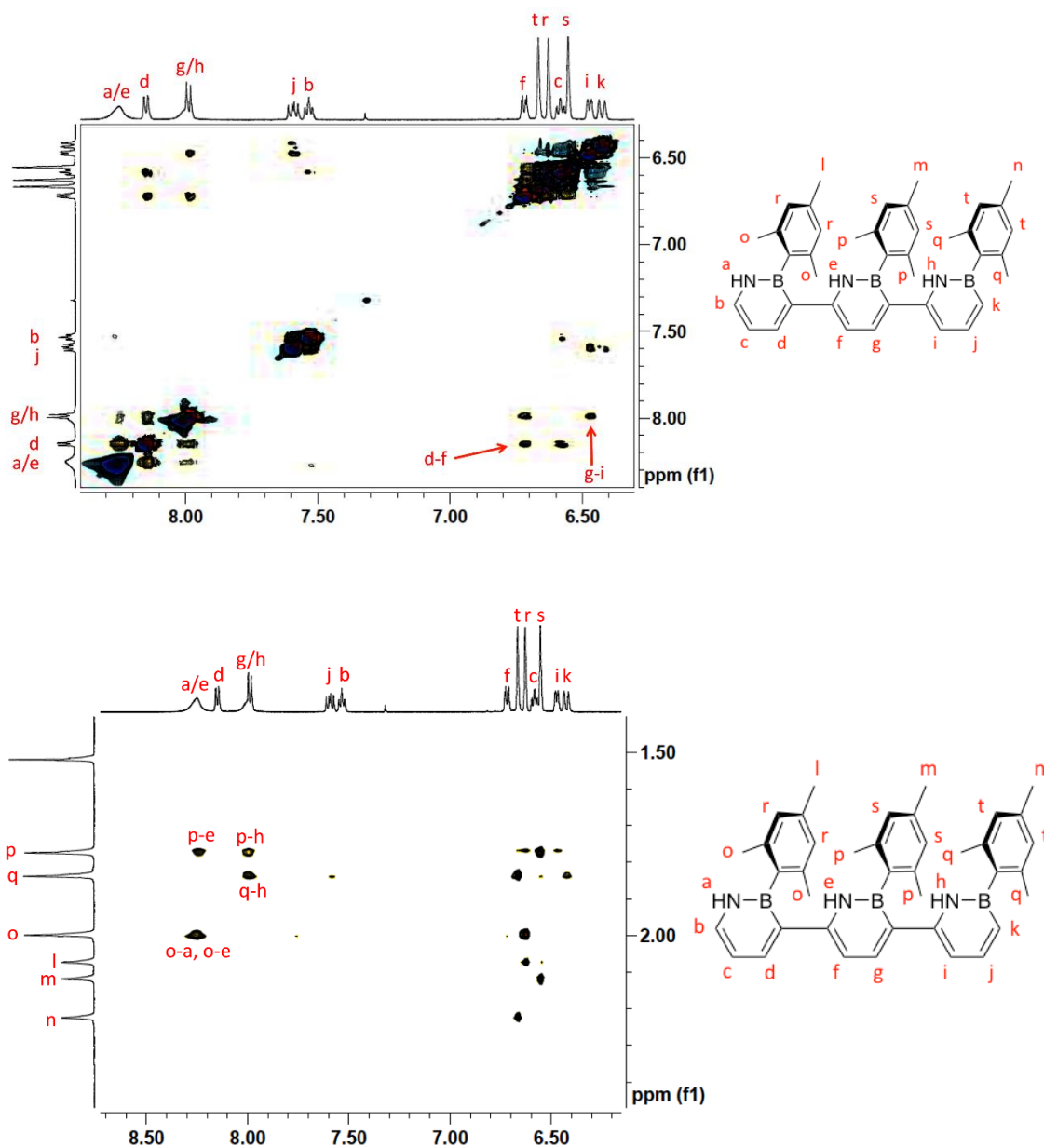
Figure 3-4b. H, H NOESY NMR spectrum of trimer **BN3** in CD$_2$Cl$_2$.

Polymerization of the AB-type monomer **BN-M** via Suzuki-Miyaura polycondensation was then examined using a range of different catalyst systems (Scheme 3-1, Table 3-1). Initial attempts under standard conditions with Pd(PPh$_3$)$_4$ or Pd$_2$(dba)$_3$/t-Bu$_3$P at 110 °C did not generate the desired polymer based on ^{1}H NMR analysis of the crude samples. GPC data indicated formation of short oligomers, and an end group

analysis by MALDI-MS suggested early termination by phosphine ligands in the case of Pd(PPh$_3$)$_4$ (Figure 3-5). Similar results were obtained when using Buchwald's Pd(dba)$_2$/SPhos catalyst system to prevent an early halt of the polymer growth due to ligand scrambling.[15]

We then decided to explore the efficacy of (t-Bu$_3$P)Pd(Ar)Br[16] initiator systems, which have recently been shown to promote chain-growth Suzuki-Miyaura-type polymerization, providing access to well-defined fluorene-containing end-functionalized polymers, star polymers and even block copolymers.[17] Indeed, polymerization of **BN-M** at room temperature in a THF / water mixture using (t-Bu$_3$P)Pd(Ph)Br as the initiator and Na$_2$CO$_3$ as the base resulted in a red-brown mixture from which the polymer was isolated as a dark purple solid after filtration through alumina gel. Further purification by preparative gel permeation chromatography (GPC) on BiobeadsTM gave **BN-P** with a number-average molecular weight of M_n = 2330 (dispersity $Đ$ = 1.40), corresponding to an average of DP$_n$ = 12 units per chain (Figure 3-6).
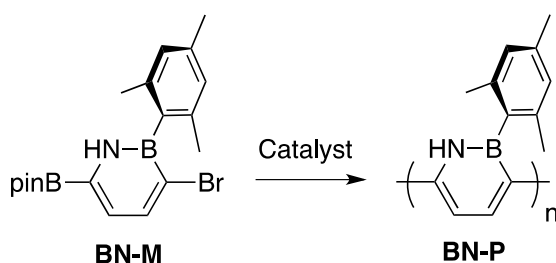
Scheme 3-1. Suzuki-Miyaura polycondensation of monomer BN-M.

Table 3-1. Conditions and results for Suzuki-Miyaura polymerization
of monomer **BN-M**

Entry	Catalyst	Added Ligand	Base	Solvent	T (°C)	Time (h)	Isolated Product	GPC-PDA λ_{max} (nm)[e]
1	Pd(PPh$_3$)$_4$ (5%)		K$_2$CO$_3$	Toluene/DMF 1:1[a]	110	48	Oligomers[c]	410
2	Pd$_2$(dba)$_3$ (2.5%)	t-Bu$_3$P (10%)	t-BuOK	Toluene/H$_2$O[a]	110	12	--	--
3	Pd(dba)$_2$ (1%)	SPhos (2%)	NaHCO$_3$	THF/H$_2$O 1:1[a]	70	48	Oligomers[c]	420
4	Pd(dba)$_2$ (5%)	SPhos (10%)	KOH	THF/H$_2$O 1:1[a]	70	48	--	--
5	(t-Bu$_3$P)Pd(Ph)Br (5%)		CsF[b]	THF/H$_2$O[a]	RT	12	Oligomers[c]	440
6	(t-Bu$_3$P)Pd(Ph)Br (5%)		Na$_2$CO$_3$	THF/H$_2$O[a]	RT	12	Polymer[d]	475

[a] Volume ratio, otherwise minimum H$_2$O was used to dissolve the base. [b] 18-crown-6 was added as a phase transfer catalyst. [c] GPC-RI/PDA analysis of the crude product after passing through a short plug of alumina shows only evidence of oligomers with n<5. [d] Polymeric product was isolated by preparative GPC. [e] Absorption maximum for highest molecular weight component based on GPC-PDA analysis.
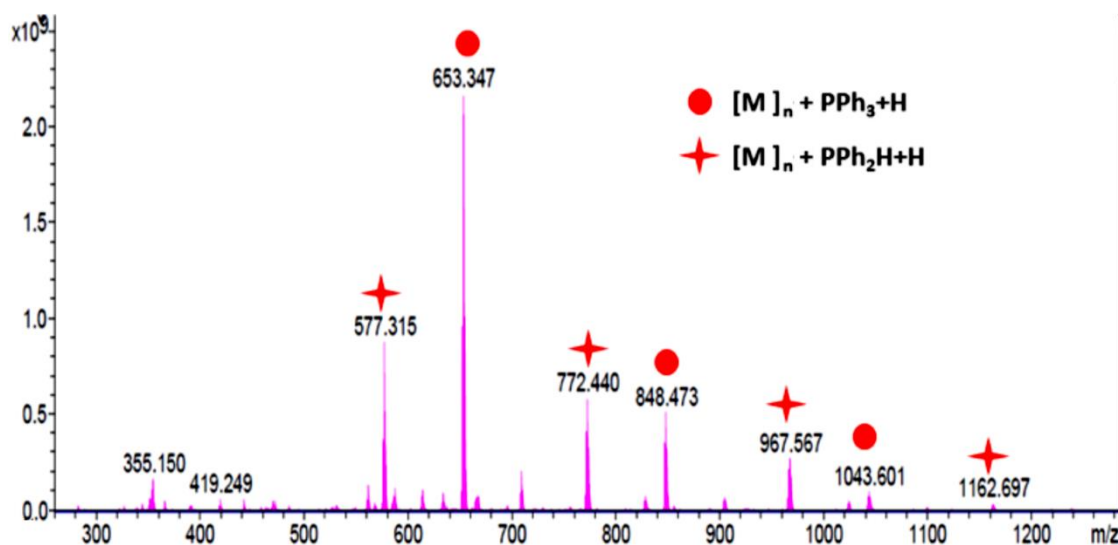
Figure 3-5. High resolution (pos. mode) MALDI-MS data of crude polymer sample (Entry 1, Table 3-1).
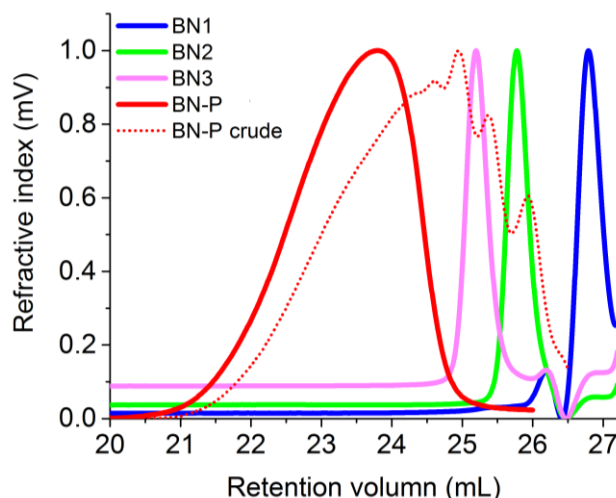
Figure 3-6. GPC-RI data for **BN-P** (Table 3-1, Entry 6; before and after fractionation by preparative GPC on Biobeads^{TM} in comparison to azaborine oligomers (THF, 1 mL/min).

The integrity of the azaborine moieties in **BN-P** was confirmed by a broad signal in the ^{11}B NMR at a chemical shift of $\delta = 37.2$ (Figure 3-7), which is close to that of the precursor **BN-M** ($\delta = 35.6$).[11] ^{1}H NMR data show chemical shifts that are comparable to those of trimer **BN3** (Figure 3-8). Further analysis by MALDI-MS (Figure 3-9) clearly confirmed the proposed polymer structure with the expected repeating units. Polymers with predominantly one Ph (from the initiator) and one H (from protonolysis) end group are observed. However, the presence of additional peak series with two Ph groups and two hydrogen end groups, respectively, suggests chain coupling and is reminiscent of competing step-growth processes.
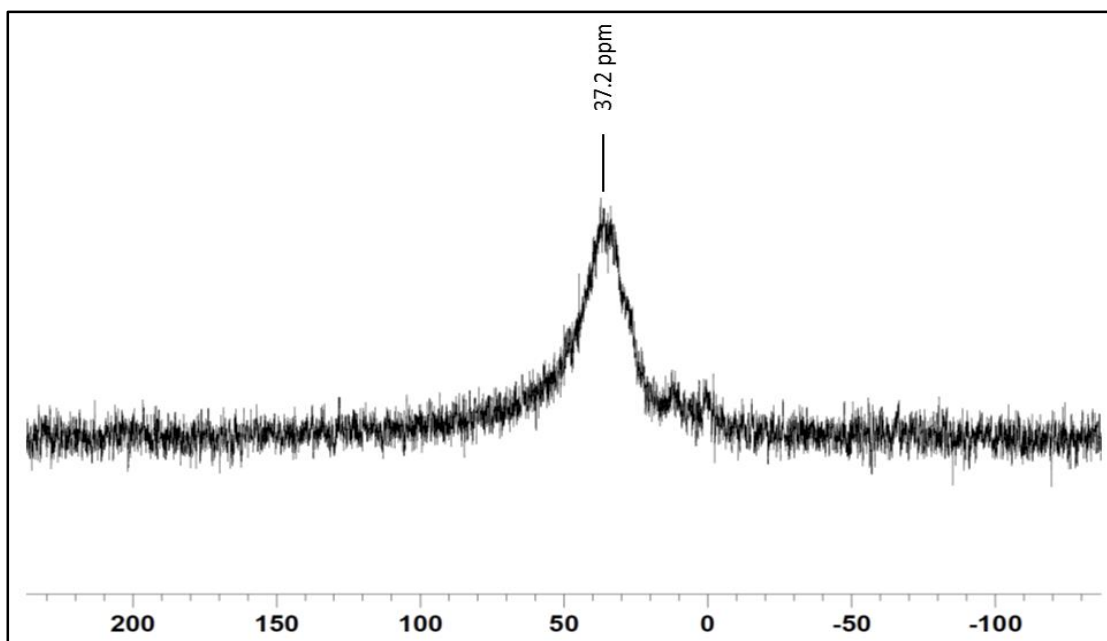
Figure 3-7. ^{11}B NMR of **BN-P** recorded in CD_2Cl_2 (δ, ppm)
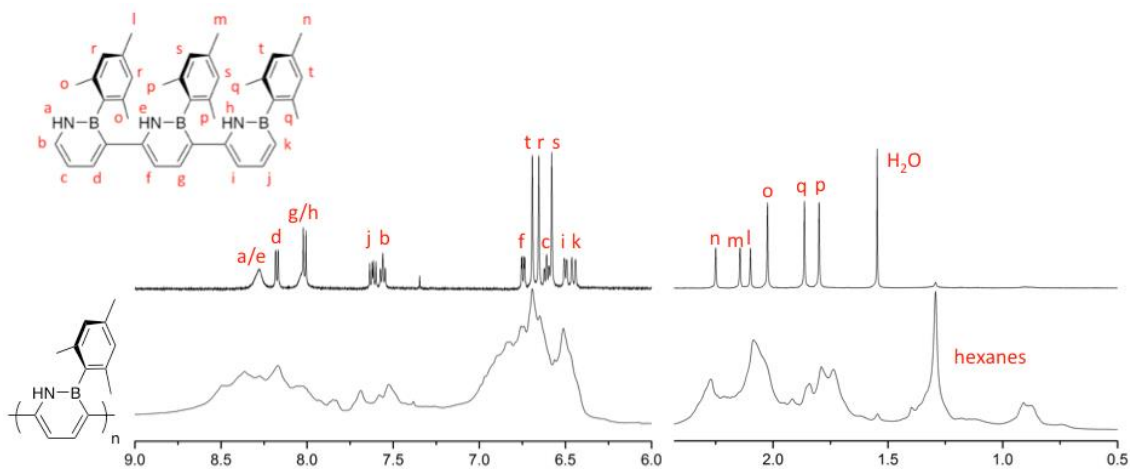
Figure 3-8. Comparison of the ^{1}H NMR spectra of **BN3** and polymer **BN-P** in CD_2Cl_2 (δ, ppm).
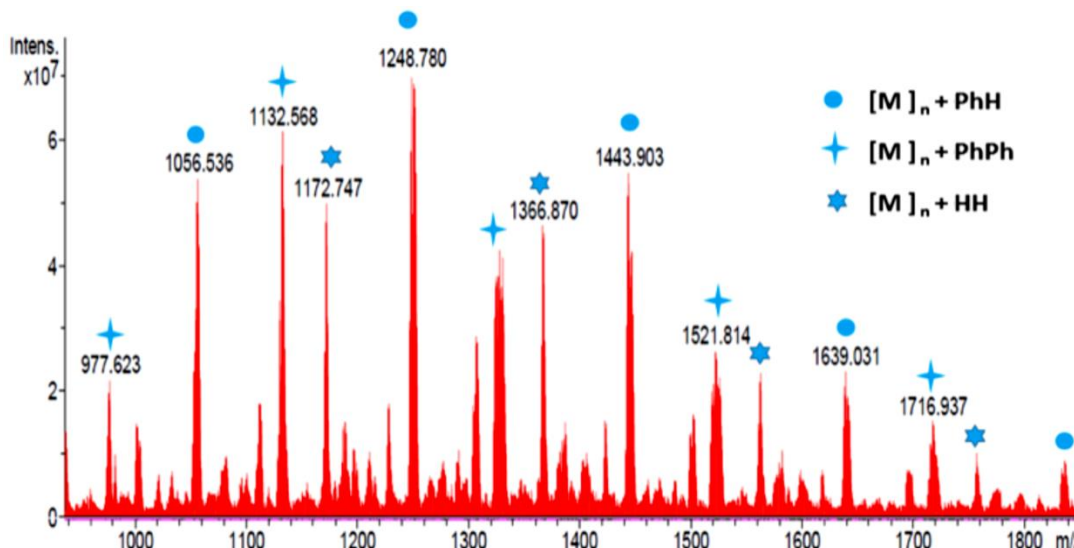
Figure 3-9. High resolution (pos. mode) MALDI-MS data of polymer after separation using preparative column Biobeads[TM] (Entry 6, Table 3-1).

UV-vis absorption and fluorescence data of the polymer were acquired in THF and compared to those of the oligomers **BN1-3** (Table 3-2, Figure 3-10). The maximum of the lowest energy absorption band experiences a dramatic bathochromic shift as the azaborine backbone is extended from **BN1** (277 nm) to **BN2** (334 nm), **BN3** (383 nm), and the isolated polymer **BN-P** (457 nm). In addition, the crude polymer sample was analyzed by GPC with a PDA detector, where the absorption spectra at different retention times can be correlated to the polymer molecular weight and vice versa. The GPC-PDA analysis revealed the presence of well-defined oligomers with absorption spectra that correlate well with those of the isolated species **BN1-3** (Figure 3-11). The absorption maximum is shifted as far as 475 nm for the highest molecular weight polymer that can be detected. This is at significantly lower energy than for related carbonaceous polymers such as poly(paraphenylene) (PPP) and even planarized poly(tetrahydropyrene)s (PTHP) (Table 3-3).[18] The absorption maxima for the azaborine oligomers also converge more slowly towards a constant value for the polymeric species than is the case for PPP and a

remarkably large effective conjugation length of ca. $n_{ECL} = 14$ is deduced from an exponential data fit (Figure 3-12),[19] which indicates more effective π-conjugation for the azaborine polymer.

Table 3-2. Molecular weight and photophysical data of azaborine oligomers and polymer BN-P

	BN1	BN2	BN3	BN-P
MW_{calcd}	197	393	588	--
Mn, GPC (Da)[a]	190	430	670	2330
$\lambda_{abs, max}$ (nm)[b]	277	334	383	457
ε (M^{-1},cm^{-1})[b]	8390	19400	29100	6360
$\lambda_{fl, max (nm)}$[b]	--	411	491	600
Φ (%)[b,c]	--	0.28	42.9	8.5
τ_{fl} (ns)[b]	--	--	2.7	1.8

[a] GPC-RI in THF vs PS standards. [b] in THF solution. [c] absolute quantum yield determined with an integrated sphere
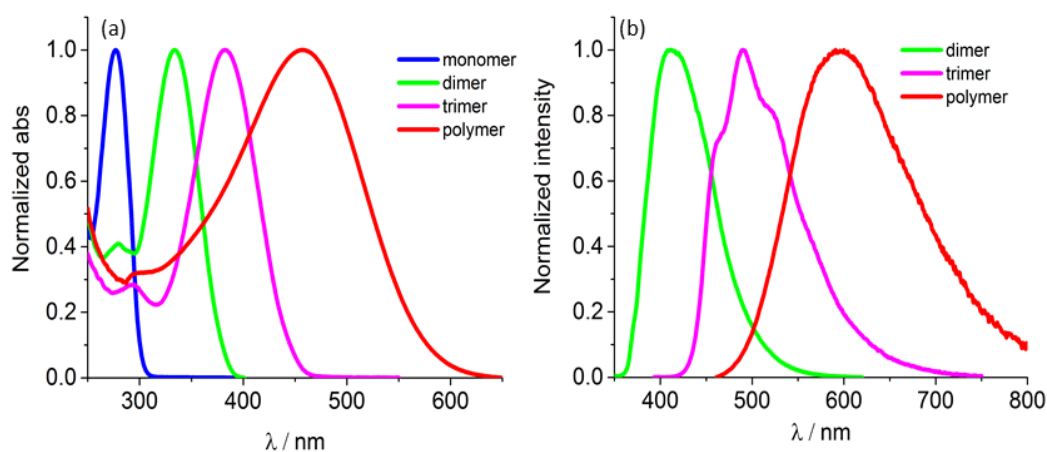
Figure 3-10. (a) UV-vis and (b) fluorescence spectra of azaborine oligomers and polymer BN-P in THF.
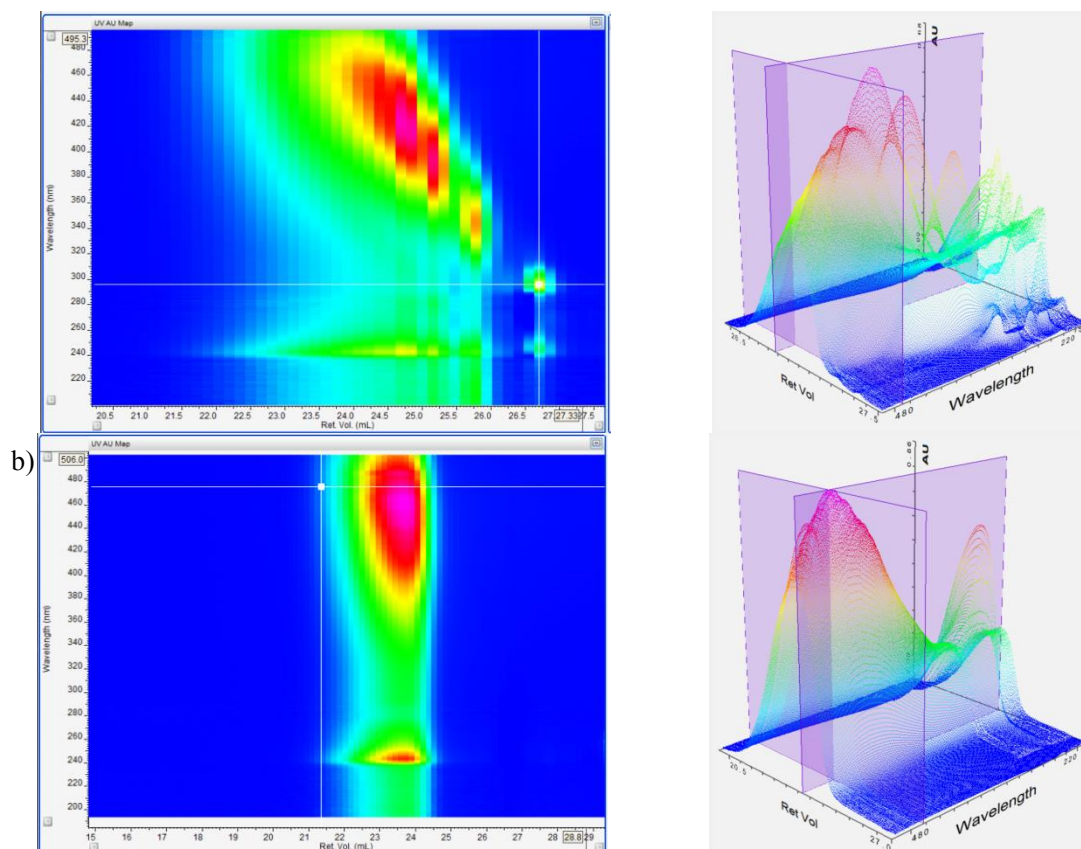
Figure 3-11a. 2D and 3D GPC-PDA data for **BN-P** (Table 3-1, Entry 6) a) before and b) after fractionation by preparative GPC on Biobeads[TM] (THF, 1 mL/min) and comparison to UV-vis absorption data of azaborine oligomers.
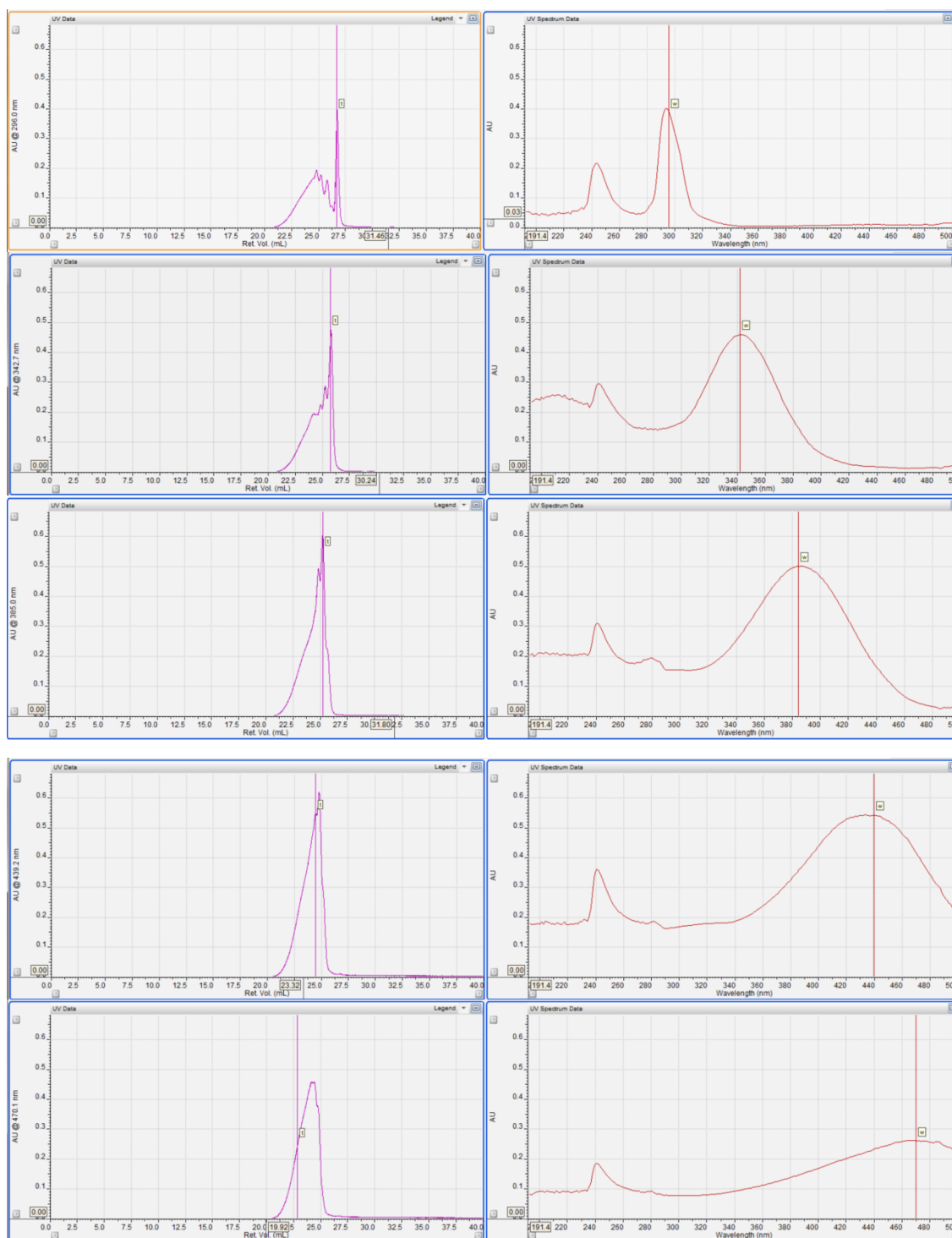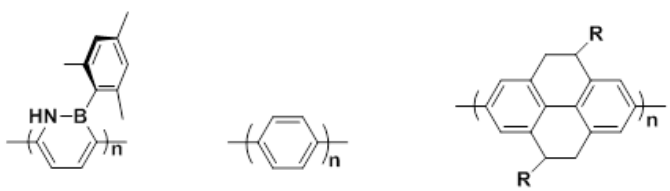
Figure 3-11b. GPC-PDA data for **BN-P** (Table 3-1, Entry 6) before fractionation: Correlation of retention time and UV-vis absorption data.

Table 3-3. Comparison of the longest wavelength absorption maxima (λ_{max} / nm) of azaborine oligomers and polymer **BN-P** with those of related **PPP**-type oligomers.

aromatic rings n	BN-P [a]	PPP [b]	PTHP [b]
1	277	200, 254 (weak)	---
2	334	252	295
3	383	279	---
4	418 [c]	292	329
5	440 [c]	299	---
6	---	308	352
7	---	---	---
8	---	---	364
10	---	---	370
~12	457 [e]	---	375
~15	475 [f]	---	---
λ_∞ [f]	474	322	384
n_{ECL} [f]	14	9	19

[a] Measured in THF solution. [b] Data taken from ref. [18] (R = alkyl). [c] Estimated by GPC-PDA analysis. [d] n_{av} for isolated polymer. [e] Estimated by GPC-PDA analysis for highest molecular weight fraction of **BN-P**. [f] Estimated using equations displayed in Figure 3-12.

$$\lambda_{max}(n) = \lambda_\infty - (\lambda_\infty - \lambda_1)e^{-b(n-1)}$$

$$n_{ecl} = \frac{\ln(\lambda_\infty - \lambda_1)}{b} + 1$$
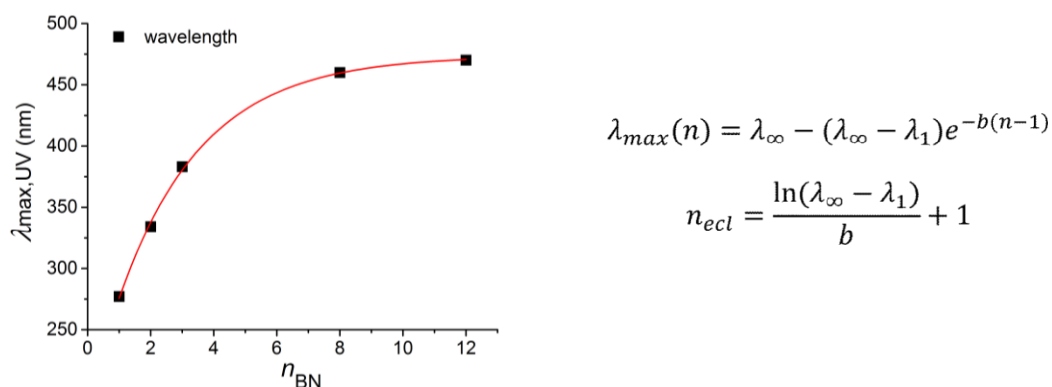
Figure 3-12. Exponential fit of absorption data for **BNn** oligomers to number of repeat units (n) according to ref. [19a]. Data for $n = 8, 12$ are estimated from GPC-PDA data of the polymer. The fit predicts an absorption maximum at infinite chain length of $\lambda_\infty = 474$ nm, an attenuation parameter of $b = 0.376$, and an effective conjugation length of $n_{ECL} = 14$. (In courtesy of Dr. P. Chen)

Except for the shortest member, **BN1**, all the azaborines are emissive. As seen in Figure 2b, the emission maximum is red-shifted with chain extension, similar to the trend for the absorption maxima. The strongest emission is observed for **BN3** with an absolute quantum yield of Φ_F = 42.9% (τ = 2.7 ns) while that of the polymer **BN-P** is comparatively less intense with a slightly shorter lifetime (Table 3-1, Figure 3-13).
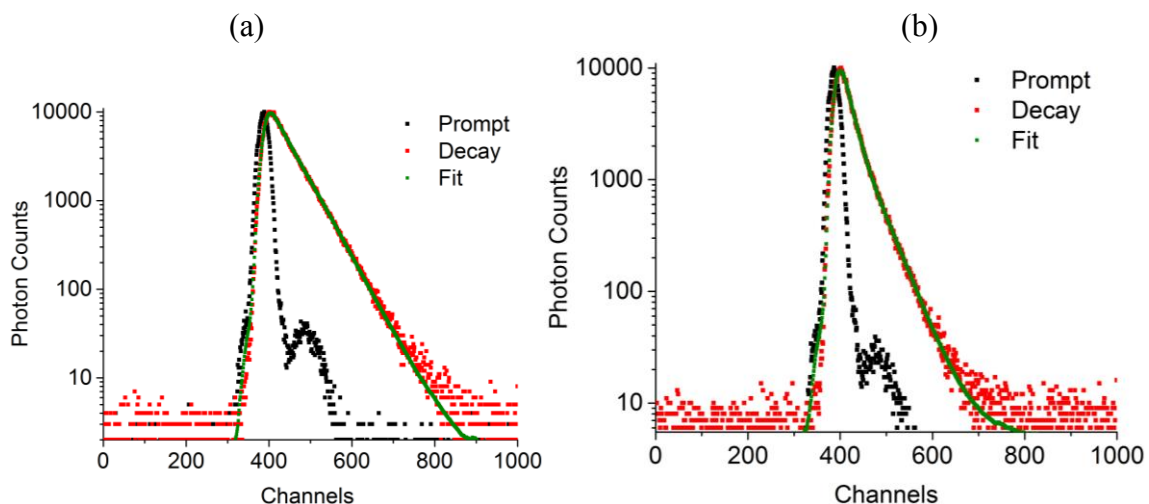
Figure 3-13. Fluorescence lifetime measurements for (a) **BN3** and (b) **BN-P** in THF solution. For **BN3:** τ = 2.74(1) ns (single exponential fit; χ^2 = 1.22); for **BN-P**: τ = 1.81(1) ns (single exponential fit; χ^2 = 2.27).

Large Stokes shifts are detected, suggesting significant structural reorganization in the excited state, possibly with further planarization of the conjugated backbone. However, the absorption and emission bands are not affected to a great extent by the solvent polarity (Table 3-4, Figure 3-14), indicating that changes in the dipole moment upon excitation are small. A similar behavior was also observed for B2N2-quaterphenyl analogues reported by Jaska et al. However, the absorption maxima for spin-coated thin films of **BN3** and **BN-P** are red-shifted (**BN3**: λ_{max} = 383 nm (THF), λ_{max} = 405 nm (film), Δ = 1418 cm^{-1}; **BN-P**: λ_{max} = 460 nm (THF), λ_{max} = 469 nm (film), Δ = 417 cm^{-1}. An even larger shift is observed in the emission spectra (**BN3**: λ_{max} = 491 nm (THF),

(λ_{max} = 572 nm (film), Δ = 2884 cm^{-1}; **BN-P**: λ_{max} = 610 nm (THF), λ_{max} = 736 nm (film), Δ = 2806 cm^{-1}; Figure 3-15) and tentatively attributed to excimer formation.

Table 3-4. Photophysical data of azaborines in different solvents and as film/powder.

		Cyclohex	Toluene	DCM	THF	MeOH	DMF	Film / powder[b]
BN1	λ_{abs} (nm)	274	281	276	277	276	279	
BN2	λ_{abs} (nm)	279, 338	338	280, 334	280, 334	276, 333	334	
BN3	λ_{abs} (nm)	287, 390	297, 389	295, 385	294, 383	296, 384	294, 383	405 (f)
BN-P	λ_{abs} (nm)	446	462	461	457	Insol.	448	469 (f)
BN2	λ_{Fl} (nm)	421	421	424	411	416	404	
BN3	λ_{Fl} (nm)	498	500	499	491	488	487	572 (f)
BN-P	λ_{Fl} (nm)	572	609	610	600	Insol.	586	736 (f)
BN2	Φ_{Fl} (%)	0.8	0.9	0.5	0.3	0.4	0.5	
BN3	Φ_{Fl} (%)	46.3	48.7	50.5	42.9	41.9	50.3	9.6 (p)
BN-P	Φ_{Fl} (%)	16	9.4	8.9	8.5	Insol.	11.1	n.d.
BN3	τ_{Fl} (ns)	3.1	2.9	3.2	2.7	2.8	2.6	2.4 (p)
BN-P	τ_{Fl} (ns) [a]	2.74 (42%) 1.38 (58%)	2.50 (47%) 1.00 (53%)	1.81	2.33 (45%) 0.97 (55%)	Insol.	2.44 (42%) 1.08 (58%)	0.34 (95%) 3.97 (5%)

[a] Double-exponential fits are used except for DCM solution. [b] Film of polymer with $M_{n,GPC}$ = 3150 Da.
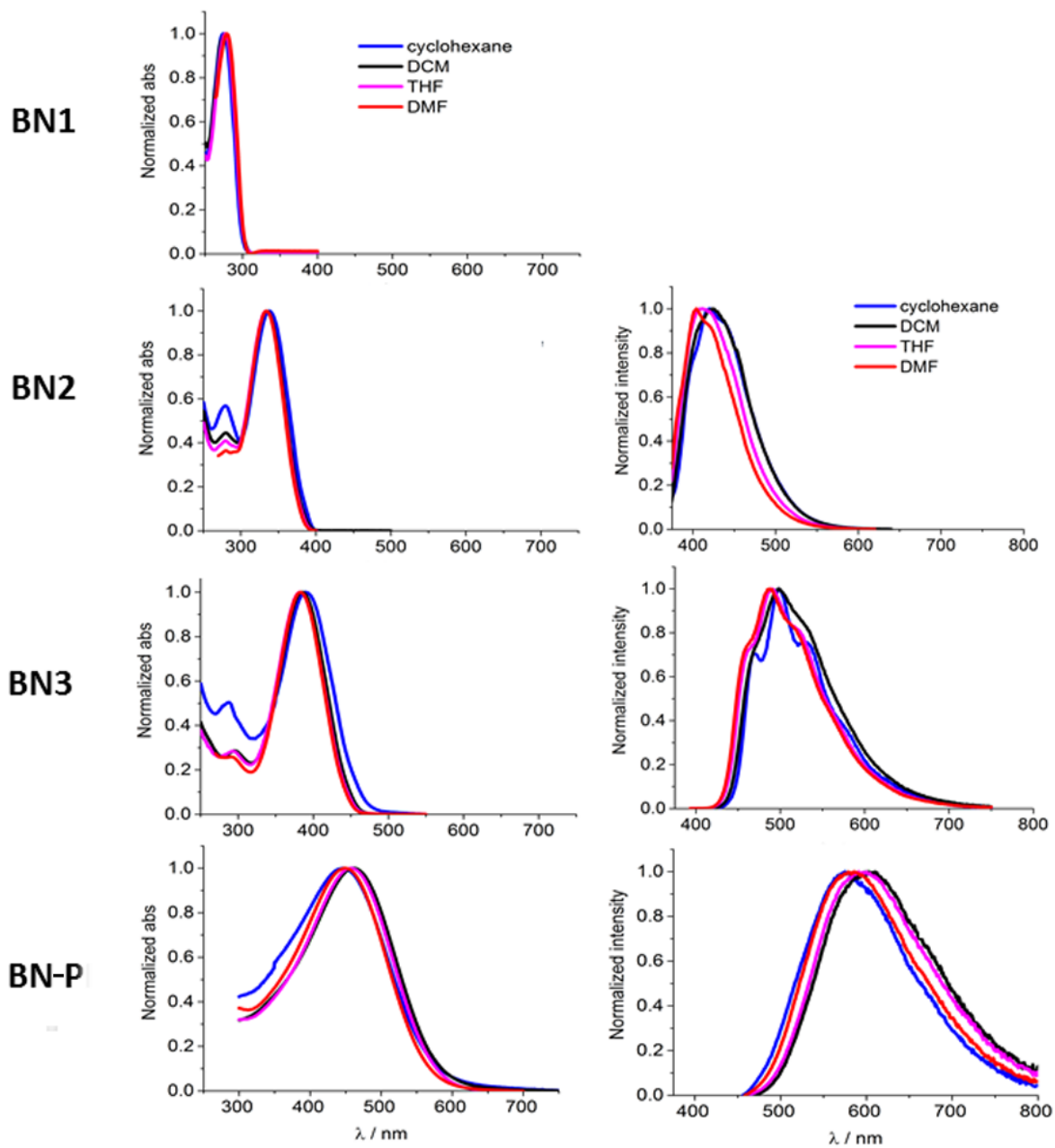
Figure 3-14. UV-vis and fluorescence spectra of azaborine oligomers and polymer **BN-P** in different solvents.
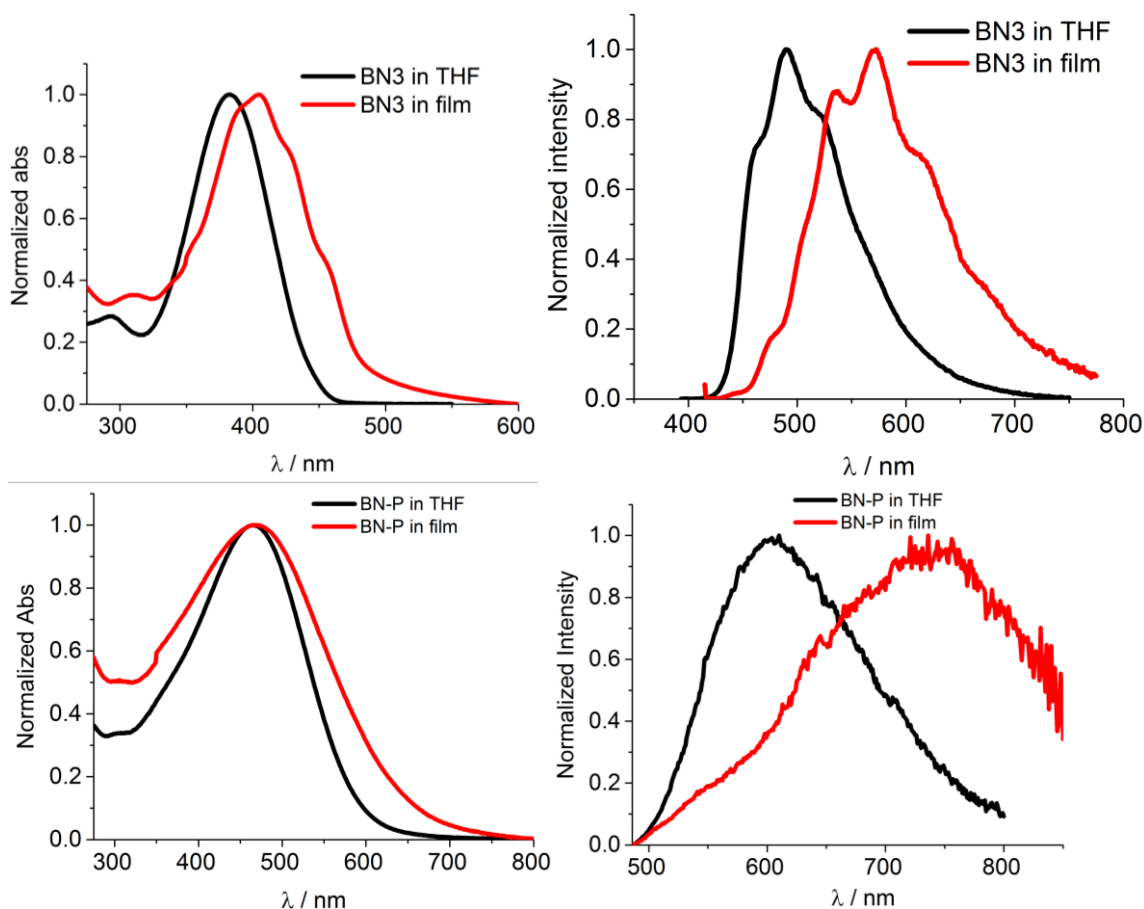
Figure 3-15. UV-vis absorption (left) and fluorescence (right) spectra of **BN3** and **BN-P** (polymer batch with $M_{n,GPC}$ = 3150 Da, $Đ$ = 1.34) in THF solution and as thin film.

To further explore the origins of the strong bathochromic shifts with extension of the conjugated main chain, DFT calculations (Gaussian 09, B3LYP, 6-31g*) were conducted on the azaborine oligomers **BN1-3**, the corresponding paraphenylenes (**PP1-3**), and cyclohexadienes (**CHD1-3**) (Tables 3-5, 3-6, 3-7).[20] The HOMO of **BN1** is mostly situated on the mesityl group and the LUMO on the azaborine heterocycle with participation of the N p-orbital and to a lesser extent the B p-orbital (Table 3-5a). The situation changes for the longer oligomers, **BN2** and **BN3**, for which both the HOMO and LUMO are localized on the azaborine moieties (Table 3-5 (b, c)). The frontier orbitals resemble those of the cyclohexadiene analogs **CHD2** and **CHD3** in that the N contributions are small and the B atoms only contribute to the HOMO. In contrast, for

PP2 and **PP3**, the HOMOs are localized on the benzene rings, with significant contribution of the mesityl groups, and all of the main chain carbon atoms participate in the LUMOs. This indicates that as the chain is extended, the 1, 2-azaborine oligomers act more like trans-cisoid polyacetylene and less like poly(paraphenylene) analogues and further points toward more effective conjugation in **BN-P** in comparison to **PPP**. In good agreement with the X-ray crystal structure data for **BN2**, all the azaborine oligomers prefer a cisoid conformation, in which the mesityl groups point into the same direction (preferred by 5.5 kJ/mol for **BN2** and 11.4 kJ/mol for **BN3** relative to the transoid conformers). The computed torsion angles for **BN2** (32.7°) and **BN3** (31.4, 31.6°) are remarkably small (Figure 3-6b) and the experimentally observed torsion of ∠C3-C4-C5-C6 = −16.8° in **BN2** crystal is even smaller.[14] This conformational preference appears to be favored by short N-H…π interactions (N-H…centroid distance of 2.610 Å in the X-ray structure of **BN2**) between the azaborines and the mesityl substituents in neighboring units.[6,21] Consistent with this interpretation is that the corresponding cyclohexadienes **CHDn** are much more twisted and the phenylene rings in **PPn** adopt an almost perpendicular orientation (Table 3-6).

Table 3-5a. Comparison of HOMO/LUMO plots for **BN1**, **CHD1**, and **PP1** (B3LYP/6-31g*)
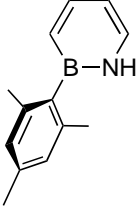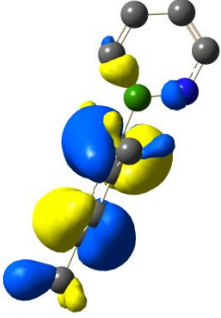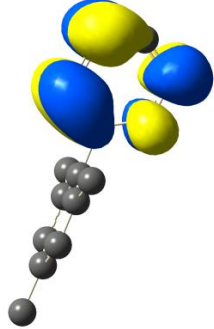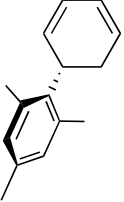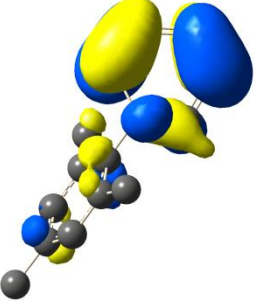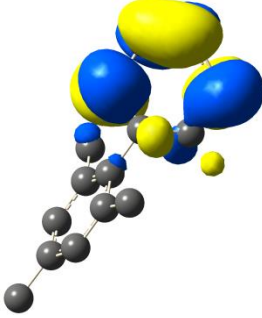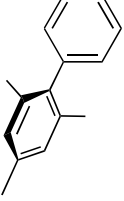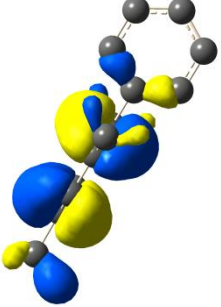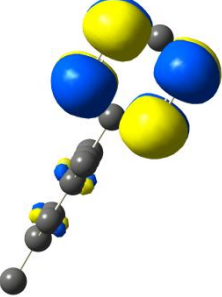
	HOMO	LUMO
BN1 $E_g = 5.38$ eV		
CHD1 $E_g = 5.02$ eV		
PP1 $E_g = 6.10$ eV		

Table 3-5b. Comparison of HOMO/LUMO plots for **BN2**, **CHD2**, and **PP2**
(B3LYP/6-31g*)
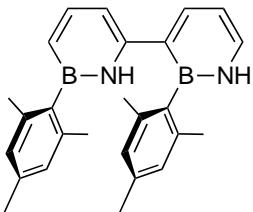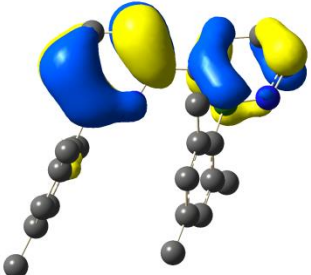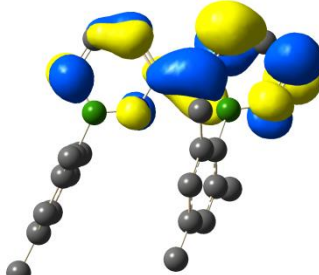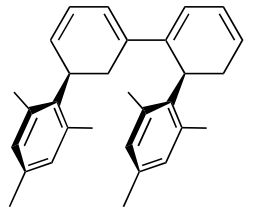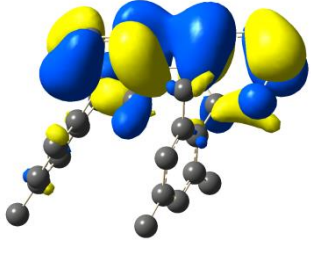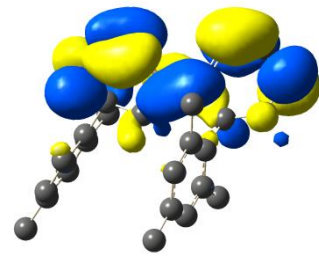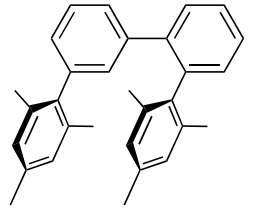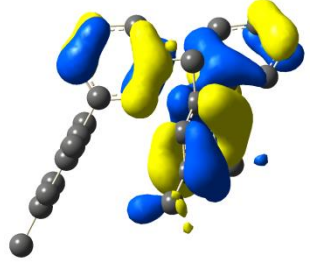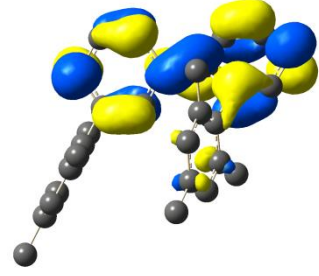
	HOMO	LUMO
BN2 E_g = 4.05 eV		
CHD2 E_g = 3.72 eV		
PP2 E_g = 5.31 eV		

Table 3-5c. Comparison of HOMO/LUMO plots for **BN3**, **CHD3**, and **PP3**
(B3LYP/6-31g*)
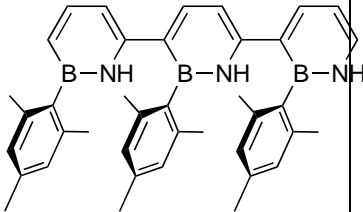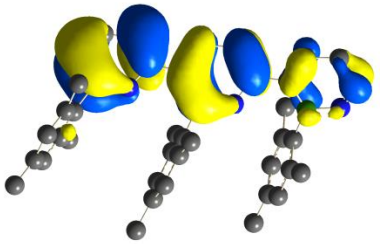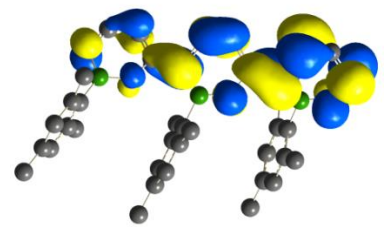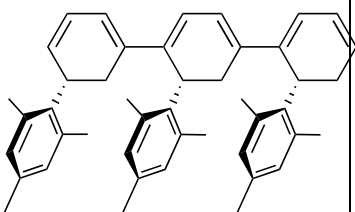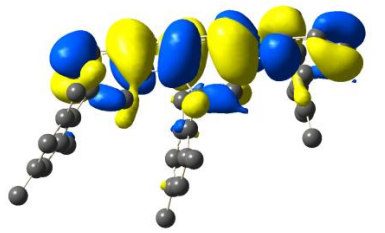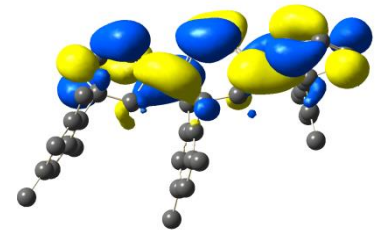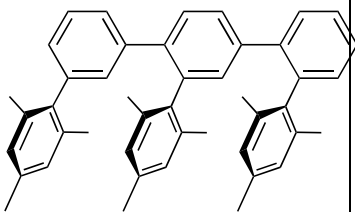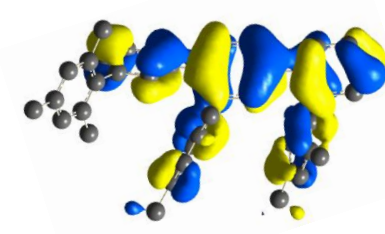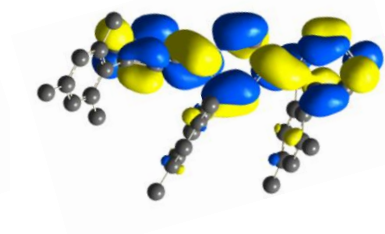
	HOMO	LUMO
BN3 E_g = 3.38 eV		
CHD3 E_g = 3.10 eV		
PP3 E_g = 4.89 eV		

Table 3-6. Comparison of calculated energy and geometry of different rotational isomers (Spartan 10, MMFF force field; Gaussian 09, DFT, B3LYP/6-31g*)

a) Comparison of calculated energy for different rotational isomers

	MMFF, Spartan (kJ/mol)	DFT, Gaussian (eV)
BN2 cis	**492.16**	**-31774.90**
BN2 trans	502.91	-31774.84
CHD2 cis	**499.86**	**-31650.93**
CHD trans (more orthogonal)	509.86	
PP2 cis	**461.84**	**-31587.67**
PP2 trans (more orthogonal)	465.04	

BN3 cis/cis	**774.13**	**-47646.26**
BN3 cis/trans	784.13	
BN3 trans/trans	792.61	-47646.14
CHD3 (rings rotating in same direction)	**766.49**	**-47460.20**
CHD3 (3rd ring in same orientation as 1st)	770.92	
PP3 (rings rotating in same direction)	**710.58**	**-47365.24**
PP3 (3rd ring in same orientation as 1st)	710.92	

b) Comparison of calculated torsion angles in different rotational isomers

	MMFF, Spartan C-C-C-C Torsions (deg)	DFT, Gaussian C-C-C-C Torsions (deg)
BN2 cis	**49.4**	**-32.7**
BN2 trans	130.7	144.8
CHD cis	**-54.9**	**-42.7**
CHD trans (more orthogonal)	143.5	--
PP2 cis	**-64.3**	**-47.9**
PP2 trans (more orthogonal)	101.2	--

BN3 cis/cis	**50.4 / 47.7**	**31.4 / 31.6**
BN3 cis/trans	-50.4 / 133.1	--
BN3 trans/trans	129.4 / -131.8	146.0 / 146.2
CHD3 (rings rotating in same direction)	**-55.1 / -55.0**	**41.7 / 41.1**
CHD3 (3rd ring in same orientation as 1st)	92.5 / -56.8	--
PP3 (rings rotating in same direction)	**64.5 / 65.0**	**47.1 / 46.7**
PP3 (3rd ring in same orientation as 1st)	--	--

Another important result is that the HOMO-LUMO energy gap strongly decreases with extension of the chain (Figure 3-16, Table 3-7), which is consistent with the experimental absorption data discussed above.[22] The HOMO energies are significantly higher and the LUMO energies lower than in the paraphenylene analogs **PPn**; they are much closer to the energy levels predicted for the cyclohexadienes **CHDn**.
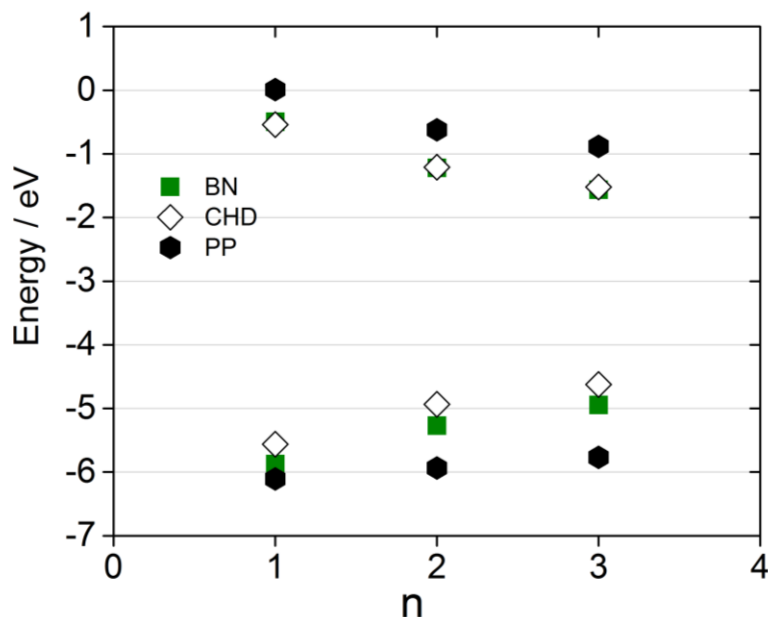
Figure 3-16. Comparison of HOMO/LUMO energy levels (eV) for azaborine oligomers with those of PPn and CHDn analogs.

Table 3-7a. Comparison of HOMO/LUMO energy levels (eV) of azaborine oligomers (DFT, B3LYP/6-31g*)

	BN1	BN2	BN3
L+2	+0.565	+0.063	-0.276
L+1	+0.249	-0.277	-0.603
LUMO	**-0.497**	**-1.220**	**-1.563**
HOMO	**-5.876**	**-5.272**	**-4.947**
H-1	-5.928	-5.646	-5.507
H-2	-6.016	-5.782	-5.658
E_g	**5.38**	**4.05**	**3.38**

Table 3-7b. Comparison of HOMO/LUMO energy levels (eV) of azaborine oligomers with corresponding all-carbon systems (DFT, B3LYP/6-31G*)

	BN1	CHD1	PP1
L+2	+0.565	0.313	+0.144
L+1	+0.249	0.163	+0.042
LUMO	**-0.497**	**-0.541**	**+0.010**
HOMO	**-5.876**	**-5.563**	**-6.108**
H-1	-5.928	-6.078	-6.215
H-2	-6.016	-6.192	-6.584
E_g	**5.379**	**5.022**	**6.12**

	BN2	CHD2	PP2
L+2	+0.063	+0.184	+0.031
L+1	-0.277	-0.057	-0.177
LUMO	**-1.220**	**-1.212**	**-0.623**
HOMO	**-5.272**	**-4.934**	**-5.936**
H-1	-5.646	-5.981	-6.041
H-2	-5.782	-6.034	-6.151
E_g	**4.052**	**3.72**	**5.31**

	BN3	CHD3	PP3
L+2	-0.276	+0.088	-0.128
L+1	-0.603	-0.496	-0.208
LUMO	**-1.563**	**-1.522**	**-0.881**
HOMO	**-4.947**	**-4.625**	**-5.770**
H-1	-5.507	-5.550	-5.956
H-2	-5.658	-5.992	-6.022
E_g	**3.384**	**3.10**	**4.89**

Cyclic voltammetry studies offer additional support for the notion that the HOMO-LUMO gap dramatically decreases with extension of conjugation. The oxidation potential decreased from $E_{ox, onset}$ = +0.58 V for **BN2** to $E_{ox, onset}$ = +0.36 V for **BN3** (Figure 3-17), consistent with an increase in energy of the HOMO with extension of π-conjugation. The irreversibility of the oxidation process might possibly be related to

oxidative deborylation.[10] The reduction potential of **BN3** ($E_{red, onset}$) is -2.55 V vs Fc/Fc$^+$ in THF/[(n-Bu)$_4$N]PF$_6$ (Figure 3-17), whereas for **BN1** and **BN2** the reduction potentials lie outside the electrochemical window of the solvent. The electrochemical oxidation of **BN-P** was attempted using CH$_2$Cl$_2$/[(n-Bu)$_4$N]PF$_6$ as the supporting electrolyte, but the scans showed no clearly discernible oxidative processes, possibly due to oxidative degradation processes. We also note that for the longest azaborine oligomer, **BN3**, both the oxidation and reduction potentials could be experimentally determined and the electrochemical gap of 2.91 eV is even lower than predicted by DFT methods .

BN2: E_{HOMO} = -(E_{ox} + 4.8) eV = -5.38 eV   ($E_{HOMO, DFT}$ = -5.28 eV)
BN3: E_{HOMO} = -(E_{ox} + 4.8) eV = -5.16 eV   ($E_{HOMO, DFT}$ = -4.96 eV)
BN3: E_{LUMO} = -(E_{red} + 4.8) eV = -2.25 eV   ($E_{LUMO, DFT}$ = -1.60 eV)
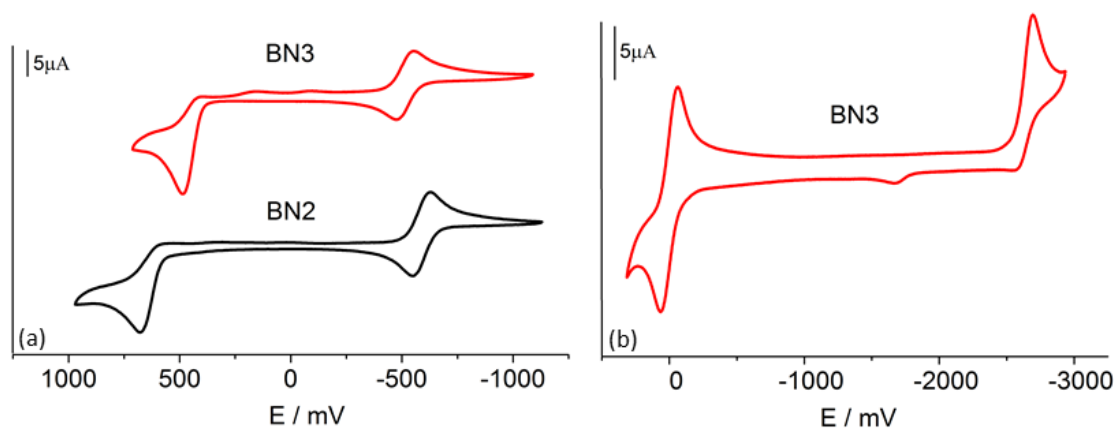
Figure 3-17. Cyclic voltammetry data for dimer **BN2** and trimer **BN3**. (a) Recorded at a scan rate of 100 mV/s with CH$_2$Cl$_2$/[(n-Bu)$_4$N]PF$_6$ (0.1 M) as the supporting electrolyte and referenced against decamethylferorrocene couple, Fc*/Fc*$^+$ (-590 mV versus Fc/Fc$^+$). (b) Recorded at scan rate of 100 mV/s with THF/[(n-Bu)$_4$N]PF$_6$ (0.1 M) as supporting electrolyte and referenced against Fc/Fc$^+$.

3.3 Conclusion

The regioregular synthesis of a conjugated polymer that is solely based on azaborine building blocks was accomplished by Suzuki-Miyaura polycondensation of an

AB type monomer. The polymer main chain is isoelectronic to poly(paraphenylene), but photophysical and computational studies indicate a closer similarity to poly(cyclohexadiene). A comparison of the absorption and emission characteristics of corresponding monodisperse oligomers reveals highly effective extension of π-conjugation that can be traced back to two distinct features: (i) the almost coplanar arrangement of the azaborines, which is favored by N-H…π interactions and (ii) the more limited contribution of N and B to the frontier orbitals in comparison to the C atoms in poly(paraphenylene). The close resemblance of poly(azaborine) to trans-cisoid poly(cyclohexadiene) suggests intriguing applications as a new class of conjugated materials.

3.4 Experimental

Materials and Methods. All oxygen- and moisture-sensitive manipulations were carried out under an inert atmosphere (N_2) using either standard Schlenk techniques or a dry box. THF, Et_2O, CH_2Cl_2, toluene, and pentane were purified by passing through a neutral alumina column under argon or distilled from Na/benzophenone (THF). The catalyst (t-Bu$_3$P)Pd(Ph)Br was prepared according to a literature procedure.[16,23] All other chemicals and solvents were purchased and used as received.

^{11}B NMR, ^{1}H NMR spectra were recorded on a Varian Unity/Inova 500 or 600 spectrometer at ambient temperature. The ^{11}B NMR spectrum of the polymer was acquired with a boron-free quartz NMR tube using a boron-free probe. ^{1}H NMR spectra are referenced internally to solvent signals; ^{11}B NMR chemical shifts are externally referenced to BF$_3$•Et$_2$O (δ 0). The two-dimensional ^{1}H NOESY[24] measurements were

obtained with the standard pulse sequence that was followed by a 90° pulse flanked by two 5 G/cm gradient for dephasing any residual transverse magnetization and suppressing potential artifacts, before the relaxation delay. A mixing time of 400 ms was applied for **BN3** (Varian Unity/Inova 500 spectrometer) and a mixing time of 600 ms was applied for **BN2** (Varian Unity/Inova 600 spectrometer). Spectra were recorded in the phase sensitive mode by employing the TPPI improvement of the States-Haberkorn-Ruben Hypercomplex method.[25] Typically, 256 t1 increments of 2K complex data points over 5.0 kHz spectral widths were collected with 32 scans per t1 increment, preceded by 16 or 32 dummy scans, and a relaxation delay of 2 s. Data sets were processed on a Sun Blade 100 workstation (Sun Microsystems Inc., Palo Alto, CA) using the VNMR software package (Varian Inc., Palo Alto, CA).

High-resolution MALDI-MS measurements were performed at Rutgers University on an Apex-ultra 7T Hybrid FT-MS (Bruker Daltonics) in positive ion mode. The samples (10 mg/mL in THF) were mixed with anthracene (10 mg/mL in THF) as the matrix in a 1:2 ratio and then spotted on the wells of a target plate.

GPC analyses were performed using a Viscotek GPCmax equipped with a VE 2001 GPC solvent/sample module, a 2600 PDA detector, a TDA 305 triple detector array and three columns, consisting of a PLgel 5 μm mixed-D and two PLgel 5 μm mixed-C columns. The system was calibrated against narrow polystyrene standards (10) in the molecular weight range from 580 to 371100 Da.

UV-visible absorption data were acquired on a Varian Cary 5000 UV-Vis/NIR spectrophotometer. The fluorescence data and lifetimes were measured using an Horiba Fluorolog-3 spectrofluorometer equipped with a 350 nm nanoLED and a FluoroHub R-

928 detector. Absolute quantum yields (Φ_F) were measured with a pre-calibrated Quanta-φ integrating sphere attached to the Fluorolog-3 instrument. Light from the sample compartment is directed into the sphere via a fiber-optic cable and the F-3000 Fiber-Optic Adapter and then returned to the sample compartment (and ultimately the emission monochromator) via a second fiber-optic cable and the F-3000.

Cyclic voltammetry (CV) experiments were carried out on a CV-50W analyzer from BASi. The three-electrode system consisted of an Au disk as working electrode, a Pt wire as counter electrode and an Ag wire as a pseudo-reference electrode. The voltammograms were recorded with ca. 10^{-3} to 10^{-4} M solutions in THF containing $Bu_4N[PF_6]$ (0.1 M) as the supporting electrolyte. The scans were referenced after the addition of a small amount of ferrocene (Fc) or decamethylferrocene (Fc*) as internal standard. The potentials are reported relative to the Fc/Fc^+ couple.

DFT calculations were performed with the Gaussian09 suite of programs.[20] The input files were generated in Chem3D and then pre-optimized in Spartan10. Geometries were then optimized in Gaussian09 using the hybrid density functional B3LYP with a 6-31g* basis set. Frequency calculations were performed to confirm the presence of local minima (only positive frequencies). Orbital representations were plotted with Gaussview 5.08 (scaling radii of 75%, isovalue of 0.03). Vertical excitations were then calculated using TD-DFT methods (B3LYP/6-31g*).

Representative Polymerization Procedure (Entry 6, Table 3-1): To a solution of monomer **BN-M** (411 mg, 1.00 mmol) in freshly distilled THF (16 mL) in a Schlenk tube was added under N_2 protection a degassed aqueous 2 M sodium carbonate solution (5 mL). A solution of the catalyst (t-Bu$_3$P)Pd(Ph)Br (23.3 mg, 0.050 mmol) in THF (10 mL) was added via syringe and the mixture was stirred overnight at room temperature. The polymerization was quenched with deionized water, extracted with DCM, passed through a short plug of alumina gel and purified by preparative GPC on Biobeads[TM] with THF as the eluent. The THF was removed by evaporation under reduced pressure and the product dried under high vacuum to give the polymer as a dark purple solid. Yield: 60 mg (15%). GPC (THF vs PS standards): M_n = 2330, $Đ$ = 1.40. ^{11}B NMR (160.4 MHz, CDCl$_3$): δ = 37.2, $w_{1/2}$ = 5300 Hz. All experiments were performed with this polymer batch except for the determination of ε and thin film measurements (Figure 3-15), for which a polymer batch of slightly higher molecular weight (M_n = 3150, $Đ$ = 1.34) was used.

BN2: ^{1}H NMR (599.7 MHz, CD$_2$Cl$_2$): δ 8.20 (br s, 1H), 8.02 (d, $^3J_{HH}$ = 7.2 Hz 1H), 7.96 (br s, 1H), 7.63 (dd, $^3J_{HH}$ = 6.6, 4.2 Hz, 1H), 7.49 (t, $^3J_{HH}$ = 6.6 Hz, 1H), 6.71 (s, 2H), 6.70 (s, 2H), 6.56-6.51 (m, 2H), 6.46 (d, $^3J_{HH}$ = 6.6 Hz, 1H), 2.24 (s, 3H), 2.15 (s, 3H), 2.02 (s, 6H), 1.89 (s, 6H).

BN3: ^{1}H NMR (499.9 MHz, CD$_2$Cl$_2$): δ 8.28 (br, 2H), 8.18 (d, $^3J_{HH}$ = 8.5 Hz, 1 H), 8.03 (br s, 1H), 8.01 (d, $^3J_{HH}$ = 8.0 Hz, 1H), 7.62 (dd, $^3J_{HH}$ = 7.5, 3.5 Hz, 1H), 7.56 (td, $^3J_{HH}$ = 7.0, 1.0 Hz, 1H), 6.76 (dd, $^3J_{HH}$ = 7.8, 2.0 Hz, 1H), 6.69 (s, 2H), 6.65 (s, 2H), 6.61 (td, $^3J_{HH}$ = 7.3, 1.5 Hz, 1H), 6.58 (s, 2H), 6.50 (d, $^3J_{HH}$ = 7.0 Hz, 1H), 6.45 (d, $^3J_{HH}$ = 10.5 Hz, 1H), 2.25 (s, 3H), 2.14 (s, 3H), 2.10 (s, 3H), 2.02 (s, 6H), 1.86 (s, 6H), 1.80 (s, 6H).
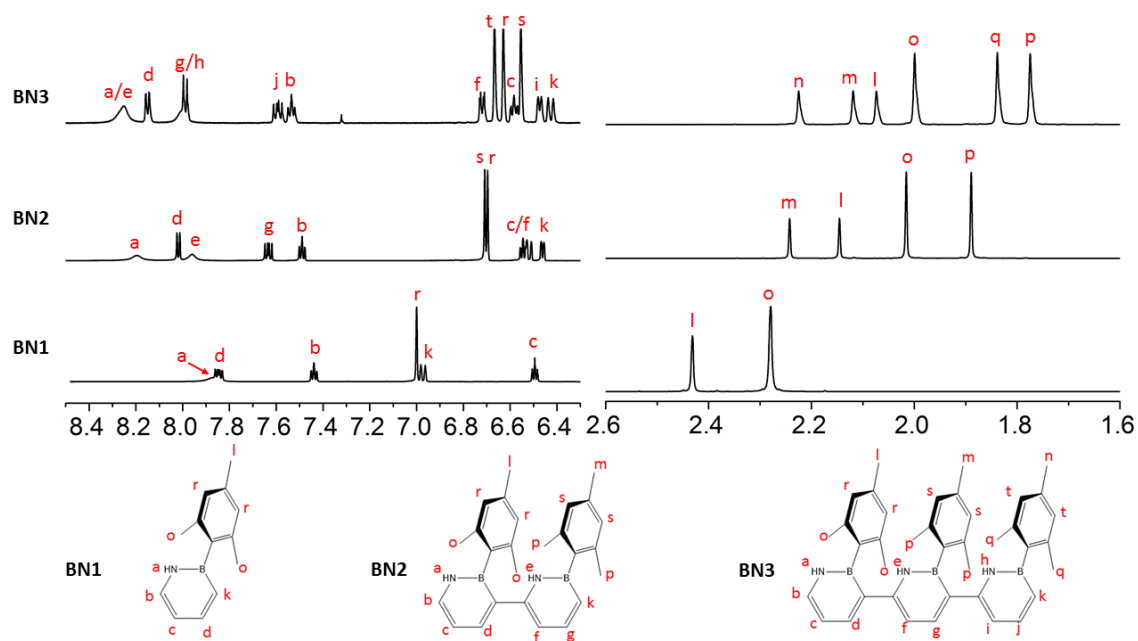
Figure 3-18. Comparison of the ^{1}H NMR spectra of **BN1, BN2, BN3** in CD$_2$Cl$_2$ (δ, ppm).

Table 3-8. TD-DFT data for **BN1** (B3LYP/6-31g*)

λ / nm	Oscillator strength	Assignment
265.68	0	H→L (0.70)
240.96	**0.168**	H-3→L+3 (0.15)
		H-2→L (0.20)
		H-1→L (0.64)
		H-1→L+3 (0.11)
215.83	**0.108**	H-2→L+2 (0.30)
		H-1→L+2 (0.14)
		H→L+1 (0.62)
202.33	0.061	H-1→L+3 (0.51)
195.59	0.016	H-7→L (0.12)
		H-4→L (0.67)
		H→L+2 (0.11)
188.50	0.406	H-2→L+1 (0.43)
		H→L+2 (0.49)
185.35	0.885	H-3→L (0.13)
		H-2→L+2 (0.58)
		H-1→L+2 (0.13)
		H→L+4 (0.13)
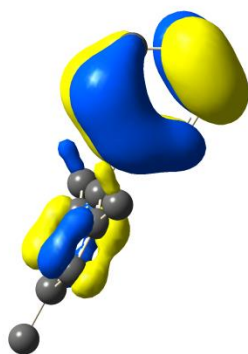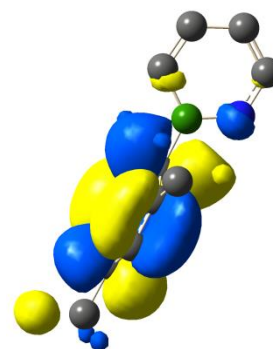
HOMO-1   **LUMO+1**

Table 3-9. TD-DFT data for **BN2** (B3LYP/6-31g*)

λ / nm	Oscillator strength	Assignment
336.27	**0.264**	**H→L (0.69)**
314.13	0.021	H-1→L (0.70)
290.70	0.023	H-3→L (0.70)
280.31	**0.083**	**H→L+1 (0.70)**
262.65	**0.133**	H-6→L (0.11)
		H-5→L (0.31)
		H→L+2 (0.61)
253.17	0.039	H-5→L (0.56)
		H→L+7 (0.11)
242.31	0.016	H-1→L+6 (0.19)
		H→L+4 (0.52)
238.29	0.076	H-3→L+1 (0.62)
236.22	0.020	H-5→L (0.14)
		H→L+5 (0.56)

Table 3-10. TD-DFT data for **BN3** (B3LYP/6-31g*)

λ / nm	Oscillator strength	Assignment
403.47	**0.511**	**H→L (0.70)**
345.25	0.013	H-1→L (0.70)
329.72	0.014	H-2→L (0.65)
328.00	0.040	H-4→L (0.12)
		H-3→L (0.63)
		H-2→L (0.27)
319.39	**0.197**	H-4→L (0.15)
		H→L+1 (0.68)
306.44	0.072	H-4→L (0.53)
305.55	0.049	H-5→L (0.58)
		H-4→L (0.35)
293.85	0.012	H-4→L (0.17)
		H→L+2 (0.64)
		H→L+3 (0.18)
279.75	0.069	H→L+3 (0.64)
267.45	0.033	H-8→L(0.15)
		H→L+5 (0.57)
260.86	0.010	H-8→L (0.51)
		H-3→L+1 (0.22)
		H→L+6 (0.36)
254.47	0.020	H-1→L+2 (0.18)
		H→L+5 (0.18)
		H→L+6 (0.47)
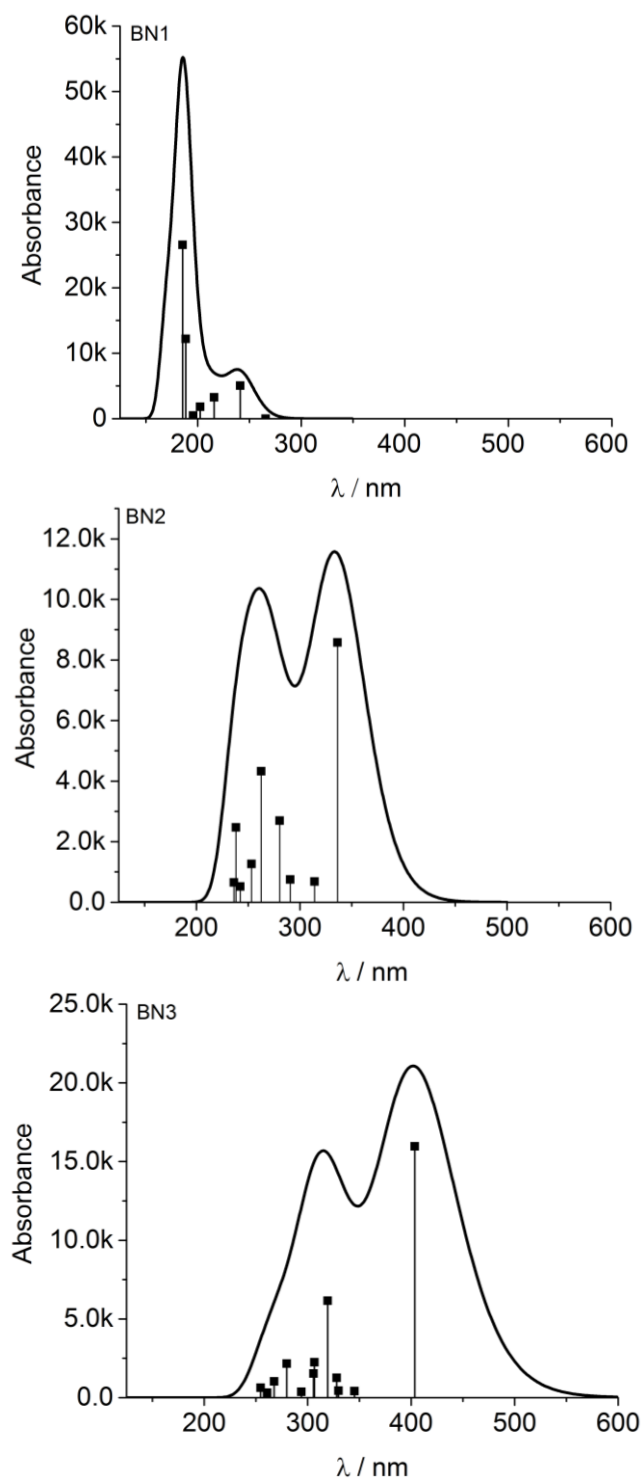
Figure 3-19. Comparison of calculated absorption spectra of **BN1**, **BN2**, and **BN3** (TD-DFT, B3LYP/6-31g*)

Table 3-11.   Coordinates (Å) for the optimized geometry of **BN1** (DFT, B3LYP/6-31g*)

Standard orientation: (Ground State)

Center Number	Atomic Number	Atomic Type	X	Y	Z
1	5	0	1.267755	-0.000071	0.090747
2	7	0	2.003980	0.000218	-1.152585
3	6	0	3.369021	0.000249	-1.239521
4	6	0	4.141623	0.000007	-0.110728
5	6	0	3.525370	-0.000269	1.173935
6	6	0	2.157060	-0.000308	1.324035
7	6	0	-0.313160	-0.000009	0.043360
8	6	0	-1.035960	-1.214120	0.025819
9	6	0	-2.434316	-1.197526	-0.010272
10	6	0	-3.154586	0.000089	-0.025503
11	6	0	-2.434254	1.197605	-0.010111
12	6	0	-1.035847	1.214110	0.025990
13	6	0	-0.309462	2.544176	0.043887
14	6	0	-0.309618	-2.544210	0.043521
15	6	0	-4.666019	0.000036	-0.027522
16	1	0	1.504949	0.000417	-2.035197
17	1	0	3.799686	0.000474	-2.236747
18	1	0	5.222348	0.000038	-0.206725
19	1	0	4.181264	-0.000443	2.045018
20	1	0	-2.975346	-2.142637	-0.025069
21	1	0	-2.975226	2.142745	-0.024774
22	1	0	0.364988	2.623263	0.905251
23	1	0	0.310103	2.682721	-0.851595
24	1	0	-1.013588	3.381355	0.090732
25	1	0	-1.013776	-3.381383	0.090011
26	1	0	0.310125	-2.682531	-0.851871
27	1	0	0.364660	-2.623534	0.904998
28	1	0	-5.067121	0.889162	-0.526383
29	1	0	-5.067108	-0.883603	-0.536119
30	1	0	-5.066953	-0.005692	0.995299
31	1	0	1.755240	-0.000510	2.336197

Table 3-12. Coordinates (Å) for the optimized geometry of **BN2** (DFT, B3LYP/6-31g*)

Standard orientation: (Ground State)

Center Number	Atomic Number	Atomic Type	Coordinates (Angstroms) X	Y	Z
1	6	0	0.693930	-3.252953	1.288295
2	6	0	-1.735018	-2.997495	1.095088
3	7	0	-0.365135	-1.353956	0.089854
4	6	0	-1.626682	-1.835182	0.352434
5	5	0	0.873706	-1.971425	0.495161
6	6	0	-0.585219	-3.692328	1.551461
7	1	0	-0.339328	-0.476418	-0.419021
8	1	0	1.527525	-3.840709	1.669601
9	1	0	-2.721499	-3.366032	1.353641
10	1	0	-0.753346	-4.600555	2.131983
11	6	0	-2.799096	-1.087551	-0.161117
12	6	0	-5.129038	-1.194329	-0.977166
13	7	0	-4.123004	0.939881	-0.788548
14	6	0	-5.204020	0.166459	-1.098820
15	5	0	-2.855015	0.438726	-0.317997
16	6	0	-3.933548	-1.803007	-0.518545
17	1	0	-5.986077	-1.804009	-1.241906
18	1	0	-4.246022	1.940415	-0.897340
19	1	0	-3.918906	-2.890434	-0.464507
20	1	0	-6.098767	0.675815	-1.443506
21	6	0	-1.719612	1.506256	-0.040189
22	6	0	0.311630	3.432772	0.453086
23	6	0	-1.394282	1.891352	1.282690
24	6	0	-1.018410	2.109516	-1.110878
25	6	0	-0.018010	3.053417	-0.849594
26	6	0	-0.397892	2.845828	1.506546
27	1	0	0.520824	3.498124	-1.684439
28	1	0	-0.164867	3.136517	2.529633
29	1	0	1.232285	5.007788	1.623124
30	6	0	1.424425	4.418861	0.719553
31	1	0	2.381286	3.900289	0.865848
32	1	0	1.555702	5.112819	-0.117580
33	6	0	-1.330806	1.753440	-2.552696
34	1	0	-1.425465	0.670908	-2.699676
35	1	0	-0.546109	2.113517	-3.225452
36	1	0	-2.276919	2.198022	-2.888817
37	6	0	-2.117161	1.279791	2.465069

38	1	0	-1.941945	0.198907	2.527027
39	1	0	-3.202889	1.422598	2.396598
40	1	0	-1.782159	1.725415	3.407168
41	6	0	2.241703	-1.289611	0.080076
42	6	0	4.711769	-0.092760	-0.664817
43	6	0	2.939409	-0.450841	0.978079
44	6	0	2.801760	-1.518403	-1.197173
45	6	0	4.016891	-0.921446	-1.549847
46	6	0	4.153066	0.131657	0.596182
47	1	0	4.433874	-1.111545	-2.538012
48	1	0	4.676969	0.774702	1.302428
49	6	0	6.042780	0.513165	-1.047235
50	1	0	6.877575	-0.145538	-0.770694
51	1	0	6.208307	1.471738	-0.542746
52	1	0	6.111179	0.683667	-2.127464
53	6	0	2.098269	-2.411326	-2.200115
54	1	0	1.850217	-3.387391	-1.765816
55	1	0	2.721526	-2.584045	-3.083882
56	1	0	1.152099	-1.973216	-2.543588
57	6	0	2.375288	-0.151591	2.352027
58	1	0	2.042930	-1.063845	2.860600
59	1	0	1.503595	0.512998	2.288583
60	1	0	3.119182	0.339363	2.988889

Table 3-13.   Coordinates (Å) for the optimized geometry of **BN3** (DFT, B3LYP/6-31g*)

Standard orientation: (Ground State)

```
-------------------------------------------------------------------------
Center   Atomic    Atomic    Coordinates (Angstroms)
Number   Number    Type       X        Y        Z
-------------------------------------------------------------------------
```

Center Number	Atomic Number	Atomic Type	X	Y	Z
1	5	0	4.979176	-0.613685	-0.570390
2	7	0	6.339788	-0.745998	-1.029057
3	6	0	6.869118	-1.871004	-1.591411
4	6	0	6.090913	-2.984386	-1.760190
5	6	0	4.736964	-2.976606	-1.342160
6	6	0	4.128866	-1.880365	-0.744705
7	6	0	2.722286	-2.005055	-0.303589
8	6	0	2.160394	-3.188845	0.144848
9	6	0	0.811875	-3.258007	0.552103
10	6	0	-0.054125	-2.170480	0.553326
11	5	0	0.524461	-0.842939	0.053457
12	7	0	1.912261	-0.896971	-0.325399
13	6	0	-1.434122	-2.363801	1.051013
14	6	0	-1.765762	-3.270277	2.044096
15	6	0	-3.106515	-3.439923	2.472884
16	6	0	-4.150256	-2.717822	1.935051
17	5	0	-3.844232	-1.694399	0.857731
18	7	0	-2.447565	-1.607011	0.509381
19	6	0	4.547964	0.783489	0.034388
20	6	0	-0.207653	0.555541	-0.097083
21	6	0	-4.884691	-0.767344	0.103727
22	6	0	4.422097	0.959210	1.433324
23	6	0	4.035596	2.200155	1.948134
24	6	0	3.749522	3.287274	1.115473
25	6	0	3.886355	3.110707	-0.263173
26	6	0	4.282315	1.885632	-0.812470
27	6	0	-0.442303	1.376950	1.030817
28	6	0	-1.083319	2.610472	0.876250
29	6	0	-1.518005	3.064140	-0.373351
30	6	0	-1.276255	2.253126	-1.484232
31	6	0	-0.629314	1.017338	-1.366324
32	6	0	-5.434945	-1.166017	-1.136847
33	6	0	-6.371669	-0.354571	-1.784049
34	6	0	-6.790024	0.863003	-1.237886
35	6	0	-6.247563	1.249529	-0.010629
36	6	0	-5.307576	0.458513	0.661493
37	6	0	4.421196	1.768197	-2.319172
38	6	0	4.699101	-0.186843	2.384373

39	6	0	3.269441	4.600376	1.686929
40	6	0	-0.388180	0.192442	-2.616701
41	6	0	-2.260071	4.372864	-0.512131
42	6	0	-4.744196	0.942197	1.982121
43	6	0	-5.025079	-2.478683	-1.774112
44	6	0	-7.788068	1.736783	-1.962893
45	1	0	6.971176	0.041074	-0.929159
46	1	0	7.910971	-1.833763	-1.894491
47	1	0	6.514769	-3.868786	-2.223065
48	1	0	4.156890	-3.880318	-1.522575
49	1	0	2.776850	-4.078448	0.204097
50	1	0	0.445716	-4.233072	0.871309
51	1	0	2.367966	-0.037816	-0.616267
52	1	0	-0.975432	-3.840845	2.518820
53	1	0	-3.285408	-4.173055	3.260972
54	1	0	-5.153936	-2.905707	2.313434
55	1	0	-2.148326	-0.926184	-0.181116
56	1	0	3.948428	2.321331	3.026542
57	1	0	3.672331	3.944762	-0.929211
58	1	0	-1.254377	3.231049	1.754668
59	1	0	-1.605056	2.586939	-2.467054
60	1	0	-6.790966	-0.682414	-2.734592
61	1	0	-6.567738	2.188529	0.439278
62	1	0	5.473273	1.767848	-2.634276
63	1	0	3.979950	0.840947	-2.704117
64	1	0	3.932009	2.606107	-2.825787
65	1	0	4.637744	0.140534	3.427099
66	1	0	3.978926	-1.003440	2.249949
67	1	0	5.697023	-0.614618	2.227427
68	1	0	3.644095	4.757670	2.704036
69	1	0	3.588670	5.448364	1.071362
70	1	0	2.172605	4.627371	1.734034
71	1	0	-0.673531	-0.857537	-2.478774
72	1	0	-0.958954	0.585060	-3.464334
73	1	0	0.670912	0.191231	-2.905727
74	1	0	-2.060901	4.847977	-1.479129
75	1	0	-3.345360	4.219452	-0.443830
76	1	0	-1.981017	5.079101	0.277471
77	1	0	-4.747066	0.148527	2.738035
78	1	0	-3.703316	1.274178	1.873454
79	1	0	-5.321290	1.786799	2.374277
80	1	0	-5.609823	-2.682522	-2.677500
81	1	0	-3.964852	-2.479392	-2.058245
82	1	0	-5.162951	-3.320865	-1.085104
83	1	0	-7.314361	2.294933	-2.782214
84	1	0	-8.595840	1.142616	-2.406234

85	1	0	-8.241657	2.471032	-1.288373
86	6	0	0.009244	0.941929	2.409468
87	1	0	1.103033	0.872331	2.467354
88	1	0	-0.392192	-0.043331	2.673327
89	1	0	-0.318728	1.652312	3.175503

Table 3-14. Coordinates (Å) for the optimized geometry of **CHD1** (DFT, B3LYP/6-31g*)

Standard orientation: (Ground State)

Center Number	Atomic Number	Atomic Type	Coordinates (Angstroms)		
			X	Y	Z
1	6	0	1.222223	0.447133	-0.124608
2	6	0	1.920642	0.248705	1.245967
3	6	0	3.427157	0.307020	1.132126
4	6	0	4.049335	-0.053191	-0.002428
5	6	0	3.282588	-0.477855	-1.177509
6	6	0	1.953819	-0.289588	-1.236442
7	6	0	-0.283175	0.187864	-0.065584
8	6	0	-0.815198	-1.117863	0.055468
9	6	0	-2.203743	-1.294913	0.098381
10	6	0	-3.096980	-0.225445	0.039189
11	6	0	-2.558048	1.057908	-0.060627
12	6	0	-1.178526	1.282624	-0.116175
13	6	0	-0.699663	2.717655	-0.227133
14	6	0	0.044514	-2.361063	0.178298
15	6	0	-4.590961	-0.450452	0.056486
16	1	0	1.359186	1.509347	-0.371365
17	1	0	1.553405	1.012279	1.942393
18	1	0	1.635664	-0.716913	1.690550
19	1	0	3.999911	0.583896	2.014925
20	1	0	5.135346	-0.055722	-0.062244
21	1	0	3.814231	-0.932163	-2.010641
22	1	0	1.385788	-0.568093	-2.121463
23	1	0	-2.595092	-2.307225	0.185736
24	1	0	-3.230105	1.913259	-0.100391
25	1	0	-0.159202	2.905056	-1.163626
26	1	0	-1.550491	3.405326	-0.200468
27	1	0	-0.027950	2.999068	0.593178
28	1	0	0.388362	-2.511192	1.210514
29	1	0	-0.530886	-3.250398	-0.099466
30	1	0	0.939399	-2.324911	-0.447775
31	1	0	-5.122120	0.414405	0.468485
32	1	0	-4.981607	-0.619143	-0.956273
33	1	0	-4.857742	-1.328111	0.655482

Table 3-15.   Coordinates (Å) for the optimized geometry of **CHD2** (DFT, B3LYP/6-31g*) Standard orientation: (Ground State)

```
--------------------------------------------------------------------------
Center   Atomic    Atomic        Coordinates (Angstroms)
Number   Number    Type      X           Y           Z
--------------------------------------------------------------------------
```

Center Number	Atomic Number	Atomic Type	X	Y	Z
1	6	0	-2.592446	-0.488449	-0.986187
2	6	0	-4.077280	-0.510361	-1.462746
3	6	0	-4.652929	-1.890264	-1.637445
4	6	0	-4.140149	-2.936928	-0.971067
5	6	0	-2.967880	-2.795104	-0.117143
6	6	0	-2.229541	-1.658366	-0.054851
7	6	0	-0.988543	-1.623881	0.740824
8	6	0	-0.909756	-2.186160	1.973987
9	6	0	0.329463	-2.196397	2.742535
10	6	0	1.505009	-1.882796	2.169283
11	6	0	1.565179	-1.582554	0.682461
12	6	0	0.252052	-0.922072	0.193939
13	6	0	2.806888	-0.815533	0.227394
14	6	0	3.158334	0.439046	0.778188
15	6	0	4.310772	1.092718	0.322108
16	6	0	5.129643	0.560680	-0.672606
17	6	0	4.760536	-0.669378	-1.220191
18	6	0	3.625196	-1.363010	-0.790382
19	6	0	3.318448	-2.693976	-1.450569
20	6	0	2.331457	1.152249	1.830626
21	6	0	6.382903	1.273470	-1.124523
22	1	0	-4.708452	0.047246	-0.754896
23	1	0	-4.140278	0.057024	-2.399880
24	1	0	-5.535736	-2.003491	-2.263240
25	1	0	-4.587321	-3.924273	-1.062281
26	1	0	-2.633860	-3.669973	0.434213
27	1	0	-1.799072	-2.617917	2.426658
28	1	0	0.284676	-2.488693	3.789402
29	1	0	2.437461	-1.929722	2.726946
30	1	0	1.599168	-2.571185	0.203182
31	1	0	0.224581	0.134528	0.484594
32	1	0	0.251263	-0.932994	-0.901683
33	1	0	4.569522	2.054621	0.761749
34	1	0	5.376019	-1.106710	-2.004415
35	1	0	2.327030	-2.710236	-1.919770
36	1	0	4.052151	-2.906797	-2.234183
37	1	0	3.350736	-3.528921	-0.739340
38	1	0	2.950464	1.874654	2.373205
39	1	0	1.503320	1.714114	1.378644
40	1	0	1.888143	0.469503	2.559766

41	1	0	7.268838	0.901720	-0.591974
42	1	0	6.565159	1.125218	-2.194870
43	1	0	6.320655	2.350934	-0.938164
44	6	0	-2.251216	0.920601	-0.490085
45	6	0	-1.657707	3.579805	0.328823
46	6	0	-2.676176	1.394289	0.773711
47	6	0	-1.552126	1.803548	-1.347692
48	6	0	-1.262626	3.104242	-0.922739
49	6	0	-2.366074	2.706455	1.154047
50	1	0	-0.716600	3.764798	-1.593697
51	1	0	-2.694907	3.053648	2.132106
52	6	0	-1.093337	1.394550	-2.734087
53	1	0	-0.349240	0.588440	-2.706991
54	1	0	-0.630663	2.242903	-3.247429
55	1	0	-1.922469	1.047122	-3.362751
56	6	0	-3.438919	0.546687	1.774175
57	1	0	-2.766210	-0.126411	2.316349
58	1	0	-4.205798	-0.079590	1.312538
59	1	0	-3.931490	1.188569	2.511904
60	6	0	-1.365922	4.999736	0.755343
61	1	0	-0.428003	5.364179	0.322148
62	1	0	-1.290824	5.083785	1.844845
63	1	0	-2.160298	5.685588	0.430848
64	1	0	-1.987489	-0.668751	-1.884294

Table 3-16.   Coordinates (Å) for the optimized geometry of **CHD3** (DFT, B3LYP/6-31g*) Standard orientation: (Ground State)

Center Number	Atomic Number	Atomic Type	X	Y	Z
1	6	0	4.695631	-1.139330	-1.170094
2	6	0	6.082770	-1.754373	-1.532692
3	6	0	6.023297	-3.164430	-2.054931
4	6	0	4.987816	-3.964519	-1.753592
5	6	0	3.850188	-3.479322	-0.984339
6	6	0	3.681583	-2.173486	-0.651603
7	6	0	2.445331	-1.736835	0.016547
8	6	0	1.862236	-2.457780	1.009275
9	6	0	0.594060	-2.087861	1.600463
10	6	0	-0.218354	-1.123768	1.088337
11	6	0	0.227260	-0.443436	-0.213736
12	6	0	1.773639	-0.431909	-0.380350
13	6	0	-1.559925	-0.908103	1.650776
14	6	0	-1.794690	-0.938678	2.989241
15	6	0	-3.134099	-0.786217	3.542491
16	6	0	-4.223972	-0.868965	2.757627
17	6	0	-4.068851	-1.193044	1.282735
18	6	0	-2.741697	-0.620116	0.727367
19	1	0	6.567859	-1.091267	-2.260102
20	1	0	6.742565	-1.734219	-0.652625
21	1	0	6.872698	-3.538569	-2.622637
22	1	0	4.970366	-4.998314	-2.091322
23	1	0	3.065751	-4.189916	-0.738169
24	1	0	2.353108	-3.352808	1.384011
25	1	0	0.241133	-2.679283	2.441229
26	1	0	1.988127	-0.189106	-1.427219
27	1	0	2.206636	0.388790	0.202932
28	1	0	-0.962238	-1.048343	3.679937
29	1	0	-3.234987	-0.631060	4.614514
30	1	0	-5.227017	-0.801123	3.172295
31	1	0	-2.571169	-1.047758	-0.266575
32	1	0	-2.825809	0.462820	0.579462
33	1	0	-3.959098	-2.286362	1.251025
34	6	0	-5.271986	-0.833226	0.411152
35	6	0	-7.520283	-0.236083	-1.228147
36	6	0	-5.885530	-1.840383	-0.372652
37	6	0	-5.792171	0.480952	0.354421
38	6	0	-6.905999	0.746321	-0.453162
39	6	0	-6.988988	-1.526006	-1.171612
40	1	0	-7.301358	1.760596	-0.474088

41	1	0	-7.450617	-2.316035	-1.761409
42	6	0	-5.190885	1.651094	1.108582
43	1	0	-4.812892	1.373061	2.095528
44	1	0	-5.936944	2.442129	1.240035
45	1	0	-4.348649	2.091548	0.558705
46	6	0	-8.701717	0.085496	-2.113660
47	1	0	-9.240689	0.969469	-1.756481
48	1	0	-9.410791	-0.748854	-2.155967
49	1	0	-8.384528	0.292108	-3.144889
50	6	0	-5.393353	-3.275340	-0.380511
51	1	0	-5.477185	-3.750675	0.604976
52	1	0	-4.342911	-3.355587	-0.686433
53	1	0	-5.982293	-3.875100	-1.081315
54	1	0	-0.157366	-1.099450	-1.006306
55	6	0	-0.304922	0.965276	-0.497326
56	6	0	-1.232188	3.575871	-1.150448
57	6	0	-0.866153	1.239502	-1.768306
58	6	0	-0.190338	2.022503	0.436493
59	6	0	-0.660091	3.296520	0.090411
60	6	0	-1.321946	2.527296	-2.067186
61	1	0	-0.570125	4.097440	0.822334
62	1	0	-1.758306	2.714321	-3.046659
63	6	0	-1.002325	0.177322	-2.842633
64	1	0	-1.678875	-0.633843	-2.544205
65	1	0	-0.041162	-0.284331	-3.099996
66	1	0	-1.408376	0.614735	-3.759765
67	6	0	-1.700275	4.968416	-1.503830
68	1	0	-2.020721	5.521530	-0.614329
69	1	0	-2.539646	4.942753	-2.207355
70	1	0	-0.898721	5.551730	-1.977201
71	6	0	0.389731	1.860973	1.829142
72	1	0	1.257635	1.199415	1.862748
73	1	0	-0.351722	1.446830	2.521140
74	1	0	0.699981	2.835265	2.220786
75	1	0	4.261173	-0.793571	-2.117366
76	6	0	4.921194	0.101484	-0.298753
77	6	0	5.434459	2.443041	1.233240
78	6	0	4.883918	1.382679	-0.899465
79	6	0	5.252925	0.003156	1.073315
80	6	0	5.497393	1.172707	1.805008
81	6	0	5.134896	2.521549	-0.127740
82	1	0	5.750736	1.080148	2.859707
83	1	0	5.098962	3.497584	-0.608209
84	6	0	4.583589	1.578617	-2.372883
85	1	0	3.564637	1.266478	-2.634804
86	1	0	5.270036	1.016750	-3.018123

87	1	0	4.675877	2.634976	-2.642932
88	6	0	5.668802	3.688000	2.056368
89	1	0	6.150196	4.475336	1.465742
90	1	0	6.302912	3.481076	2.925124
91	1	0	4.723516	4.100235	2.434639
92	6	0	5.349472	-1.312794	1.821900
93	1	0	4.356940	-1.701386	2.074735
94	1	0	5.897744	-1.171055	2.758949
95	1	0	5.858879	-2.095734	1.254475

Table 3-17.   Coordinates (Å) for the optimized geometry of **PP1** (DFT, B3LYP/6-31g*)
Standard orientation: (Ground State)

Center Number	Atomic Number	Atomic Type	X	Y	Z
1	1	0	1.413548	0.000077	2.148336
2	6	0	1.958714	0.000044	1.207589
3	6	0	3.358385	-0.000043	-1.201630
4	6	0	1.241633	0.000001	0.001438
5	6	0	3.354637	0.000042	1.211068
6	6	0	4.058875	-0.000001	0.005816
7	6	0	1.962470	-0.000043	-1.202477
8	1	0	3.891842	0.000074	2.156157
9	1	0	5.145695	-0.000002	0.007508
10	1	0	1.420234	-0.000075	-2.144920
11	1	0	3.898523	-0.000077	-2.145044
12	6	0	-0.257369	0.000002	-0.000577
13	6	0	-3.082766	0.000002	-0.008303
14	6	0	-0.964354	1.220238	-0.004060
15	6	0	-0.964356	-1.220239	-0.004039
16	6	0	-2.362890	-1.197557	-0.009246
17	6	0	-2.362894	1.197558	-0.009266
18	1	0	-2.903400	-2.142494	-0.015522
19	1	0	-2.903398	2.142498	-0.015560
20	6	0	-0.235146	2.545945	-0.006578
21	1	0	0.413426	2.650360	-0.884384
22	1	0	0.411767	2.654014	0.872002
23	1	0	-0.943084	3.380590	-0.008935
24	6	0	-0.235140	-2.545943	-0.006518
25	1	0	0.413441	-2.650378	-0.884314
26	1	0	-0.943074	-3.380591	-0.008858
27	1	0	0.411763	-2.653980	0.872073
28	6	0	-4.593872	-0.000006	0.019299
29	1	0	-5.004346	0.886181	-0.476808
30	1	0	-4.974164	0.000068	1.049850
31	1	0	-5.004330	-0.886273	-0.476677

Table 3-18. Coordinates (Å) for the optimized geometry of **PP2** (DFT, B3LYP/6-31g*)
Standard orientation: (Ground State)

Center Number	Atomic Number	Atomic Type	X	Y	Z
1	1	0	-4.503184	0.929276	-1.492156
2	6	0	-4.148599	-0.058893	-1.209883
3	6	0	-3.255376	-2.561674	-0.452099
4	6	0	-4.927776	-1.178603	-1.493555
5	6	0	-2.914141	-0.160381	-0.547863
6	6	0	-2.456005	-1.442286	-0.157631
7	6	0	-4.475504	-2.441023	-1.111686
8	1	0	-5.879288	-1.063812	-2.005948
9	1	0	-5.064450	-3.328018	-1.329567
10	1	0	-2.893144	-3.546728	-0.170857
11	6	0	-1.171318	-1.675138	0.565887
12	6	0	1.238911	-2.232559	1.908550
13	6	0	-1.157053	-2.490564	1.710603
14	6	0	0.047981	-1.147390	0.112658
15	6	0	1.257059	-1.418506	0.766466
16	6	0	0.036885	-2.762009	2.377166
17	1	0	-2.091683	-2.900025	2.084531
18	1	0	0.064985	-0.523840	-0.774752
19	1	0	0.029144	-3.388765	3.265307
20	1	0	2.170946	-2.449361	2.424258
21	6	0	-2.170831	1.111731	-0.258823
22	6	0	-0.861122	3.566643	0.253441
23	6	0	-2.196975	1.671993	1.036292
24	6	0	-1.504500	1.792287	-1.300984
25	6	0	-0.858394	3.001788	-1.024423
26	6	0	-1.543069	2.887187	1.266525
27	1	0	-0.340063	3.515875	-1.831787
28	1	0	-1.574762	3.317348	2.266003
29	6	0	2.547454	-0.862096	0.243720
30	6	0	4.986740	0.173887	-0.735053
31	6	0	3.271835	-1.567813	-0.739609
32	6	0	3.044841	0.360465	0.739764
33	6	0	4.255739	0.853954	0.242139
34	6	0	4.477759	-1.038036	-1.209634
35	1	0	4.637131	1.796422	0.631260
36	1	0	5.034485	-1.589929	-1.965017
37	6	0	-1.472354	1.242207	-2.711383
38	1	0	-1.178093	0.186710	-2.733662
39	1	0	-0.765754	1.803996	-3.330167
40	1	0	-2.455382	1.298998	-3.194517

41	6	0	-2.929926	0.995891	2.173117
42	1	0	-3.956251	0.733003	1.893196
43	1	0	-2.973415	1.649784	3.049771
44	1	0	-2.433042	0.066121	2.474596
45	6	0	-0.132914	4.860139	0.536688
46	1	0	0.902832	4.673181	0.850734
47	1	0	-0.617606	5.425266	1.340259
48	1	0	-0.091436	5.500516	-0.350999
49	6	0	2.291284	1.142117	1.793101
50	1	0	1.304901	1.458824	1.433843
51	1	0	2.848720	2.038190	2.084548
52	1	0	2.118098	0.544533	2.695617
53	6	0	2.769376	-2.887084	-1.284274
54	1	0	3.465326	-3.294311	-2.024353
55	1	0	1.789801	-2.780652	-1.765079
56	1	0	2.646019	-3.632408	-0.489586
57	6	0	6.276370	0.742587	-1.280502
58	1	0	6.973914	-0.050727	-1.570900
59	1	0	6.776888	1.380317	-0.543933
60	1	0	6.096101	1.357282	-2.172938

Table 3-19.   Coordinates (Å) for the optimized geometry of **PP3** (DFT, B3LYP/6-31g*)
Standard orientation: (Ground State)

Center Number	Atomic Number	Atomic Type	X	Y	Z
1	6	0	-3.844155	-1.029600	1.208588
2	6	0	-1.606870	-1.697937	2.763128
3	6	0	-3.989684	-1.334673	2.569923
4	6	0	-2.562415	-1.062127	0.643737
5	6	0	-1.428525	-1.395278	1.401887
6	6	0	-2.875210	-1.664761	3.340440
7	1	0	-4.979258	-1.312996	3.019346
8	1	0	-2.453628	-0.834647	-0.411029
9	1	0	-2.994144	-1.895571	4.396047
10	1	0	-0.741367	-1.945702	3.371755
11	6	0	-0.066203	-1.487212	0.801339
12	6	0	2.573910	-1.802458	-0.227107
13	6	0	0.700865	-2.632701	1.075064
14	6	0	0.507581	-0.481489	-0.013664
15	6	0	1.809716	-0.660116	-0.501027
16	6	0	1.986472	-2.795966	0.571718
17	1	0	0.265358	-3.419874	1.684383
18	1	0	2.233953	0.127999	-1.113468
19	1	0	2.546803	-3.696364	0.809105
20	6	0	3.940556	-2.006254	-0.787944
21	6	0	6.484220	-2.564594	-1.873922
22	6	0	4.220598	-3.238094	-1.406855
23	6	0	4.967985	-1.033946	-0.715701
24	6	0	6.224330	-1.339237	-1.263447
25	6	0	5.472340	-3.521236	-1.946424
26	1	0	3.425985	-3.975626	-1.479817
27	1	0	7.014207	-0.595936	-1.189564
28	1	0	5.652674	-4.480531	-2.424256
29	1	0	7.468796	-2.769385	-2.285941
30	6	0	4.799403	0.299527	-0.046905
31	6	0	4.552568	2.824762	1.204388
32	6	0	4.684297	1.471760	-0.827521
33	6	0	4.810483	0.396458	1.359866
34	6	0	4.684300	1.656496	1.957507
35	6	0	4.555222	2.708085	-0.188859
36	1	0	4.696120	1.723762	3.043843
37	1	0	4.451022	3.604528	-0.797542
38	6	0	-0.195741	0.796470	-0.370459
39	6	0	-1.449661	3.231019	-1.077668
40	6	0	-0.273788	1.849988	0.564971

41	6	0	-0.724342	0.972124	-1.667467
42	6	0	-1.345564	2.182053	-1.994474
43	6	0	-0.899658	3.044972	0.193604
44	1	0	-1.758708	2.306534	-2.993779
45	1	0	-0.950662	3.855594	0.918451
46	6	0	-5.037465	-0.685217	0.368639
47	6	0	-7.290979	-0.040297	-1.208942
48	6	0	-5.698212	-1.691743	-0.365890
49	6	0	-5.506583	0.643681	0.316997
50	6	0	-6.624830	0.940259	-0.469574
51	6	0	-6.812678	-1.351361	-1.139404
52	1	0	-6.984418	1.967227	-0.503731
53	1	0	-7.321576	-2.133731	-1.699864
54	6	0	4.687096	1.417073	-2.340766
55	1	0	4.409860	2.387595	-2.763878
56	1	0	3.987441	0.666557	-2.726165
57	1	0	5.674389	1.151580	-2.738021
58	6	0	4.436408	4.177365	1.868281
59	1	0	3.654128	4.786810	1.401209
60	1	0	5.374426	4.743005	1.789959
61	1	0	4.198866	4.081691	2.932725
62	6	0	4.966569	-0.826721	2.235426
63	1	0	5.806596	-1.451118	1.911361
64	1	0	4.070850	-1.458968	2.210060
65	1	0	5.139796	-0.538011	3.276946
66	6	0	0.326078	1.720845	1.947103
67	1	0	1.388378	1.454476	1.900320
68	1	0	-0.176889	0.944407	2.535459
69	1	0	0.237764	2.663863	2.495912
70	6	0	-0.633181	-0.119624	-2.712628
71	1	0	-1.254233	0.121836	-3.580898
72	1	0	-0.958682	-1.090332	-2.321693
73	1	0	0.395266	-0.258502	-3.067878
74	6	0	-2.152497	4.518172	-1.442390
75	1	0	-2.069820	4.731086	-2.513716
76	1	0	-1.737496	5.371090	-0.894329
77	1	0	-3.223388	4.468787	-1.203265
78	6	0	-5.225311	-3.128478	-0.323978
79	1	0	-5.195855	-3.515240	0.701391
80	1	0	-4.210006	-3.233302	-0.724866
81	1	0	-5.886376	-3.773809	-0.910872
82	6	0	-4.821053	1.746524	1.093213
83	1	0	-4.818165	1.543546	2.170735
84	1	0	-5.325999	2.704729	0.933903
85	1	0	-3.772852	1.861501	0.793438
86	6	0	-8.478155	0.310180	-2.076283

```
87      1       0       -9.184133   -0.524553   -2.146441
88      1       0       -8.165967    0.557198   -3.100158
89      1       0       -9.018476    1.178629   -1.684299
---------------------------------------------------------------------------
```

3.5 References

(1)   (a) Liu, Z.; Marder, T. B. *Angew. Chem. Int. Ed.* **2008**, *47*, 242; (b) Bosdet, M. J. D.; Piers, W. E. *Can. J. Chem.* **2009**, *87*, 8; (c) Campbell, P. G.; Marwitz, A. J. V.; Liu, S.-Y. *Angew. Chem. Int. Ed.* **2012**, *51*, 6074.

(2)   (a) Burroughes, J. H.; Bradley, D. D. C.; Brown, A. R.; Marks, R. N.; Mackay, K.; Friend, R. H.; Burns, P. L.; Holmes, A. B. *Nature* **1990**, *347*, 539; (b) Grimsdale, A. C.; Müllen, K. *Macromol. Rap. Comm.* **2007**, *28*, 1676; (c) Scherf, U.; List, E. J. W. *Adv. Mater.* **2002**, *14*, 477.

(3)   (a) Jäkle, F. *Chem. Rev.* **2010**, *110*, 3985; (b) Tanaka, K.; Chujo, Y. *Macromol Rapid Comm* **2012**, *33*, 1235; (c) Jäkle, F. *Top. Organomet. Chem.* **2015**, *49*, 297; (d) Guo, F.; Yin, X.; Pammer, F.; Cheng, F.; Fernandez, D.; Lalancette, R. A.; Jäkle, F. *Macromolecules* **2014**, *47*, 7831; (e) Dou, C.; Ding, Z.; Zhang, Z.; Xie, Z.; Liu, J.; Wang, L. *Angewandte Chemie International Edition* **2015**, *54*, 3648.

(4)   Taniguchi, T.; Yamaguchi, S. *Organometallics* **2010**, *29*, 5732.

(5)   (a) Jaska, C. A.; Piers, W. E.; McDonald, R.; Parvez, M. *J. Org. Chem.* **2007**, *72*, 5234; (b) Lukoyanova, O.; Lepeltier, M.; Laferrière, M.; Perepichka, D. F. *Macromolecules* **2011**, *44*, 4729.

(6)   Marwitz, A. J. V.; Lamm, A. N.; Zakharov, L. N.; Vasiliu, M.; Dixon, D. A.; Liu, S.-Y. *Chem. Sci.* **2012**, *3*, 825.

(7)   (a) Yamaguchi, S.; Jin, R.-Z.; Itami, Y.; Goto, T.; Tamao, K. *J. Am. Chem. Soc.* **1999**, *121*, 10420; (b) Yamaguchi, S.; Shirasaka, T.; Akiyama, S.; Tamao, K. *J. Am. Chem. Soc.* **2002**, *124*, 8816; (c) Baumgartner, T.; Reau, R. *Chem. Rev.* **2006**, *106*, 4681; (d) Zhan, X.; Barlow, S.; Marder, S. R. *Chem. Commun.* **2009**, 1948; (e) He, G.; Kang, L.; Delgado, W. T.; Shynkaruk, O.; Ferguson, M. J.; McDonald, R.; Rivard, E. *J. Am. Chem. Soc.* **2013**, *135*, 5360; (f) Jahnke, A. A.; Djukic, B.; McCormick, T. M.; Domingo, E. B.; Hellmann, C.; Lee, Y.; Seferos, D. S. *J. Am. Chem. Soc.* **2013**, *135*, 951; (g) He, X.; Baumgartner, T. *RSC Adv.* **2013**, *3*, 11334; (h) Linshoeft, J.; Baum, E. J.; Hussain, A.; Gates, P. J.; äther, C. N.; Staubitz, A. *Angew. Chem. Int. Ed.* **2014**, *53*, 12916

(8)   (a) Barbarella, G.; Favaretto, L.; Sotgiu, G.; Zambianchi, M.; Bongini, A.; Arbizzani, C.; Mastragostino, M.; Anni, M.; Gigli, G.; Cingolani, R. *J. Am. Chem. Soc.* **2000**, *122*, 11971; (b) Dell, E. J.; Capozzi, B.; Xia, J.; Venkataraman, L.; Campos, L. M. *Nature Chem.* **2015**, *7*, 209; (c) Busby, E.; Xia, J.; QinWu; Low, J. Z.; Song, R.; Miller, J. R.; Zhu, X.-Y.; Campos, L. M.; Sfeir, M. Y. *Nature Mater.* **2015**, *14*, 426.

(9)   Wei, S.; Xia, J.; Dell, E. J.; Jiang, Y.; Song, R.; Lee, H.; Rodenbough, P.; Briseno, A. L.; Campos, L. M. *Angew. Chem. Int. Ed.* **2014**, *53*, 1832.

(10)   (a) Yamamoto, T.; Saito, H.; Osakaa, K.; Ando, I.; Kikuchi, M. *Polym. Bull.* **1992**, *29*, 597; (b) Chen, L.; Mahmoud, S. M.; Yin, X.; Lalancette, R. A.; Pietrangelo, A. *Org. Lett.* **2013**, *15*, 5970.

(11)   Baggett, A. W.; Vasiliu, M.; Li, B.; Dixon, D. A.; Liu, S.-Y. *J. Am. Chem. Soc.* **2015**, *137*, 5536.

(12)   (a) Sakamoto, J.; Rehahn, M.; Wegner, G.; Schlüter, A. D. *Macromol. Rap. Comm.* **2009**, *30*, 653; (b) *Conjugated Polymer Synthesis: Methods and Reactions*; Chujo, Y., Ed.; Wiley-VCH: Weinheim, 2010.

(13)   (a) Teramae, H. *J. Chem. Phys.* **1986**, *85*, 990; (b) Wu, C. Q.; Miao, J.; Yu, J.-Z.; Kawazoe, Y. *Phys. Rev. B* **1998**, *57*, 6.

(14)   Baggett, A. W.; Guo, F.; Li, B.; Liu, S.-Y.; Jäkle., F. *Angew. Chem. Int. Ed. 2015, DOI: 10.1002/anie.201504822*.

(15)   Hohl, B.; Bertschi, L.; Zhang, X.; Schlüter, A. D.; Sakamoto, J. *Macromolecules* **2012**, *45*, 5418.

(16)   Barrios-Landeros, F.; Carrow, B. P.; Hartwig, J. F. *J. Am. Chem. Soc.* **2008**, *130*, 5842.

(17)   (a) Yokoyama, A.; Suzuki, H.; Kubota, Y.; Ohuchi, K.; Higashimura, H.; Yokozawa, T. *J. Am. Chem. Soc.* **2007**, *129*, 7236; (b) Beryozkina, T.; Boyko, K.; Khanduyeva, N.; Senkovskyy, V.; Horecha, M.; Oertel, U.; Simon, F.; Stamm, M.; Kiriy, A. *Angew. Chem. Int. Ed.* **2009**, *48*, 2695; (c) Zhang, H.-H.; Xing, C.-H.; Hu, Q.-S. *J. Am. Chem. Soc.* **2012**, *134*, 13156; (d) Gutacker, A.; Lin, C.-Y.; Ying, L.; Nguyen, T.-Q.; Scherf, U.; Bazan, G. C. *Macromolecules* **2012**, *45*, 4441; (e) Fischer, C. S.; Baier, M. C.; Mecking, S. *J. Am. Chem. Soc.* **2012**, *135*, 1148; (f) Elmalem, E.; Biedermann, F.; Johnson, K.; Friend, R. H.; Huck, W. T. S. *J. Am. Chem. Soc.* **2012**, *134*, 17769; (g) Fischer, C. S.; Jenewein, C.; Mecking, S. *Macromolecules* **2015**, *48*, 483.

(18)   Grimme, J.; Kreyenschmidt, M.; Uckert, F.; Müllen, K.; Scherf, U. *Adv. Mater.* **1995**, *7*, 292.

(19)   (a) Meier, H.; Stalmach, U.; Kolshorn, H. *Acta Polymerica* **1997**, *48*, 379; (b) Martin, R. E.; Diederich, F. *Angewandte Chemie International Edition* **1999**, *38*, 1350.

(20)   M. J. Frisch, G. W. T., H. B. Schlegel, G. E. Scuseria, M. A. Robb, J. R. Cheeseman, G. Scalmani, V. Barone, B. Mennucci, G. A. Petersson, H. Nakatsuji, M. Caricato, X. Li, H. P. Hratchian, A. F. Izmaylov, J. Bloino, G. Zheng, J. L. Sonnenberg, M. Hada, M. Ehara, K. Toyota, R. Fukuda, J. Hasegawa, M. Ishida, T. Nakajima, Y. Honda, O. Kitao, H. Nakai, T. Vreven, J. A. Montgomery, Jr., J. E. Peralta, F. Ogliaro, M. Bearpark, J. J. Heyd, E. Brothers, K. N. Kudin, V. N. Staroverov, R. Kobayashi, J. Normand, K. Raghavachari, A. Rendell, J. C. Burant, S. S. Iyengar, J. Tomasi, M. Cossi, N. Rega, J. M. Millam, M. Klene, J. E. Knox, J. B. Cross, V. Bakken, C. Adamo, J. Jaramillo, R. Gomperts, R. E. Stratmann, O. Yazyev, A. J. Austin, R. Cammi, C. Pomelli, J. W. Ochterski, R. L. Martin, K. Morokuma, V. G. Zakrzewski, G. A. Voth, P. Salvador, J. J. Dannenberg, S. Dapprich, A. D. Daniels, O. Farkas, J. B. Foresman, J. V. Ortiz, J. Cioslowski, and D. J. Fox, Gaussian, Inc., Wallingford CT, 2009, Gaussian 09, Revision A.1.

(21)   A bis-BN-tolan showed evidence of intermolecular N-H…π hydrogen bondingin the solid state consistent with the N-H moiety possessing a hybrid character between an arene C-H and an amine N-H bond. See ref. 6.

(22)   According to TD-DFT calculations (B3LYP, 6-31G*), the lowest energy vertical transitions corresponds to HOMO-LUMO excitation, except for **BN1**. See Tables 3-8, 9, 10.

(23)   Stambuli, J. P.; Incarvito, C. D.; Buhl, M.; Hartwig, J. F. *J. Am. Chem. Soc.* **2004**, *126*, 1184.

(24)   (a) Jeener, J.; Meier, B. H.; Bachmann, P.; Ernst, R. R. *J. Chem. Phys.* **1979**, *71*, 4546; (b) Muller, L. *J. Am. Chem. Soc.* **1979**, *101*, 4481.

(25)   States, D. J.; Haberkorn, R. A.; Ruben, D. J. *J. Magn. Reson.* **1982**, *48*, 286.

Conclusions

With the development of various synthetic methods and characterization techniques, the family of organoborane-functionalized conjugated polymers have grown to a scope which goes beyond any single discipline. In this thesis, we demonstrated the incorporation of organoborane functionality into different π-conjugated polymers: (i) side-chain organoborane-functionalized polythiophenes, (ii) boronic acid-functionalized polyolefins covalently linked to polythiophenes, (iii) B-N for C=C substitution as a new paradigm for conjugated materials development. Interesting optical and electronic properties of these newly developed polymers suggest that they hold great promise in new organic electronics and sensory applications.

List of Publications

Publications on Ph.D work

1. "Regioregular Synthesis of Azaborine Oligomers and Polymer with a syn-Conformation that is Stabilized by N-H…π Interactions," Baggett, A. W.; **Guo, Fang**.; Li, B.; Liu, S.-Y.; Jäkle, F. *Angew. Chem. Int. Ed*. **2015**, *54*, 11191-11195. **(Equal Contribution)**
   - Selected as Polymerization/Hot Paper
   - Cover Picture, *Angew. Chem. Int. Ed*. **2015.**

2. "Regioregular Organoborane-Functionalized Poly(3-alkynylthiophene)s" **Fang Guo**, X.Yin, F. Pammer, F. Cheng, D. Fernandez, R. A. Lalancette, and F. Jäkle. Macromolecules, **2014**, *47*, 7831-7841.

3. "Air- and Water-Stable, Fluorescent Oligomers of 9,10-Dihydro-9,10-diboraanthracene" Christian Reus, **Fang Guo**, Alexandra John, Marcel Winhold, Hans-Wolfram Lerner, Frieder Jäkle, and Matthias Wagner. *Macromolecules*, **2014**, *47*, 3727–3735.

4. "Synthesis, Structures, and Hydroboration of Oligo- and Poly(3-alkynylthiophene)s" Pammer, F.; **Guo, Fang**.; Lalancette, R. A.; Jäkle, F. *Macromolecules* **2012**, *45*, 6333.